

SCOURING AROUND A GROUP OF PIERS

A thesis Submitted

in partial fulfilment of the requirements for the award of the degree of

DOCTOR OF PHILOSOPHY

In

CIVIL ENGINEERING

By

GEETA DEVI

(Roll. No. - 2K17/PhD/CE/09)

Under the supervision of

Prof. MUNENDRA KUMAR



**DEPARTMENT OF CIVIL ENGINEERING
DELHI TECHNOLOGICAL UNIVERSITY
SHAHBAD DAULATPUR, BAWANA ROAD, DELHI - 110042 (INDIA)**

2023



DELHI TECHNOLOGICAL UNIVERSITY

(Formerly Delhi College of Engineering, Since 1941)

Shahbad Daulatpur, bawana road, Delhi- 110042

DECLARATION

I hereby declare that the research work presented in this thesis entitled "Scouring around a group of piers" is original and carried out by me under the supervision of Prof. Munendra Kumar, Professor, Department of Civil Engineering, Delhi Technological University, Delhi, and being submitted for the award of Ph.D. degree to Delhi Technological University, Delhi, India. The content of this thesis has not been submitted either in part or whole to any other university or institute for the award of any degree or diploma.

Date: 10/05/2023

Place: DTU, Delhi.

(Geeta Devi)

Roll. No. – 2k17/PhD/CE/09



DELHI TECHNOLOGICAL UNIVERSITY

(Formerly Delhi College of Engineering, Since 1941)

Shahbad Daulatpur, bawana road, Delhi- 110042

Date: - 10/05/2023

CERTIFICATE

This is to certify that the PhD thesis entitled “Scouring around a group of piers” is being submitted by Mrs. Geeta Devi, for the fulfilment of the requirements for the award of the degree of Doctor of Philosophy in Civil Engineering to the Department of Civil Engineering, Delhi Technological University, Delhi, India. She has a bonafide record of original research work carried out by her under my guidance and supervision. The results embodied in this thesis have not been submitted to any other university or institution for the award of any degree or diploma.

Prof. Munendra Kumar

Supervisor

Department of Civil Engineering

Delhi Technological University

Delhi – 110042.

ACKNOWLEDGEMENTS

I would like to express my appreciation to the people who have helped me most during my research work. First and foremost, I am deeply grateful to my thesis advisor Prof. Munendra Kumar, Professor, Department of Civil Engineering, Delhi Technological University, for his enduring patience, constant encouragement, guidance and support throughout this research, without which successful completion would not have been possible. It has been an honor to be associated with such a great supervisor and learn from his experience.

I want to pronounce my utmost gratitude to Sh. Kewal Singh, retired senior lab technician, Mr. Anil Agnihotri, lab technician, and Nitesh, lab attendant, Department of Civil Engineering, for their valuable help. I also express my gratitude to my colleagues Deepak Singh, Monika Sharma, Neevetika Verma, Noopur Awasthi, Rahul Kumar, Ruchika Dabas, Shailesh Kumar Gupta, and Vijay Kaushik for providing me sensible guidance, faultless planning, helpful advice, kind cooperation, and friendly discussion at various stages of the work.

My inexplicable gratitude goes to the Head of the Civil Engineering Department (Prof. Vijay K. Minocha), and all the faculty members for providing me sensible guidance, faultless planning, helpful advice, and kind cooperation at various stages of the work. I am also thankful to the lab staff and office staff of the Civil Engineering Department for providing the kind cooperation and necessary facilities to carry out the study.

Finally and most importantly, I would like to express my love and thanks to my parents, my brother Shubham Sharma, my sister Priyanka Sharma and grandparents for their encouragement and support, who stood by me like a rock and provided constant motivation during the years. I want to extend special thanks to my husband Ajay Bhardwaj his support and constant motivation. All my family members have shown enormous patience during this process and have cheerfully sacrificed the time that rightfully belonged to them. Finally, I extend a profound expression of respect to all elders in the family and especially my parents, who have always showered me with their blessings and made me

who I am today. At the end of this Ph.D. research, I want to thank all the people who helped, supported, and encouraged me all these five years.

LIST OF PUBLICATIONS

- Devi, Geeta, and Munendra Kumar. "Estimation of local scour depth around twin piers using gene expression programming (local scour around twin piers)." *Water Supply* 22, no. 6 (2022): 5915-593.
- Devi, Geeta, and Munendra Kumar. "Characteristics assessment of local scour encircling twin bridge piers positioned side by side (SbS)." *Sādhanā* 47, no. 3 (2022): 1-13.
- Devi, Geeta, and Munendra Kumar. "Experimental study of the local scour around the two piers in the tandem arrangement using ultrasonic ranging transducers." *Ocean Engineering* 266 (2022): 112838.

LIST OF CONFERENCES

- Devi, Geeta, and Munendra Kumar. "Countermeasures against Local Scouring at Circular Bridge Piers Using Collar and Combination of Slot and Collar." In *River Hydraulics*, pp. 289-296. Springer, Cham, 2022. (Scopus)
- Devi, Geeta, and Munendra Kumar. "Review paper of different scouring Monitoring Techniques and Instruments." (2018), *International Conference on New Frontiers in Engineering, Science & Technology, NFEST*, Delhi.

LIST OF BOOK CHAPTERS

- Devi, Geeta, and Munendra Kumar. "Last century evolution in local scour measuring techniques." In *Current Directions in Water Scarcity Research*, vol. 7, pp. 513-529. Elsevier, 2022.
- Devi, Geeta, and Munendra Kumar. "Countermeasures against Local Scouring at Circular Bridge Piers Using Collar and Combination of Slot and Collar." In *River Hydraulics*, pp. 289-296. Springer, Cham, 2022.
- Devi, Geeta, and Munendra Kumar. "A Review on Estimation Methods of Scour Depth around Bridge Pier." In *River Dynamics and Flood Hazards*, Springer Nature 2022.

ABSTRACT

Scour is caused by the erosive action of flow of water, which erodes and takes away sediments from the river bed, as well as from the area of bridge piers and abutments. This process of scour is well-known for its complicated behaviour, and this process becomes more complex for the group of piers. As per the literature available, scour is a major contributor for the collapse of the bridge structures. Hence it becomes essential for the researches to predict the scour depth accurately. To fulfill this necessity, the deep understanding of the flow-field around the piers and factors affecting the scour depth is important. Numerous studies are available in the literature on the flow-field and local scour, but majority of them are focused only on single pier. However, multiple piers are more common in the bridge designing due to economical and geotechnical considerations. Engineers across the world are predominately considering single pier characterization for the group of piers, although all bridge structures are laid on the group of piers. The design considerations developed for a single pier mostly ignores the most significant group effects for multiple piers such as: pier sheltering, pier spacing and mutual interference effect. It is demonstrated by the fact that inadequate research and development for the multiple piers have been observed. Therefore, it is utmost important to investigate the factors affecting the multiple piers and develop an equation by considering all the variables for accurate prediction of scour depth.

The primary aim of this research is to investigate the effect of the pier spacing (P_s) between the piers and temporal scour development on scour depth and propose a new equation for scour depth estimation. In order to meet the objectives of this research, detailed experimental study has been conducted for, single pier, two piers, and three piers. In total, 232 experiments have been carried out for various pier spacing and pier arrangements on uniformly graded sediment in the Hydraulic Engineering Laboratory of Delhi Technological University, Delhi, India. Pier arrangements studied in this research are: single pier, two piers in tandem arrangement, two piers in side-by-side arrangement, two piers at an angle of 15 and 30 degrees to the direction of flow, three piers in tandem arrangement, three piers in side-by-side arrangement and three piers in staggered

arrangement. The instantaneous 3-D velocity measurement is conducted by utilizing SonTek 16-MHz Micro-ADV (Acoustic Doppler Velocimeter) has been used. For profoundly understanding and continuous monitoring of scour evolution SeaTek Ultrasonic ranging system have been used.

The Experimental observations for the temporal scour evolutions and scour hole development pattern for all the pier arrangements under various pier spacing has been presented in the graphical and pictorial form. The findings of this research shed light on the factors that causes scour: pier spacing, flow depth, Froude number, and scour development pattern. These are all important variables, which needs to consider in order to accurately predict the maximum scour depth. Results shows that, the flow-field around the group of piers is much more complex than single pier and pier spacing plays a major role in the scour depth estimation. The results also exemplify that non-dimensional scour depth increases with the increase in the Froude number and velocity of flow. The effect of pier spacing shows that the scour depth increases as the pier spacing increases at a certain P_s range, then it decreases. Furthermore, two semi empirical equations has been proposed for the tandem and side-by-side arrangements by using GEP, and the comparison of the proposed GEP equation with the well-known equation and experimental results shows that the GEP is better prediction tool for scour depth. Lastly, to evaluate the influence of various parameters on the scour depth sensitivity analysis has been conducted, and concluded that pier spacing plays an important role in scour estimation. The findings of this study can be further used for the evaluation of the research data.

TABLE OF CONTENTS

DECLARATION.....	II
CERTIFICATE.....	III
ACKNOWLEDGEMENTS	IV
LIST OF PUBLICATIONS	VI
ABSTRACT.....	VII
TABLE OF CONTENTS	IX
LIST OF TABLES	XIX
LIST OF ABBREVIATIONS	XXI
CHAPTER 1	1
1.1 GENERAL BACKGROUND.....	1
1.2 SCOUR.....	4
1.2.1 General scour	4
1.2.2 Localized scour.....	5
1.2.3 Bend scour	6
1.2.4 Confluence scour	6
1.3 LOCAL SCOUR AROUND A GROUP OF PIERS.....	7
1.4 OBJECTIVES.....	9
1.5 SCOPE AND LIMITATION	9
1.6 ARRANGEMENT OF THESIS	10
CHAPTER 2	11
2.1 INTRODUCTION.....	11
2.2 LOCAL SCOUR AROUND SINGLE PIER	11
2.3 LOCAL SCOUR AROUND TWO PIERS.....	14
2.4 LOCAL SCOUR AROUND THREE PIERS.....	19
2.5 PROBLEM STATEMENT.....	23
2.6 MECHANISM OF LOCAL SCOUR	23

2.7	VARIABLES AFFECTING THE LOCAL SCOUR.....	27
2.7.1	<i>Flow shallowness</i>	27
2.7.2	<i>Effect of Sediment Coarseness, D/d_{50}</i>	29
2.7.3	<i>Effect of Sediment Non-uniformity, σ_g</i>	30
2.7.4	<i>Effect of pier alignment, K_θ</i>	32
2.7.5	<i>Effect of Pier Shape</i>	33
2.7.6	<i>Effect of Flow Intensity, V/V_c</i>	34
2.7.7	<i>Effect of Viscosity</i>	36
2.8	TEMPORAL SCOUR DEPTH.....	37
2.9	APPROACHES FOR SCOUR DEPTH ESTIMATION.....	40
2.9.1	<i>Semi empirical equations used for scour depth estimation</i>	40
2.9.1.1	Melville and Coleman Equation.....	40
2.9.1.2	HEC-18 Equation.....	42
2.9.1.3	IRC 1998 &2000 (Indian Roads Congress) Equation.....	43
2.9.1.4	Sheppard/Melville Equation (S/M equation).....	44
2.9.1.5	Laursen and Toch.....	45
2.9.2	<i>AI based Approaches for scour depth estimation</i>	46
2.10	SUMMARY AND GAPS IN LITERATURE.....	47
CHAPTER 3	49
3.1	INTRODUCTION.....	49
3.2	EXPERIMENTAL SETUP.....	49
3.2.1	<i>Rectangular Flume and its Components</i>	49
3.2.2	<i>Vernier Point Gauge</i>	51
3.2.3	<i>Venturimeter</i>	51
3.2.4	<i>V-Notch</i>	52
3.2.5	<i>SeaTek ultrasonic ranging system</i>	53
3.2.6	<i>Pier Models arrangements</i>	55
3.3	MATERIAL USED AND SEDIMENT TRANSPORTATION.....	56
3.4	DIMENSIONAL ANALYSIS.....	58
3.5	VELOCITY MEASUREMENT.....	60
3.5.1	<i>Micro-ADV (Acoustic Doppler Velocimeter)</i>	60

3.5.2	<i>Flow Probe</i>	62
3.6	EXPERIMENTAL PROCEDURE AND DATA ACQUISITION	64
3.7	COMPUTATIONAL ANALYSIS	66
3.7.1	<i>General overview of GEP</i>	66
3.7.2	<i>GEP Modelling</i>	68
3.7.3	<i>Modification</i>	68
3.7.3.1	Replication	69
3.7.3.2	Mutation	69
3.7.3.3	Transposition and insertion sequence elements	69
3.7.3.4	Recombination	69
3.8	SUMMARY	70
CHAPTER 4	71
4.1	INTRODUCTION	71
4.2	SINGLE PIER	71
4.2.1	<i>Experimental programme and flow characteristics</i>	72
4.2.2	<i>Results and Discussion</i>	74
4.2.2.1	Temporal evolution of scour depth around single pier	74
4.2.2.2	Scour Hole Formation	77
4.2.2.3	Flow Shallowness (h/D) effect	78
4.2.2.4	Froude Number Effect on the Scour Depth around Single Pier	79
4.2.2.5	Flow-Field using CFD	80
4.3	TWO PIERS IN TANDEM ARRANGEMENT	87
4.3.1	<i>Experimental Programme and flow characteristics</i>	87
4.3.2	<i>Results and Discussion</i>	89
4.3.2.1	Temporal evolution of scour depth around two piers (tandem arrangement)	90
4.3.2.2	Effect of Froude number on scour depth around two piers in tandem arrangement	95
4.3.2.3	Effect of Reynolds Number on Maximum Scour Depth	97
4.3.2.4	Effect of Relative Velocity on Maximum Scour Depth	99
4.4	TWO PIERS IN SIDE-BY-SIDE ARRANGEMENT	102

4.4.1	<i>Experimental Programme and flow characteristics</i>	102
4.4.2	<i>Results and Discussions</i>	104
4.4.2.1	Temporal evolution of scour depth around two piers (side-by-side arrangement)	104
4.4.2.2	Froude number effect	107
4.5	TWO PIERS AT AN ANGLE OF 15° AND 30° ARRANGEMENT	110
4.5.1	<i>Experimental Programme and flow characteristics</i>	110
4.5.2	<i>Results and Discussions</i>	111
4.5.2.1	Temporal evolution of scour depth around two piers (angle arrangement)	111
4.5.2.2	Effect of Pier Spacing on the Non-Dimensional Scour Depth.....	113
4.6	THREE PIERS IN TANDEM ARRANGEMENT	115
4.6.1	<i>Experimental Programme and flow characteristics</i>	115
4.6.2	<i>Results and discussion</i>	116
4.6.2.1	Temporal evolution of scour depth around three piers in tandem arrangement.....	116
4.6.2.2	Effect of pier spacing on the three piers in tandem arrangement.....	118
4.6.2.3	Froude number effect on the scour depth around three piers in tandem arrangement.....	121
4.7	THREE PIERS IN SIDE BY SIDE ARRANGEMENT.....	124
4.7.1	<i>Experimental Programme and flow characteristics</i>	124
4.7.2	<i>Results and discussion</i>	125
4.7.2.1	Temporal evolution of scour depth around three piers in side-by-side arrangement.....	125
4.7.2.2	Effect of pier spacing on the three piers in side-by-side arrangement ..	130
4.7.2.3	Froude number Effect on the Scour Depth.....	131
4.8	THREE PIERS IN STAGGERED ARRANGEMENTS.....	132
4.8.1	<i>Experimental Programme and flow characteristics</i>	132
4.8.2	<i>Results and discussion</i>	133
4.8.2.1	Temporal evolution of scour depth around three piers in staggered arrangement.....	133

4.8.2.2	Effect of pier spacing on the three piers in staggered arrangement .	Error!
	Bookmark not defined.	
4.9	GENE EXPRESSION PROGRAMMING FOR TANDEM ARRANGEMENT.....	139
4.9.1	<i>GEP for scour depth prediction.....</i>	<i>139</i>
4.9.2	<i>GEP Modelling.....</i>	<i>140</i>
4.9.3	<i>GEP model performance analysis for equilibrium scour depth.....</i>	<i>145</i>
4.10	GENE EXPRESSION PROGRAMMING FOR SIDE BY SIDE ARRANGEMENT	146
4.10.1	<i>Brief overview of Gene Expression Programming (GEP).....</i>	<i>146</i>
4.10.2	<i>GEP Application: Formulation for Scour Depth.....</i>	<i>147</i>
4.10.3	<i>Performance analysis of the GEP model for equilibrium scour depth.....</i>	<i>151</i>
4.10.4	<i>Sensitivity Analysis.....</i>	<i>153</i>
CHAPTER 5	156
5.1	SUMMARY	156
5.1.1	<i>Pier arrangements</i>	<i>156</i>
5.1.2	<i>Traditional equation.....</i>	<i>158</i>
5.1.3	<i>GEP</i>	<i>158</i>
5.2	CONCLUSION.....	159
5.3	RECOMMENDATION FOR FURTHER WORK	161
REFERENCES	162

LIST OF FIGURES

Fig. 1.1 Bridge failures: (a) Hintze Ribeiro, Castelo-de-Paiva, northern Portugal, (b) Queen Isabella Causeway, Texas, United State, (c) Tadcaster Bridge, England, U.K. (d) Viadotto Madonna del Monte, Italy,(e) Logan River bridge, Australia, and (f) Tinau River Bridge, Nepal	2
Fig. 1.2 Local scour around the circular pier	6
Fig. 2.1 Two piers in tandem arrangement on the Vivekananda Bridge and Nivedita Bridge.....	15
Fig. 2.2 Flow-field around isolated bridge pier with primary vortices adapted from (Ettema et al. 2011).....	24
Fig. 2.3 Flow Shallowness (h/D) effect on the Non-Dimensional Scour depth Y_s/D adapted from Moreno (2016).....	29
Fig. 2.4 Sediment coarseness effect (D/d_{50}) on non- dimensional scour depth (Y_s /D) adapted from Melville and Coleman (2000).....	30
Fig. 2.5 Effect of sediment non-uniformity on the non-dimensional scour depth for (a) clear water bed condition and (b) live bed condition.....	31
Fig. 2.6 Influence of pier alignment factor with the pier angle adapted from (Melville and Coleman 2000).....	32
Fig. 2.7 Basic shapes of bridge piers	33
Fig. 2.8 Classification of the scour depth on the basis of flow intensity adapted from Melville and Coleman (2000).....	34
Fig. 2.9 Effect of flow intensity (V/V_c) on the scour depth with the Factor of Flow intensity K_I (a) Uniform sediment, (b) Non-Uniform sediment, adapted from Melville and Coleman (2000)	35
Fig. 2.10 Variation of Froude number on the Non-dimensional scour depth adapted from Ettema et al. (2006).....	36
Fig. 2.11 Temporal scour depth evolution for clear water and live bed condition adapted from Ettema et al. (2006).....	37
Fig. 3.1 Schematic Diagram of the rectangular recirculating open channel flume.....	49
Fig. 3.2 Rectangular masonry flume and its components.....	50

Fig. 3.3 Schematic diagram of the venturimeter.....	52
Fig. 3.4 Schematic representation of the V-Notch.....	53
Fig. 3.5 SeaTek Ultrasonic Transducers.....	54
Fig. 3.6 Particle size distribution curve	57
Fig. 3.7 Micro-ADV (Acoustic Doppler Velocimeter).....	62
Fig. 3.8 Flow Probe.....	63
Fig. 3.9 (a) Placement of sand bed; (b) placement of the pier	64
Fig. 3.10 Installation of SeaTek transducers around the pier	64
Fig. 4.1 Mechanism of bridge scour around single pier	71
Fig. 4.2 Experimental setup of hydraulic flume for single pier	72
Fig. 4.3 Position of ultrasonic transducers around the bridge pier at P ₁ , P ₂ , P ₃ , and P ₄ ...	73
Fig. 4.4 Temporal scour depth at the Observation points (a) P ₁ and (b) P ₄	75
Fig. 4.5 Temporal scour depth at the observation points (a) P ₂ and (b) P ₃	76
Fig. 4.6 Elevation of scour hole developed after 72 hours of experimental run.....	77
Fig. 4.7 Flow shallowness effect on the equilibrium time t _e	78
Fig. 4.8 Trend of scour depth at four observation points for the single pier with the increasing Froude number.....	79
Fig. 4.9 Meshing of the circular cylinder.....	82
Fig. 4.10 Boundary condition for the channel section	83
Fig. 4.11 Velocity contour of the flow around the bridge pier; (a) Initial stage, (b) Intermediate Stage, (c) Final Stage.....	85
Fig. 4.12 Streamlines contours for the bridge pier at (a) Initial stage, (b) Intermediate Stage, (c) Final Stage	86
Fig. 4.13 Schematic diagram of two piers in tandem arrangement	87
Fig. 4.14 Experimental setup of hydraulic flume	87
Fig. 4.15 Pier positioning and observation points.....	88
Fig. 4.16 Scour-hole geometry for front and rear piers in tandem arrangement at the end of experimental run	91
Fig. 4.17 Temporal scour evolution at two piers for rate of flow 0.0295 m ³ /sec	92
Fig. 4.18 Temporal scour evolution at two piers for rate of flow 0.0361 m ³ /sec	93
Fig. 4.19 Temporal scour evolution at two piers for rate of flow 0.0428 m ³ /sec	93

Fig. 4.20 Temporal scour evolution at two piers for rate of flow $0.0486 \text{ m}^3/\text{sec}$	94
Fig. 4.21 Temporal scour evolution at two piers for rate of flow $0.0537 \text{ m}^3/\text{sec}$	94
Fig. 4.22 Effect of densimetric Froude number on non-dimensional scour depth at front and rear pier at (a) upstream side (b) downstream side (c) right side and (d) left side.....	96
Fig. 4.23 Non-dimensional scour depth variation with Densimetric Froude number (F_d)	97
Fig. 4.24 Reynolds number effect on the non-dimensional scour depth for the front pier	98
Fig. 4.25 Reynolds number effect on the non- dimensional scour depth for the rear pier	99
Fig. 4.26 Non-dimensional scour depth (Y_s /D), versus relative velocity (u/u_c), with the increasing non-dimensional pier spacing (P_s /D) at (a) upstream side (b) downstream side (c) right side and (d) left side	101
Fig. 4.27 Schematic diagram of the experimental set-up.....	102
Fig. 4.28 Laboratory set-up for experimental work	102
Fig. 4.29 Experimental set-up for different arrangements of the piers with increasing center-to-center clear spacing between the piers	103
Fig. 4.30 Scour hole evolution after drainage of water for eight pier spacing arrangements	104
Fig. 4.31 Maximum scour depth in case of $2.5 D$ spacing (a) Experimental results (b) contour plot for maximum scour bed level in cm	105
Fig. 4.32 Equilibrium scour depth for the seven-sets of rate of flow in m^3/sec	106
Fig. 4.33 Equilibrium scour depth for the seven-sets of rate of flow (m^3/sec) for (a) Left Pier, and (b) Right Pier.	107
Fig. 4.34 Effect of the Froude number on scour depth upstream of the two piers in side-by-side arrangement.....	109
Fig. 4.35 Effect of the Froude number on scour depth downstream of the two piers in side-by-side arrangement	109
Fig. 4.36 Two piers aligned at 15° angle of attack to the direction of flow.....	110
Fig. 4.37 Two piers aligned at 30° angle of attack to the direction of flow	111
Fig. 4.38 Temporal Evolution of scour depth around two piers aligned at (a) 15° and (b) 30°	113
Fig. 4.39 Effect of angle of attack on the non-dimensional scour depth at two piers aligned at an angle of (a) 15° and (b) 30°	114

Fig. 4.40 Three piers positioned in the tandem arrangement.....	116
Fig. 4.41 Temporal evaluation of scour depth around three piers in the tandem arrangement at 0.0295 m ³ /s rate of flow	117
Fig. 4.42 Temporal evaluation of scour depth around three piers in the tandem arrangement at 0.0428 m ³ /s rate of flow	117
Fig. 4.43 Temporal evaluation of scour depth around three piers in the tandem arrangement at 0.0537 m ³ /s rate of flow	118
Fig. 4.44 Scour depth around the three piers in the tandem arrangement	120
Fig. 4.45 Variation of non-dimensional scour depth with the pier spacing on the upstream side of the piers for the Froude number (a) 0.206, (b) 0.217 and (c) 0.237	122
Fig. 4.46 Variation of non-dimensional scour depth with the pier spacing on the right side of the piers for the Froude number (a) 0.206, (b) 0.217 and (c) 0.237	122
Fig. 4.47 Variation of non-dimensional scour depth with the pier spacing on the left side of the piers for the Froude number (a) 0.206, (b) 0.217 and (c) 0.237	123
Fig. 4.48 Variation of non-dimensional scour depth with the pier spacing on the downstream side of the piers for the Froude number (a) 0.206, (b) 0.217 and (c) 0.237	124
Fig. 4.49 Three piers in side by side arrangement	125
Fig. 4.50 Temporal evolution of scour depth on the upstream side of the side-by-side pier arrangement for V= 0.224 m/sec	126
Fig. 4.51 Temporal evolution of scour depth on the upstream side of the side-by-side pier arrangement for V= 0.262 m/sec	127
Fig. 4.52 Temporal evolution of scour depth on the upstream side of the side-by-side pier arrangement for V= 0.3 m/sec	127
Fig. 4.53 Temporal evolution of scour depth on the downstream side of the side-by-side pier arrangement for V= 0.224 m/sec	128
Fig. 4.54 Temporal evolution of scour depth on the downstream side of the side-by-side pier arrangement for V= 0.262 m/sec	129
Fig. 4.55 Temporal evolution of scour depth on the downstream side of the side-by-side pier arrangement for V= 0.3 m/sec	129
Fig. 4.56 Scour depth around the three piers in side-by-side arrangement.....	131

Fig. 4.57 Effect of Froude number on scour depth for side-by-side arrangement at (a) upstream side, (b) right side, (c) left side, and (d) downstream side	132
Fig. 4.58 Three piers in staggered arrangement.....	133
Fig. 4.59 Temporal scour depth around three piers aligned in staggered arrangement for $V= 0.224$ m/sec	134
Fig. 4.60 Temporal scour depth around three piers aligned in staggered arrangement for $V= 0.262$ m/sec	135
Fig. 4.61 Temporal scour depth around three piers aligned in staggered arrangement for $V= 0.30$ m/sec	135
Fig. 4.62 scour depth around the three piers aligned in staggered positioning.....	138
Fig. 4.63 Expression tree	144
Fig. 4.64 Comparison of the GEP equation with the existing equations: (a) IRC equation; (b) Laursen and Toch equation; (c) Melville and Coleman equation; and (d) HEC-18 equation.....	146
Fig. 4.65 Proposed GEP formulation in the form of expression tree's (ET's)	149
Fig. 4.66 GEP predicted equilibrium scour depth (Y_{su}) versus observations from the current Experimental Study (a) Training; and (b) Testing.....	152
Fig. 4.67 Observed versus Predicted equilibrium scour depth using different equations: Present study (GEP) versus (a) Laursen and Toch; (b) Melville and Coleman; (c) HEC-18; (d) Sheppard/Melville	153

LIST OF TABLES

Table 2.1 Research work available in the literature for scour around two bridge piers ...	16
Table 2.2 Scour classification on the basis of pier size and floe depth purposed by Melville and Coleman (2000)	28
Table 2.3 Shape factor for different pier shapes adapted from Richardson and Davis (2001)	33
Table 2.4 Correction factors for the Melville and Coleman equation	41
Table 2.5 Values of K_1 factor of correction for pier shapes adapted from Richardson and Davis (2001)	42
Table 2.6 Values of K_2 factor of correction for various angle of attacks Richardson and Davis (2001)	43
Table 2.7 Values of K_3 factor of correction for condition of bed Richardson and Davis (2001)	43
Table 3.1 Specifications of the Seatek Ultrasonic ranging system	54
Table 3.2 Arrangement of piers	55
Table 3.3 Specifications of the Micro-ADV	61
Table 3.4 Specifications of Flow Probe	63
Table 4.1 Hydraulic parameters for the experimental study	73
Table 4.2 Flow parameters	89
Table 4.3 Characteristics flow conditions of the present study and similar studies	89
Table 4.4 Experimental results of first category (Single pier) for all the five flow conditions	100
Table 4.5 Flow characteristics for the two-pier aligned at an angle of 15 and 30 degree	111
Table 4.6 Flow characteristics for the three piers in the tandem and side by side arrangement	115
Table 4.7 Outline of the dimensional factors utilised in the formulation of the GEP	141
Table 4.8 Description of the variables used in the proposed investigation to formulate GEP	143
Table 4.9 Values of gene constants used in the proposed equation	143

Table 4.10 Statistical analysis for the GEP and traditional regression based equations for the present experimental results.....	145
Table 4.11 List of the dimensional variables used for GEP formulation.....	148
Table 4.12 Definition of the parameters used in GEP formulation.	150
Table 4.13 Statistical error measures for the GEP and traditional regression based equations	152
Table 4.14 sensitivity analysis of the influencing parameters	155

LIST OF ABBREVIATIONS

ADV	Acoustic Doppler Velocimeter
AVDP	Acoustic Doppler Velocity Profilers
ANN	Artificial Neural Networks
ANFIS	Adaptive Network-based Fuzzy Inference Systems
DES	Detached-Eddy Simulation
ET	Expression Tree
FDOT	Florida Department of Transportation
GA	Genetic Algorithms
GEP	Gene Expression Programming
GMDH	Group Method of Data Handling
GP	Genetic Programming
IRC	Indian Roads Congress
LES	Large-Eddy Simulation
MSD	Maximum Scour Depth
NCH	National Cooperative Highway
PIV	Particle Image Velocity
RBF	Radial Basis functions
RANS	Reynolds-Averaged Navier-Stokes

CHAPTER 1

INTRODUCTION

1.1 General Background

From the beginning of history, bridges have been required in order to cross the waterways for transportation systems. As transportation means seem to have been considered an essential factor for the economic, social and cultural improvement of a country. Since then, humans have been required to construct bridges to span bodies of water, mountains, and highways. Bridge components such as piers and abutments, which support the bridge superstructure, play a significant part in structural stability and security. Undermining of bridge components owing to silt transport, riverbed erosion, scouring, and floods are widely acknowledged as key challenges in the growth of a country. According to Melville (1975), variables influencing changes in bed elevation at a bridge site is primarily divided into three groups: (a) progressive aggradation and degradation of the river bed, (b) temporary scour, and (c) presence of a hydraulic structure. Thus scouring and flooding of the riverbed near the bridge site is considered as primary cause of bridge failure among these difficulties.

In the history of bridge failure flooding events has been identified as the leading cause of failure, although significant advances have been made in this research area. Smith (1976), examined the 143 bridge failure that occurred in various nations between the years 1961-1975, out of these failures roughly 45% might be linked to the scour around bridge piers. According to Melville (1992), 29 of the 108 bridge collapses recorded in New Zealand between the years of 1960-1984, had also attributed to scour. As per Melville and Coleman (2000) study, the scour of the bridge foundation can be held responsible for at least one severe bridge failure per year in New Zealand. Additionally, Parola et al. (1997); Richardson and Davis (2001), and Arneson et al. (2012) also stated that, the bridge scour is a major problem in the United States and is primary factor in around 60% of all U.S. highway bridge collapses. Additionally, it has been stated that over 2,500 bridges were demolished in 1993 as a result of scour brought on by extreme flooding. In 1994, there were also reports of over 1,000 bridges being closed in Georgia due to flooding.

More than 500 bridge collapses in the United States between the years 1989-2000 had analyzed (Wardhana and Hadipriono 2003).

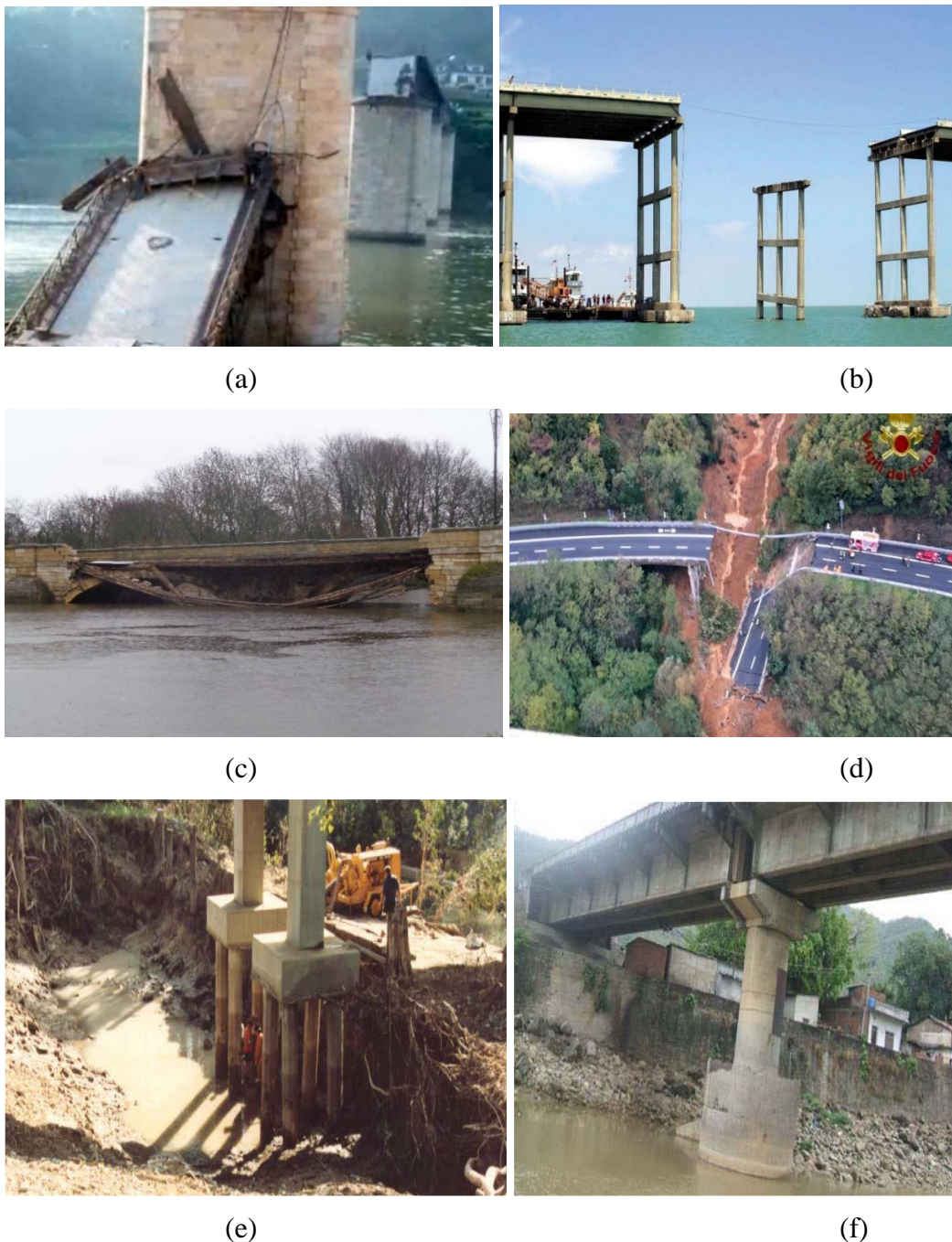


Fig. 1.1 Bridge failures: (a) Hintze Ribeiro, Castelo-de-Paiva, northern Portugal, (b) Queen Isabella Causeway, Texas, United State, (c) Tadcaster Bridge, England, U.K. (d) Viadotto Madonna del Monte, Italy, (e) Logan River bridge, Australia, and (f) Tinau River Bridge, Nepal

A series of bridge failures that occurred after 2000 have been reported here; according to the information provided on Wikipedia-contributors, on the night of March 4, 2001, a reinforced cement concrete bridge named Hintze Ribeiro Bridge, Castelo de Paiva, northern Portugal, collapsed due to scouring of piers shown in **Fig. 1.1**. Fifty Nine individuals had died in the catastrophe, and three automobiles had also crushed in the collapsing part. Following the disaster, the bridge was dismantled and replaced with a new bridge, and hundreds more bridges around Portugal had blocked for emergency repair. On September 15, 2001, the second-longest bridge fell due to pier failure named 'Queen Isabella Causeway, Texas, United States. Because the Causeway serves as the only route connecting South Padre Island to Port Isabel, the collapse had a significant economic impact on the region. On October 29, 2005, the Valigonda rail catastrophe happened at Valigonda, Hyderabad, India. Interstate 88 washed out as a result of the June 2006 floods in upstate New York and northern Pennsylvania. A 20-metre portion of the railway bridge Broadmeadow viaduct in Ireland fell in August 2009 owing to tidal scouring of foundations. On Nov 2009, due to excessive rainfall and flooding, seven bridges had destroyed or damaged beyond repair in England.

The Colorado Department of Transportation, projected that at least 30 state highway bridges had demolished and 20 suffered major flood damage in 2013 (Novey). CPR Bonnybrook ridge, Calgary, Canada, got partially collapsed due to scouring from flooding in 2013. The Plaka Bridge on Arachthos River in Greece, one of the most outstanding examples of popular Greek architecture, failed on February 1, 2015 as a result of the flash flood. The flood ripped the foundations of the bridge from the riverbanks and swept away the central section of the bridge; this bridge has been repaired in July 2020. The I-10 Bridge and the Bob White covered bridges in the United States had destroyed mainly by water and rainstorms in 2015. Tadcaster Bridge in England, U.K., got collapsed in December 2015 owing to flooding. In March 2017, floods damaged the foundation of two piers at Pfeiffer Canyon Bridge in the United States. On September 17, 2017, the provincial road ksanthi-lasmos river bridge in Greece fell, and the likely reason for failure was scour. Cancura Bridge in Chile collapsed in June 2018, owing to pier foundation failure caused by high floods. Bridge scour induced instability and contributed to the structural failure of the northern arch on the Bishops ford Road Bridge in London, United Kingdom, on June 2019.

On November 2019, in Viadotto Madonna del Monte a concrete bridge in Italy, fell due to severe rain and pier failure. On November 27, 2021, Logan river bridge, Australia, collapsed due to a major flooding event and bridge pier failures. Lastly, on July 25, 2022, a bridge on the Kaliasot River in Madhya Pradesh, India caved in early this morning due to the heavy rainfall in the first year of functioning. As a result, there has been claimed to be very significant chance of bridge failure. According to the analysis above, bridge scour is one of the biggest global issue with bridge safety.

1.2 Scour

Scour around bridge piers may be characterized as a complicated sediment removal process caused by the significant interaction of a 3-D turbulent flow-field and presence of hydraulic structure (piers and abutments) positioned in flowing water. Scour phenomenon is primarily caused by the erosive action of the flowing water, which erodes and takes away the sediment particles from the river bed and from the area around the hydraulic structures (Breusers et al. 1977). According to Melville and Coleman (2000) scour can also be defined as the lowering of the riverbed due to the erosive tendency of the water such that the foundation of the bridge pier gets exposed.

There are four main types of scour which encounters at the bridge crossing waterways:

- 1) General scour
- 2) Localized scour
- 3) Bend scour
- 4) Confluence scour

1.2.1 General scour

The reduction in the actual longitudinal profile of river bed level caused by man-made structures or natural sources is referred to as general scour (Melville and Coleman 2000). General scour occurs regardless of whether the bridge is present and can manifest as either degradation or aggradation. Degradation or aggradation are the consequences of a variation in flow intensity caused by recurrent floods and climate variability. The progressive loss of sediment from the river bed due to continuous river flow and human activity is referred to as degradation. On the other hand, aggradation is the progressive deposit of sediment on the river bed produced by several flooding incidents over time. According to Melville and

Coleman (2000), general scour may be categorized into two types based on the period of occurrence. Short-term scour development is often triggered by a single enormous flood event or a series of modest flood occurrences. Long-term scour, on the other hand, happens over time as a result of progressive deterioration and bank erosion.

1.2.2 Localized scour

According to Melville and Coleman (2000) localized scour is a combination of contraction scour and local scour, due to the increase in the flow velocity, the flow width is converged as the flow approaches the hydraulic structure, this is termed as contraction. This increase in velocity flow generates high-intensity erosive forces on the river bed. These erosive forces around the bridge pier increase the transportation of the sediment material and lower the riverbed level. Contraction scour is further categorized as clear-water scour and live-bed scour. The occurrence of clear water scour is monitored prior to the transportation of the sediment when the rate of flow is low, and it does not erode the river bed. It develops up to a significant depth as flow velocity increases, but only immediately before the riverbed sediment begins to move, which is at rest on upstream of the bridge pier. And, it is the maximum scour depth when no material is being moved. Live-bed scour arises when the deposition of sediment materials into the pier scour hole equals the transportation of sediment material on the upstream of pier (Johnson et al. 2015; Melville and Coleman 2000).

Local scour occurs due to the presence of an obstruction in the form of hydraulic structures such as piers and abutments in the waterway of a flowing river, the sudden surge in flow accelerates the erosive activities around these hydraulic structures. The most common type of scouring is local scour at bridge piers. According to Debnath and Chaudhuri (2010), the combined effect of bed shear, downward flow, increase in velocity, turbulence in flow, vortex shedding, and the formation of scour holes, which erode bridge foundations and cause bridge failures all over the world. **Fig. 1.2** illustrates the flow around a bridge pier. The removal rate of this river bed sediment during a flood is generally quick and aggressive (Deng and Cai 2010), which may lead to the bridge collapse, which may become more common due to climate change. Local scour at hydraulic structures gets affected by angle of attack, bed material size, characteristics of the pier or abutment, depth of flow, duration

of flow and flow intensity. Local scour occurs in both conditions, clear water as well as in live-bed.

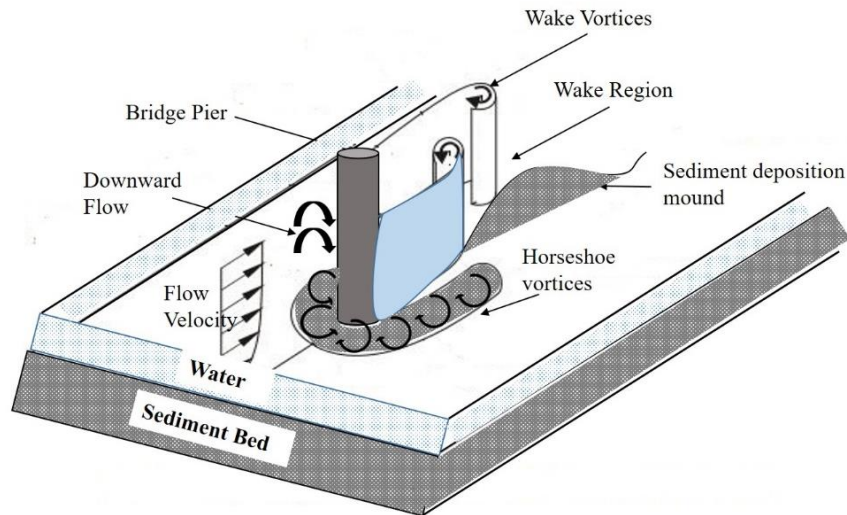


Fig. 1.2 Local scour around the circular pier

1.2.3 Bend scour

Bend scour arises at bends as a consequence of variable stream flow and the steepest region of the bend. Bend scour is related with the flow around the meander section of river bends. Bend scour is influenced by curvature of bend, sediment gradation and, bank erosion. In addition to bend scour, floating wooden material that diverts flow creates trouble for bridges situated at bends. Researchers have investigated sediment transport under steady and unsteady flow circumstances, the influence of sediment gradation, and flow rate and river characteristics at the bends during steady flow rates.

1.2.4 Confluence scour

It is explained as natural scour. When two or more rivers meet at one point or when the channels of a river/stream converge in a braided river stretch is termed as confluence scour. As confluence channels intersect the crossing of a bridge at some angle, along with the movement of sediment material, it evolves the scour holes around structures such as piers or abutments. Confluences enhance scour at bridge piers and abutments due to the higher transport rate of sediment material caused by flowing water just at the meeting point (Melville and Coleman 2000). Confluence scour is affected by the flow angle, channel size,

bed material characteristics, rate of flow of the confluence channels, and channel depth. The literature has just a few research on scour at bridges placed at confluences.

1.3 Local Scour around a group of piers

Numerous investigations on the scour around the bridge pier have been conducted during the previous half-century. Still, unfortunately, understanding the scour mechanism and scour flow field is a challenging problem for hydraulic researchers. Although the studies focused on the single pier can be categorized based on the (a) Scour mechanism and the flow-field around the single pier have been included in studies (Ahmed and Rajaratnam 1998; Dargahi 1989; Dey and Raikar 2007), (b) Temporal evolution of the maximum scour depth has been studied by Kothyari and Kumar (2012); Melville and Chiew (1999); Oliveto and Hager (2002) and (c) the influence of flow characteristics and sediment characteristics have been included in the (Ettema 1976, 1980; Klinga and Alipour 2015; Laursen and Toch 1956; Melville 1984; Melville and Coleman 2000; Shen et al. 1969; Sheppard et al. 2004). However, for geotechnical and economic reasons, bridge designs prefer pier groups or complex piers. This leads to problems if the results of single piers are directly applied to piers group or complex piers.

The current state of practice is to use a single pier equation either by multiplying a correction factor or by redefining an equivalent pier width. In order to provide more insight into the scouring process, a comprehensive understanding of the flow structure can help with scour depth prediction. Despite a huge number of analyses focused on single piers, only a limited number of studies have focused on a group of piers or complex piers. Few studies focused on the group of the pier are discussed here, such as Akilli et al. (2004); Ataie-Ashtiani and Aslani-Kordkandi (2012); Behzad and Abolfazl (2013); Das et al. (2015); Keshavarzi et al. (2018); Yang et al. (2018).

Akilli et al. (2004) used particle image velocimetry to investigate the flow characteristics around two and three circular cylinders positioned in side-by-side arrangement. Acoustic Doppler Velocimeter (ADV) flow patterns around two circular piers oriented in tandem and side by side had shown by (Ataie-Ashtiani and Aslani-Kordkandi 2012; Behzad and Abolfazl 2013). Das et al.(2015) has carried out an experimental study for investigated the horseshoe vortex flow pattern in an equilibrium

scour hole surrounded by two eccentric circular piers. (Beheshti and Ataie-Ashtiani 2016) studied the flow-field around complex pier that included a pier column, a pile cap, and a pile group. Ali Keshavarzi et al. (2017) utilized particle image velocity (PIV) to examine the flow structure around a single pier and two piers in tandem under flat-bed conditions. Yang et al. (2018) investigated the flow parameters surrounding a pile group in a scour hole at four distinct phases of the scouring process.

The literature has been extensively explored the phenomenon of scour around individual piers, yet there exists a noticeable gap in research that specifically investigates the scour patterns and characteristics arising when a group of piers are closely positioned. Understanding the intricate dynamics involved, such as how neighboring piers influence scour development, flow patterns, and sediment transport, holds paramount importance for the design of efficient and secure bridge or offshore structures. Particularly, when the spacing between piers is minimized, the resulting flow interference effects can give rise to intricate flow patterns and scour processes. Therefore, it becomes imperative to delve deeper into the impact of flow interference on local scour, as this knowledge is crucial for precise prediction of scour depths and the subsequent development of appropriate countermeasures. To this end, extensive research efforts are required to comprehensively understand how various pier configurations and spacing parameters influence flow interference effects and the consequential scour development.

Moreover, the accurate prediction of scour depths around a group of piers necessitates the establishment of reliable sediment transport and scour prediction models. Existing models primarily rely on data obtained from experiments conducted solely on individual piers, thereby potentially limiting their applicability to scenarios involving groups of piers. Consequently, there is a pressing need for further research to significantly enhance the accuracy and reliability of sediment transport models when applied to the intricate arrangements inherent in complex pier groupings. Addressing this research gap will pave the way for more robust and effective design methodologies, ensuring the safety and longevity of structures exposed to scour hazards. By undertaking comprehensive studies that specifically focus on scour phenomena around groups of piers and by improving the reliability of sediment transport models, we can advance our understanding of these complex processes. This will enable engineers and researchers to develop innovative and

efficient strategies to mitigate scour and enhance the resilience of bridge and offshore structures in the face of challenging hydraulic conditions.

1.4 Objectives

The primary objective of this study is to conduct an experimental investigation of three-dimensional flow structure and scour around a group of piers. It is proposed that the effects of pier spacing on flow structure and local scour near bridge piers be thoroughly investigated. The following concrete objectives are offered:

1. To deeply understand the flow-structure and scour mechanism around single bridge pier.
2. To analyze the effect of the group of pier and pier spacing on the local scour around the bridge piers.
3. To identify the key parameters influencing the local scour around the bridge pier by accessing and analyzing the traditional equations for the prediction of local scour.
4. To simulate the local scour around the piers by applying computational modelling.

1.5 Scope and Limitation

The most generally used approach for obtaining reliable and precise results is experimental investigation owing to the complicated nature of flow field around bridge piers and multiple limitations on various parameters influencing the scour depth. As result, the present research work involves conducting an experimental investigation. However, there are certain limitations:

- The present research work has been conducted for the uniform circular piers of diameter 50 mm and uniformly graded sediment material has been used to carry out the experimentation.
- The maximum number of three round cylindrical columns for bridge piers were used during the entire proposed study.
- The pier spacing for the various pier arrangements has been considered in the range of 1D-5D only.

- All the experiments have been conducted under steady flow condition.

1.6 Arrangement of Thesis

This thesis is divided into five chapters. Each chapter is summarized below:

Chapter I provides a general overview on bridge scour and the related challenges. Additionally, this chapter also provides a brief introduction to the scour phenomenon and types of scour around the bridge pier, objectives of the study, along with scope and limitation.

Chapter II presents a review of relevant literature dealing with the evaluation and estimation of the scour around bridge piers and identifying the research gaps that has to be addressed for the objectives of this study. In addition, a discussion of the flow regime near bridge piers, temporal evolution of scour depth, and approaches for predicting scour depth are also included in this chapter.

Chapter III presents details of the methodology used to conduct the experimentation and thorough overview of the experimental facilities and equipment.

Chapter IV presents the results of experimental tests for scour depth around bridge piers. The experimental results of the single pier, two piers, and three pier are compared in order to determine the influence of pier spacing between the piers on scour depth.

Chapter V contains the summary and conclusions of the thesis. The recommendations for further work are also included.

- A list of publications published during the present study is included at the end of the thesis.
- References and Appendices.

CHAPTER 2

LITERATURE REVIEW

2.1 Introduction

Local scour was caused by the presence of three-dimensional flow distribution force and an unstable flow field on the river bed. Local scour can be induced by either natural events (heavy rain, floods) or by artificial constructions (buildings built in the riverbed). The characteristics of the flow, fluid, pier, and bed material all have an influence on the scouring process. Additionally scouring is a time-dependent process. Numerous investigations in the domain of scour around have been done in recent decades. Using the most relevant and significant information, this chapter highlights the various features of scour processes at the group of bridge piers.

2.2 Local scour around single pier

As bridge scour is the most common cause of the catastrophic bridge failures across the world, so it has been investigated in the past by number of researchers (Breusers et al. 1977; Dey et al. 1995; Muzzammil and Gangadhariah 2010; Okhravi et al. 2022; Pandey et al. 2020a). According to these researchers the process of local scour is majorly dependent on the hydraulic characteristics, sediment characteristics and duration of flow. Hydraulic characteristics have been studied in detail by researchers (Chabert and Engeldinger 1956; Dey and Raikar 2007; Ettema 1980; Guan et al. 2019; Majedi-Asl et al. 2021; Muzzammil and Gangadhariah 2010; Yanmaz and Altinbilek 1991) and sediment characteristics have been highlighted by (Aguirre-Pe et al. 2003; Cheng et al. 2020a; Debnath and Chaudhuri 2010; Lauth and Papanicolaou 2008; Umeda et al. 2010). Temporal evolution around the hydraulic structures has been carried out by (Kothyari et al. 1992a; Melville and Chiew 1999; Oliveto and Hager 2002; Yang et al. 2020; Yanmaz and Kose 2007). Kothyari et al., (1992b) conducted a study for the temporal evolution around the circular pier for the uniform sediment, in his research the duration of experimental run has been kept for 800 minutes. (Melville and Chiew 1999) conducted an experimental study for the circular bridge pier and proposed a formulation for computing equilibrium time t_e . (Oliveto and

Hager 2002) performed experimental study by incorporating six sediments (3-uniform and 3-non uniform graded) and purposed an equation for temporal scour depth. Whereas, (Yang et al. 2020) studied the temporal scour depth effect for the complex pier. However, (Yanmaz and Kose 2007) conducted a time-dependent scour depth study for the bridge abutments. When considering temporal effects, poor correlation among scour depths is occasionally reported in the field and in the experiment.

The majority of the research has been done through experimental work with various techniques, including ADV (Acoustic Doppler Velocimetry), ADVP (Acoustic Doppler Velocity Profilers), and PIV (Particle Image Velocimetry) in plane bed and scoured beds under the live bed condition and clear-water bed condition. The flow field and its structural interaction have also been shown using numerical techniques like LES (Large-Eddy Simulation), RANS (Reynolds-Averaged Navier-Stokes), DES (Detached-Eddy Simulation), and RANS-LES-hybrid.

Scour around the circular pier has been thoroughly studied and characterized. Some of the many outstanding insights to this literature include (Laursen and Toch, 1956; Shen et al., 1969; Melville and Sutherland, 1988; Melville and Coleman, 2000; Oliveto and Hager 2002; Mia and Nago, 2003; Sheppard et al., 2004; Kothyari et al., 2007). Flow structure encircling non-circular piers has not been thoroughly investigated in recent years (Diab et al. 2009; Raikar and Dey 2008). They both performed experiments using square piers to identify how the turbulent horseshoe vortex flow developed at various stages of the scour process till achievement of equilibrium scour depth. An ADV was used to take the flow measurements. They examined the Reynolds stresses, turbulence intensities, and horseshoe vortex size at various azimuthal planes. Furthermore, Chang et al. (2010) revealed that these vortices are the primary characteristics of the flow field and turbulence structure around rectangular pier for small angle of attack.

Chabert and Engeldinger (1956) conducted the first and most thorough experimental investigation on bridge pier scour. Different sediment sizes, pier shapes, and protection systems had all the objective of experimental investigation. In total over Three-hundred experiments had been conducted for the duration lasting from a few hours to days.

The regime change from clear water to level bed caused the most scouring. No general scour relationship was proposed despite the enormous data set. So yet, there has not been a systematic and logical analysis of these results.

In the live-bed regime, the local scour depth and mean approach flow velocity relationship has been formulated by Melville (1984). Cylindrical piers had been used in experimental studies where the pier size, mean particle size of sediment, and average rate of flow had systematically changed. The results of the present study fall within the fine or intermediate zones, where the scour depth is roughly independent of D/d_{50} to achieve these results uniform sediments had utilized, to ensure that the impacts of sediment non-uniformity are not included. The results of the study concludes that, the ratios between the maximum scour depth and pier diameter can reach 2.4 to 2.5. As a result, it poses a serious risk to the stability of bridge structural and load-bearing capacity.

In addition to the experimental study, few numerical studies have also been reported in the literature, for analyzing the flow-field and scour evolution (Alborzi and Osouli 2017; Alemi and Maia 2018; Behzad and Abolfazl 2013; Chang and Constantinescu 2015; Ettema et al. 2006; Huang et al. 2009; Roulund et al. 2002, 2005; Török et al. 2017; Zaid et al. 2019). (Alborzi and Osouli 2017) utilized ANSYS fluent, Eulerian multiphase model to simulate the soil-water interaction, and results of the numerical simulation has been compared with the regression based equations. Alemi and Maia (2018) simulated the pier scour around the single pier and complex pier with the FLOW-3D software, and results are validated with the already published results. Behzad and Abolfazl (2013) in his study, conducted numerical and experimental investigation of the flow pattern around a tandem arrangement of two piers in a moderately rough flat bed. Huang et al. (2009), conducted computational simulations using a 3D-CFD model to examine scale effects on turbulent flow and sediment scour. Although, CFD has been found useful for understanding the complex pier flow-field structure (Chang and Constantinescu 2015; Ettema et al. 2006; Kirkil et al. 2008, 2009), CFD also holds patent promise for substantial use in design estimation of scour depth. However, despite some recent success for simple geometry piers, CFD has ability to simulate erosion and scour at a pier is limited, thus hampering its present practicality for scour-depth estimation Roulund et al. (2002, 2005). A compiled review

study has been reported by Ettema et al. (2017), includes the work carried out in the last 60 years and in light of the ongoing need to further resolve the problem of pier scour. According to the findings of the review study, the characteristics of pier flow-fields demand additional examination in order to benefit design estimate of scour depth the necessity for improved design estimation of scour depth drives scour research. This assessment also shows that much of the effort toward understanding scour evolution is done a long time ago and requires more examination. In order to fulfill these research gaps and by considering the paucity of data the present study has been planned and conducted. The principal aim of the present analysis is to provide the most recent laboratory data in order to analyze the impact of flow duration on the evolution of scour holes and to analyze the flow field.

2.3 Local scour around two piers

Numerous investigations have been performed to determine the factors influencing scour around bridge piers to better understand the complicated behaviour of scour by (Breusers et al., 1977; Devi and Kumar, 2022a; Dey and Raikar, 2007; Hong et al., 2018; Jain et al., 2021; Lança et al., 2013; Melville and Raudkivi, 1977; Muzzammil and Gangadhariah, 2010; Pandey et al., 2020a; Pu et al., 2021; Tipireddy et al., 2019; Vijayasree and Eldho, 2021). According to these investigations, scouring around bridge piers is among the most significant aspects of the failure of river bridges. Most of these investigations are centered on single pier scour. Although, in practice, new bridges spans are usually broad, and two or more circular piers are required to support the structure, positioned in the flow direction. Many new bridges have been built beside older bridges in recent years as the automobile population has increased. Such an example is in Kolkata, West Bengal, India, at which a new bridge, Nivedita Bridge, has successfully opened directly downstream of an existing bridge, Vivekananda Bridge. If two bridges are situated near to one other, the piers of one must have an impact on the piers of the other as shown in Error! Reference source not found..

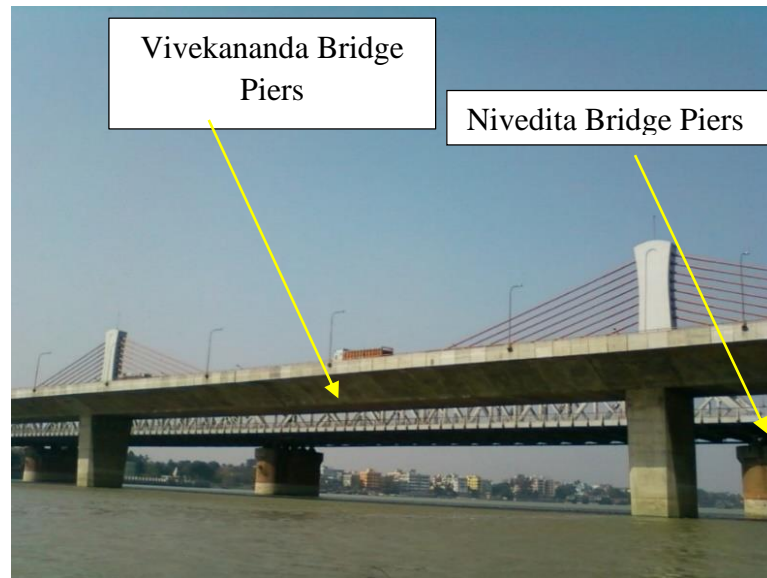


Fig. 2.1 Two piers in tandem arrangement on the Vivekananda Bridge and Nivedita Bridge

As a consequence of rapid economic development in developing countries, the number of bridges constructed has been increased. A complete understanding of the scour around pier groups is highly needed. Some of the studies based on two piers in the tandem arrangement has been conducted experimentally in order to highlight few important factors for the design consideration of the bridge pier, pier spacing, mutual interference, size of the bridge pier, bridge pier shape and countermeasures such as (Amini et al., 2014, 2011; Beg and Beg, 2015; Behzad and Abolfazl, 2013; Behzad and Beheshti, 2006; Elliott and Baker, 1985; Garg et al., 2021; Hosseini and Amini, 2015; Keshavarzi et al., 2018; Memar et al., 2020). Amini et al. (2012) experimentally studied the scour depth under clear water conditions and concluded the dependency of scour on the diameter of piles, spacing between piles, and the ratio of an immersion. They also developed a technique for predicting scour depth for a wide range of an immersed and unimmersed group of piers. The influence of the approaching flow characteristics (depth of flow and velocity of flow) and sediment characteristics (density of particle, size of sediment particles, and gradation effect) is subjected to the variation in local scour depth.

An increase in non-uniformity of sediment leads the creation of an armored layer at the foot of the scour hole, lowering the scour depth in clear-water scour. The decrease is clearly

linked to the gradation factor or geometrical standard deviation, σ_g , which is defined as $\sqrt{\frac{d_{84}}{d_{16}}}$, where d_{84} and d_{16} signify the grain size at the eighty-fourth and sixteenth percentiles, respectively (Cheng et al. 2020b). The influence of densimetric Froude number on maximum scour depth and scour deposit has not been explored directly by researchers. It ought to be highlighted that the design equation does not contain characterization of the densimetric Froude number. Additionally, the maximum scour depth also depends on geometric characteristics (pier diameter of piers, spacing between piers, and width of piers) (Zhou et al. 2020). However, until now, researchers have been incapable of finding out the behaviour of the pier, the influence of the pier spacing, influence of densimetric Froude number and temporal scour depth. **Table 2.1** lists previously conducted research work for the two piers, along with their finding and founding.

Table 2.1 Research work available in the literature for scour around two bridge piers

Pier Models	Reference	Investigation	Finding	Founding		
				Y_t	F_d	P_s
One	(Cheng et al. 2020b)	Assessing the sediment gradation effects under clear water for bridge pier scour	An increase in the grading of sediment particles results in reducing the scour depth.	-	C	-
Two	(Wang et al. 2016a)	Time development and flow variation of the scouring depth	Scour Zone of the rear pier was divided into four new categories.	C	-	-
Two	(Keshavarzi et al. 2018)	The significance of pier spacing over scour depth was investigated experimentally.	The findings indicate maximum scour depth at the front pier at spacing = 2.5 D.	C	-	C
Two	(Behzad and Abolfazl 2013)	This Experimental study compares flow patterns on a rough surface for a single pier and two piers.	The findings show that a rear pier significantly affects the flow pattern, especially in the vicinity zone.	-	-	C
Two	(Das et al. 2015)	The study experimentally investigates the scour development and the influence of pier shape and	The greater scour hole was generated when circular piers are replaced with the equilateral triangular and	-	-	C

		mutual interference on the scour.	square pier of the same dimensional width under same flow conditions.			
Two and Three	(Khaple et al. 2017)	An experimental study, to evaluate the pier for, two piers positioned in tandem and side by side, and three piers positioned in staggered arrangements.	Findings of the study, represents the influence of pier spacing on different arrangements.	C	-	C
Two	(Garg et al. 2021)	Experimental investigation of the influence of collar plate on the individual bridge pier and combined collar plate for two piers.	The results of the study, concludes that the collar plate of diameter 2.5 D for single pier and two piers, reduces the scour depth completely.	-	-	C
Two	(Memar et al. 2020)	The objective of the experimental study was to evaluate the, the influence of the size and positioning of circular collars over the pier, on scour for two piers in tandem position.	The study concludes that, the location of the collar plate on the bed surface results in maximum scour reduction.	C	-	-
Two	(Beg and Beg 2015)	The study investigates factors affecting the scour depth under clear water scour conditions. Including mutual interference between two bridge piers of unequal sizes and pier spacing,	The results conclude that, maximum scour was observed at 66 mm upstream of the front pier and minimum at 33 mm rear piers.	-	-	C
Present Study				C	C	C

Where Y_t is temporal scour depth; F_d is the densimetric Froude number and P_s is the pier spacing factor. *C conducted

Latest and significant studies of local scour has been included in Bordbar et al. (2021); Jain et al. (2021); Khan et al. (2017); Nagel et al. (2020); Pandey et al. (2020a); Qi et al. (2019) and Malik et al. (2021). Furthermore, several investigations on a set of piers are also conducted by researchers, such as the work of (Sumner et al. 1999) used flow visualization, particle image velocimetry (PIV) and hot-film anemometry to explore the flow field for two and three circular cylinders positioned side-by-side, with the pier spacing pitch ratio expanding. Their observations reinforce the concept that the arrangement of circular cylinders needs Reynolds number independence. Similarly, the work of (Akilli et al. 2004) utilised the particle image velocimetry (PIV) approach to analyses flow around two and three side-by-side cylindrical piers, and findings indicate that in the case of side-by-side bridge piers, the flow structure behind the cylinders is asymmetrical and that in the case of three cylinders both an asymmetrical and a symmetrical flow was observed. In addition, authors (Ataie-Ashtiani and Aslani-Kordkandi 2012) conducted an experimental study to analyse the flow characteristics of two piers placed in a side-by-side configuration and validated the results with the numerical simulations. It is concluded that the impacts of these flow vortices between the piers should be incorporated into the semi-empirical equations for a better estimation of the scour depth for side-by-side piers arrangement. All of the above-mentioned literature studies are focused on the flow field around the two and three piers. Despite extensive laboratory studies, the regression-based equations have involved tedious calculations and have not provided promising predictions (Gaudio et al. 2013).

The angle of attack is the angle between the flow direction and the principal axis of the pier alignment. Angle of attack is an essential feature that must be considered during the experimental investigations. Two angles of attack have been used in this section. As per the (Breusers and Raudkivi 1991) the scour depth is a function of projected width of the pier (width of the pier in the normal direction of flow). As the angle of attack is increased, projected width of the pier is also increased and hence the scour depth is increased (Melville and Coleman 2000). Practically, angle of attack in the river section may be significantly changed due to the flooding and meandering of river. Firstly, (Laursen and Toch 1956) investigated the influence of the shape of pier and angle of attack and proposed a coefficient for angle of attack. The results of the study concludes that, the length of the

round nosed pier has no influence on scour depth at zero degree angle of attack. (Chabert and Engeldinger 1956) also investigated the influence of the angle of attack on the scour depth by utilizing various pier shapes and provided the values of the coefficient of angle of attack for the rectangular pier with round nose for various hydraulic conditions. (Hannah 1978) investigated the scour phenomenon around the single and group of piers for the tandem and side-by-side positioning by varying pier spacing and angle of attack. And concluded that the equilibrium scour depth has been attained first by the front pier and then by the rear pier. Author also proposed an adjustment factor for estimating the equilibrium scour depth. (Nazariha 1996) studied the local scour around the single and two piers for two hours of experimental duration. The effect of angle of attack and pier spacing has been studied for the two piers. The result of the study concludes that, for small pier spacing larger the angle of attack, greater will be the equivalent diameter of the pier and, consequently, larger will be the scour depth. In case of two piers, zero angle of attack has also been studied by (Nazariha 1996), and it has been concluded that the for small pier spacing ratio $L/D = 1$, the piers behaves as single pier scour. For the spacing range of $1 < L/D \leq 4$ increase in scour depth has been reported and for spacing $4 < L/D \leq 5$ and reached upto the value of single pier scour. Furthermore, for $L/D > 5$ separate two scour holes has been formed around two piers.

Research on scour around bridge piers is crucial as it allows us to expand our knowledge of scour processes, accurately assess scour vulnerability, validate design guidelines, devise effective mitigation measures, bolster bridge resilience and safety, address climate change impacts, and foster knowledge sharing. Through dedicated research, we can enhance the overall design, construction, and maintenance practices of bridges, ensuring their long-term performance and the safety of the public. Consequently, the present study incorporates the investigation of various pier arrangements, including tandem, side-by-side, and angled piers, within its objectives.

2.4 Local scour around three piers

Plethora literature is available on bridge scour subject, but only a handful literature is available for the group of bridge piers. Bridge structure consists of multiple piers are structurally more economical and geotechnically more viable than the single pier design,

due to this reason the designing of the multiple piers becomes more popular in recent years (Behzad and Beheshti 2006; Melville and Coleman 2000; Parola et al. 1997). The Pima County department of transportation has corroborated the successive functioning of the bridge structure laid on the group of piers (three piers in tandem arrangements). And proposed the utilization of the two and three piers in tandem arrangement for new bridge structure (Zhou et al. 2020). Despite this progression, research on group of piers is inadequate, with only a few studies available for a group of piers (Jones and Sheppard 2004; Khassaf and Shakir 2013; Wang et al. 2017; Zhou et al. 2020b). However, popularly used engineering manuals, HEC-18, offer almost no guidelines on predicting scour depth around a group of piers. Concurrent turbulence structures surrounding the piers change as scour progresses, as do the scour mechanisms (Amini and Mohammad 2017; Ataie-Ashtiani et al. 2010; Behzad and Beheshti 2006). Jiao and Wu (2018) states that, the Concurrent turbulence structures, such as the horseshoe and wake vortices that form around group of piers in tandem or staggered configuration, generate drag and lift forces on the sediment material on the bottom of the bed and inducing local scour.

Some research work has been conducted in the past for group of piers are (Akilli et al. 2004; Amini Baghbadorani et al. 2018; Ataie-Ashtiani and Aslani-Kordkandi 2012; Coleman 2005; Muzzammil et al. 2015; Muzzammil and Gangadhariah 2010; Sumner et al. 1999). In addition to the above, Heidarpour et al. (2010) examine the spacing impact and countermeasures on scour depth around group of piers, and concluded that as the distance between the piers expands, the region between the piers without protection is washed away and resulting into the formation of deeper scour holes at the upstream side of the piers. The study conducted by authors (Behzad and Beheshti 2006), concludes that, the interference between the piers relies on the angle of attack, the geometry of the pier model, and spacing of piers.

Bridge pier scour prediction has been focused on a single pier of varying sizes, geometries, and angle of attack of flow. Regardless of pier separation or angle of attack, widely used manuals still propose adopting single-pier scour equations with an equivalent diameter for multiple piers. (Cheng et al. 2018; Kim et al. 2017; Wang et al. 2017b) has proposed using a single-pier scour equation with variable empirically corrected coefficients to predict the

scour depth around the group of piers. Although many studies have been completed to assess the depth of scour at single piers, much less effort has been done to investigate scour at the pile groups (Amini et al. 2012; Coleman 2005; Richardson and Davis 2001). On the other hand, only a few studies are available in the literature that provides regression-based equations for the group of piers (Amini Baghbadorani et al. 2018; Coleman et al. 2005; Gaudio et al. 2013). (Coleman et al. 2005) proposed a new equation to evaluate local scour depth at a complex pier, which is named as Melville and Coleman equation. HEC-18 and Florida Department of Transportation (FDOT) equations are reviewed in Amini Baghbadorani et al. (2018), and a new equation for the protective benefit of pile cap frontal extension has been suggested.

In addition, several studies for flow-field analysis around the pier group are also carried out, such as Sumner et al. (1999) studied flow mechanism around two and three circular piers placed in side-by-side positioning by utilized flow-visualization, hot-film anemometry, and particle image velocimetry (PIV). Similarly, Akilli et al. (2004) also studied flow mechanism around two and three side-by-side circular piers by utilizing PIV approach. The results show that the flow-field in the rear of the pier is asymmetrical for two and symmetrical and asymmetrical for three piers. Furthermore, Ataie-Ashtiani and Aslani-Kordkandi (2012) carried a numerical simulation with two piers positioned side by side. Results suggested that, the effect of flow vortices between both the piers must be considered into semi-empirical equations to even more accurate estimation of scour depth. Ataie-Ashtiani et al. (2010) carried over 70 experimental runs by using complex piers of varying geometrical characteristics and concluded that both the Coleman (2005) and HEC-18 (Arneson et al. 2012) approaches underestimated the scour depth.

Furthermore, few studies have been carried out for the three piers in the staggered arrangements such as Das et al. (2014); Jaman et al. (2017); Malik and Setia (2020a); Pasupuleti et al. (2022). (Das et al. 2014) conducted an experimental study for the group of piers under clear water condition for the increasing Froude number and spacing between the piers. Two piers in the tandem and eccentric arrangement, and three piers in the staggered arrangement have been utilized. The observations made from the two piers arrangement states that scour depth increases for the closely placed piers, and for three

piers scour volume is larger in case of 3D than 2D pier spacing. Jaman et al. (2017) carried out an experimental study for analyzing the flow-field, flow characteristics, and formation of scour hole around three piers aligned in tandem and staggered arrangement. The result of the study concludes that the three pier interference plays a key role in the evolution of the greater scour hole. Malik and Setia (2020a) investigated the mutual interference of the piers for the three piers in staggered arrangement. Experimental results observed have been compared with the results of the regression based model. The results of the study states that for the pier spacing more than 5D, the vortex shedding effect is almost negligible. Pasupuleti et al. (2022) carried out an experimental study for investigating the flow-field for the tandem and staggered arrangement. For the three pier staggered arrangement, bi-vortex has been observed in the opposite direction in the space between the piers. As the literature available on this topic is very limited, hence, this section of the dissertation has been planned for three piers in the staggered arrangement to evaluate the influence of the pier spacing and rate of flow on the scour depth.

Rising urbanization and the growing volume of traffic necessitate the construction of new bridges alongside existing ones, leading to pier interference issues. Additionally, using a group of piers is often preferred for economic and safe bridge design. However, designing bridge piers that are both safe and cost-effective requires accurate forecasting of the scour depth around them, taking into account the interference of upstream piers on the scour at downstream piers. Moreover, when concurrent bridges, such as a railway and a road bridge, or a newly-built bridge alongside an existing one, are present, the presence of an upstream pier can significantly influence the scour at the downstream piers. This creates a unique environment where the complex interaction between the flow of water and the piers can result in scour patterns that differ from those observed around isolated piers.

Therefore, the problem of local scour around a group of piers is multifaceted and requires a thorough understanding of the hydraulic processes involved, the influence of upstream piers on downstream scour, and the specific characteristics of concurrent or adjacent bridges. Addressing this problem is crucial for ensuring the safe and cost-effective design, construction, and maintenance of bridges in such complex scenarios. Though this issue has been given attention in the present study.

2.5 Problem statement

In the present study, the issue of local scour around a group of piers has received significant attention. The researchers recognized the growing need for constructing new bridges alongside existing ones due to urbanization and increased traffic volume. They also acknowledged the preference for using a group of piers to achieve economical and safe bridge designs. However, they identified that designing piers in such scenarios requires a thorough understanding of the scour depth forecast, taking into account the interference of upstream piers on the downstream pier scour. To address this issue, a comprehensive investigation has been conducted for the scour phenomena around a group of piers. We focused on accurately predicting the scour depth and patterns to ensure safe and cost-effective bridge design. Special attention has been given to understanding the hydraulic interactions between the flow of water and the piers, considering the presence of upstream piers and their influence on scour at the downstream piers.

To achieve the objectives of the present study, we have employed a combination of approaches, including laboratory experiments, numerical modeling technique and advanced computational technique. As laboratory experiments replicated the hydraulic conditions and bridge configurations to study scour phenomena in a controlled environment. Additionally, numerical models were developed and validated to simulate and predict scour depths accurately, considering the interference of upstream piers. The findings and insights contributes to an improved understanding of local scour phenomena and offered valuable recommendations for potential risks associated with scour around group piers. By addressing this issue in the present study, the researchers made a significant contribution to the field of bridge engineering.

2.6 Mechanism of local scour

The vortex system that characterizes the flow-field encircling the bridge pier includes horseshoe vortex, bow vortex, and wake vortex. Horseshoe vortex are generated around the toe of the pier, whereas bow wave are originated on the top surface of the flowing water. Horseshoe vortices are found on the upstream of the pier, and a wake vortex are found just behind the bridge pier and they grows up to the depth of flow as shown in **Fig.**

2.2, these characteristics include an extremely complicated flow structure. The flow field is identified as turbulent structure with a wide variety of sizes, as well as a prominent down-flow near the pier edge (Kirkil et al. 2009). Melville (1975) noted that the prime source of the scour is the vortex formation (horseshoe and wake vortices) generated around the bridge pier. The horseshoe vortex raises velocities closer to the bed, thereby increasing the potential of sediment transport. Due to this complex vortex structures, understanding and prediction of scour depth become a challenging task.

To reliable prediction of scour depth understanding the flow-field around the bridge piers is very essential. Many investigators, such as Ahmed and Rajaratnam (1998); Baker (1979); Chiew (1984); Ettema (1980); Gazi and Afzal (2020); Kumar and Kothiyari (2012); Melville (1975); Melville and Coleman (2000); Melville and Raudkivi (1977); Meneghini et al. (2001); Muzzammil and Gangadhariah (2010); Qadar (1981); Richardson and Panchang (1998); Salim and Jones (1996); Sheppard et al. (2004); Yang et al. (2010) have conducted research on flow structures around bridge piers.

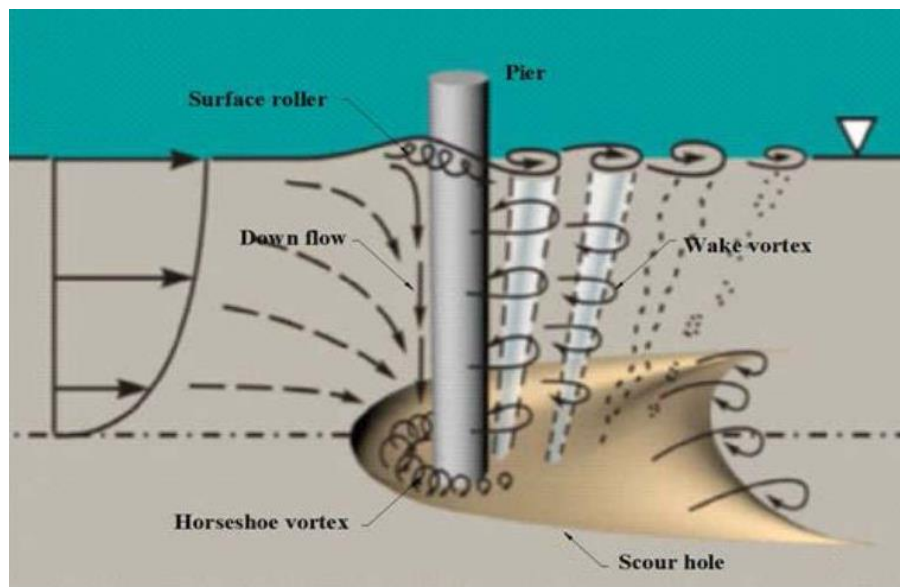


Fig. 2.2 Flow-field around isolated bridge pier with primary vortices adapted from (Ettema et al. 2011)

To reliable prediction of scour depth understanding the flow-field around the bridge piers is very essential. Many investigators, such as Ahmed and Rajaratnam (1998); Baker (1979); Chiew (1984); Ettema (1980); Gazi and Afzal (2020); Kumar and Kothiyari (2012); Melville (1975); Melville and Coleman (2000); Melville and Raudkivi (1977); Meneghini et al. (2001); Muzzammil and Gangadhariah (2010); Qadar (1981); Richardson and Panchang (1998); Salim and Jones (1996); Sheppard et al. (2004); Yang et al. (2010) have conducted research on flow structures around bridge piers.

According to the findings of the aforementioned investigations, the primary processes that generates the local scour at cylindrical piers are as follows:

1. The flow velocity on the upstream of the pier drops to zero (stagnation point). At this point the water surface level increases and generates a wave on the form of surface roller commonly known as bow wave. Stagnation pressure present on the upstream of the pier results in lowering of the down-flow. The resultant down-flow functions as a vertical jet, which erode the sediment on the front side of the pier and creates a scour hole and weakening the already developed scour hole slope.
2. As the process of scour continues the down-flow keeps rolling and its interaction with the flow results into the generation of the complex vortex is known as horseshoe vortex. At the upstream face of the pier flow gets separated by the horseshoe vortex. These vortices erodes and transports the sediment particles to the rear side of the pier from the scour hole. The scour depth and horseshoe vortex are linearly related to each other, as the strength of horseshoe vortex increases the scour depth also increases. These vortices are a part of turbulence system, along with down-flow waves and flow acceleration around the pier (Zhao and Huhe 2006).
3. Wake vortices are formed on the rear side of the pier. As the flow approaches the sides of the pier, flow gets separated and approaches the downstream side of pier, and generates Wake vortex. These vortices also erode and transport sediment from the bed to the downstream of the flow.

The scour depth is influenced by a numerous parameters, including flow characteristics, sediment characteristics, and bridge pier characteristics. As per Sheppard et al. (2004), the

mechanism of scour is also affected by D/d_{50} ratio. The existence of hydraulic structure in the direction of flow causes this phenomenon, which forms a pressure gradient field. The force exerted by the pressure gradient on the sediment material of the bed, is greater than the intensity of the drag force originated from the flowing water over the sediment particles. As the value of D/d_{50} grew, the pressure force induced by this pressure gradient reduced. Three types of pier flow fields based on pier width (D) and flow depth (h) proposed by Ettema et al. (2011) are :

1. Narrow piers (h/D more than 1.4)
2. Transitional piers (h/D range 0.2-1.4)
3. Wide piers (h/D more than 0.2)

Furthermore, Muzzammil and Gangadhariah (2010) conducted an experimental investigation around the circular pier under clear water condition for assessing the phenomenon of scour evolution and horseshoe vortex. In order to provide more accuracy for vortex mechanism Mudflow visualization technique was developed. The vortex characteristics had measured for three bed conditions: rigid flat, solidified, and mobile. Additionally, extensive characterization of horseshoe vortex has also been carried out for vortex dimension, tangential velocity, and strength for all three flow conditions. Results for rigid bed demonstrates that the size of primary horseshoe vortex is around 20 % of D , whereas the tangential velocity of vortex is 50 % of V ($10^4 \leq Re_D \leq 1.4 \times 10^5$). As it evolves, the horseshoe vortex entirely sinks into scour hole, and the size of the vortex increases linearly with scour depth.

As per Ettema et al. (2011), the flow field around the narrow pier includes; flow vortices (down-flow, horseshoe, and wake), flow convergence and divergence, sediment transportation, flow turbulence and dissipation of flow. Similarly, same flow field occurred for the transition pier. Consequently, the down-flow begins to alter as the flow depth decreases or size of the pier increases. In case of broad pier, flowing water curves and flows on the sides of the pier surface before converging the flow around the pier. The weak down-flow waves resulting in less scour on the upstream side of the pier. The presence of broad

pier the obstruction in the flow is increased, hence the horizontal distribution of the flow gets affected for the large channel span before the pier positioning.

Das et al. (2015) describes the influence of mutual interference between piers with varied longitudinal separation on local scour at the equilibrium stage for the two circular, square, and triangular-shaped piers. The extent of total scour depth for triangle pier was found to be less than that of a circular or square pier, and scour depth at the rear pier increases with three times eccentricity and longitudinal spacing.

2.7 Variables affecting the local scour

In this section various parameters influencing the scour depth are discussed: such as (1) flow shallowness; (2) effect of sediment coarseness; (3) effect of sediment non-uniformity; (4) effect of pier alignment; (5) effect of pier shape; (6) effect of flow intensity; (7) effect of viscosity.

In order to study the influence of the factors affecting the scour depth around the bridge piers many studies have been carried out in the past few decades, these are Ettema (1980); Ettema et al. (2011); Laursen and Toch (1956); Melville and Coleman (2000); Melville and Sutherland (1988); Raudkivi and Ettema (1983); Yanmaz and Altinbilek (1991). Most of these studies have aimed to describe the influences of different parameters on the scour around bridge piers. Despite this, there are significant gaps in our general comprehension of the scour process and scour depth estimation. This is owing to the challenges in performing experimental work on the large sized pier models or a lack of accurate field data for validation of the experimental results. Melville and Coleman (2000) presented detailed studies that explained the mechanisms influencing scour at bridge piers. They utilised laboratory data to examine the impact of various factors.

2.7.1 Flow shallowness

The “flow shallowness effect” is the ratio of the approaching flow depth (h) to the diameter of the pier (D) which is achieved at the equilibrium scour depth. Raudkivi (2020), states that the influence of the flow shallowness effect becomes negligible on the scour depth, if the scour depth is greater than $3D$. He also stated that, if there is a decrease in the scour

depth than the intensity of the surface rollers (due to bow waves) formed will also be reduced. As a result, no specific relationship between approaching flow depth and scour depth has been established. Flow shallowness effect has been classified in three different categories for pier classes in term of D/h ratio as shown in **Table 2.2** proposed by Melville and Coleman (2000). These are:

- a) Narrow Pier (Deep Flow) – in this case when depth of the flow comparatively greater than pier width, for this case the scour depth is independent of depth of flow and is in linear relationship with the pier width.
- b) Intermediate Pier (Intermediate Flow) – in this case when the depth of the flow and width of the pier are intermediate the scour depth is dependent on both the depth of flow and the width of pier.
- c) Wide Pier (Shallow Flow) – in this case when the depth of the flow is comparatively very less than the width of the pier the scour depth is in linear relationship with the flow depth and is independent of width of the pier.

Table 2.2 Scour classification on the basis of pier size and flow depth proposed by Melville and Coleman (2000)

Category	D/h	Dependency of scour depth
Narrow Pier (Deep Flow)	Less than 0.7	Linear – width of pier Independent – flow depth
Intermediate Pier (Intermediate Flow)	0.7-5	$Y_s \propto (Dh)^{1/2}$
Wide Pier (Shallow Flow)	Greater than 5	Independent – width of pier Linear – flow depth

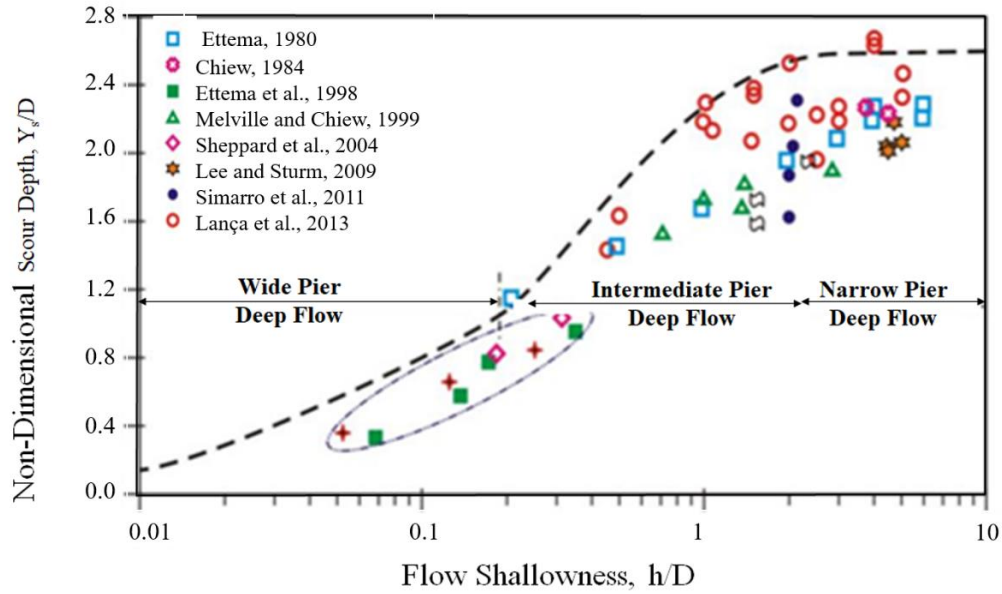


Fig. 2.3 Flow Shallowness (h/D) effect on the Non-Dimensional Scour depth Y_s/D adapted from Moreno (2016)

The literature data from Chiew (1984); Ettema (1980); Ettema et al. (1998); Lança et al. (2013); Lee and Sturm (2009); Melville and Chiew (1999); Sheppard et al. (2004); Simarro et al. (2011) has been utilized for these three classifications. These data sets are plotted in **Fig. 2.3**, Non-dimensional scour depth Y_s/D (y-axis) and h/D (x-axis) for the cylindrical piers. The range of the various parameters to minimize the effect of the other parameters for these data sets are such as $D/d_{50} = (30-100)$, $d_{50} \geq 0.6 \text{ mm}$, $\sigma_g \leq 1.5$, and $U/U_c = (0.8-1)$. **Fig. 2.3** shows the classification of the wide pier, intermediate pier and narrow pier clearly with the solid line from left to right of the.

2.7.2 Effect of Sediment Coarseness, D/d_{50}

The “effect of sediment coarseness” is the effect of relative sediment size (D/d_{50}) on the equilibrium scour depth. As per the research results of the Melville and Coleman (2000); Melville and Sutherland (1988); Raudkivi and Ettema (1983), the effect of D/d_{50} in case of narrow pier on scour depth will be negligible if its value is greater than 100. However, if the $D/d_{50} \leq 50$, than the effect of relative sediment size will be considered. The relationship of scour depth and the sediment coarseness is well depicted in the **Fig. 2.4**. Additionally, Lança et al. (2011, 2013); Lee and Sturm (2009); Sheppard et al. (2004, 2014); Sheppard

and Renna (2010), shown that the D/d_{50} has a significant influence on the scour depth. These studies shows that non dimensional scour depth (Y_s/D) increases with the increase in the relative sediment size D/d_{50} . Furthermore, Ettema et al. (2011) from his study concludes that, the scour depth will be affected by the relative sediment size only if the sediment size is either relatively large or small, and if the sediments used are uniformly graded than this effect is negligible. When the $D/d_{50} < 8$, in this case the scour will be reported due to the erosion of the sediment on the sides of the piers and hence scour depth will be reduced.

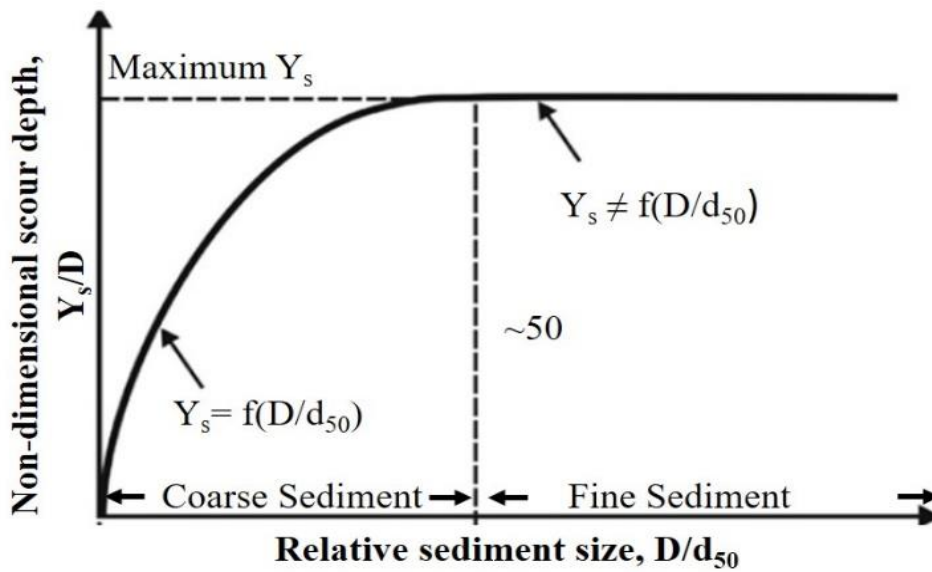
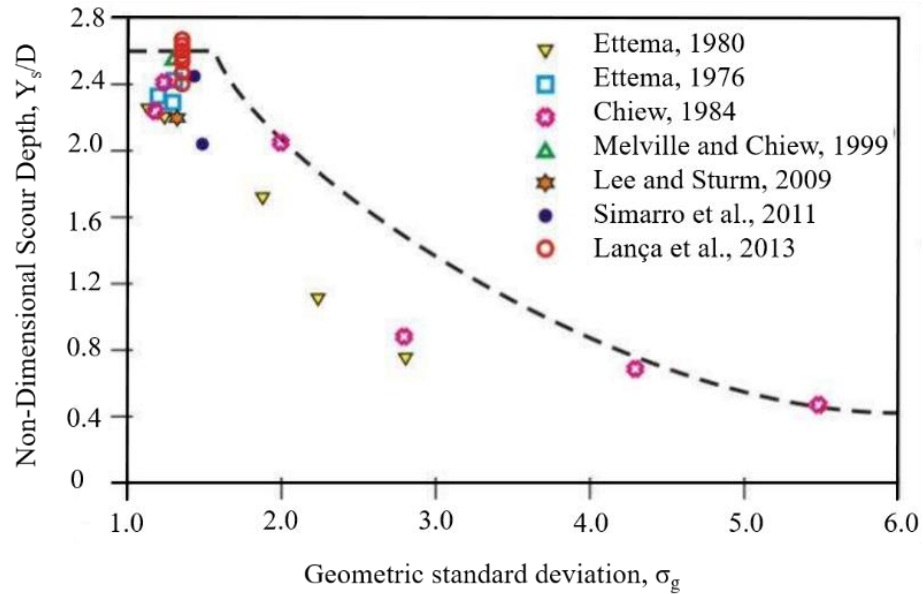


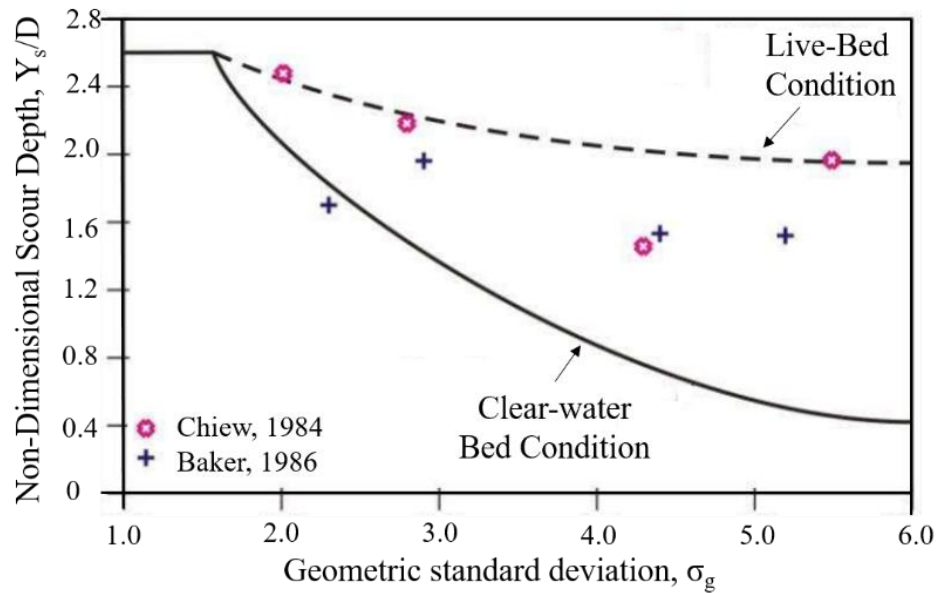
Fig. 2.4 Sediment coarseness effect (D/d_{50}) on non- dimensional scour depth (Y_s /D) adapted from Melville and Coleman (2000)

2.7.3 Effect of Sediment Non-uniformity, σ_g

Geometric standard deviation, σ_g of the sediments used is characterized as a sediment non-uniformity. The expression proposed by Şarlak and Tiğrek (2011) for the $\sigma_g = \sqrt{d_{84}/d_{16}}$, signifies the grain size at the eighty-fourth and sixteenth percentiles, respectively. The variation in the particle size has been used in the above mentioned expression, because this has a considerable effect on the scour depth. Ettema (1976) and Chiew (1984) conducted an experimental study for evaluating the influence of the sediment non-uniformity on scour depth, experimental tests had been carried out for varying values of the σ_g under clear water condition. Results of these studies conclude that Y_s/D decreases with the increase in the σ_g values.



(a)



(b)

Fig. 2.5 Effect of sediment non-uniformity on the non-dimensional scour depth for (a) clear water bed condition and (b) live bed condition

Experimental results of the Baker (1986); Chiew (1984); Ettema (1976, 1980); Lanca et al. (2013); Lee and Sturm (2009); Melville and Chiew (1999); Simarro et al. (2011) for evaluating the influence of the σ_g on the scour depth under clear water and live bed condition has been presented in **Fig. 2.5 (a) and (b)**. The corresponding range of the parameters used in the fig are such as $U/U_c = (0.8-1)$, $D/d_{50} = (30-100)$, $h/D \geq 2$. **Fig. 2.5**

(a) and (b) represents the trend of the σ_g with the Y_s/D for the clear water condition and live bed condition respectively. In case of clear water condition the values of σ_g is increased a decrease in the Y_s/D has been observed, whereas this decrease is comparatively very less in case of live bed condition. In both the cases for the $\sigma_g \leq 1.5$ the Y_s/D is can be considered as constant.

2.7.4 Effect of pier alignment, K_θ

The pier alignment angle can be defined as the angle between the longitudinal axis of the flow and direction of the flow. Laursen and Toch (1956) first investigated the influence of bridge pier alignment angle on scour depth formed around those piers. As per Melville and Coleman (2000), the angle of attack at the pier considerable affect the scour depth for all the pier shapes except cylindrical pier. Effect of the increase in the angles of attack with the scour depth are very well elaborated by the Melville and Coleman (2000) as presented in **Fig. 2.6**. As the angle of attack and width of the pier is increased scour depth is also increased. They proposed a multiplying factor K_θ , for most of the existing scour estimation equations. At zero angle of attack, effect of length of the pier becomes negligible, whereas if this angle deviates from zero, than substantial effect will be experienced by pier. The effect of angle of attack on the aspect ratio L/B , of rectangular pier is presented in the **Fig. 2.6**.

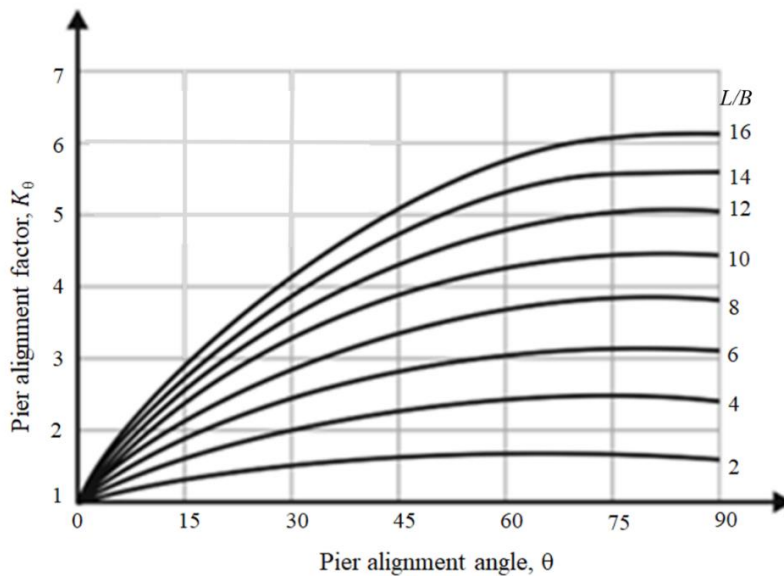


Fig. 2.6 Influence of pier alignment factor with the pier angle adapted from (Melville and Coleman 2000)

Breusers and Raudkivi (1991) also considered pier width as a function of scour depth, and they suggested that for $\theta = 5^\circ-10^\circ$ the effect of angle of attack can be neglected. Ettema et al. (2011), reported that the effect of angle of attack varies with h/D and D/d_{50} . Although the effects of θ , h , and d_{50} are interrelated, ongoing study on scour depth prediction have acknowledged these as mutually independent components.

2.7.5 Effect of Pier Shape

Bridge piers exist in various shapes, some of the commonly used geometries of the bridge piers are shown in the **Fig. 2.7** to evaluate the scour depth for different pier shapes a multiplying shape factors has been proposed by number of researchers such as : Ettema et al. (2011); Laursen and Toch (1956); Melville and Coleman (2000); Richardson and Davis (2001); Sheppard and Miller (2006) Values of the shape factors for the commonly used piers are tabulated in **Table 2.3**. These values are only applicable in case of isolated pier.

Table 2.3 Shape factor for different pier shapes adapted from Richardson and Davis (2001)

Sr. No	Shape of the pier	Shape factor
1	Cylindrical Pier	1
2	Rectangular sharp-nosed pier	0.9
3	Rectangular round-nosed pier	1
4	Oblong pier	1

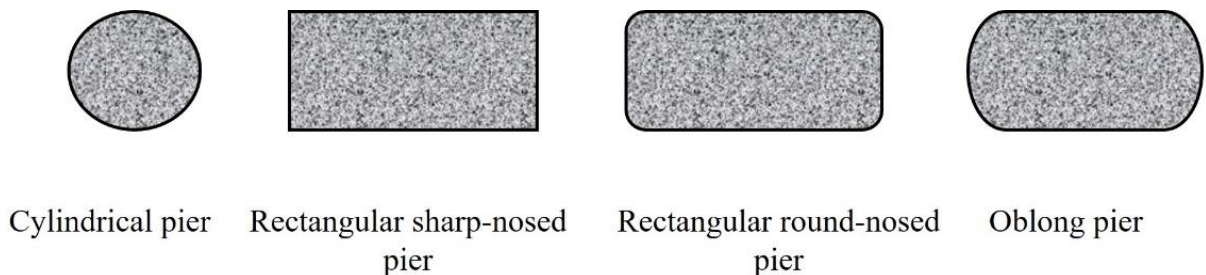


Fig. 2.7 Basic shapes of bridge piers

2.7.6 Effect of Flow Intensity, V/V_c

Flow intensity can be defined as the ratio of the flow velocity (V) to the critical flow velocity (V_c). Melville and Coleman (2000), classified the local scour into clear water and live-bed condition on the bases of the flow intensity as shown in **Fig. 2.8**. If the flow intensity approaches to one than clear water scour takes place, and if the flow intensity if greater than one than it is termed as live bed scour. In case of clear water scour no sediment material will be transported from the scour hole along the flow to the downstream of the channel. Whereas in case of live bed scour sediment material moves along the direction of the flow.

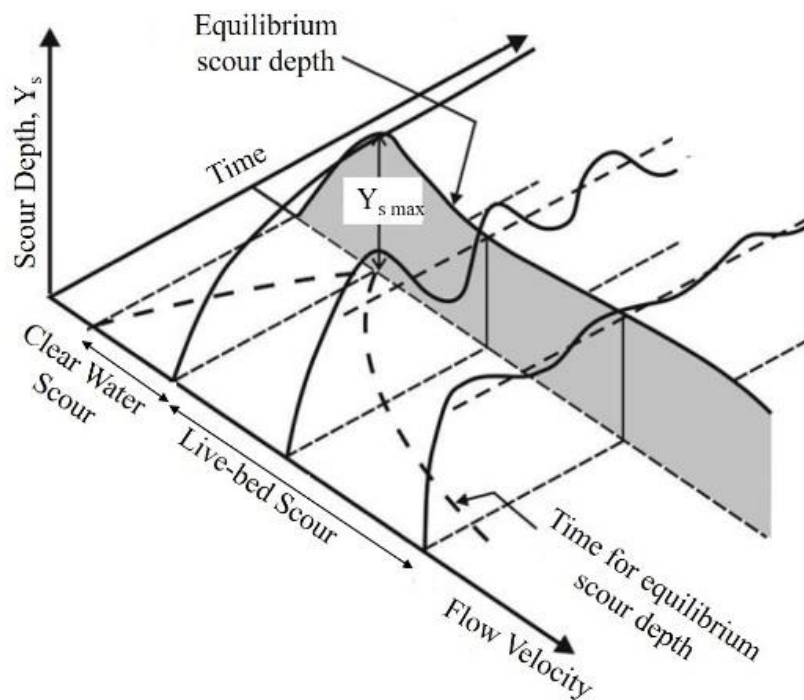


Fig. 2.8 Classification of the scour depth on the basis of flow intensity adapted from Melville and Coleman (2000)

Scour depth in case of uniformly graded sediment under the clear water condition has linear relationship with flow intensity at the maximum threshold peak for $V/V_c \approx 1$. As the $V/V_c > 1$, the scour depth firstly decreases and starts increasing until the second peak is attained which is termed as live bed condition peak. According to Ettema et al. (2011), the live bed scour is weakly dependent on the velocity of flow. Melville and Coleman (2000) presented

a summarized data of the scour given by Chabert and Engeldinger (1956); Chee (1982); Chiew (1984); Ettema (1980); Hancu (1971); Shen et al. (1966) for the uniform sediment and non-uniform sediment to evaluate the influence of the flow intensity on the scour depth under clear water and live bed condition in **Fig. 2.9 (a) and (b)** respectively. However, under live bed conditions, the flow intensity is insignificant for the variation of local scour depth for both sediment types.

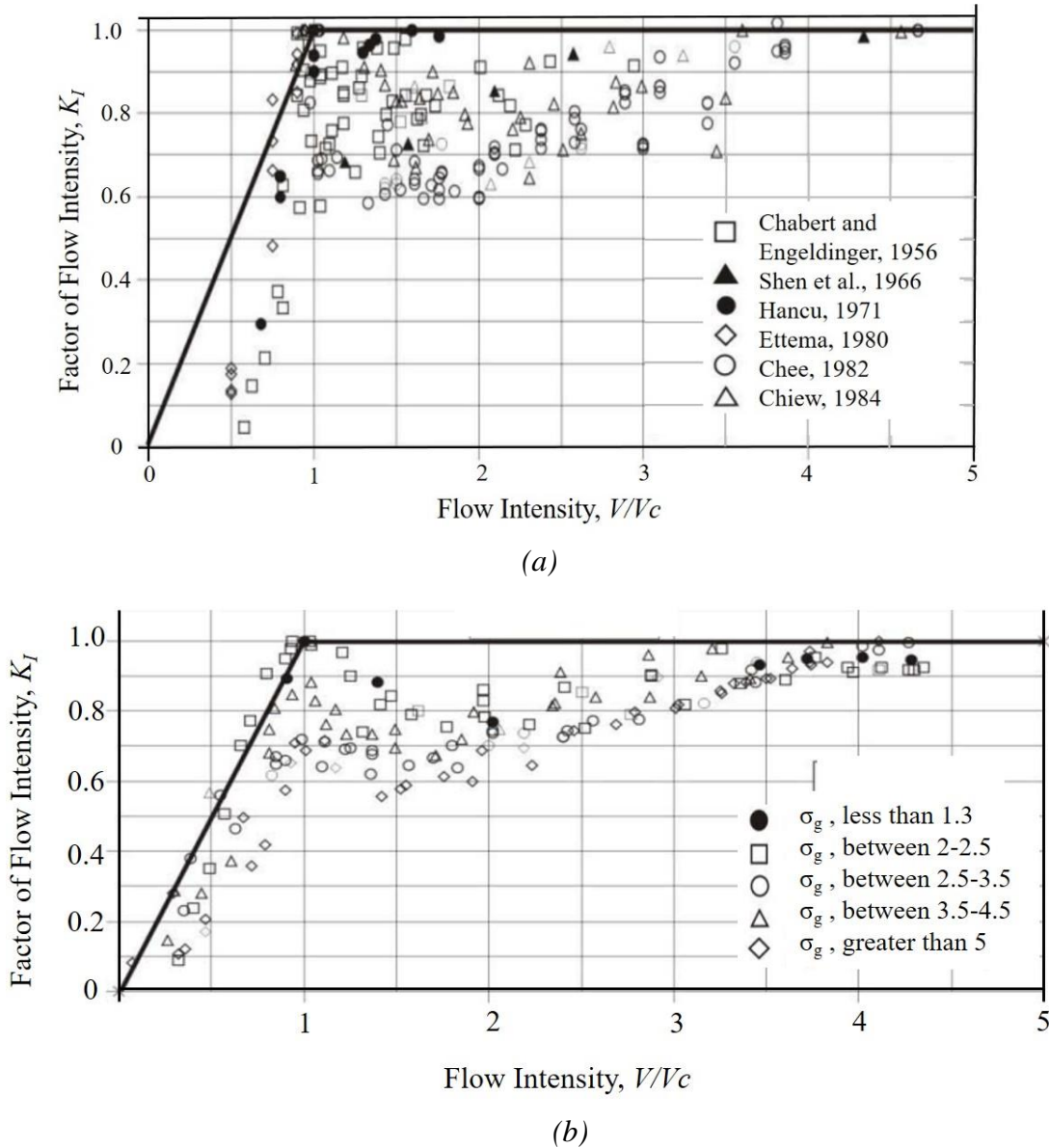


Fig. 2.9 Effect of flow intensity (V/V_c) on the scour depth with the Factor of Flow intensity K_I (a) Uniform sediment, (b) Non-Uniform sediment, adapted from Melville and Coleman (2000)

2.7.7 Effect of Viscosity

The effect of viscosity has not been considered by numerous researchers such as Chiew (1984); Ettema (1980); Lança et al. (2013); Melville and Chiew (1999); Oliveto and Hager (2002); Sheppard et al. (2004) these are focused only on single pier scour studies. These researchers neglected the effect of the viscosity, due to the presence of the turbulent flow field around the bridge pier. In contrary, researchers as M. Lança et al. (2016); Shen et al. (1969), considered the Reynolds number as an important factor. Ettema et al. (1998) concluded that, for precise scour depth prediction, bridge pier should be scaled linearly with the flow and sediment particles. Due to the non-linear behaviour of the piers, a larger and deeper scour hole is formed. As per their results, Reynolds number is insignificant for pier scour and Froude number can describe the gradient of energy. For the small width piers (narrow pier) larger will be the Froude number and hence the scour depth will be reduced. Further Ettema et al. (2006), on the basis of the experimental results proposed a relationship curve for the Non-dimensional scour depth and Froude number as shown in **Fig. 2.10**.

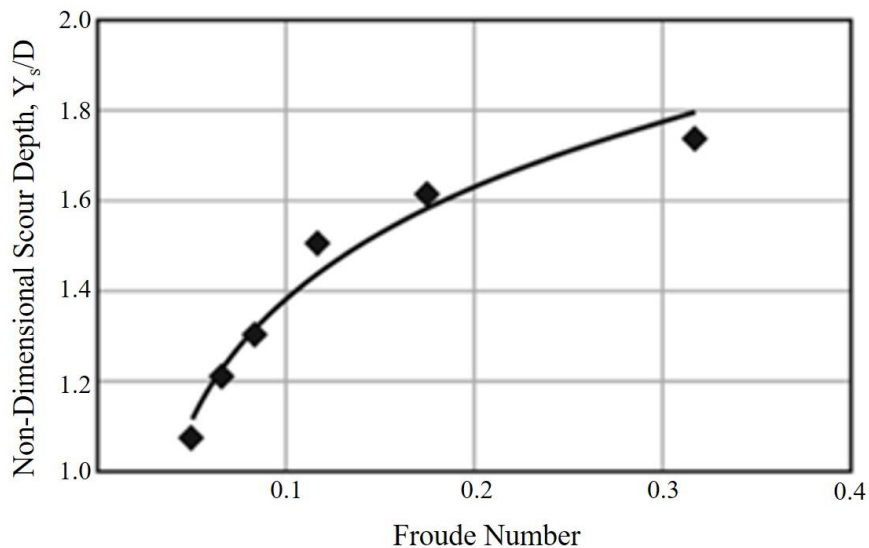


Fig. 2.10 Variation of Froude number on the Non-dimensional scour depth adapted from Ettema et al. (2006)

2.8 Temporal scour depth

Scour depth is a time dependent phenomenon. Local scour attains the equilibrium state with time, and this time to attain the equilibrium may be infinite as proposed by Breusers et al. (1977); Melville and Chiew (1999). The basic concept of scour attainment under both clear water and live bed condition purposed by Ettema et al. (2011) as shown in **Fig. 2.11**. Equilibrium scour depth attained early under clear water condition in comparison with the live. **Fig. 2.11** depicts the asymptotic growth of scour depth to attain the equilibrium state under clear water scour condition. Whereas, under live bed conditions, the equilibrium scour depth is attained more rapidly, and the scour depth then fluctuates as sediment materials passes across the bridge piers. As a result, throughout most circumstances for the scour under live bed conditions, the temporal development of scour depth is insignificant.

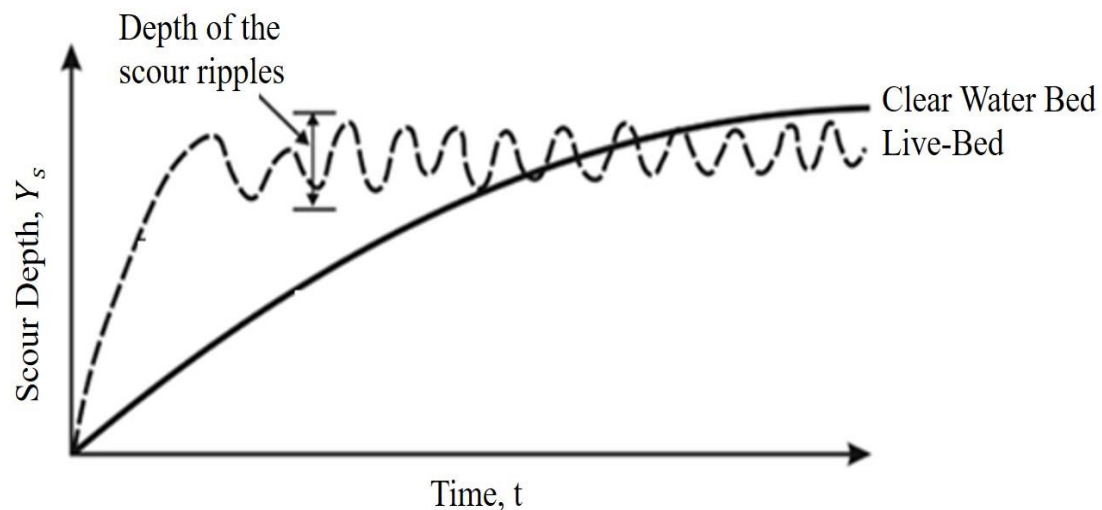


Fig. 2.11 Temporal scour depth evolution for clear water and live bed condition adapted from Ettema et al. (2006)

Extensive study has been carried out in the past for the temporal scour depth by numerous researchers Chabert and Engeldinger (1956); Ettema (1980); Hannah (1978); Kothyari (2007); Kothyari et al. (1992b); Melville and Chiew (1999); Melville and Coleman (2000); Oliveto et al. (2003, 2005); Oliveto and Hager (2002); Yanmaz and Altinbilek (1991). Estimation of the maximum scour depth within a specific time frame is extremely

challenging due to the complexities of the scour process. As a result, several researchers have investigated various methods for assessing the correlation of temporal scour depth. The variation of the scour depth with time is essential for the safe and economical design of bridge piers.

The very first study for introducing the effect of time and velocity on the scour depth under clear water condition has been conducted by Chabert and Engeldinger (1956). They have conducted a number of experimental study for the long duration of experiments reaching from hours to days. Additionally they also evaluated the functioning of the protection devices. Hannah (1978) studied the temporal scour depth using a single pile and two piles. The experimental duration was spanned to seven hours. The results of the study, does not provide any correlations encompassing temporal variation of scour depth. As per the Ettema (1980), equilibrium scour depth around the bridge pier was completely attained in fourteen days. He categorized the equilibrium scour depth attainment phase into three stages, Initial, erosion, and equilibrium stage. In initial stage the scour erosion rate is high, in erosion stage the scour hole formation is accompanied with the horseshoe vortices and lastly in the equilibrium stage the amount of sediment entered into the scour hole becomes equal to the sediment eroded from the scour hole.

Yanmaz and Altinbilek (1991) conducted experimental study to assess the temporal evolution of scour depth, by taking the test durations as *5, 20, 60 and 150 minutes*. They proposed a semi empirical equation for scour depth estimation by considering the time, this equation was based on the continuity equation of the sediments. Kothyari et al. (1992b) studied the temporal scour depth experimentally for the uniform and non- uniform sediment material under clear water condition (steady flow and unsteady flow). They developed a procedure to evaluate the temporal variation in scour depth, this procedure was based on the fact that the principal agent of scour generation is the primary vortices at the nose of the pier. Nazariha (1996) conducted long duration (90 hours) experimental runs for temporal scour depth evaluation. Results of his study reveals that, the maximum scour depth occurs in first 30 minutes of the experimental run, and after that, the rate of scour evolution decreases. He also concluded that the *80%* of the total scour takes place in first *120 minutes*.

Melville and Chiew (1999) carried out an experimental study under clear water condition in uniform sand beds for temporal scour depth. Due to the asymptotic nature of the scour, the equilibrium scour depth may be attained after infinite time. To overcome this difficulty, authors have used a new term t_e , time taken to achieve equilibrium scour depth. This is defined as the, time taken in scour hole evolution till the rate of sediment scour reaches the 5% of pier diameter in the last twenty-four hours of experimental run. The temporal scour evolution equations proposed by the authors are written below:

$$\frac{Y_s}{Y_{se}} = \exp \left\{ -0.03 \left| \frac{V_c}{V} \ln \left(\frac{t}{t_e} \right) \right|^{1.6} \right\} \quad 1$$

Where t_e can be obtained from **Eq. 2 and Eq. 3** are written as:

$$t_e \text{ (days)} = 48.26 \frac{D}{V} \left(\frac{V}{V_c} - 0.4 \right) \quad \text{for} \quad \frac{h}{D} > 6, \quad \frac{V}{V_c} > 0.4 \quad 2$$

$$t_e \text{ (days)} = 30.89 \frac{D}{V} \left(\frac{V}{V_c} - 0.4 \right) \left(\frac{h}{D} \right)^{0.25} \quad \text{for} \quad \frac{h}{D} < 6, \quad \frac{V}{V_c} > 0.4 \quad 3$$

Where, D = Diameter of the pier; V = Velocity of flow; V_c = Critical velocity of flow; h = Depth of flow

Oliveto and Hager (2002) , investigated the temporal scour for bridge pier and abutment for six different sediments. They proposed an equation for scour depth, which depends on the pier or abutment length, densimetric Froude number and dimensionless. The results of the study, concludes that with the increase in the time scour depth also increases but asymptotically till the attainment of the equilibrium state. However, the time taken to achieve the equilibrium scour depth has not defined accurately yet, but still there are few equation as given in literature. The equations proposed by Melville and Chiew (1999), is very simple in using and gives almost precise results, so these equation are incorporated into present study for evaluating the temporal scour depth. A method for computing the temporal variation of scour depth for circular pier under clear water condition for uniform sediment have been developed by Mia and Nago (2003). The experiments has been kept running till the scour was less than 1 mm or no scour in last 1 hour . The conclusion of their

study shows that, scour does not develop when the critical shear stress has been attained, at this stage equilibrium scour depth and respected time can be computed.

2.9 Approaches for scour depth estimation

2.9.1 Semi empirical equations used for scour depth estimation

Numerous empirical and semi-analytical approaches for estimating the scour depth around uniform piers are available in the literature. A detailed description of the estimation of equilibrium depth of scour can be found in Ettema (1980); Garde and Raju (2000); Kothyari (1989); Melville (1975). Hence the same is not repeated herein. Typically the maximum of the investigation carried out on either experimental data or field based data. Due to the disparities in various test and field conditions, the results obtained are either over predicting or under predicting the scour depth. So, a brief description on the most commonly used methods for the estimation of equilibrium or maximum depth of scour is presented herein.

1. Melville and Coleman Equation
2. HEC-18 Equation
3. IRC (1998 &2000)
4. Sheppard/Melville Equation
5. Laursen and Toch

2.9.1.1 Melville and Coleman Equation

Initially, Melville (1997) proposed an equation for scour depth estimation, later on this equation was modified by Melville and Coleman (2000) and named as Melville and Coleman Equation, a new factor considering time has been added into the equation after Melville and Chiew (1999) suggestion. The various parameters influencing the scour depth has been considered into the proposed equation in term of the multiplying factor. The modified form of the Melville equation has been written in **Eq.4**:

$$Y_s = K_h K_I K_{sd} K_\alpha K_s K_g K_t \quad 4$$

Where, Y_s is the local scour depth; K_h is the flow depth factor; K_I is the Flow Intensity factor; K_{sd} is the sediment size factor; K_α is the alignment of pier factor; K_s is the shape of pier factor; K_g is the channel geometry factor; K_t is the time factor. Correlation factors for the Melville and Coleman equation are tabulated in **Table 2.4** below:

Table 2.4 Correction factors for the Melville and Coleman equation

Sr. No.	Factor	Conditions		
1	Flow depth factor	$K_h = 2.4$	$\frac{D}{h} < 0.7$	5
		$K_h = 2\sqrt{hD}$	$0.7 < \frac{D}{h} < 5$	6
		$K_h = 4.5h$	$\frac{D}{h} > 5$	7
2	Flow Intensity factor	$K_I = \frac{V - (V_a - V_c)}{V_c}$	$\frac{V - (V_a - V_c)}{V_c} < 1$	8
		$K_I = 1$	$\frac{V - (V_a - V_c)}{V_c} \geq 1$	9
3	Sediment size factor	$K_{sd} = 0.57 \log \left(2.24 \frac{D}{d_{50}} \right)$	$\frac{D}{d_{50}} \leq 25$	10
		$K_{sd} = 1$	$\frac{D}{d_{50}} > 25$	11
4	Alignment of pier factor	$K_\alpha = \left(\frac{b_p}{D} \right)^{0.65}$	$\frac{b_p}{D} = 1$ for $\alpha = 0$	12
5	Shape of pier factor	Circular pier – 1 Round nose pier – 1 Square nose pier – 1.1 Sharp nose pier – 0.9		
6	Time factor	Time factor can be computed from equations given in temporal scour depth section.		

2.9.1.2 HEC-18 Equation

HEC-18 equation has been proposed by Richardson et al. (1987), in the NCH (National Cooperative Highway) research program and this equation has been commonly used in U.S. this equation was originally based on the laboratory data developed at the Colorado State University for circular bridge piers. With time progressive modifications have been made into this equation by Arneson et al. (2012); Richardson and Davis (2001). This equation can be used in both (Clear Water and live bed) conditions. The modified equation can be written as in **Eq.13** :

$$\frac{Y_s}{h_u} = 2.0 k_1 k_2 k_3 k_w \left(\frac{D}{h_u}\right)^{0.65} F_r^{0.43} \quad 13$$

where: Y_s is the scour depth (m); h_u is the flow depth on upstream of the pier (m); D is the diameter of pier (m); K_1 , K_2 , K_3 and K_w is the factors of correction; F_r is the Froude number; g is the acceleration due to gravity; V is the mean velocity of flow (m/s). The values of the K_1 , K_2 , K_3 for the HEC-18 equation has been tabulated below in **Table 2.5, Table 2.6 and Table 2.7.**

Table 2.5 Values of K_1 factor of correction for pier shapes adapted from Richardson and Davis (2001)

Sr. No.	Pier shape	K_1
1	Square nosed Pier	1.1
2	Round Nosed Pier	1
3	Sharp Nosed Pier	0.9
4	Circular Cylindrical Pier	1
5	Pier Group	1

Table 2.6 Values of K₂ factor of correction for various angle of attacks Richardson and Davis (2001)

Sr. No.	Angle of Attack	L/4 =D	L/8 =D	L/12 =D
1	0°	1	1	1
2	15°	1.5	2	2.5
3	30°	2	2.75	3.5
4	45°	2.3	3.3	4.3
5	90°	2.5	3.9	5

Table 2.7 Values of K₃ factor of correction for condition of bed Richardson and Davis (2001)

Sr. No.	condition of bed	Height of dune,(ft.)	K ₃
1	Clear Water flow	-	1.1
2	Plane bed without dunes	-	1.1
3	Small dunes	2-10	1.1
4	Medium dunes	10-30	1.1-1.2
5	Large dunes	>30	1.3

The values of the factor K_w can be calculated from the equations written below in **Eq.14** and **Eq.15** :

$$K_w = 2.58 \left(\frac{h}{D}\right)^{0.34} Fr^{0.65} \quad \text{for } \frac{V}{V_c} < 1.0 \quad 14$$

$$K_w = 1.0 \left(\frac{h}{D}\right)^{0.13} Fr^{0.25} \quad \text{for } \frac{V}{V_c} < 1.0 \quad 15$$

2.9.1.3 IRC 1998 &2000 (Indian Roads Congress) Equation

The Indian Road Congress (Congress 2016) code is widely used in India to obtain the standards required for the design of roadway bridges. The IRC equation has been published in Indian standard codes - IRC:5, IRC:SP:13 & IRC 78 and this equation has been utilized to construct bridges. The equation is formulated on the basis of the Lacey's formula. Unlike most scour formulations, the IRC equation does provide any separate criteria for local,

constriction, and global scour. The maximum scour depth is considered to be two times Lacey's scour depth. Standard IRC equation can be written as in **Eq.16** and **Eq. 17**:

$$Y_s = 0.473 \left(\frac{Q}{f} \right)^{1/3}, \text{ when } \frac{L}{B} \geq 1 \quad 16$$

$$Y_s = 1.34 \left(\frac{q^2}{f} \right)^{1/3}, \text{ when } \frac{L}{B} \leq 1 \quad 17$$

where; Q = Design discharge (m^3/sec), Y_s = Scour depth (m), q = Intensity of discharge ($m^3/s/m$), Q/L & f = Silt factor given by Lacey's equation, L = Clear waterway (m), and B = Mean width of channel (regime width) (m).

2.9.1.4 Sheppard/Melville Equation (S/M equation)

S/M equation is a combination of the equilibrium scour depth prediction equation proposed by Melville (1997); Sheppard and Miller (2006). In order to make a new suitable equation with the better prediction accuracy, this equation was modified and renamed as Sheppard/Melville equation (S/M equation). The proposed S/M equation can be written in **Eq.18**, **Eq.19** and **Eq.20**:

$$\frac{y_s}{D} = 2.5 f_1 f_2 f_3 \quad \text{for } 0.4 \leq \frac{V}{V_c} \leq 1.0 \quad 18$$

$$\frac{y_s}{D} = f_1 \left[2.2 \left(\frac{\frac{v}{v_c} - 1}{\frac{v_{IP}}{v_c} - 1} \right) + 2.5 f_3 \left(\frac{\frac{v_{IP}}{v_c} - \frac{v}{v_c}}{\frac{v_{IP}}{v_c} - 1} \right) \right] \quad \text{for } 1 \leq \frac{V}{V_c} \leq \frac{V_{IP}}{V_c} \quad 19$$

$$\frac{y_s}{D} = 2.2 f_1 \quad \text{for } \frac{V}{V_c} > \frac{V_{IP}}{V_c} \quad 20$$

Here, V_{IP} can be computed from **Eq.21** and **Eq.22** by considering the maximum value of V_{IP} :

$$V_{IP} = 0.6\sqrt{gh} \quad 21$$

$$V_{lp} = 5V_c \quad 22$$

where, Y_s = Scour depth below the bed level (m), D = Diameter of pier (m), f_1, f_2, f_3 = S/M's coefficients, V = Mean velocity of flow (m/s), V_c = Critical Velocity of flow (m/s), V_{IP} = Live bed peak velocity of flow (m/s).

The values of the S/M coefficients can be computed from the **Eq.23**, **Eq.24** and **Eq.25** :

$$f_1 = \tanh \left[\left(\frac{h}{D} \right)^{0.47} \right] \quad 23$$

$$f_2 = \left\{ 1 - 1.2 \left[\ln \left(\frac{V}{V_c} \right) \right]^2 \right\} \quad 24$$

$$f_3 = \left[\frac{\left(\frac{D}{d_{50}} \right)}{0.4 \left(\frac{D}{d_{50}} \right)^{1.2} + 10.6 \left(\frac{D}{d_{50}} \right)^{-0.13}} \right] \quad 25$$

2.9.1.5 Laursen and Toch

Laursen and Toch (1956) on the basis of the prototype model study, generated design criteria in the form of curves. Later these curves had established in the form of mathematical expressions by Neill (1964). The expression can be written as in **Eq.26**:

$$Y_s = 1.35 D^{0.7} h^{0.3} \quad 26$$

where Y_s = Scour depth below the bed level (m), D = Diameter of the pier (m), and h = Head of flow (m)

The estimation of scour depths around group of piers is analogous to scour depths around a single pier, but with various empirically calculated coefficients Liang et al. (2017). Only a few studies published in the literature provide regression-based equations for group piers (Amini Baghbadorani et al. 2018; Coleman et al. 2005; Gaudio et al. 2013). To evaluate local scour depth at a complex pier, proposed a new methodology called the Melville and Coleman equation (Coleman et al. 2005). Amini Baghbadorani et al. (2018), reviewed the HEC-18 and Florida Department of Transportation (FDOT) equations, and as well as

recommended a new equation. Behzad and Beheshti, (2006) developed a coefficient for estimating scour depth around a group of piers. Ataie-Ashtiani et al. (2010) performed more than seventy experimentations by utilizing complex piers and discovered that both the Coleman (2005) and Richardson and Davis (1995) methods overestimate the scour depth. Despite the extensive experiments, the regression-based equations require time-consuming analyses and did not yield significant improvement in results (Gaudio et al. 2013). For a group of piers, the current standard is to use single pier equation by multiplying a correction factor or redefining an equivalent pier width.

2.9.2 AI based Approaches for scour depth estimation

In very recent work, Artificial intelligence (AI) techniques has also utilized as alternative solutions to predict scour depth (Sharafati et al. 2020). Computational techniques have greatly simplified scour estimation and made it more acceptable than conventional methods (Muzzammil et al. 2015). Adaptive Network-based Fuzzy Inference Systems, Artificial Neural Networks, Genetic Algorithms, Gene Expression Programming, Genetic Programming, Group Method of Data Handling and Radial Basis functions are some of the AI techniques now being employed to solve various hydraulics engineering challenges. A few of the studies are Akib et al. (2014); Choi et al. (2017) used the ANFIS method to examine various scour issues, while Pandey et al. (2020c; b) have used the GA method to estimate scour depth.

Furthermore, Najafzadeh et al. (2015) and Najafzadeh and Azamathulla (2013) demonstrated the use of GMDH to estimate the scour depth. It used the Levenberg-Marquardt (LM) approach and evaluated by comparing its results to those of ANFIS, RBF-NN, and other empirical equations. The GMDH-LM was found to provide more accurate estimations than the others. Even though ANN models perform better than traditional regression-based methodologies, unlike GEP, they cannot provide a direct relation between scour depths and the variables affecting them.

In addition, the works in Azamathulla (2012); Bateni et al. (2019); Guven and Gunal (2008); Muzzammil et al. (2015); Najafzadeh et al. (2016) utilized the GEP approach to estimate scour depth and evaluated their findings to certain other regression-based

equations, leading to the conclusion that GEP is the most admirable modelling methodology for scour depth investigation, among some other methods. As a result, the primary objectives of the present study are to provide new experimental data for scour depth around a group of piers, to identify the factors influencing scour development, and to establish an empirical relationship for estimating scour depth.

Although CFD models (e.g., RANS, LES, and DNS) are capable of revealing the complex 3D turbulence flow field around bridge pier, their applications to engineering design are not common due to the limitation of their capabilities of simulating sediment transport and the high computing cost (Cheng et al. 2018; Escauriaza and Sotiropoulos 2011; Kim et al. 2017). Artificial intelligence techniques has also used as alternatives to predict scour depth, such as ANN (Artificial Neural Networks) (Choi and Cheong 2006), ANFIS (Adaptive Neuro-Fuzzy Inference System) (Bateni et al. 2007; Jahangirzadeh et al. 2014b; Najafzadeh 2015) GMDH (Group Method of Data Handling) (Najafzadeh 2015; Najafzadeh et al. 2013, 2015; Najafzadeh and Azamathulla 2013; Sharafati et al. 2020), MT (Model Tree) (Ghaemi et al. 2013; Najafzadeh and Oliveto 2021), SVM (Support Vector Machine) (Azamathulla 2012; Goel and Pal 2009; Jahangirzadeh et al. 2014a; Sreedhara et al. 2019) and extreme learning machine (Ebtehaj et al. 2018). Lastly,(Zaid et al. 2019) conducted a CFD numerical simulation based RANS (Reynolds Average Navier Stokes Equation) using k- ϵ approach for predicting the flow field around square and cylinder piers. Results of their study does not captured any vortex shedding, and authors suggested further research should be conducted on this topic.

2.10 Summary and gaps in Literature

A detailed review of the literature based on the scour around the bridge pier has been presented in the present chapter. This chapter includes the brief description of the local scour phenomenon around the single and group of piers, Mechanism of local scour, variables affecting the sour depth, temporal scour depth and various approaches used for the estimation of the scour depth. Basically, the scour phenomenon is the study of the relationship between the flow field and the hydraulic structures placed in the flowing water stream, as a consequence of this interplay sediment material starts eroding from the bed and around the hydraulic structures. Section 2.2 describes the scour phenomenon around

the single pier under various flow and sediment characteristics with the help of already published literature. Section 2.3 elaborates the mechanism of scour evolution around the different shapes of the bridge pier with previously published research. Local scour has been classified on the basis of the volume of the sediment transported into the scour region and ability of the flowing water to take away the sediment. There are two main classification: clear water- bed and live bed. In section 2.4, scour around the group of pier has been summarized for the various laboratory conditions. In addition, various factor influencing the scour depth are discussed in section 2.5 and the graphical trends of the scour dependency on the various factors have also been presented here. Furthermore, attainment of the equilibrium scour depth and temporal evolution of the scour depth has been discussed in details in section 2.6. Lastly, in Section 2.7 various approaches used for the scour depth estimation are studied: Semi empirical equations and AI based approaches. Various equation used for the scour estimation are listed in the section 2.7 with the details of the coefficient factors used in the equations.

According to the review conducted in this chapter, it has been found that the numerous amount of literature is available for the study of flow structure, mechanism of scour and scour prediction, but majority of this literature is based on the single pier study. Only a limited amount of literature is available for the group of the pier. However in actual practice, all the bridge structures consists of more than one pier. On the basis of this literature survey some gaps has been outlined:

- Scour depth and flow field around the group of bridge pier has not in investigated well in past.
- Influence of pier spacing on the scour depth around the two or more than two piers have not been investigated.
- Number of studies have been carried out but still there is not a single equation for accurate estimation of scour depth.

Hence, this study is mainly focused on the experimental investigation of the scour depth group of bridge piers aligned in various position and the effects of the pier spacing on the scour depth has also been evaluated.

CHAPTER 3

EXPERIMENTAL METHODOLOGY

3.1 Introduction

This chapter provides the details of the experimental setup and methodology adopted in the present study. In order to understand the complex scour mechanism, the influence of pier spacing and the rate of flow, this study has been carried out. In total, 232 experiments have been carried out for various pier spacing and arrangements on uniformly graded sediment in the Hydraulic Engineering Laboratory of Delhi Technological University, Delhi, India.

3.2 Experimental Setup

3.2.1 Rectangular Flume and its Components

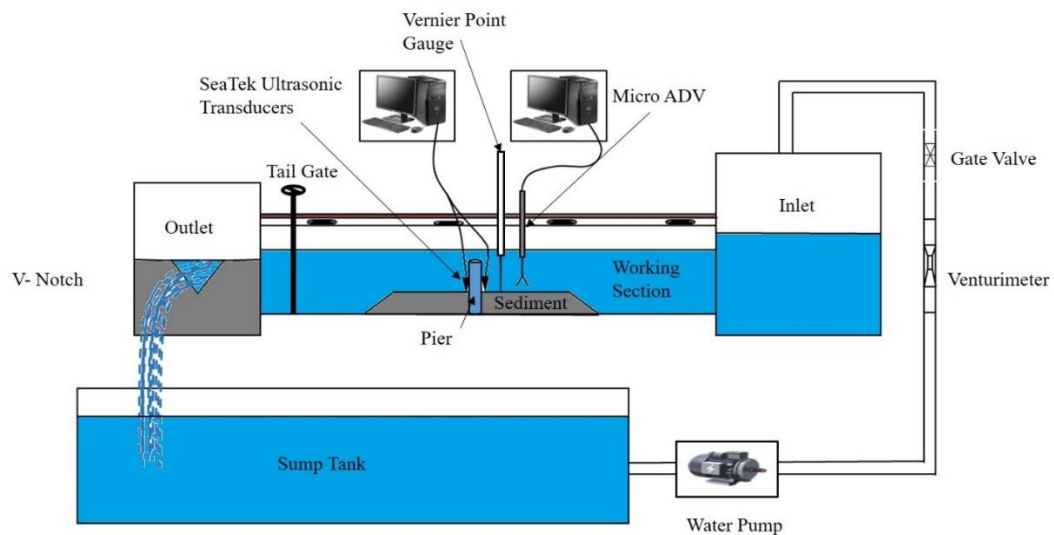


Fig. 3.1 Schematic Diagram of the rectangular recirculating open channel flume

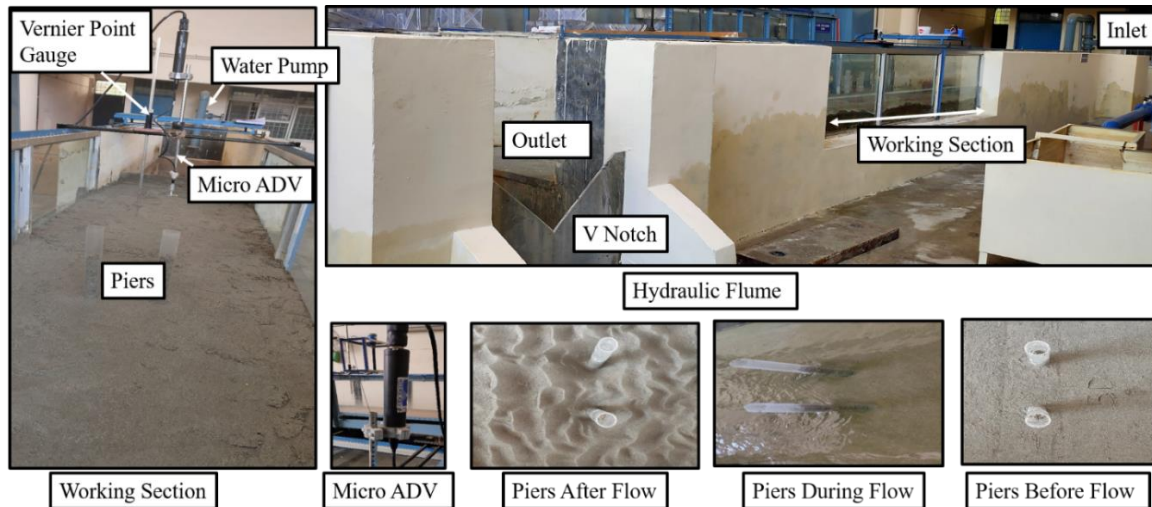


Fig. 3.2 Rectangular masonry flume and its components

Experimental work has been carried out in the hydraulic laboratory using recirculating masonry flume at Delhi Technological University, New Delhi, India. **Fig. 3.1** depicts a schematic diagram of the flume detailing the flow sections. The flume has a length of 14 meters, a width of 1.10 meters, and a depth of 0.80 meters. The flume section has a working area that is 5 meters long, 1.10 meters wide, and 0.80 meters deep, and it is located 5 meters downstream from the inlet of the flume. The side of the working section is made up of a glass wall to facilitate the clear visualization of the scour around the piers as shown in **Fig. 3.2**. The working area has been filled with a uniformly graded sand bed. Acrylic pipes of diameter D , 50 mm, have been used as pier models, laid in the centre of the working section at pier spacing. A vernier point gauge with ± 0.1 mm accuracy has been equipped in the working section for bed elevation measurements. Tailgate has been provided at the outlet ends of the working section to adjust the flow depth in the flume. And a gate valve is provided upstream of the inlet tank to regulate the flow.

Additionally, two settling chambers have also been provided in both the inlet and outlet tank for settling the floating particles. These settling chambers are provided for collecting the floating sediments during the flow. For providing continuous flow during the experimental run, a sump tank and a water pump have been provided. Water from the sump tank is pumped to the inlet tank through a venturimeter and gate valve and then to the working section, and in the end, falls into the outlet tank. To measure the rate of flow in

the flume section, a venturimeter, a V-notch, has been installed, and to find out the continuous point velocity Micro ADV has been installed in the working section. SeaTek ultrasonic transducers have been installed around the bridge piers to precisely measure the scour depth.

3.2.2 Vernier Point Gauge

A vernier point gauge with $\pm 0.1 \text{ mm}$ accuracy has been used for the measurement of the bed elevation around the bridge piers and in the sediment bed after the drainage of all the water from the channel section. This has been mounted on the flume section on a moveable trolley so that the pointer gauge can be moved in any direction, as shown in **Fig. 3.2**.

3.2.3 Venturimeter

Venturimeter is used for the measurement of the rate of flow by observing the change in the pressure head at converging and diverging ends. It converts pressure energy into kinetic energy. It was named after Giovanni Battista Venturi, an Italian physicist (1746-1822). Venturimeter is based on the principles of Bernoulli's Equation, and venture effect has been used to measure the pressure reduction at the joint section. Bernoulli's Equation is the summation of the pressure head ($P/\rho g$), velocity head ($V^2/2g$) and datum head (z). Venturimeter consists of three parts which are presented in **Fig. 3.3**:

1. Converging end
2. Throat
3. Diverging end

$$\frac{P}{\rho g} + \frac{V^2}{2g} + z = \text{constant} \quad 27$$

$$\frac{P_1}{\rho g} + \frac{V_1^2}{2g} + z_1 = \frac{P_2}{\rho g} + \frac{V_2^2}{2g} + z_2 \quad 28$$

Where P_1 is the pressure at section 1; P_2 is the pressure at section 2; V_1 is the velocity at section 1; V_2 is the velocity at section 2; at point 1, d_1 is the pipe diameter at section 1 and d_2 is the pipe diameter at section 2.

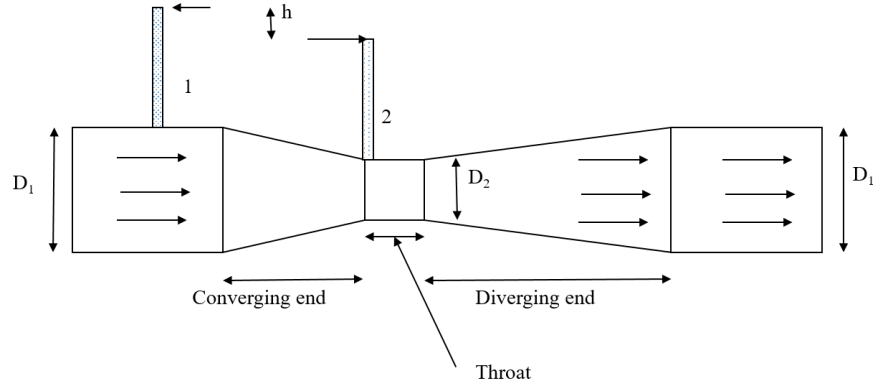


Fig. 3.3 Schematic diagram of the venturimeter

3.2.4 V-Notch

V-notch is a type of weir; weirs are the barrier provided in the river way for altering the flow to prevent a flood. Weirs are also used as flow measurement devices for the river flow. V notch is in the form of a plate, and edges are sharply crested, as shown in **Fig.**

3.4. The expression for the measurement of flow velocity can be derived as:

$$Q = \int_0^{H_1} dh(2(H_1 - H_2) (\tan \theta/2)(\sqrt{2gH_2}) \quad 29$$

$$Q = 2\sqrt{2g} \tan(\theta/2) \int_0^{H_1} (H_1 - H_2) \sqrt{h} dh \quad 30$$

$$Q = 2\sqrt{2g} \tan(\theta/2) \int_0^{H_1} (H_1 h^{1/2} - H_2^{3/2}) dh \quad 31$$

$$Q = 2\sqrt{2g} \tan(\theta/2) \left[\frac{4}{15} H_1^{5/2} \right] \quad 32$$

$$Q = \frac{8}{15} \sqrt{2g} \tan(\theta/2) [H_1^{5/2}] \quad 33$$

$$Q_{th} = \frac{8}{15} C_d \sqrt{2g} \tan(\theta/2) [H_1^{5/2}] \quad 34$$

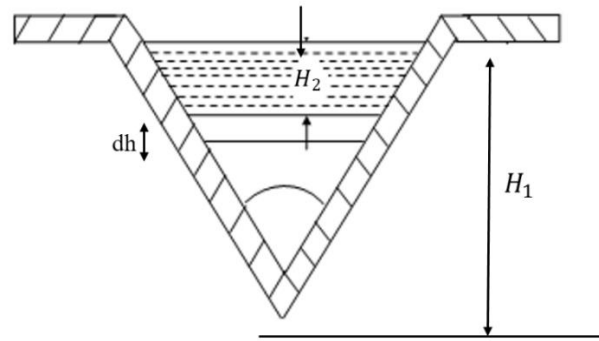


Fig. 3.4 Schematic representation of the V-Notch

3.2.5 SeaTek ultrasonic ranging system

The primary function of the SeaTek Ultrasonic ranging system is to measure the 3D bed profile in an open channel. This system consists of eight transducers, an array of stainless steel, and for communication, an electronics package; the working frequency of these transducers is 5MHz. The centre-to-centre spacing between the transducers is eight centimeters. This system can support a maximum of 32 transducers in a group of four each, as shown in **Fig. 3.5**. Each transducer has a diameter of 1 cm and is packed in stainless steel covering. The closest measurement range for these transducers is 3.5 cm, and the farthest measurement range is 110 cm. Each transducer has been number labelled at the ends of the cable, as shown in **Fig. 3.5**. For the data communication, the RS232 communicator has been used in the data logger. The number of these transducers will be shown in the computer after the plug-in of the cable into the appropriate connector. To form long arrays of 8.4 feet, a group of 4 arrays are mounted, and the operating frequency of these arrays is 2MHz. The electronic package samples the data during the run by accessing the BNC input from the four analogue channels. During a run, these channels often record the X and Y coordinates of the scour data. This data is sent back to a monitoring Computer through RS232 serial connections and recorded using provided SeaTek software. For the data recording from these transducers, SeaTek software has been utilized. Individual transducers, in addition to fixed arrays, can be utilized to construct arrays. Individual transducers have the benefit of being able to vary the numbering and spacing of transducers to match the requirements of the laboratory setup. The specification of the SeaTek are listed in **Table 3.1**.



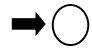

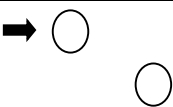
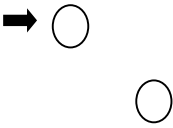
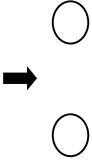

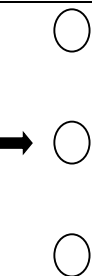
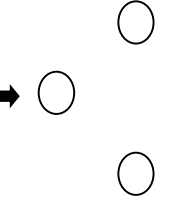
Fig. 3.5 SeaTek Ultrasonic Transducers

Table 3.1 Specifications of the Seatek Ultrasonic ranging system

Range	3.5cm to 110cm
Accuracy	± 5%
Transducer	32
Threshold Voltage	Threshold Value between 600 and 2600 mV
Maximum Range	Greater than the threshold voltage, up to 100cm
Temperature	20°C
The number of pings that must be processed for each return.	Individuals range up to 20 pings
Analogue inputs	up to external analogue channels, inputs 0-5 volts
Testing ports	2
Software for Data logger	Ultrasonic Ranging System
Warranty	12 Months
Detailed	Hardware & application training must be provided by the vendor

3.2.6 Pier Models arrangements

Table 3.2 Arrangement of piers

Sr. No.	No. of Piers	Angle of Attack	Position of Piers	Pier Spacing
1	1	0°		0
2	2	0°		1.5D to 5D
3	2	15°		1.5D to 5D
4	2	30°		1.5D to 5D
5	2	90°		1.5D to 5D
6	3	0°		1 D to 5D
7	3	90°		1 D to 4D
8	3	0°		1.5D to 5D

Acrylic pipes of diameter D , 50 mm, have been used as pier models; it has been laid in the centre of the working section at various pier spacing (P_s) ranging from 1.5- 5 times the diameter of the pier (D). The whole experimental study has been carried out in three configurations (a) single pier and (b) two piers in tandem positioning, side-by-side and at 15° and 30° angles (c) Three piers in tandem, side-by-side and staggered arrangement. The arrangement of piers considered in this dissertation is presented below in **Table 3.2**. The diameter of the pier has been adopted carefully so that the effect of contraction on the scour depth can be neglected.

For the selection of the flume size and pier geometry (Melville and Coleman 2000) proposed a few criteria. These universal criteria needed to be satisfied for the smooth conduction of experimental work such as:

- a) **Contraction effect:** For the absence of the contraction effect, the ratio of the bed width of the channel, B , to the diameter of a pier, D , should not be less than 6.5. In this dissertation contraction effect has been neglected, $B/D = 110/5 = 22$.
- b) **Flow shallowness effect:** If the ratio of the diameter of the pier to the flow depth is less than 0.7, then the flow shallowness effect can be neglected. The ratio of D/h for the present study is between 0.31 and 0.4, which is less than 0.7, so the flow shallowness effect is neglected in this dissertation.
- c) **Sediment particle effect:** If the ratio of pier diameter, D , to the mean particle size of sand, D_{50} is greater than 50, then the sediment particle effect is not present. In this dissertation, the sediment particle effect has been neglected, as the ratio is greater than 50, $D/D_{50} = 83.33$.

3.3 Material Used and Sediment Transportation

The flume section has a working area that is 5 meters long, 1.10 meters wide, and 0.80 meters deep, and it is located 5 meters downstream from the inlet of the flume. The working area has been filled with a uniformly graded sand bed (180 mm thickness) laid on a slope of 1/250. The characteristic properties of the sand are mean particle size, $d_{50} = 1.75$ mm, uniformity coefficient, $C_u = 2$ and curvature coefficient, $C_c = 1$. The particle size distribution curve for the sediment used has been presented in **Fig. 3.6**.

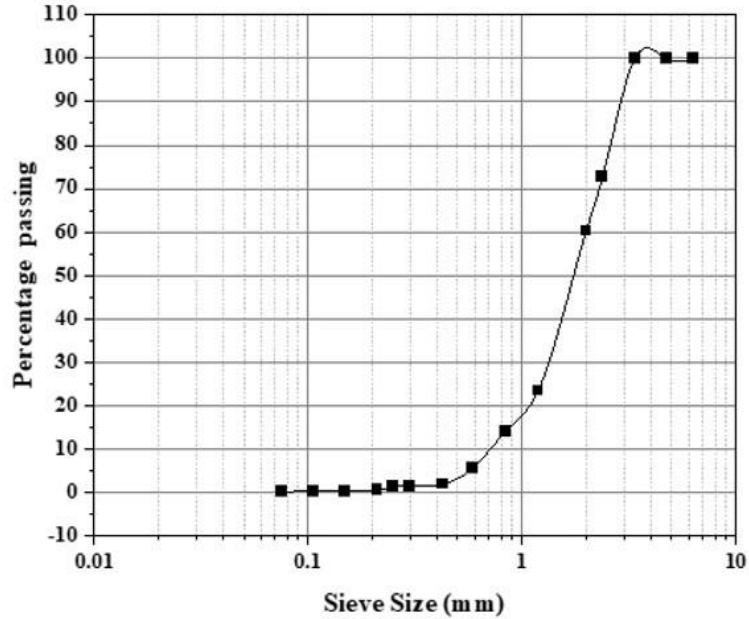


Fig. 3.6 Particle size distribution curve

The condition of sediment transport along the approach bed is influenced by various factors that impact the movement of sediment particles, such as sand, gravel, or silt, by water, wind, or ice. These factors include flow velocity, sediment size and composition, bed slope, sediment availability, vegetation and obstructions, as well as hydrological or meteorological events. Events like rainfall, flooding, or storms can have a substantial effect on sediment transport conditions, as they can increase water flow or wind intensity, resulting in higher velocities and sediment transport rates. The velocity of the water or wind passing over the sediment bed is a critical factor in sediment transport. Higher velocities have the ability to dislodge and transport larger sediment particles, whereas lower velocities may only move smaller particles. Deposition occurs in areas where the flow velocity decreases or when the sediment supply exceeds the transport capacity. This can lead to sediment buildup, altering the bed elevation and potentially affecting the hydraulic performance of nearby structures.

On the other hand, if the flow velocity exceeds the sediment's critical threshold, erosion can take place. Erosion removes sediment particles from the approach bed, which can result in scour or undermine structures. Sediment particles vary in size, shape, and density. Coarser particles are typically more resistant to movement and require higher velocities to

be transported. In contrast, fine particles like silt and clay can be easily entrained in lower velocities. The slope of the approach bed plays a significant role in sediment transport. Steeper slopes enhance the energy of the flowing medium, promoting sediment movement. However, excessively steep slopes can lead to erosion and instability. Understanding sediment transport conditions along the approach bed is crucial for engineering designs, such as those related to bridge foundations, river channel management, or coastal protection structures. By considering the factors that influence sediment transport, engineers can design structures and implement mitigation measures to ensure stability and longevity.

All experiments have been conducted under the live bed condition. The live bed condition is state in which sediment transport is actively occurring within the flow of water. It is characterized by the movement of sediment particles, such as sand, gravel, or silt, along the bed of a channel or river. Live bed condition has been adopted for the present study, because in live bed the behavior of sediment particles can be observed and analyzed under realistic hydraulic conditions. This allows for a better understanding of sediment transport processes, including erosion, deposition, and the overall dynamics of the sediment bed. Additionally, The results obtained from experiments conducted in the live bed condition provides valuable insights for various applications, such as river engineering, bridge and dam design, flood management, and environmental assessments. Understanding how sediment behaves in the live bed condition is essential for making informed decisions and implementing effective measures to mitigate the impacts of sediment transport in natural or engineered systems.

3.4 Dimensional Analysis

There is a number of parameters on which scour depth is dependent such as flow characteristics, sediment properties, and bridge pier characteristics. To understand the scour depth, the relationship of these parameters with the scour depth has been studied through dimensional analysis, as it is difficult to study analytically. Dimensional analysis is an effective tool for investigating the functional relationship of the influencing parameters. To simplify this analysis, a few assumptions are made, such as (a) the sediment used is uniformly graded, (b) there is no viscous effect, and (c) the effect of approach flow

depth is negligible. In the functional relationship for these conditions, the equilibrium scour depth is written as:

$$y_s = f(\rho, \rho_s, g, h, d, u, u_c, d_{50}, P_s, t, t_e) \quad 35$$

where, y_s = scour depth; ρ = water density; ρ_s = density of sediments; g = acceleration due to gravity; d = pier diameter; u = averaged velocity of approaching flow; u_c = critical velocity of the approaching flow; d_{50} = mean particle size of the sediment; P_s = pier spacing; t = time taken for each experimental evaluation; and t_e = time taken for achieving equilibrium scour depth.

From **Eq.35**, dimensionless parameters are obtained using the Buckingham π dimensional analysis method. Three repeating variables are $h, u,$ and ρ representing the geometric, flow and fluid parameters.

$$\begin{aligned} \Pi_1(g) &= \frac{u^2}{gh}, \Pi_2(u_c) = \frac{u}{u_c}, \Pi_3(\rho_s) = \frac{\rho}{\rho_s}, \Pi_4(d_{50}) = \frac{h}{d_{50}}, \Pi_5(d) = \frac{h}{d}, \Pi_6(P_s) \\ &= \frac{h}{P_s}, \Pi_7(t) = \frac{h}{t}, \Pi_8(t_e) = \frac{h}{t_e} \end{aligned} \quad 36$$

$$\begin{aligned} \Pi_4(d_{50}) \times \frac{1}{\Pi_5(d)} &= \frac{h}{d_{50}} \times \frac{1}{h/d} \\ &= \frac{d}{d_{50}}, \Pi_5(d) \times \frac{1}{\Pi_6(P_s)} = \frac{h}{d} \times \frac{1}{h/P_s} = \frac{P_s}{d}, \Pi_8(t_e) \times \frac{1}{\Pi_7(t)} \\ &= \frac{h}{t_e} \times \frac{1}{h/t} = \frac{t}{t_e} \end{aligned} \quad 37$$

By re-arranging these variables, the non-dimensional relationship can be obtained as:

$$\frac{y_s}{d} = f\left(\frac{u^2}{gh}, \frac{u}{u_c}, \frac{d}{d_{50}}, \frac{P_s}{d}, \frac{t}{t_e}\right) \quad 38$$

where $\frac{u^2}{gh}$ is defined as the Froude number (F_r), which represents the intensity of the bulk flow in comparison to the settling velocity of the particles. $\frac{u}{u_c}$ is the relative velocity; $\frac{t}{t_e}$ is the ratio of the time taken for an experimental duration to the time taken to achieve the

equilibrium scour depth; $\frac{P_s}{d}$ is the non-dimensional pier spacing factor; and $\frac{d}{d_{50}}$ is the same for all the flow conditions. Therefore, the impact of three independent dimension-less variables, namely F_d , u/u_c , t/t_e , P_s/d has been studied.

3.5 Velocity Measurement

The velocity measurement has been primarily carried out with the Micro-ADV (Acoustic Doppler Velocimeter), and the point velocity at various points in the flume section flow probe is also used.

3.5.1 Micro-ADV (Acoustic Doppler Velocimeter)

The instantaneous 3-D velocity measurement is conducted by utilizing SonTek 16-MHz Micro-ADV. As illustrated in **Fig. 3.7**, ADV accurately measures the 3-Dimensional velocity components of flowing water, and it is a single-point current meter that works in both high and low flow conditions. The specifications of the ADV are presented in **Table 3.3**. Velocities are measured at the head of the probe in sampling volumes. A signal transmitter is located in the centre of the probe head. The probe head has made up of a single transmitter located in the centre of the probe head. The transmitter generates an acoustic pulse narrow beam projected through the water. The reflection of these pulses from the particles or “scatterers” is reflected and received by the ADV receiver. The location of the sampling volumes is designated by the receiver axes intersection. ADV probes are majorly classified into four types, namely:

- i. 3-Dimensional down-looking probe
- ii. 3-Dimensional up-looking probe
- iii. 3-Dimensional side-looking probe
- iv. 2-Dimensional side-looking probe

A 3-Dimensional down-looking probe has been utilized in this experimental investigation. The X-axis of the down-looking probe represents velocity in the flow direction, and the downward direction is considered positive; the Y-axis represents the velocity of flow in the transverse direction, and the Z-axis represents the velocity of the down-flow; the downward direction is considered positive.

Table 3.3 Specifications of the Micro-ADV

Rate of Sampling (Hz)	0.1 to 50
The volume of Sampling (cc)	0.09
Sampling Volume Distance (cm)	5
Resolution (cm/sec)	0.01
Velocity range (Programmed) (cm/sec)	3, 10, 30, 100, 250
Accuracy of velocity measurement	1% of measured velocity, 0.25 cm/s
Maximum Depth (m)	60
Sensor for Temperature	0.1°C
Compass/Tilt Sensor-Heading, Pitch, Roll Resolution	0.1 Degree
Accuracy of Compass/ Tilt sensor –Heading	± 2 Degree
Accuracy of Compass/ Tilt Sensor – Pitch, Roll	± 1 Degree
Accuracy of Pressure Sensor Strain Gauge (%)	0.1
Accuracy percentage of Resonance Pressure Transducer (%)	0.01
Power of Input	12 – 24 VDC
Typical Power Consumption (W)	2.5 – 4

SonTek 16-MHz Micro-ADV with a 5 *cm* distance to Sampling Volume, which had a maximum sampling rate of 50 *Hz* and volume of 0.09 *cc*, has been employed. In our study, the sampling rate for the data collection has been selected as 25 *Hz*. The output data from the ADV are filtered by neglecting the negative values. In order to achieve the time-independent average velocity, the sampling duration has been fixed to 5 minutes by considering the turbulence intensity of flow. The ADV readings are taken at four vertical lines upstream and downstream of the pier and the inlet and outlet at the working section. Each vertical line consists of three horizontal points where ADV reading has recorded at bed level, surface level, and at 0.6 *h* (average velocity).

However, the vertical resolution of the measurements has higher above the scour hole. According to (Sarker 1998), the range of velocity should be kept as small as feasible, if the greatest estimated velocity is 8 cm/sec, the range of velocity should be adjusted to 10 cm/sec. This is due to the fact that data noise grows with an increase in the velocity range and thus degrades accuracy at high sampling rates. SonTek's Horizon ADV software (v1.20) has been used for the data collection in this dissertation.

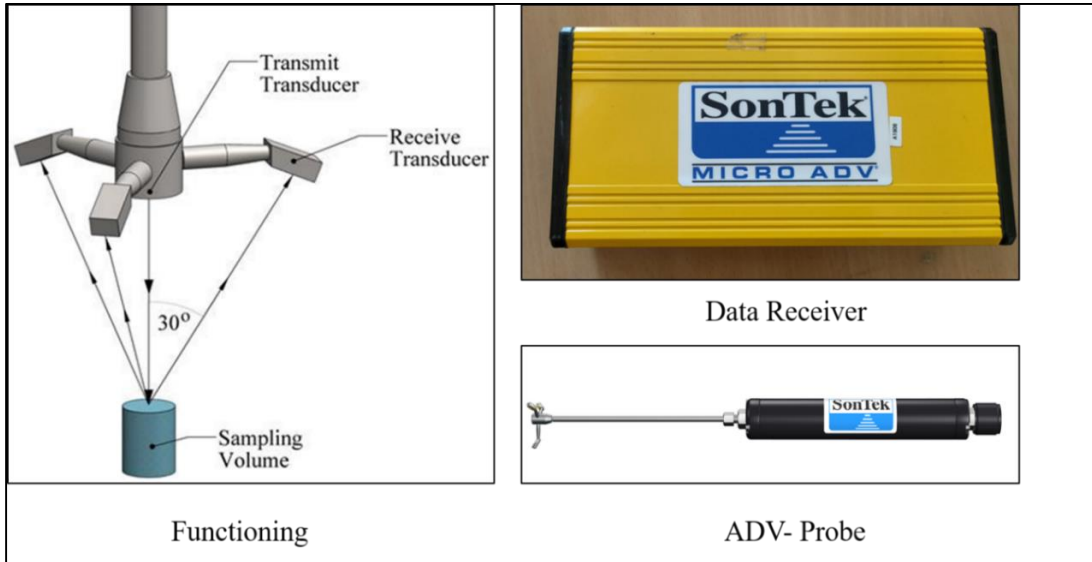


Fig. 3.7 *Micro-ADV (Acoustic Doppler Velocimeter)*

3.5.2 Flow Probe

The Flow Probe is a device that measures flow in open channels and pipes flow. As illustrated in **Fig. 3.8**, the velocity probe comprises a turbo propeller-type sensor probe handle with a digital display. Actual velocity averaging is used in the water flow meter to obtain precise flow measurements. The flow probe specifications are shown in **Table 3.4**.



Fig. 3.8 Flow Probe

Table 3.4 Specifications of Flow Probe

Range of velocity meter (m/sec)	0.1 to 6.1
Precision Accuracy (FPS)	0.1
Averaging	Actual digital running average and updates per sec.
Digital Display	LCD, Glare and UV Protected
Display Control	Four button
Data Logger	30 data sets
Working Power	Internal Lithium Battery
Operating Temperature (°C)	-20 to 70
Storage Temperature (°C)	-30 to 80

3.6 Experimental Procedure and Data Acquisition

1. **Placement of the bed material:** The first step is the placement of the uniformly graded Yamuna River sand in the working section (5m length) shown in **Fig. 3.9 (a)**. The whole sand bed has been levelled carefully with the help of the wooden bar. To check the level of the bed, a vernier point gauge is utilized (by checking bed elevation at random points).



Fig. 3.9 (a) Placement of sand bed; (b) placement of the pier

2. **Placement of the bridge pier:** A hollow cylindrical pier model of diameter 5 cm has been installed in the centre of the working section, as shown in **Fig. 3.9 (b)**. The pier model has been installed in a vertical direction to achieve better results.



Fig. 3.10 Installation of SeaTek transducers around the pier

3. **Placement of the ultrasonic transducers:** Once the pier is installed properly, the ultrasonic transducers have been mounted on the pier model to measure the accurate scour depth around the pier, as shown in **Fig. 3.10**. The details of the ultrasonic transducers have been provided in section 3.2.5.
4. **Water filling:** To fill the water up to the desired water depth, a tailgate has been closed, and water is filled into the flume section at a very low rate of flow. The flow rate is kept low, so there will be zero particle movements from the bed. As the desired depth of flow is achieved, the rate of flow is increased gradually up to the design discharge. Once the flow rate becomes constant, the tailgate is opened to maintain the desired water depth. This step should be carried out very carefully, as flow depth and rate of flow are directly related.
5. **Velocity measurement:** Velocity measurement has been carried out with Micro-ADV, venturimeter, and Velocimeter. For the three-point velocity at various points, Micro ADV has been utilized, and details of the Micro-ADV have been provided in **section 3.5.1**. The flow velocity of the water venturimeter and V notch has been utilized.
6. **Duration of run:** A series of experiments were conducted for durations of 72 hours and 8 hours to examine the scour depth characteristics over time. Specifically, five experiments were performed for the 72-hour duration, while the remaining 227 experiments were conducted for the 8-hour duration.
7. **Data collection:** Transducer data has been recorded after every 10 minutes for the first 60 minutes and after every 30 minutes till the completion of the experimental duration around the pier. Along with the transducers, experimental data has also been recorded manually with the vernier point gauge.
8. **Scour depth measurement:** At the end of each experimental test, the water pump has been switched off, and the flume section has been emptied. After 24 hours of water drainage, the bed level measurements have been recorded with a vernier point gauge (least count 0.1 mm).

3.7 Computational Analysis

3.7.1 General overview of GEP

Gene Expression Programming (GEP) is a genetic programming extension (GP). GEP combines the advantageous aspects of GAs and GP approaches to overcome some of the limitations of AI. GEP is a proficient computing technique of genotype/phenotype system, with the separate functioning of genotype and phenotype, whereas these functions are mixed in GP Ferreira (2006) and Guven and Gunal (2008). The fundamental difference between these three algorithms is based on their nature: (a) GA: the individuals are of fixed length and are stringed linearly; (b) GP: the individuals are of different shapes and sizes and are stringed nonlinear; (c) GEP: individuals have a definite length and are encoded in linear strings with fixed lengths chromosomes, which are represented as expression trees with various sizes and shapes.

The advantages of the GEP are:

1. Chromosomes are basic entities: they are linear, compact, and relatively tiny, making them easy to change genetically (replicate, mutate, recombine, transpose, etc.).
2. Expression trees (ET's) are only the expression of their particular chromosomes; they are the entities upon which selection operates, and they are selected to reproduce with change based on fitness.

The chromosomes in GEP are composed of one or more than one gene pair of linear and fixed-length symbolic string. Despite the fixed length of these chromosomes, GEP can code ET's of different shapes and sizes. Genes consist of a head and tail; the head contains the function set and terminal set, whereas the tail contains only the terminal. Each programming head is selected, and the tail can be evaluated from **Eq. 39**, as the tail works as a head function.

$$t = H(n - 1) + 1 \quad 39$$

Where, t = tail length, H = head length, and n = number of argument

Seeing the potential of GEP in terms of simple modelling, easy coding, and faster computations, it has gained popularity over other tools. GEP develops computer programmes, which are subsequently encoded in linear chromosomes and generated or interpreted into ET's. ET's are complex computer programs that, in most cases, are created to address a specific problem and are chosen based on their functionality. As genetic operators act at the chromosomal level, an advantage of the GEP technique is that it simplifies the creation of genetic variation. Genetic operations, including mutation, inversion, transposition, and recombination, are used to reconfigure chromosomes containing one or more genes. After that, one of the fitness function equations available in the literature is used to evaluate the fitness of each chromosome in the original population. The second advantage of GEP is that it is mutagenic, allowing for the growth of more sophisticated applications. Seeing these benefits, GEP seems an excellent choice for a perfect mathematical model the scour depth. For more insight on GEP, readers are encouraged to see Ferreira (2006) and Teodorescu and Sherwood (2008)

A linear chromosome, or expression tree, contains the genetic information of GEP models. ETs are fully advanced computational models typically designed to address a certain issue and are chosen based on how well they do. The big discovery made by GEP is the development of chromosomes that could represent any expression tree. The information on the GEP chromosomes is in a new language known as the Karva language, developed by Ferreira (2001). Furthermore, the chromosomal layout enabled the creation of a large number of genes. Regardless of how much or how deeply we modify the chromosomes, the structural and functional arrangement of GEP genes always ensures the development of correct programmes. The genes are organized structurally into a head and a tail.

GEP begins by generating a random population of distinct chromosomes. Chromosomes have a constant length and can comprise one or even more genes. Based on their fitness value, the roulette wheel technique chooses the best chromosomes. The chosen chromosomes are then replicated with minor alterations made by genetic operators; this operation is continued till the desired number of generations or the requisite precision is obtained. The most frequent genetic operators used to change chromosomes include mutation, inversion (which reverses the sequencing inside the head of a gene), insertions

sequence transport, root insertions sequence transport, gene transport, single or double crossover, and gene crossover (Ferreira 2002, 2006).

3.7.2 GEP Modelling

The advanced software programme Gene Xpro Tools 5.0 has been used to encourage the creation of GEP-based models for estimating the maximum scour depth. The GEP parameters and processes are then described in six phases to stimulate the production of the mathematical formula required to estimate the local scour.

1. To begin with, GEP modelling's first step is generating an initial population. As suggested by (Ferreira 2001), any population can be utilized in the underlying populace, but a population of 30 to 100 offers optimal results.
2. After instating the population size, the fitness function is measured for measurement of fitness function for each chromosome by assessing RMSE.
3. After choosing the RMSE as a fitness factor, the following stage is to select the function and terminals for each chromosome.
4. The next advance is managing the architecture of the chromosomes by choosing the Gene numbers and length of head and tail for every gene.
5. The connecting function between the sub-expression trees (sub-ETs) will be chosen in the following stage.
6. Following the preceding stage, genetic operators for chromosome design are chosen. Transposition (gene transposition, IS, and RIS), mutation (gene recombination, both one-point and two-point), inversion, and DC-specific genetic operations and their rates are among these genetic operators.

3.7.3 Modification

Individuals are selected to reproduce with modification based on fitness and the luck of the roulette wheel, resulting in the genetic diversification required for long-term evolution. Except for replication, in which all selected individual chromosomes are rigidly replicated, all of the remaining operators choose chromosomes randomly to be modified. Except for mutation, each operator can only edit a chromosome once. We will now go into further details about the operators in GEP.

3.7.3.1 Replication

Although necessary, replication is the least intriguing operator: it adds little to the operation on its own. Chromosomes are faithfully replicated in the subsequent programmes based on fitness and the luck of the roulette wheel. As a result, the chromosomes of the chosen individuals are replicated as many times as the results of the roulette.

3.7.3.2 Mutation

Mutations can develop at any point along the chromosome. The structural organization of chromosomes, on the other hand, must be preserved. Any symbol in the heads can change into another function or terminal; the terminal can only convert into terminals in the tails. The structural structure of chromosomes is preserved in this manner. It is important to note that there are no limitations in GEP on the type of mutation or the number of mutations in a chromosome: all newly produced programmes are syntactic and semantic accurate programmes.

3.7.3.3 Transposition and insertion sequence elements

GEP transposable elements are pieces of the chromosome that can be activated and hop to another location on the chromosome. There are three kinds of transposable elements in GEP:

1. A sequence of transposition of insertion
2. A sequence of root transposition
3. A sequence of gene transposition

3.7.3.4 Recombination

In all circumstances, two parent chromosomes are chosen randomly and matched to exchange material. There are three types of recombination in GEP:

1. Rate of one-point recombination
2. Rate of two-point recombination
3. Rate of gene recombination

3.8 Summary

This chapter presents a comprehensive explanation of the experimental setup and methodology employed in the study. Section 3.1 offers a general introduction to the topic, providing an overview of the research area. In Section 3.2, we describe the rectangular recirculating flume used, which has dimensions of 14 meters in length, 1.10 meters in width, and 0.8 meters in depth. This section also includes information about the flow rate measurement devices utilized, namely the V-Notch and Venturimeter. To accurately and reliably measure the scour depth around the piers, we employed the SeaTek Ultrasonic ranging system, and details about this instrument are provided as well. Additionally, the arrangement of the piers used in the experiments is listed in this section.

Section 3.3 focuses on the materials used for the experimentation, including the sediment transportation process. In Section 3.4, we conduct dimensional analysis by considering the parameters that influence the scour depth. Section 3.5 provides details about the velocity measurement devices employed, specifically the Micro ADV and Flow Probe. In Section 3.6, we present a detailed account of the experimental procedure, including the data acquisition process. Lastly, in Section 3.7, we outline the methodology and approach used for the computational modeling component of the study.

CHAPTER 4

RESULTS AND DISCUSSION

4.1 Introduction

This chapter provides the details of the experimental results conducted for the fulfillment of the objectives of this dissertation. Experiments data set for local scour around the single pier, two piers and three piers have been analyzed for varying pier spacing and rate of flow. Influence of the factors affecting the scour depth has been carried out in detail. Furthermore, this chapter also describes the temporal evolution of scour depth and scour hole development pattern. Additionally, semi-empirical equations derived by using GEP modelling tool for scour depth estimation are also proposed.

4.2 Single pier

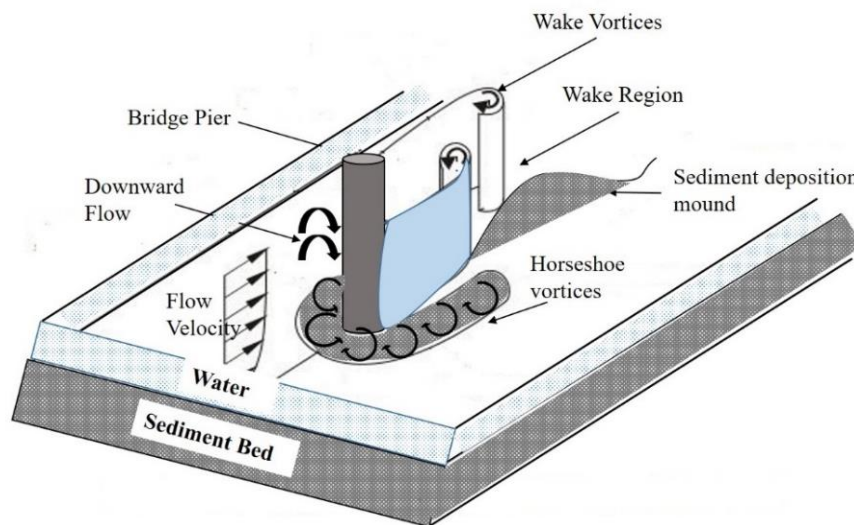


Fig. 4.1 Mechanism of bridge scour around single pier

The never-ending search for improved materials, building methods, and analysis and design methodologies has solved the majority of the early obstacles in bridge construction. However, since man learnt to construct piers and abutments in the stream channel to cross rivers, scour of the stream bed has been identified as one of the primary causes of bridge failures. Nonetheless, every year, bridge failures are added to the list of disasters that have happened due to scouring of the stream bed around the hydraulic structures. This scour

phenomenon can be described as, the erosion and deposition sediment on the riverbed around the bridge supports such as piers and abutments due to the flow field, it is a resultant of the vortex action of accelerated water around the base of the bridge pier. Vortex action enhances sediment transport and creates a scour hole around the pier; material is also deposited on the downstream side of the pier in the form of a sediment mound. The flow pattern and vortices formation around the pier are described in the **Fig. 4.1**.

4.2.1 Experimental programme and flow characteristics

Details of the experimental setup and instruments used has been discussed in the chapter 3. As discussed in previous chapter all the experiments has been carried out in a recirculating masonry flume, and experimental setup for single pier has been shown in **Fig. 4.2**. Experimental programme has been conducted for uniform sediments under five rate of flow for the single pier. Flow characteristics used for single pier study has been presented in **Table 4.1**. The values of Coefficient of uniformity, C_u and Coefficient of curvature C_c are $C_u < 6$ and $1 < C_c < 3$, hence the sand sediment will be considered as uniformly graded, as stated by (Arneson et al. 2012). Pier model of diameter, D , 50 mm made up of acrylic sheet is laid in the center of the working section. Pier model has been mounted with the SeaTek ultrasonic ranging transducers at the four point (P_1 , P_2 , P_3 , and P_4) around the cylindrical pier as shown in **Fig. 4.3**. The details of the SeaTek ultrasonic ranging transducers are provided in chapter 3, Section 3.2.5.

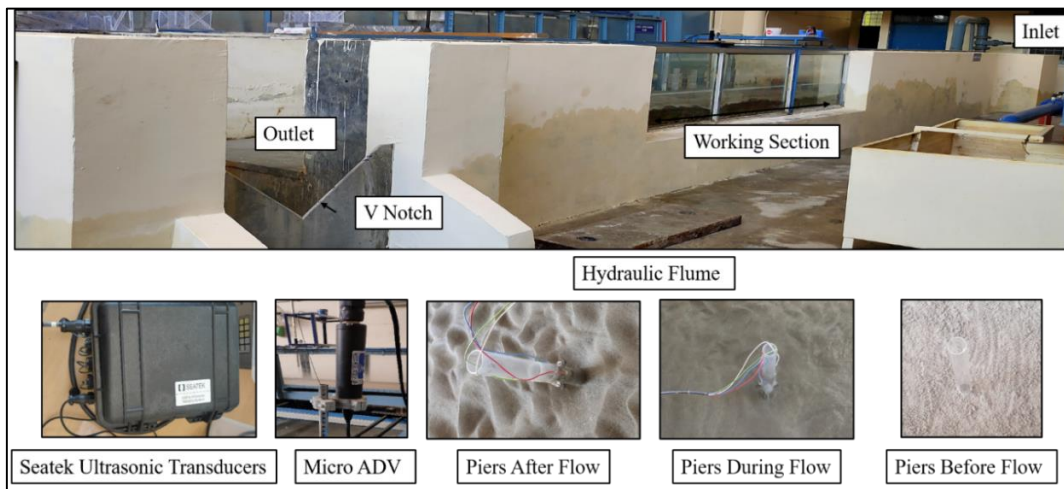


Fig. 4.2 Experimental setup of hydraulic flume for single pier

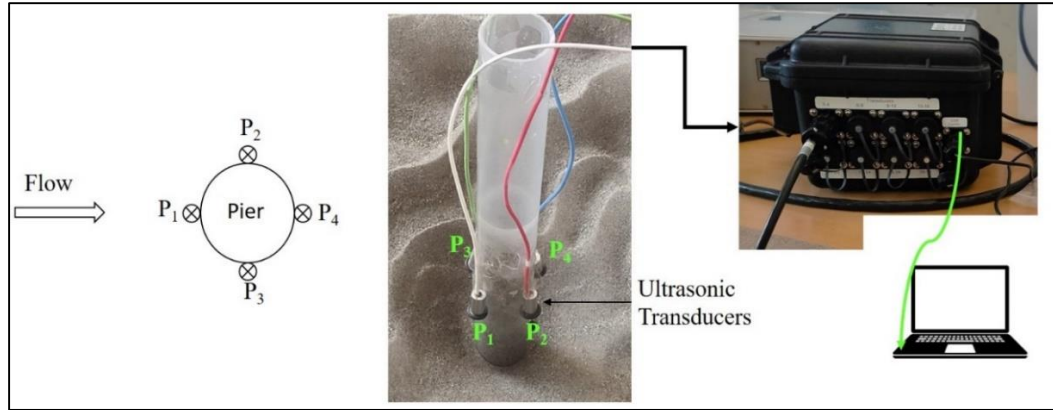


Fig. 4.3 Position of ultrasonic transducers around the bridge pier at P_1 , P_2 , P_3 , and P_4

Table 4.1 Hydraulic parameters for the experimental study

Rate of Flow Q ($\text{m}^3\text{sec}^{-1}$)	Depth of flow h (m)	Average velocity V (ms^{-1})	Critical velocity V_c (ms^{-1})	Froude Number $F_r = V/\sqrt{gh}$	Relative velocity V/V_c
0.031	0.145	0.195	0.242	0.163	0.81
0.037	0.163	0.205	0.247	0.162	0.83
0.045	0.184	0.223	0.252	0.166	0.89
0.050	0.192	0.238	0.254	0.185	0.94
0.058	0.21	0.252	0.257	0.175	0.98

For precisely measuring the pattern of the scour evolutions, bed measurements have been recorded with the SeaTek ultrasonic ranging transducers. Transducers data has been recorded after every 10 minutes for the first one hour, and after every 30 minutes for the next (71 hours) 4,260 minutes of the experimental duration. At the end of each experimental test, the water pump has been switched off, and the flume section has been emptied. After the 24 hours of water drainage, the bed level measurements has been recorded with a vernier point gauge.

To finding the equilibrium scour depth for the bridge pier has always been controversial. Few studies, explains the equilibrium scour depth criteria these are included in this section. According to (Melville and Chiew 1999) and (Grimaldi 2005), equilibrium scour depth is

achieved, if the increase in the scour depth is 5% less than the diameter of pier in last 24 hours of experimental run. Additionally, Cardoso and Bettess (1999) stated that if the gradient of scour evolution curve is approaching to zero than it can be said that, the equilibrium scour depth has been achieved. To obtain equilibrium state in small-scale lab experiments on clear-water scour depth evolution at bridge supports, the experiments must be run for an extended period of time. Keeping in mind the aforementioned criterion, duration for single pier experimental run lasted for 72 hours, and the increase in scour depth has been found to be less than 5% of the pier diameter.

4.2.2 Results and Discussion

4.2.2.1 Temporal evolution of scour depth around single pier

The temporal scour depth for the uniform graded sediment under clear water condition shows a linear relationship with the rate of flow. The evolution of scour depth with the time is investigated at the four observation point P₁, P₂, P₃, and P₄, by utilizing the ultrasonic transducers. The results of the temporal evolution of scour for are plotted in **Fig. 4.4** and **Fig. 4.5**. On the basis these results the whole temporal scour evolution process has been classified into three zones, i.e. Zone 1, Zone 2 and Zone 3. In zone 1, evolution of scour around the pier at P₁, P₂, P₃, and P₄ is increasing at the rate of 0.0137 mm/sec, 0.0088 mm/sec, 0.00904 mm/sec and 0.0099 mm/sec respectively up to 500 minutes of experimental duration. The rate of scour evolution at P₁ and P₄ is higher than the rate at P₂ and P₃ due to the active participation of the (horseshoe and wake) vortices on the upstream and downstream sides of the pier in the initial phase of experiments. In Zone 2 (500-3000 minutes), the rate of scour evolution at P₁, P₂, P₃, and P₄ is 0.00075 mm/sec, 0.00048 mm/sec, 0.00055 mm/sec and 0.00066 mm/sec respectively. The rate of scour evolution in the zone 2, is decreased by 94.5%, 94.5%, 93.91% and 93.33% than the rate of scour evolution in Zone 1. In zone 3 (3000- 4320 minutes), the scour evolution rate at P₁, P₂, P₃, and P₄ is observed as 0.00051 mm/sec, 0.00039 mm/sec, 0.00023 mm/sec and 0.00026 mm/sec respectively. The rate of scour evolution is decreased by 98.1%, 97.72%, 98.6% and 98.5% than the Zone 1. After the lapse of the 3000 minutes (50 hours) of experimental run, the scour evolution rate is approximately 3% and the gradient of the curve is almost approaching to zero. Which clearly states that the equilibrium condition has been achieved,

but in order to evaluate the further trend of the scour evolution experiment kept running till 4320 minutes (72 hours).

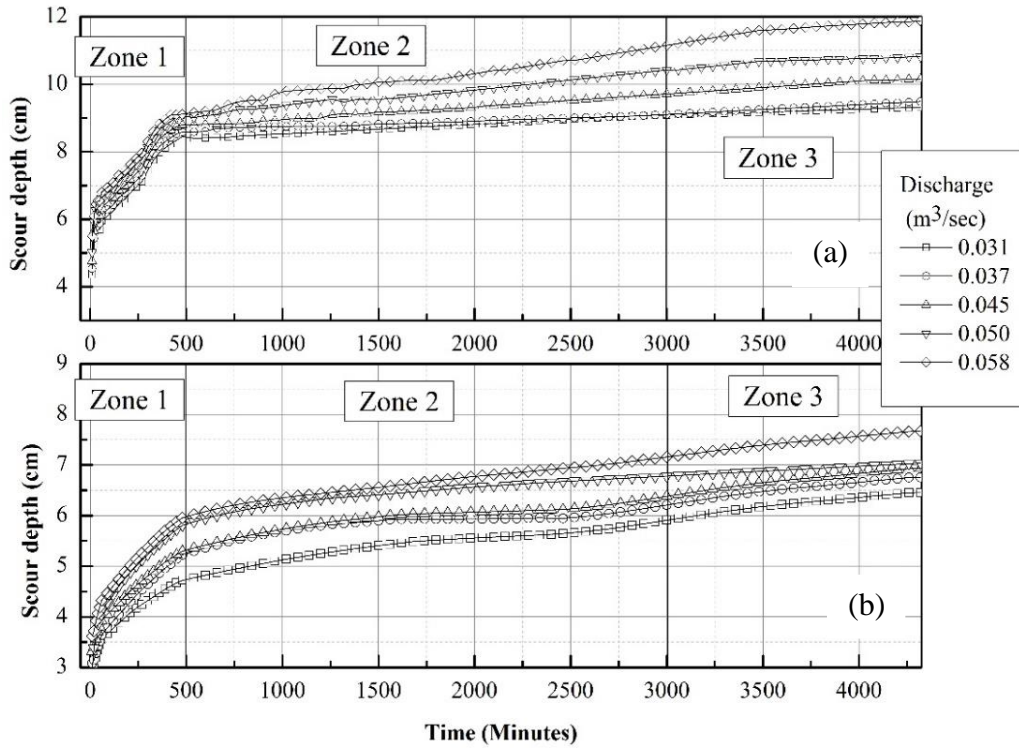


Fig. 4.4 Temporal scour depth at the Observation points (a) P_1 and (b) P_4

The results are in corroboration with the criteria proposed by (Melville and Chiew 1999), written in **Eq. 40**

$$\frac{d(Y_s)}{dt} \leq \frac{5\% \text{ of diameter of the pier}}{24 \text{ hours}} \quad 40$$

The value of $\frac{d(Y_s)}{dt}$ has been computed approximately 3% of D. From the results presented here, it can be concluded that, approximately 90% of the scour depth is achieved in the initial 500 minutes of the experimental run. So, it can be said that, the minimum duration for the scour experiments should be kept 500 minutes for the uniform sediment.

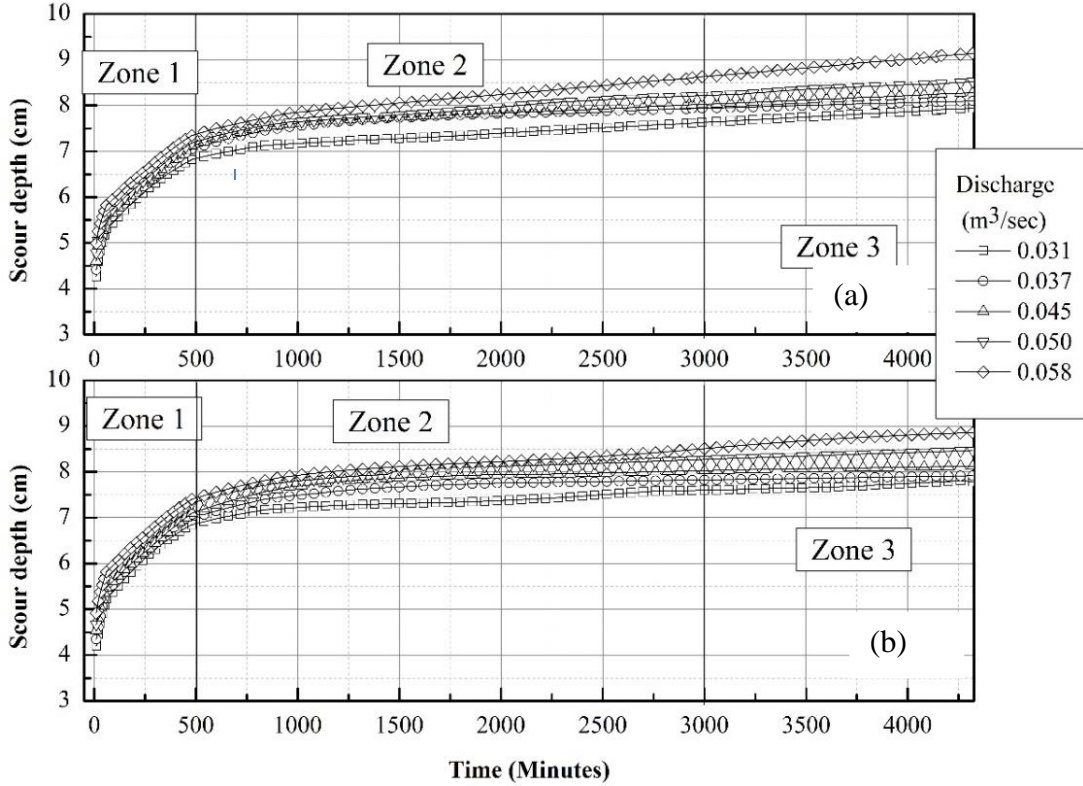


Fig. 4.5 Temporal scour depth at the observation points (a) P_2 and (b) P_3

The maximum scour depth has been calculated by using the Melville and Chiew, (1999) equations, written below in **Eq. 41** and **Eq.42**. Despite the fact that various equations have been developed to estimate the time of equilibrium scour depth development, (Melville and Chiew 1999) equation have been utilized. Because this equation is observed to be very practical and simple, with the ability to predict a reasonably precise outcome. As a result, this equation has been utilized for additional analysis of temporal development scour depth around bridge piers.

$$Y_{t_e} = \exp \left\{ -0.03 \left| \frac{V_c}{V} \ln \left(\frac{t}{t_e} \right) \right|^{1.6} \right\} \quad 41$$

Where, t_e is given as:

$$t_e \text{ (days)} = 30.89 \frac{D}{V} \left(\frac{V}{V_c} - 0.4 \right) \left(\frac{h}{D} \right)^{0.25} \quad \text{for } \frac{h}{D} < 6, \frac{V}{V_c} > 0.4 \quad 42$$

Where, Y_{t_e} = scour depth percentage attained at equilibrium time; V_c = approaching flow critical velocity; t = duration of the experiment; t_e = time needed to achieve equilibrium scour depth; D = diameter of the pier; h = depth of flow.

4.2.2.2 Scour Hole Formation

The formation of scour hole around the single pier is a resultant of the interplay of vortex formations and sediment erosion. **Fig. 4.6** depicts the scour hole formed after 72 hours of experimental run, with the flow discharge as a third parameter. The maximum scour depth is recorded at the nose of the pier. However, scour created downstream of the pier is smaller than the scour hole developed at upstream of the pier. In the early hours of the experiment, or in zone 1, the scour hole formation around the pier grows in both directions X (Flow direction) and Z (Depth of scour hole). Following that, the scour hole evolution rate in the Z direction is seen to be much slower than in zone 1, yet the scour hole has developed in the X direction by depositing sediment brought from the pier and from within the scour hole. This sediment deposition is getting close to 4 cm above the bed level. The maximum width and depth of scour hole is observed for rate of flow $0.058 \text{ m}^3/\text{sec}$. The scour hole extends on the upstream of the pier up to 20 cm and on the downstream side up to 75 cm. The scour depth does not grow much or at all as the scour hole in zone 3 is not developing further.

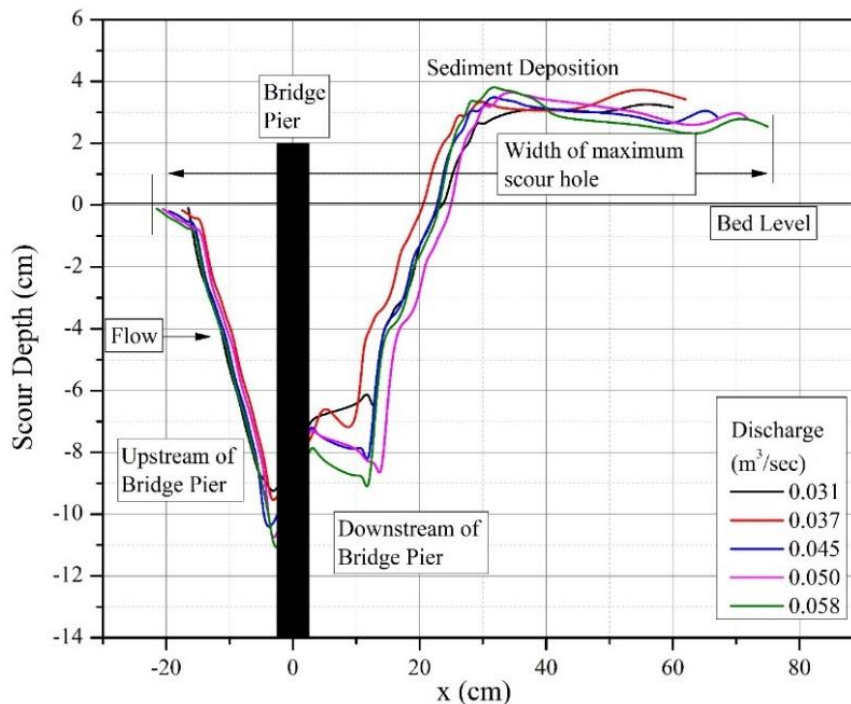


Fig. 4.6 Elevation of scour hole developed after 72 hours of experimental run

4.2.2.3 Flow Shallowness (h/D) effect

The influence of flow shallowness is less well understood due to the difficulties of obtaining credible data in flowing river (Yang et al. 2019). The effect of the flow shallowness on the equilibrium time (t_e in minutes) of the scour depth attainment has been presented in the **Fig. 4.7**. The equilibrium time (t_e) has been computed by using the Melville and Chiew (1999) expression written below in **Eq. 43-45**

$$\frac{Y_s}{Y_{se}} = \exp \left\{ -0.03 \left| \frac{V_c}{V} \ln \left(\frac{t}{t_e} \right) \right|^{1.6} \right\} \quad 43$$

$$t_e \text{ (days)} = 48.26 \frac{D}{V} \left(\frac{V}{V_c} - 0.4 \right), \quad \text{for } \frac{h}{D} > 6 \quad 44$$

$$t_e \text{ (days)} = 30.89 \frac{D}{V} \left(\frac{V}{V_c} - 0.4 \right) \left(\frac{h}{D} \right)^{0.25}, \quad \text{for } \frac{h}{D} \leq 6 \quad 45$$

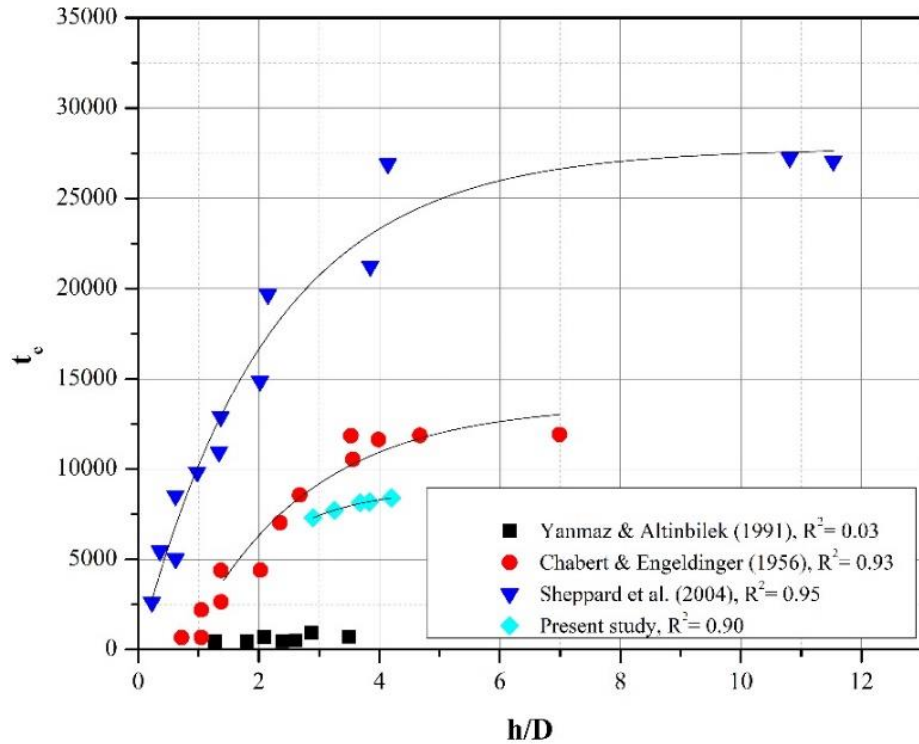


Fig. 4.7 Flow shallowness effect on the equilibrium time t_e

Fig. 4.7 shows the relationship of the flow h/D and t_e for the Yanmaz and Altinbilek (1991), Chabert and Engeldinger (1956), and Sheppard et al. (2004) with the value of

coefficient of determination as 0.03, 0.93, and 0.95 respectively. The value of coefficient of determination for the present study has been observed as 0.90.

4.2.2.4 Froude Number Effect on the Scour Depth around Single Pier

As the Froude number has been increased from 0.162 to 0.175, the scour depth increases with the increase in the Froude number. As we know that the Froude number is the ratio of the inertial force and gravitational force, it is dependent on the velocity of flow and depth of flow in the channel section. So, as the rate of flow increases, Froude number also increases whereas with the increase in the flow depth Froude number decreases and hence the scour depth increases. Same trend has been observed in case of single pier, as shown in **Fig. 4.8**. At the nose of the pier maximum scour depth has been observed for the $F_r = 0.175$ and **Fig. 4.8** also shows the trend of the scour depth at all the four observation points around the single pier with the increasing Froude number values.

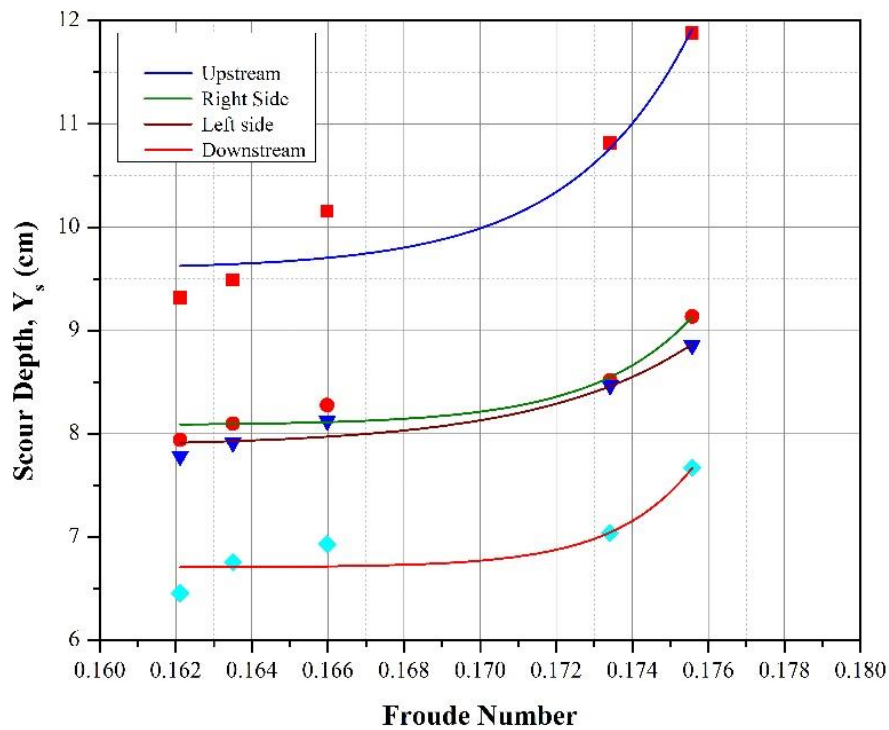


Fig. 4.8 Trend of scour depth at four observation points for the single pier with the increasing Froude number

4.2.2.5 *Flow-Field using CFD*

The flow-field around the single pier is mainly characterized by the presence of various vortices around the pier. These vortices formed as a result of the pier presence in the flow direction, which blocks a major portion of the flow, causing the flow to slow as it approaches the pier. The approaching flow divides and spreads around the pier edges some distance in front of the pier. The incoming flow to the pier is diverted into upward and downward flow. The downward flow is accelerated by the considerable pressure differential created by the vertical flow velocity and behaves as an imping jetting on the bed surface, causing weak circulation near the bed and resulting in the development of the horseshoe vortex. Near the free surface around the pier, circulation waves are generated which are termed as bow waves. These bow waves enhance the flow depth upstream of the pier. The bow wave interacts with horseshoe vortex and weakens them in shallow flow depths. The wake vortices creates intense circulation over the full flow depth, and generating a wake zone behind the pier. Wake vortices are often identified by small-scale eddies at the surface of the water behind the pier that fade as they flow downstream. The axes of the wake vortices are practically vertical, and they work like a vacuum cleaner, sucking and suspending the bed material into the main flow-field. Because of the separation and formation of many vortices, the flow-field around a pier is exceedingly complicated vortices (horseshoe, wake, and bow).

In order to comprehend the scour process and predict the scour pattern and equilibrium scour depth understanding of the flow-field around a pier is mandatory. The flow-field surrounding the pier has been simulated using ANSYS fluent software. In Ansys Fluent two-phase modelling has been used for simulating the combination of water and sediment. The Flowing water is considered as one phase and sediment is considered as another phase. These two phases flows together at their own velocity, density, temperature and viscosity. Two phase modelling is appropriate for the accurate simulation of the bridge scour during the flooding events (Xiong et al. 2017). Two phase modelling is applicable to Volume of fluid model, Eulerian Model, and Mixture Model. In this dissertation Eulerian model has been utilized for the modeling, because in Eulerian model each phase has independent fraction of volume and velocity flow field. the technical details of the Eulerian two-phase

modelling are described in Xiong et al. (2016). To solve the two phase system, water is termed as an incompressible fluid without any exchange of heat. So, the three basic conservation laws are applicable, these are: conservation of mass law, conservation of momentum law and conservation of energy law.

1. Conservation of mass law

Conservation of mass law states that mass can neither be created nor be destroyed, or mass of a system remains constant over a period of time.

$$\frac{\partial \rho}{\partial t} + \nabla(\rho V) = 0 \quad 46$$

$$\nabla \cdot V_w = 0 \quad 47$$

$$\nabla \cdot V_s = 0 \quad 48$$

Where, ρ is the density of water, V_w and V_s is the velocity of water and sediment.

2. Conservation of momentum law

Conservation of momentum law states that the total momentum of two or more bodies operating on one other in an isolated system remains constant until an external force is introduced.

$$\frac{\partial}{\partial t}(\alpha_w \rho_w V_w) + \nabla \cdot (\alpha_w \rho_w V_w V_w) \quad 49$$

$$= -\alpha_w \nabla p + \nabla \cdot \tau_w + \alpha_w \rho_w g + [K_{ws}(V_s - V_w)] + \alpha_w \rho_w F_w$$

$$\frac{\partial}{\partial t}(\alpha_s \rho_s V_s) + \nabla \cdot (\alpha_s \rho_s V_s V_s) = -\alpha_s \nabla p + \nabla \cdot \tau_s + \alpha_s \rho_s g + [K_{sw}(V_w - V_s)] + \alpha_s \rho_s F_s \quad 50$$

Where α_w and α_s are the volume fraction of water and sediment, respectively; ρ_w and ρ_s are the density of water and sediment, respectively; V_w and V_s are the velocity of water and sediment, respectively; τ_w and τ_s are the shear stress of water and sediment, respectively; F_w and F_s are the body force of water and sediment, respectively; K_{ws} and K_{sw} are the coefficient of momentum exchange, respectively.

3. Conservation of energy law

The entire energy of an isolated system is represented by an energy conservation equation that remains constant. The energy conservation equation and the momentum conservation equation are not totally independent in this investigation. As a result, if the momentum

conservation equation is already met, there is no need to add an energy conservation equation.

The flow-field originates and directs the progression of a local scour pattern around a pier, which affects the flow-field via continual interactions. In this section scour evolution has been studied by dividing the whole process in three stage, (a) initial stage, (b) intermediate stage, and (c) final stage. The scour geometry profile has been updated by applying the dynamic mesh technique herein from the commercial simulating program ANSYS Fluent. Using this technique, the computational grid of the scoured riverbed mesh has been developed, meshing is shown in **Fig. 4.9**. The k- ϵ model has been utilized for predicting the influence of turbulence and for simulating the flow field around the bridge pier.

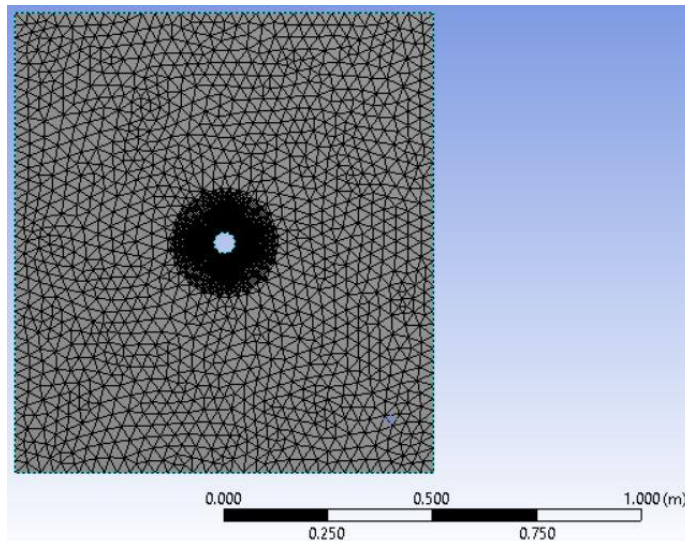


Fig. 4.9 Meshing of the circular cylinder

To provide the boundary conditions wall functions have been utilized for the turbulent sediment transport around the pier. The distribution of velocity at the entrance section plays an essential role in the flow field. The velocity distribution can be determined by using numerical flow model, by considering the velocity distribution of suspended sediment particles and by the concentration of the suspended sediment. The design for the boundary conditions has been shown in **Fig. 4.10**. The side walls are smooth and bottom wall is rough, the smooth layers have been used due to the fluid domain, and bottom wall is rough because it acts as a fluid and sediment interface.

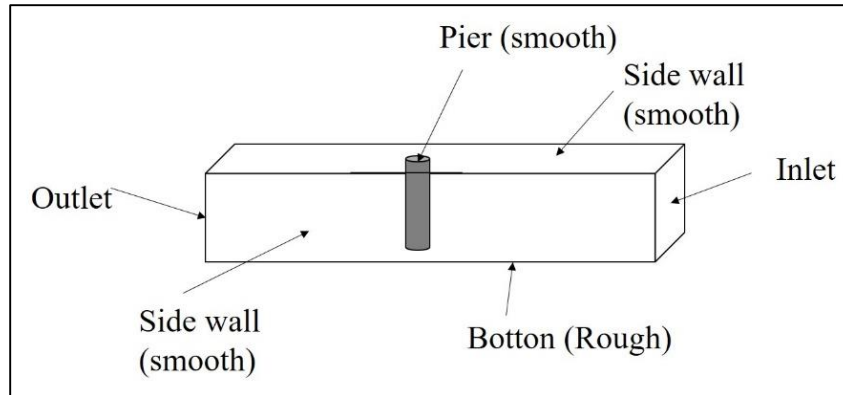
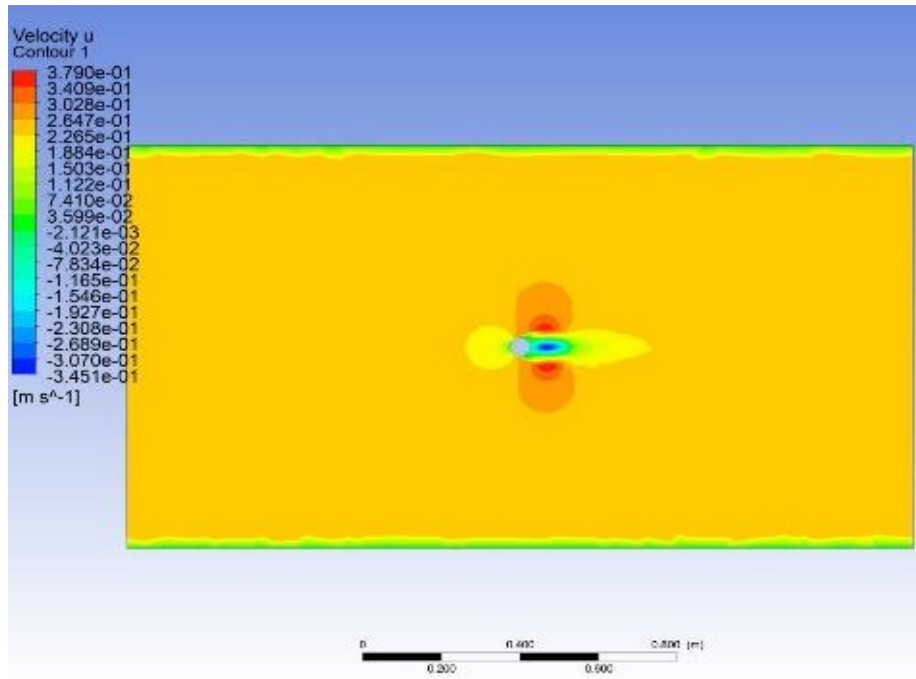


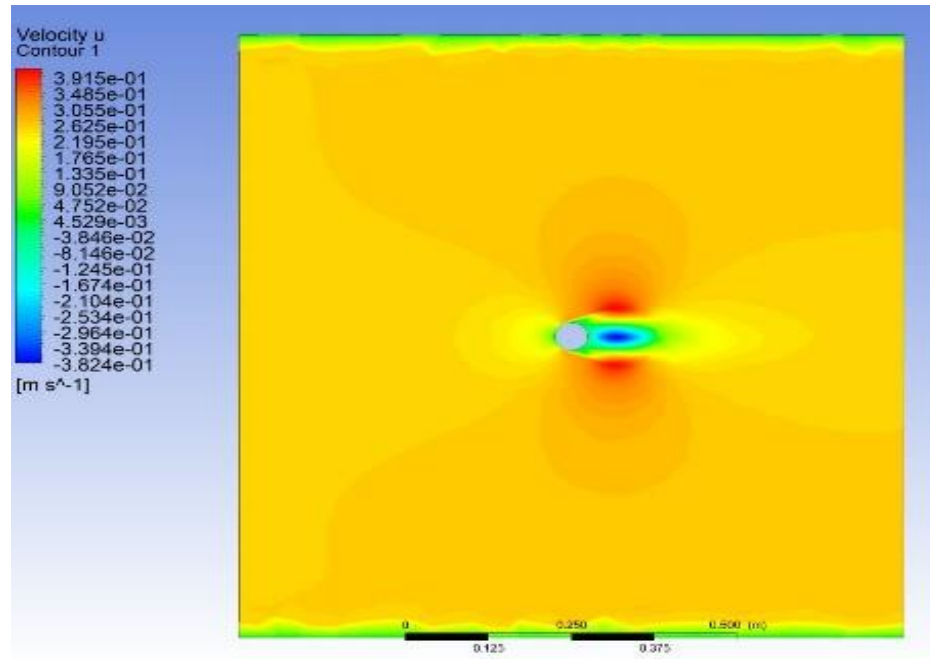
Fig. 4.10 *Boundary condition for the channel section*

Fig. 4.11 shows the velocity contours and **Fig. 4.12** shows the contours of streamline around the single pier for three stages (a) initial (b) intermediate and (c) final stage respectively. Here the instantaneous velocity component is represented by 'u'. In the initial stage of the simulation, the velocity contours are observed in the close vicinity of the pier. As the flow velocity and time of experimental study is increased the velocity distribution over the whole bed and around the pier started evolving this stage is termed as intermediate stage, while the flow-field is growing and the formation of vortices around the pier has started. In the final stage of the simulation, the formation of vortices around the pier is present on the upstream of the pier and on the downstream side of the pier von Kármán vortices have been observed. Von Kármán vortices are formed due to the repetitive presence of the swirling vortex, which are resultant of the vortex shedding. These vortices are the reason of flow separation around the cylindrical pier.

(a)



(b)



(c)

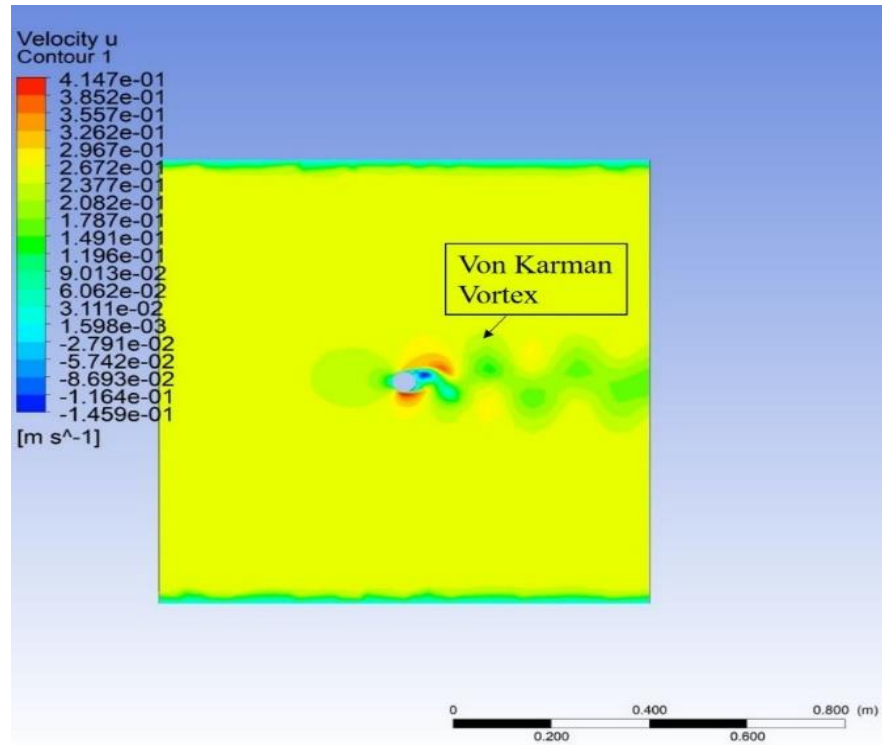
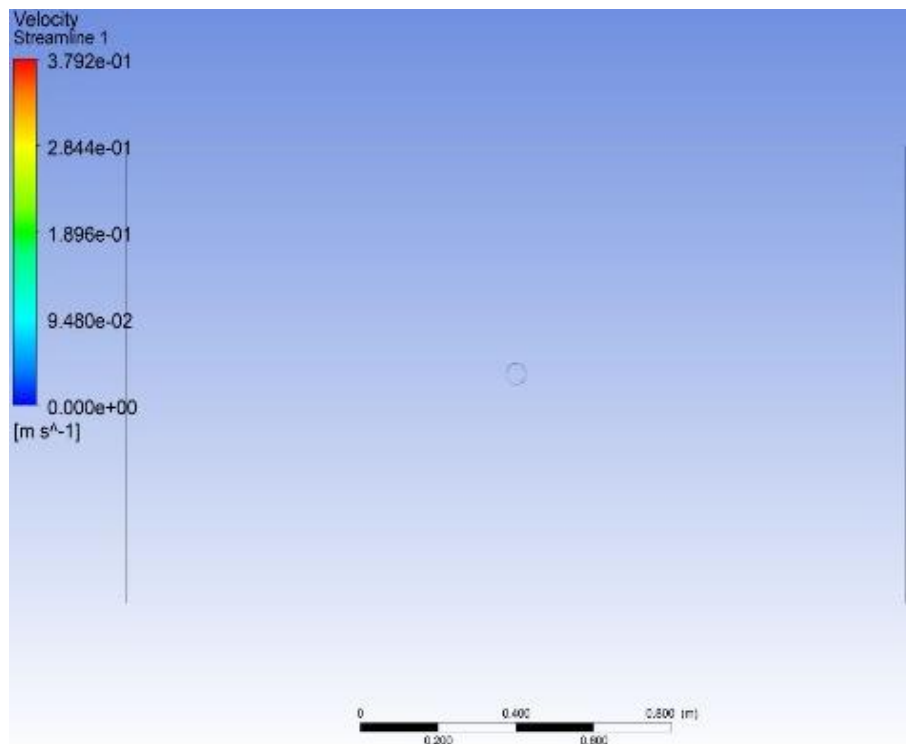


Fig. 4.11 Velocity contour of the flow around the bridge pier; (a) Initial stage, (b) Intermediate Stage, (c) Final Stage.

(a)



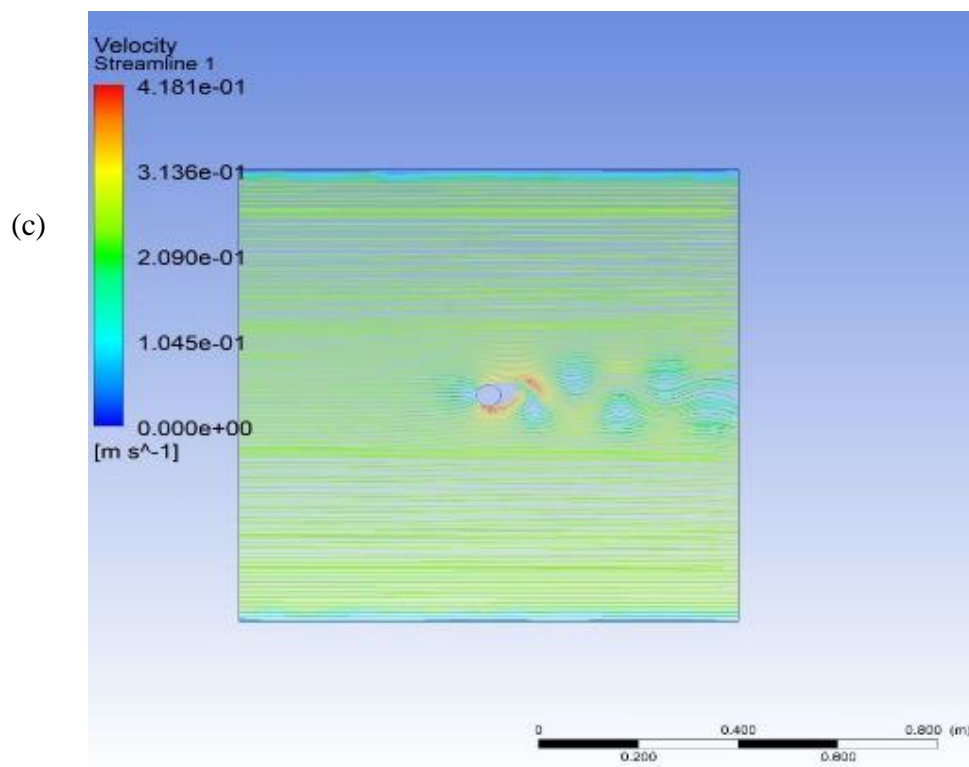
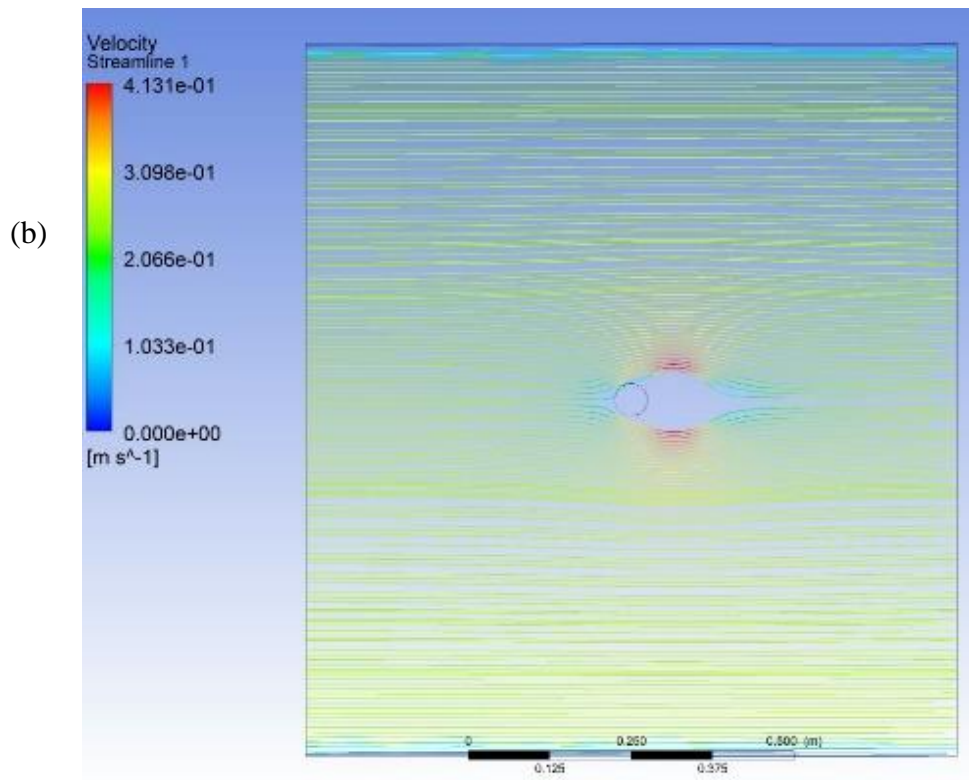


Fig. 4.12 Streamlines contours for the bridge pier at (a) Initial stage, (b) Intermediate Stage, (c) Final Stage

4.3 Two piers in tandem arrangement

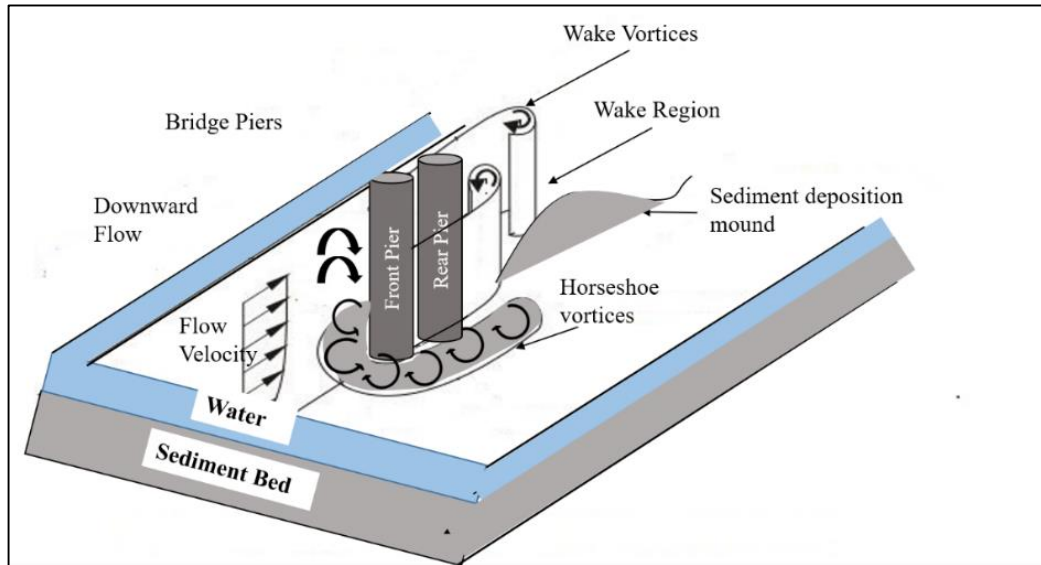


Fig. 4.13 Schematic diagram of two piers in tandem arrangement

4.3.1 Experimental Programme and flow characteristics

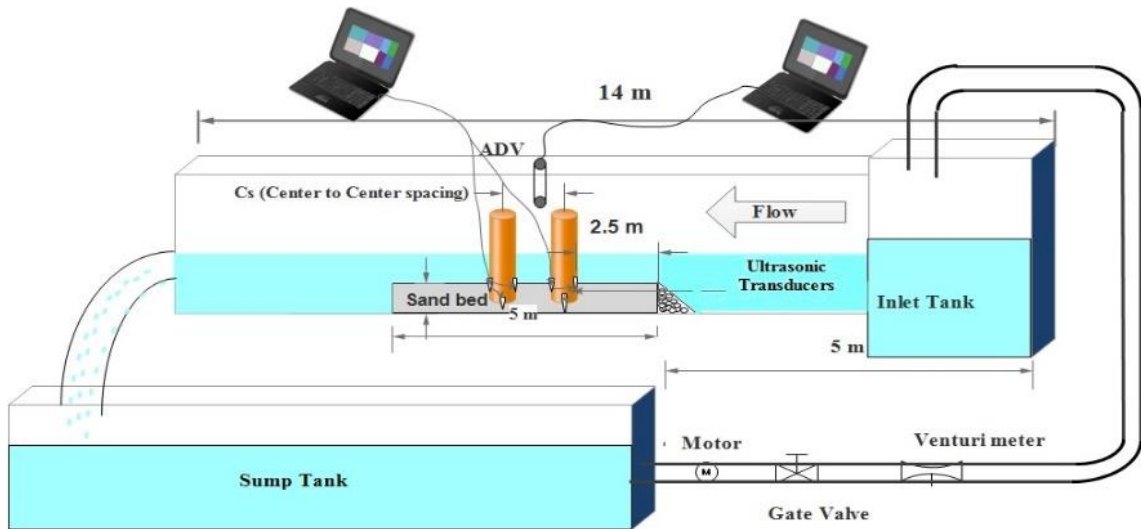


Fig. 4.14 Experimental setup of hydraulic flume

Acrylic pipes of diameter, D , 50 mm, have been used as pier models, laid in the center of the working section at centre-to centre pier spacing, $P_s = 1.5, 2, 2.5, 3, 3.5, 4, 4.5,$ and 5 times the diameter of the pier. Pier models mounted with the ultrasonic transducers in the respective P_s ($S1, S2, S3, S4, S5, S6, S7,$ and $S8$) are shown in **Fig. 4.15**. The whole experimental study has been conducted for five rates of flow (Q) classified as A, B, C, D,

and E, and eight P_s ratios. To analyze the scour process accurately, this wide range of pier spacing has been adopted. Forty experiments have been performed using two piers in tandem arrangement. The experimental run has been conducted for 480 minutes. As concluded from single pier study and from Setia (2008), Yanmaz and Altinbilek (1991) and Mia and Nago (2003) study, the maximum Scour Depth, MSD takes place in the initial 180-240 minutes of the experimental run. Considering these references and results of single pier study, the experiment duration for each run has been fixed as 480 minutes. For precisely measuring the pattern of the scour evolutions, bed measurements have been recorded with the SeaTek ultrasonic ranging transducers. Transducers data has been recorded after every 10 minutes for the first 60 minutes, and after every 30 minutes for the next 420 minutes of the experimental duration, for the eight observation points around the two piers. The water pump has been turned off at the finish of each experimental test, and water has been drained from the flume section. For final sand bed level measurements, a vernier-point gauge measurement with a precision of ± 0.1 mm has been utilized. The scour depth has been measured after 24 hours of water drainage using a vernier point gauge with ± 0.1 mm resolution, and an intense light has been used to read the scour depth.

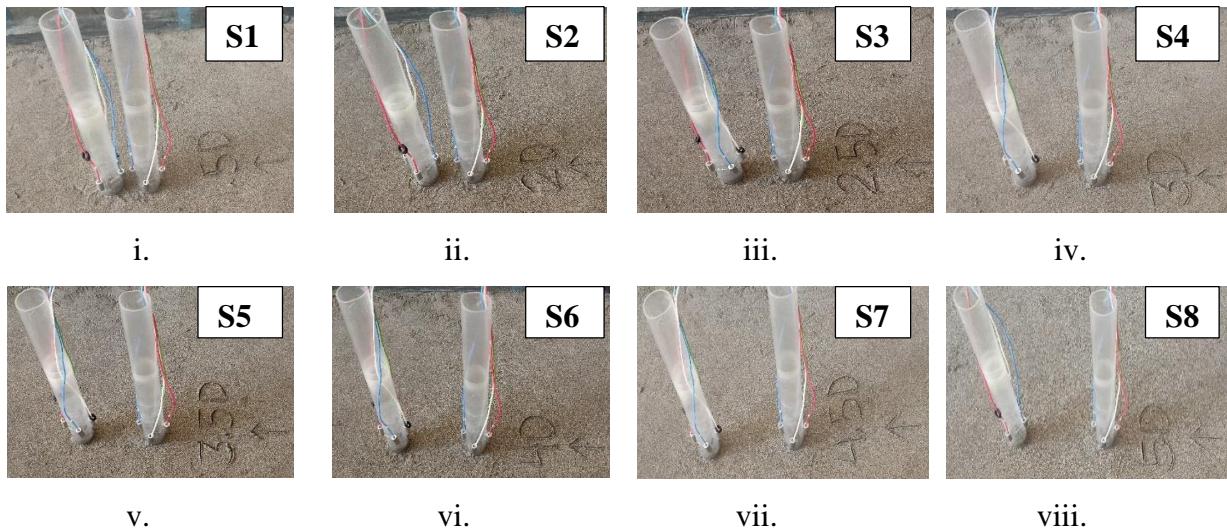


Fig. 4.15 Pier positioning and observation points

Flow variables such as discharge, Froude number, flow head, the velocity of flow, and critical velocity, for experimental conditions, has been presented in **Table 4.2**. Whereas

the characteristic flow conditions considered in this section and other similar studies are presented in **Table 4.3**.

Table 4.2 Flow parameters

Test classification	<i>D</i> (mm)	<i>d</i>₅₀ (mm)	<i>h</i> (m)	<i>V</i> (m/sec)	<i>Q</i> (m ³ /sec)	<i>F</i>_r	<i>V</i>_c (m/sec)	<i>V/V</i>_c
A	50	1.75	0.120	0.224	0.0295	0.206	0.235	0.955
B	50	1.75	0.135	0.243	0.0361	0.211	0.239	0.974
C	50	1.75	0.149	0.262	0.0428	0.217	0.243	0.987
D	50	1.75	0.154	0.287	0.0486	0.233	0.244	0.996
E	50	1.75	0.163	0.300	0.0537	0.237	0.247	0.980

Where, *D* = pier diameter; *d*₅₀ = mean particle size; *h* = water depth above the sand bed; *V* = averaged velocity of approaching flow; *Q* = rate of flow; *F*_r = Froude number; *V*_c = critical velocity of the approaching flow.

Table 4.3 Characteristics flow conditions of the present study and similar studies

Study	<i>d</i>₅₀	<i>h</i>	<i>σ</i>_g	<i>D</i>	<i>F</i>_{d84}
(Ettema 1976)	0.55-4.1	0.6	1.3-4.6	0.1	1.7-3.4
(Albert Molinas 2004)	0.75	0.29-0.40	1.4-3.4	0.18	0.9-3.8
Present study	1.75	0.120-0.163	1.68	0.05	1.4-1.8

where, *d*₅₀ = mean particle size in mm; *h* = depth of water above the sand bed in m; *σ*_g = geometric standard deviation the particle size, *D* = pier diameter in m; *F*_{d84} = densimetric Froude number at *d*₈₄ (84 percentage of the particles are finer than the whole sample).

4.3.2 Results and Discussion

The following results have been presented in this section: (1) temporal evolution of scour depth around the piers, (2) effect of densimetric Froude number on MSD, (3) effect of *u/u*_c on MSD, (4) comparison of the existing equations with the proposed GEP equation. The results of each subsection are presented at the end of each section.

4.3.2.1 Temporal evolution of scour depth around two piers (tandem arrangement)

In this section, the temporal scour depth around the two piers in the tandem arrangement has been provided. Scour phenomenon around the group of piers has been classified as global scour and local scour by Sumer et al. (2005) and Jiang and Lin, (2022, 2021). Global scour is shallow in depth and wide around the pile group and depression across in the surrounding area, and local scour is steep-sided and depression is only around the individual piles.

Fig. 4.16 depicts the scour hole dimensions for both the pier in the tandem arrangement. The local and global scour has been observed around the piers in case of $P_s = 1.5D - 5D$. For small $P_s = 1.5D - 2D$, only global scour hole has been observed, for the $P_s = 2.5D - 5D$ both localized and global both the scour holes has been observed. This is because of the strong scouring intervention at individual piers, which removes out the sediments between the piers. As the P_s increases localized scour hole at individual piers emerge as the waning interference of scouring between individual piers. Scour hole interference increases while the localized scour hole dominates the global scour at the piers as a result hydraulic group effect has vanished. The down flow erodes the sediments surrounding the front pier, and wake vortices began to form around the rear pier. For the small pier spacing $1.5D - 2D$ the scour hole development around the piers is in the shape of a single scour hole. However, due to the large pier spacing $2.5D - 5D$, the development of two independent scour holes commenced, as did the formation of horseshoe vortices around the rear pier.

Non-dimensional temporal scour depth for two piers under five rate of flow conditions has been presented in **Fig. 4.17**, **Fig. 4.18**, **Fig. 4.19**, **Fig. 4.20** and **Fig. 4.21** respectively. A detailed comparison of the scour depth evolution at all the observation points (upstream, downstream, right and left side of the pier) is presented here. The scour depth at the upstream face of the front pier is greater than the scour at upstream face of rear pier. Similarly, the scour rate on the left and right side of the front pier is greater, than the left and right side of the rear pier.

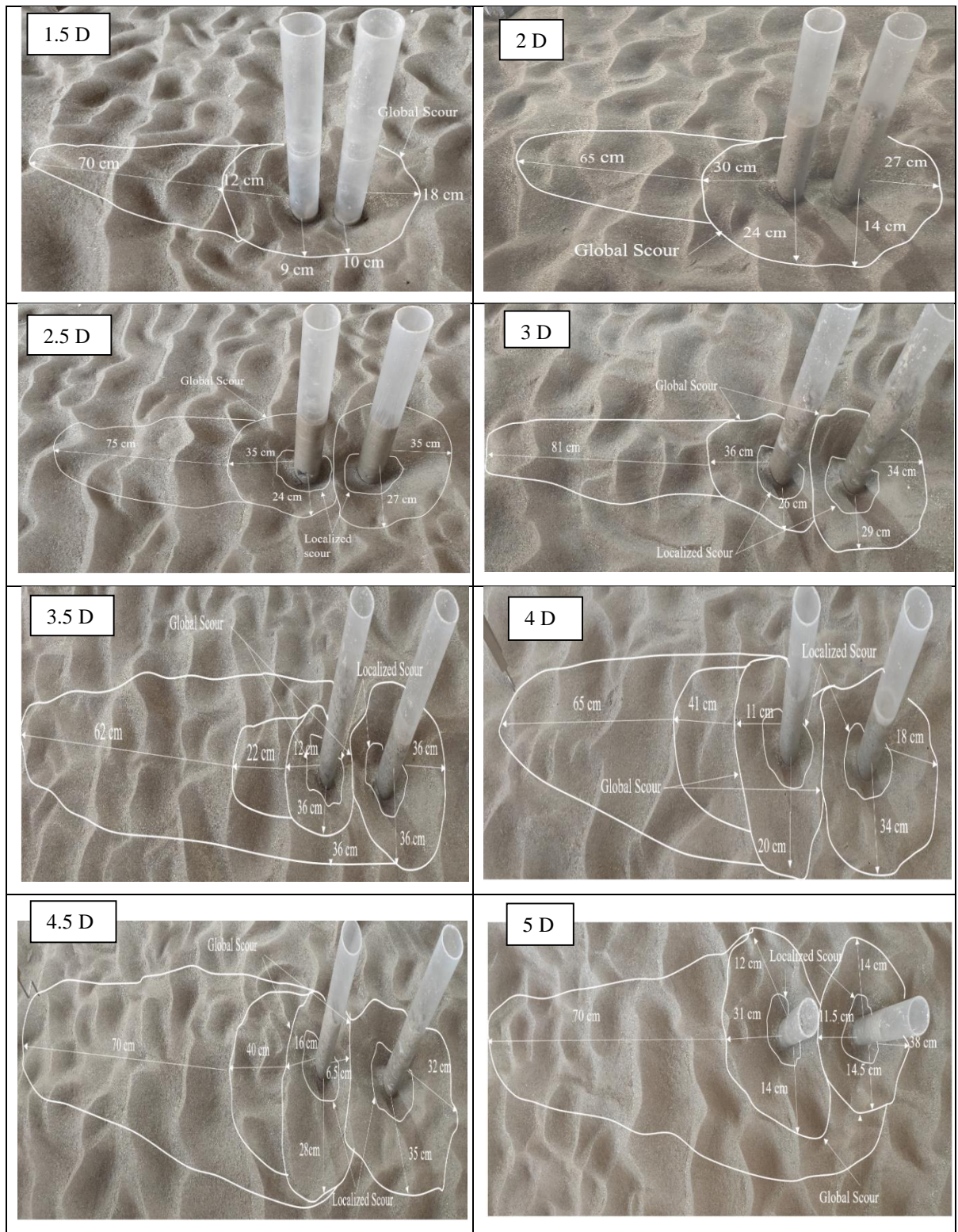


Fig. 4.16 Scour-hole geometry for front and rear piers in tandem arrangement at the end of experimental run

Therefore, this can be also said that the scour pattern at both piers is not identical. The maximum scour depth is observed at the upstream side of the front pier and minimum scour depth is observed at the downstream side of the rear pier. Hence the maximum scour depth is observed at $P_s/d = 2.5$, which is 24 % greater than the scour at a single pier, and the minimum scour depth is observed at the P_s/d ratio 5, which is 17 % less than the scour depth at the front pier. As non-dimensional pier spacing (P_s/d) is increased, the extent of scour depth is decreased upto P_s/d ranging 3, after this the scour started evolving, and piers started behaving individually. Up to P_s/d ratio 2.5, the scour hole developed is acting like a single body; however, after P_s/d ratio 3-5, the formation of two separate scour holes is witnessed. Scour around the front pier is similar as around the isolated pier, similar scour behaviour has been observed by (Wang et al. 2016a). Scour around the front pier in group of piers has been observed nearly as it was around an isolated pier for large pier spacing. So, we can conclude that the maximum influence of the front pier on the rear pier has predominating up to P_s/d ratio equal to 3; after that it starts reducing.

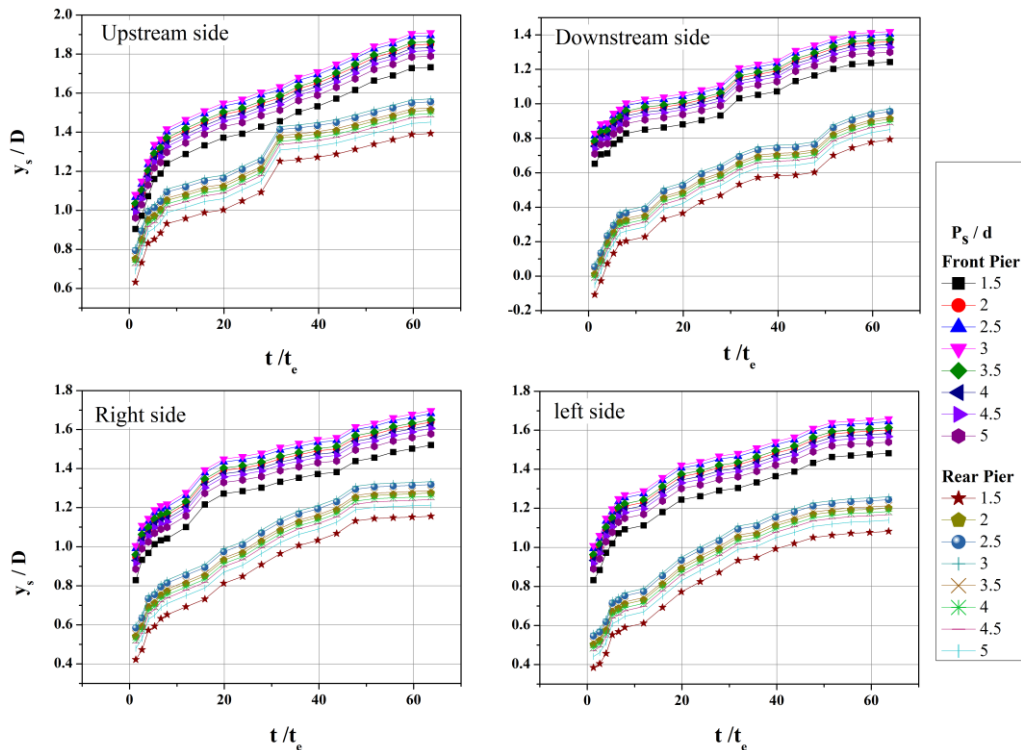


Fig. 4.17 Temporal scour evolution at two piers for rate of flow $0.0295 \text{ m}^3/\text{sec}$

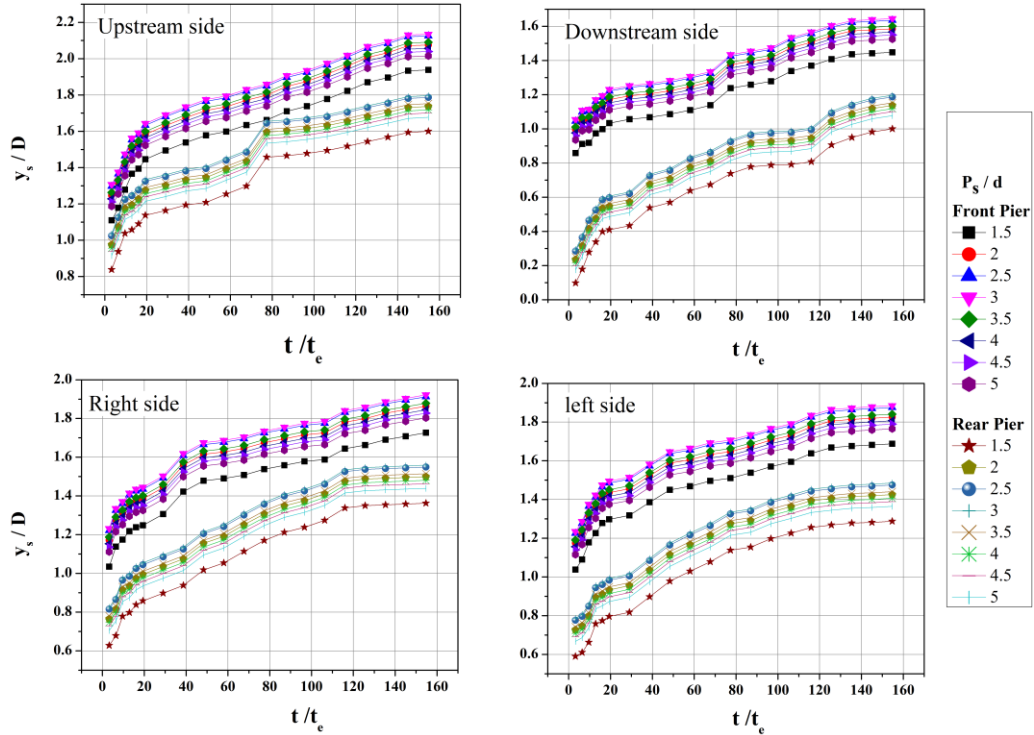


Fig. 4.18 Temporal scour evolution at two piers for rate of flow $0.0361 \text{ m}^3/\text{sec}$

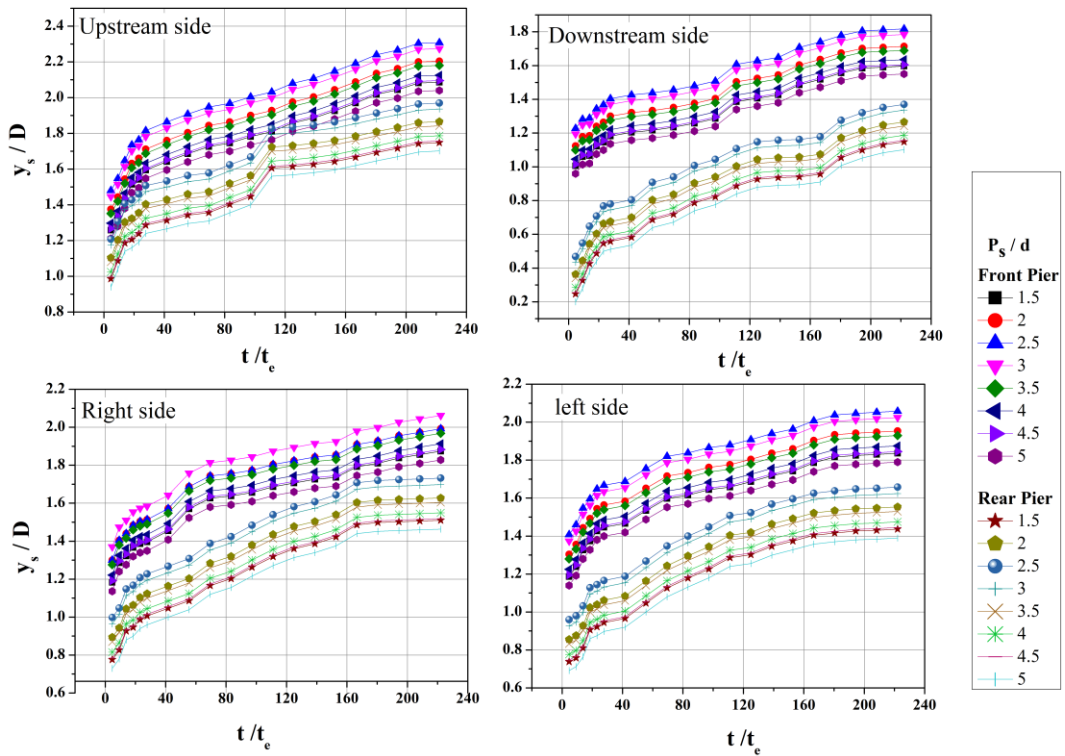


Fig. 4.19 Temporal scour evolution at two piers for rate of flow $0.0428 \text{ m}^3/\text{sec}$

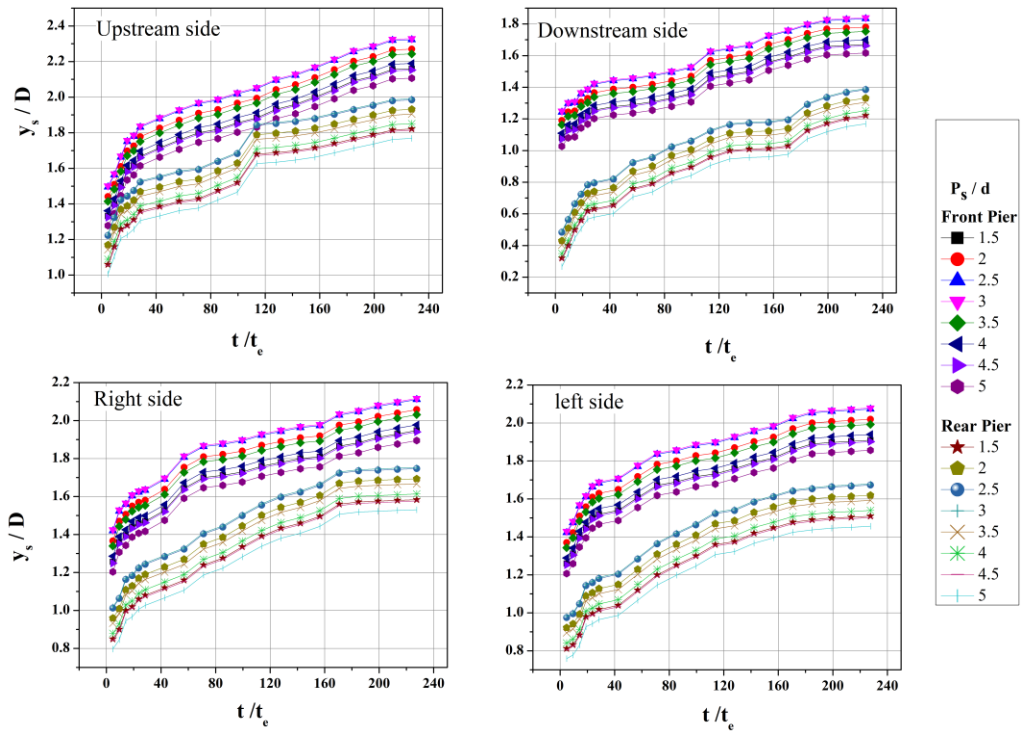


Fig. 4.20 Temporal scour evolution at two piers for rate of flow $0.0486 \text{ m}^3/\text{sec}$

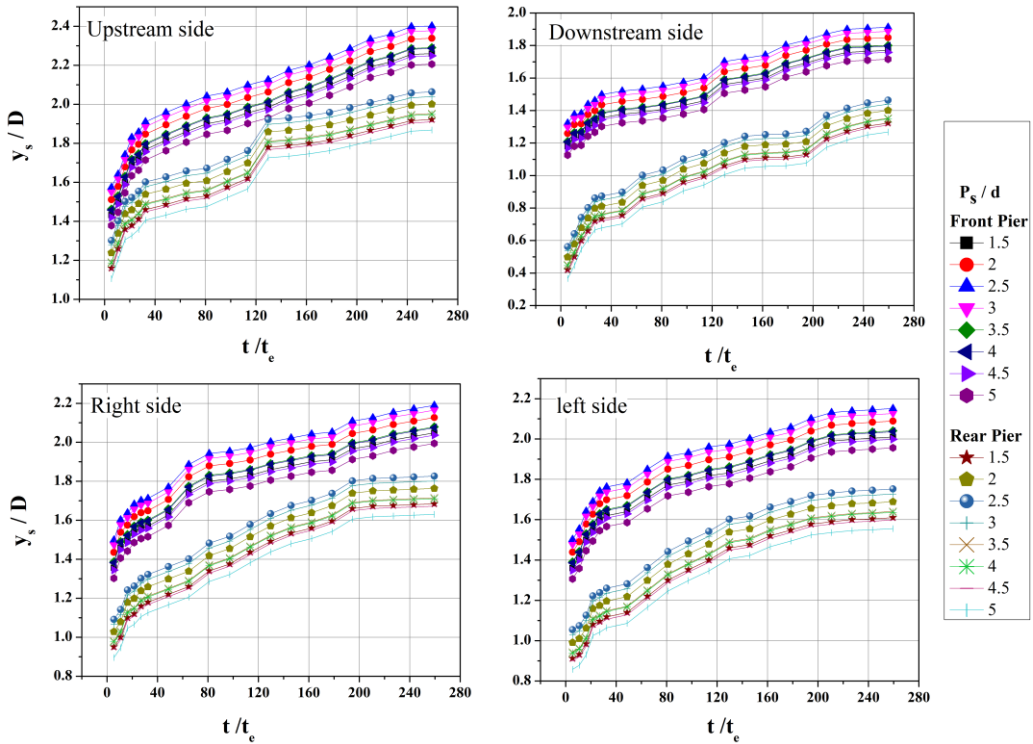


Fig. 4.21 Temporal scour evolution at two piers for rate of flow $0.0537 \text{ m}^3/\text{sec}$

4.3.2.2 Effect of Froude number on scour depth around two piers in tandem arrangement

The densimetric Froude number is essential in determining the MSD around bridge piers. In the present study, densimetric Froude number (F_d) has been used instead of Froude number (F_r). According to Cheng et al. (2020) the size of representative bed particles cannot be described using only the median diameter d_{50} in non-uniformly distributed sediments, and conducted a study using the different particle diameters, including d_{16} , d_{35} , d_{50} , d_{65} , d_{84} , d_{90} , d_{95} , and d_{99} . Study results show that the best results are obtained by using the d_{84} particle size, so in the present study d_{84} particle has been utilized rather than d_{50} . The expression proposed by Cheng et al. (2020) has been used to compute the densimetric Froude number is $F_d = \frac{u^2}{\sqrt{g}d_{84}}$, where d_{84} is the representative size of the sediment material is given by Cheng et al. (2020). The values of the sediment size d_{84} is interpolated from the sieve analysis curve, presented in **Fig. 3.6**, and can be written as in **Eq. 51**:

$$y = y_o + \frac{A}{w\sqrt{\pi/2}} e^{-2\frac{(x-x_c)^2}{w^2}} \quad 51$$

The results of the present study are illustrated in **Fig. 4.22**, the effect of densimetric Froude number on non-dimensional scours depth with non-dimensional pier spacing P_s/d . **Fig. 4.22** shows that, F_d ranges from 1.4- 1.8, and as the value of the Froude number increases, the MSD also increases. For all the flow conditions, the same range of Froude number has been adopted to evaluate the change in the MSD evolution pattern. The maximum non-dimensional scour depth is 2.4, observed at the upstream of the front pier for $P_s/d = 2.5$, at the highest value of the densimetric Froude number $F_{d84} = 1.83$. And the minimum non-dimensional scour depth is 1.5, observed at the downstream side of the rear pier at the lowest value of the $F_{d84} = 1.37$, which is 21.6 % less than that of MSD at the upstream side of a single pier. As the value of densimetric Froude number increases, non-dimensional scour depth also increases. For the value of $F_{d84} \leq 1.6$, the minimum scour depth is observed for the $P_s/d = 1.5$, and for the $F_{d84} > 1.6$, the minimum scour depth is observed in the case of $P_s/d = 5$. The MSD for $F_{d84} = 1.4 - 1.8$ occurs at the $P_s/d = 2.5$ at the upstream side of

the front pier. As a result, the bridge scour was more sensitive on the upstream side of the front pier.

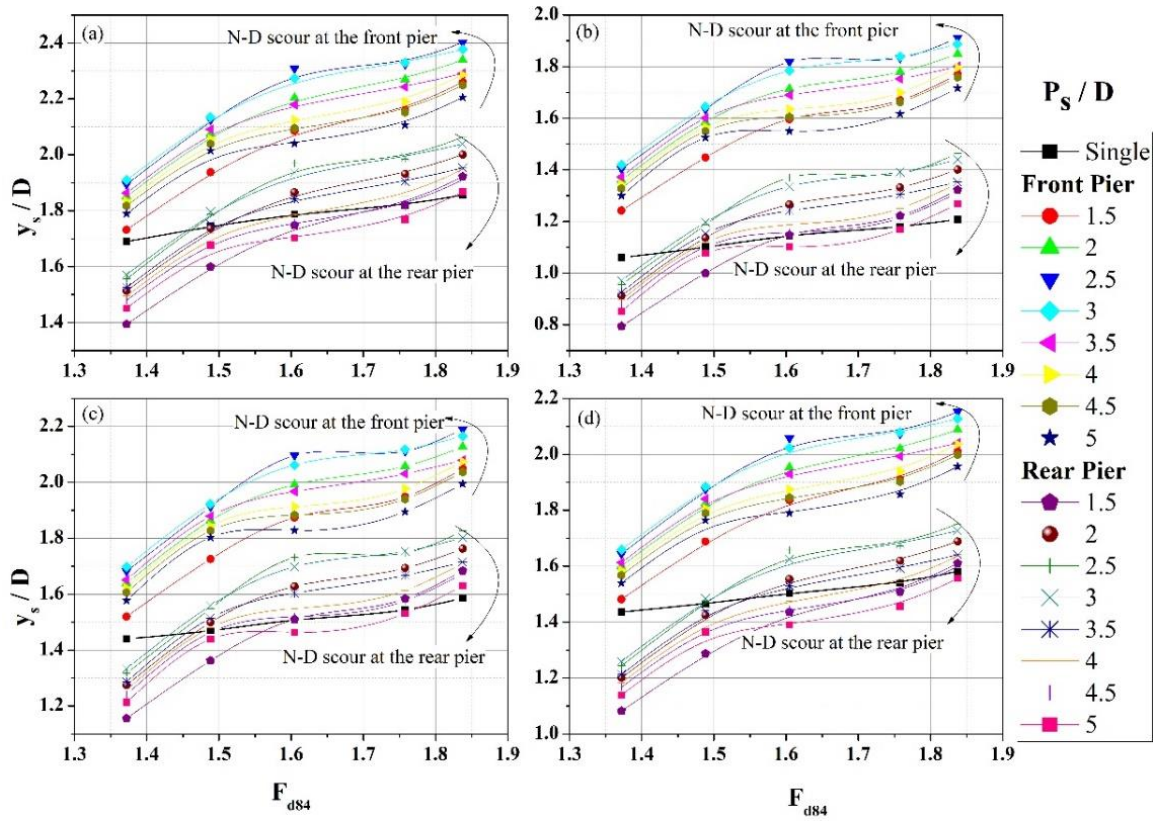


Fig. 4.22 Effect of densimetric Froude number on non-dimensional scour depth at front and rear pier at (a) upstream side (b) downstream side (c) right side and (d) left side

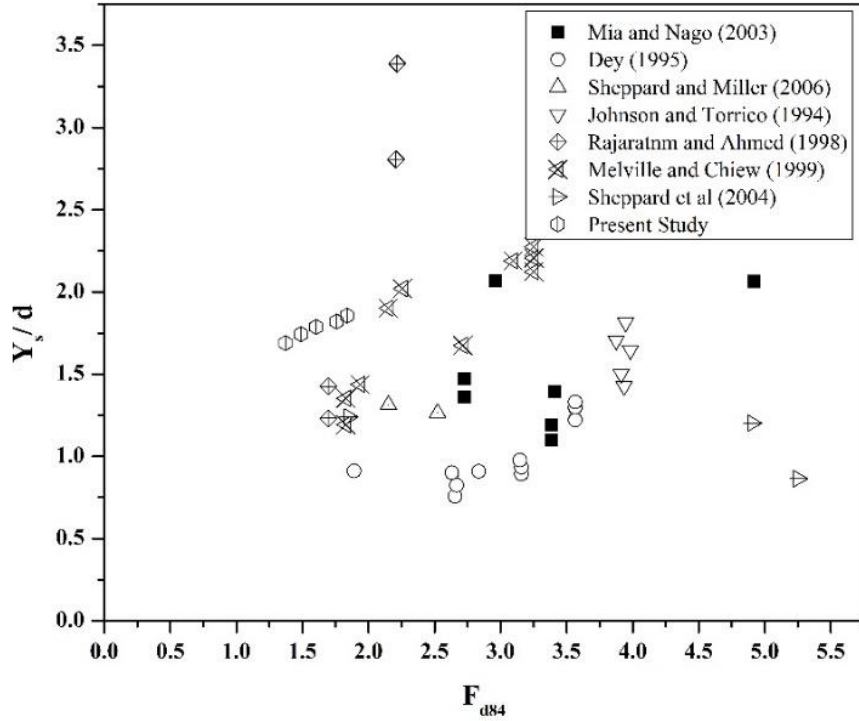


Fig. 4.23 Non-dimensional scour depth variation with Densimetric Froude number (F_d)

4.3.2.3 Effect of Reynolds Number on Maximum Scour Depth

Effect of Reynolds number on the non-dimensional scour depth has been studied with the variation on the pier spacing. The Reynolds number based on the depth-averaged approach velocity (U) and the diameter of the obstacle (D), $Re = UD/\nu$, where ν is the kinematic viscosity of the fluid. The variation in the non-dimensional scour depth for the front and rear pier has been depicted in **Fig. 4.24** and **Fig. 4.25**. As shown in the **Fig. 4.24**, for the single pier the Y_s/D curve is linearly varying with the increase in the Reynolds number. As the P_s/D range in between 1.5- 3 then the scour depth has been increased and the Y_s/D curve slightly flattened on the higher side of the curve, whereas for the $P_s/D = 3-4.5$ the curve is flattened more on the higher side. The maximum change in the individual curves have been observed for the $Re = 17,000-27,000$. For the P_s/D in between 1.5- 3, at $Re = 17,000$, slight increase in the non-dimension scour have been obtained. For the $P_s/D = 3-4$ the Y_s/D curve flatted for the range of Re 17,000-25,000 and for the $P_s/D = 4.5-5$ the Y_s/D curve attains the least values for the $Re = 20,000-27,000$.

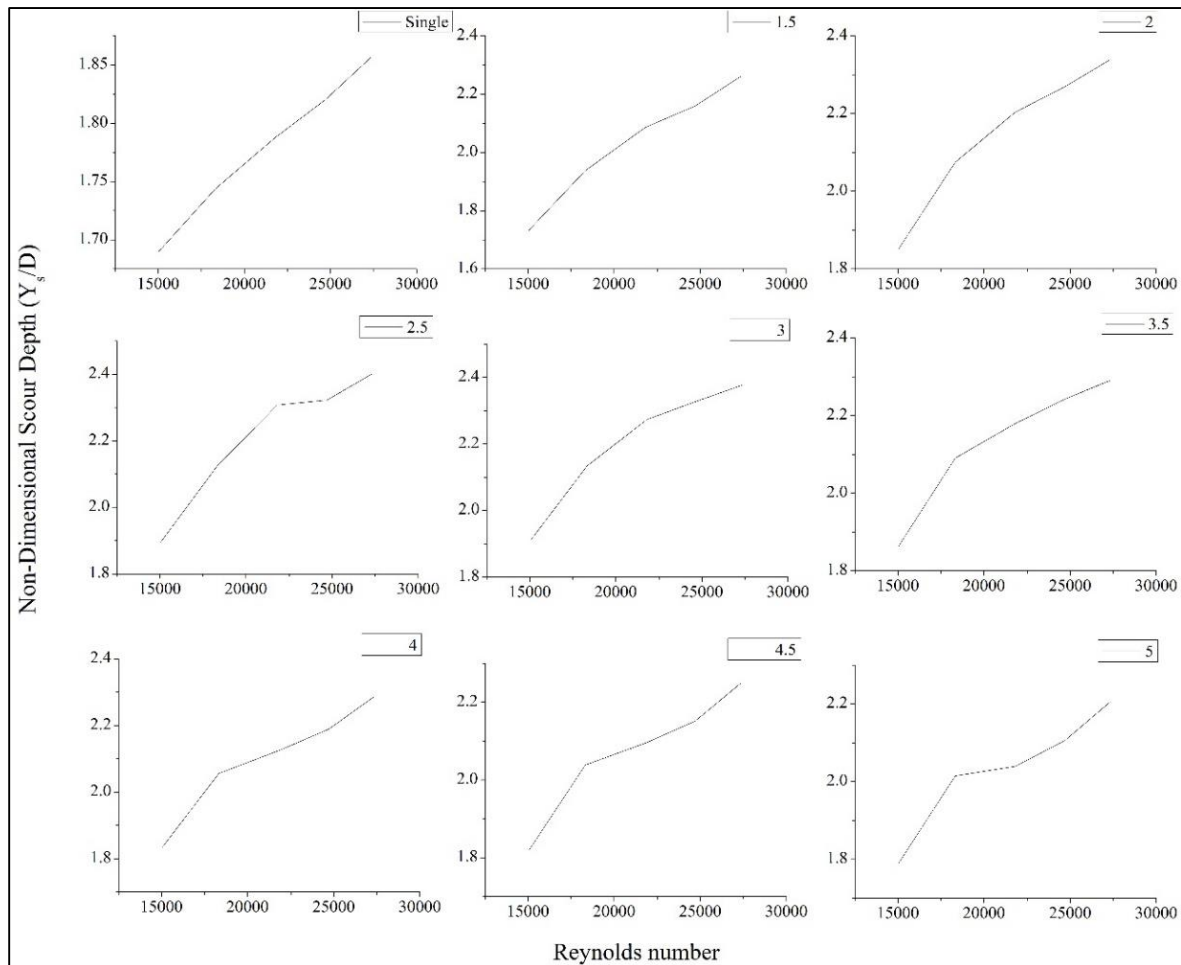


Fig. 4.24 Reynolds number effect on the non-dimensional scour depth for the front pier

Fig. 4.25 depicts the Reynolds number effect on the non-dimensional scour depth for the rear pier. The Y_s/D curve is linearly varying with the increase in the Reynolds number as in case of front pier but the curve observed in case of rear pier is more flattened. As the P_s/D range in between 1.5- 2.5 then the scour depth has been increased and the Y_s/D curve is flattened more than single pier and front pier. Whereas for the $P_s/D = 3-4.5$ the curve is more flattened but maximum flat curve is observed at the $P_s/D = 5$. The maximum change in the individual curves have been observed for the $R_e = 17,000-27,000$. This fattening of the curve is the resultant increased pressure gradients induced by the piers trigger the separation of the incoming flow and involvement of the wake vortices with the horseshoe vortices in the pier spacing area.

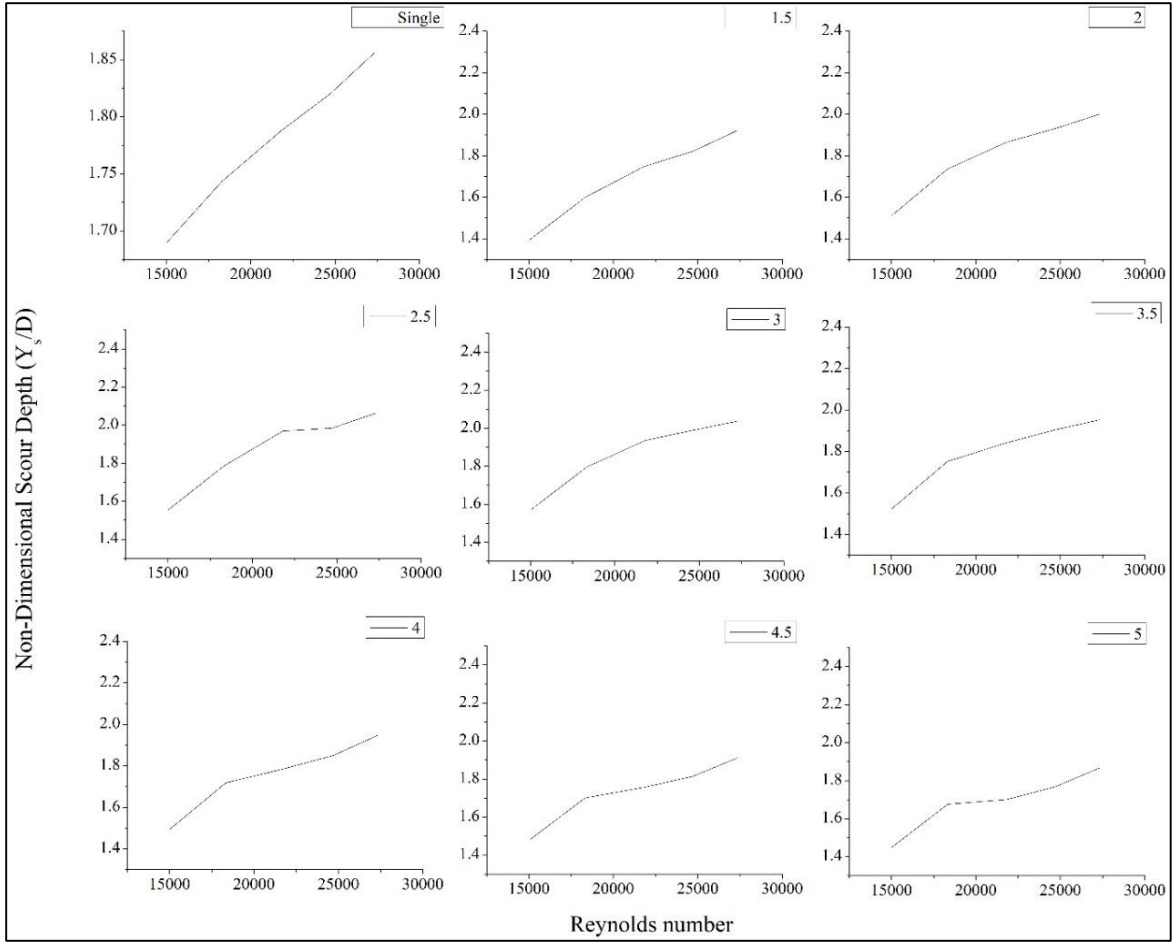


Fig. 4.25 Reynolds number effect on the non- dimensional scour depth for the rear pier

4.3.2.4 Effect of Relative Velocity on Maximum Scour Depth

In this section, the effect of relative velocity (u/u_c) on the non-dimensional scour depth (Y_s/D) has been presented for the non-dimensional pier spacing (P_s/D); results are presented in **Fig. 4.26**. In the first category of the experimental study, the rationality of the study is demonstrated for the single pier in **Table 4.4**. The experimental results of this section agree closely with the equation proposed by (Aguirre-Pe et al. 2003) and also used by authors in studies (Wang et al. 2016a; b), is written in **Eq. 52**

$$\frac{Y_s}{D} = 2.865 \frac{u}{u_c} - 1.332 \quad 52$$

Where, Y_s = scour depth; D = pier diameter; u = averaged velocity of approaching flow; and u_c = critical velocity of the approaching flow.

Table 4.4 Experimental results of first category (Single pier) for all the five flow conditions

Run No.	Y_{SU} (cm)	Y_{SR} (cm)	Y_{SL} (cm)	Y_{SD} (cm)
A	8.45	7.2	7.18	5.3
B	8.72	7.34	7.33	5.5
C	8.94	7.53	7.52	5.72
D	9.10	7.72	7.69	5.90
E	9.28	7.92	7.90	6.04

Where, Y_{SU} = scour depth at the upstream side of the pier; Y_{SR} = scour depth at the right side of the pier; Y_{SL} = scour depth at the left side of the pier; Y_{SD} = scour depth at the downstream side of the pier.

The coefficient in **Eq. 52** is slightly less than in Chiew's equation. Because the duration of the experiments used in this section is somewhat less than that taken to obtain real-time equilibrium, and the physical properties of the sediment used varies considerably with those of river sand used by (Chiew 1995; Qi et al. 2013). The mean value of critical velocity agrees well with the Schamovis equation (Tang et al. 2013), earlier used by (Wang et al. 2016a; b). Schamovi's equation can be written as in **Eq. 53**:

$$u_c = 1.14 \sqrt{gd_{50} \frac{\rho_s - \rho}{\rho}} \left(\frac{h}{d_{50}} \right)^{1/6} \quad 53$$

Where, ρ = specific gravity of the water; ρ_s = specific gravity of the sediment; g = acceleration due to gravity; and d_{50} = mean particle size.

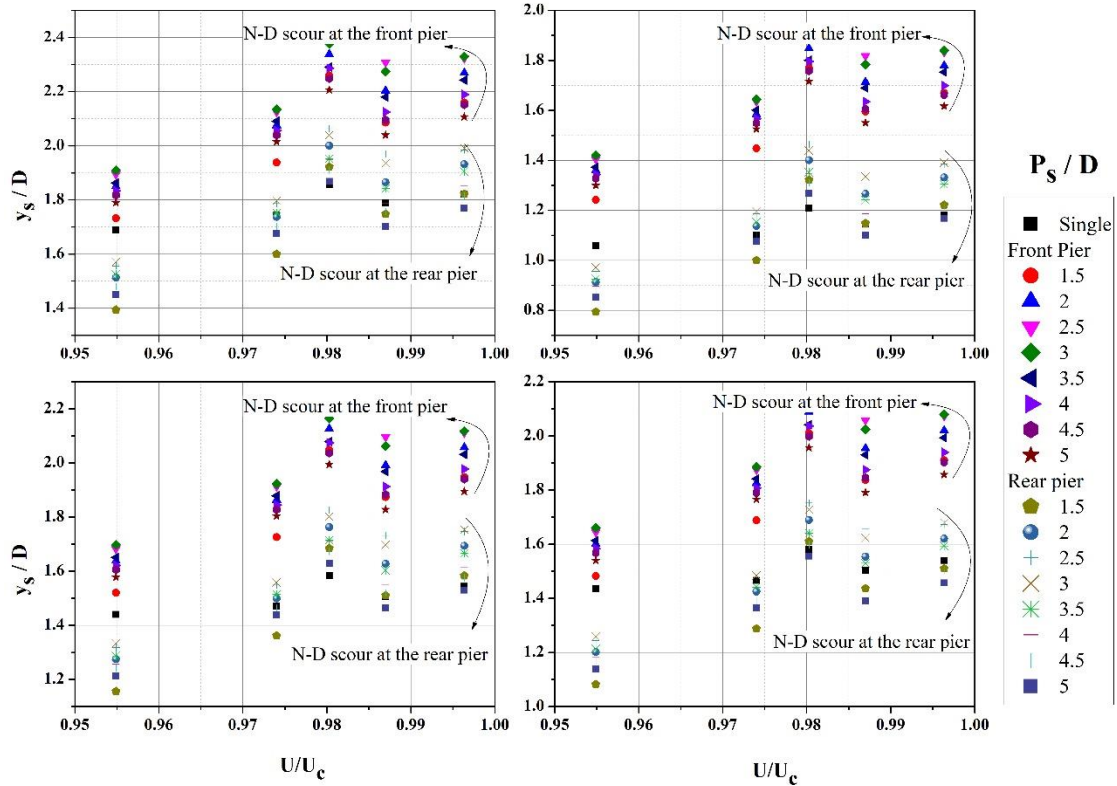


Fig. 4.26 Non-dimensional scour depth (Y_s/D), versus relative velocity (u/u_c), with the increasing non-dimensional pier spacing (P_s/D) at (a) upstream side (b) downstream side (c) right side and (d) left side

In the second category of the experimental programmes, two piers in the tandem position has been considered with the increasing P_s between the piers. The results show that, at P_s equals to zero, both the piers behave like a single body of different shapes and diameters, this case can be treated the same as a single pier. Piers act like a one body because of smaller P_s between the piers, the front pier exerts the sheltering effect on the rear pier. Because of this sheltering effect, the upstream nose of the front pier behaves like a single pier, and there is no scour effect on the rear pier; similar results are also obtained in their research by Breusers et al.(1977) and Shen et al.(1969).

As the value of P_s/D between the piers increased, the relationship between the Y_s/D and u/u_c for five flow conditions agrees well with the Eq. 53 as shown in Fig. 4.26. The findings of the this section illustrates that the scour hole developed at the front pier is larger in size than that of the rear pier and single pier; these results are similar with the results obtained by Hannah (1978) and Behzad and Beheshti (2006).

4.4 Two piers in side-by-side arrangement

4.4.1 Experimental Programme and flow characteristics

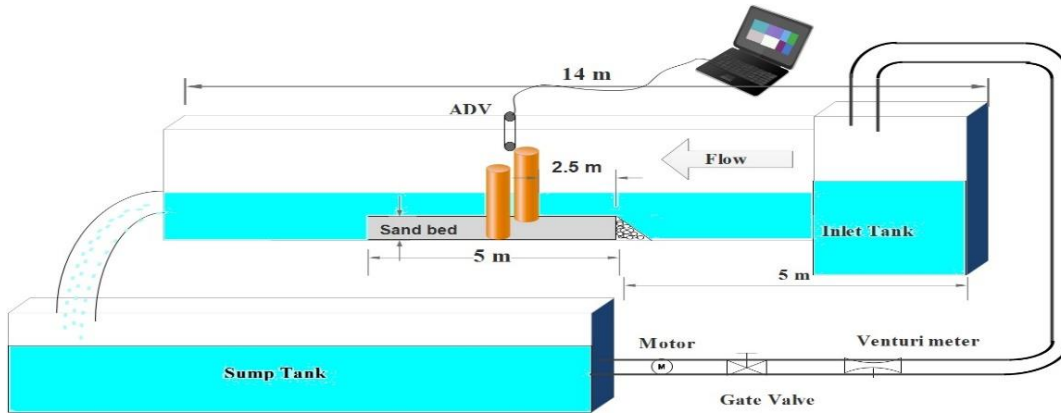


Fig. 4.27 Schematic diagram of the experimental set-up

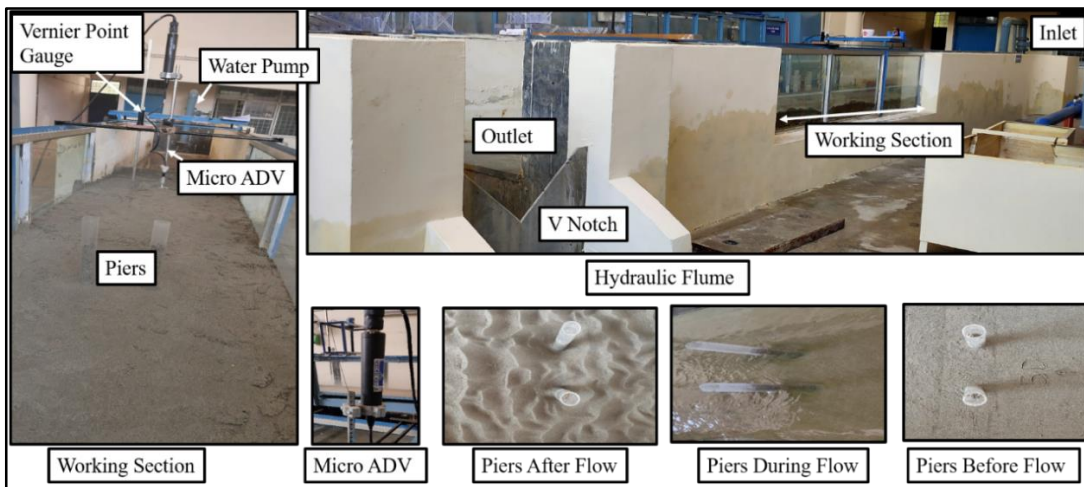


Fig. 4.28 Laboratory set-up for experimental work

The schematic diagram of the experimental set-up is depicted in **Fig. 4.27** and laboratory set-up in **Fig. 4.28**. The working section of 5 m length, 1.10 m width, and 0.20 m depth has been filled with sand, is located 5 m downstream from the inlet section of the flume. Flow depth in the working section is regulated using the sluice gate mounted downstream of the working section. The experimental investigation for two piers, placed transverse to the direction of flow has been carried out. The rate of flow (Q) ranges from 0.0295 to 0.0537 m^3/sec , water flow depth 0.12 to 0.163 meters and center to center pier spacing (P_s) from 0 to 25 cm.

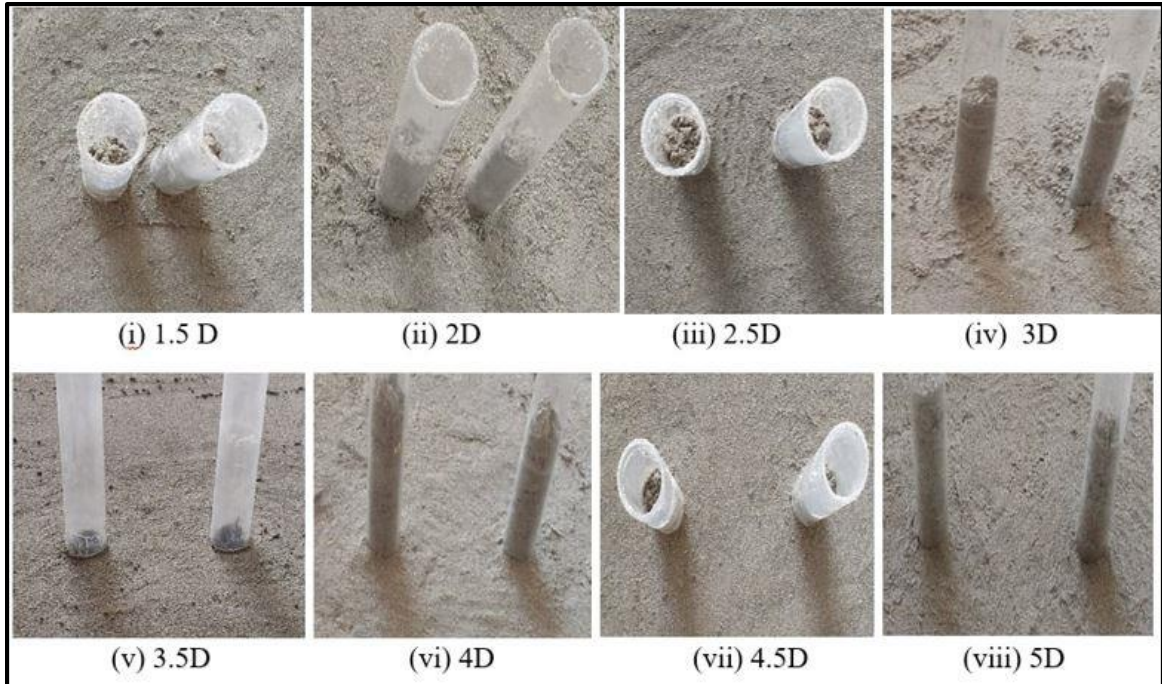


Fig. 4.29 *Experimental set-up for different arrangements of the piers with increasing center-to-center clear spacing between the piers*

As depicted in **Fig. 4.29**, experiments are carried out for eight centre-to-centre pier spacing (P_s) between the piers that are 1.5, 2, 2.5, 3, 3.5, 4, 4.5 and 5 times the diameter of the pier. Two cylindrical piers of acrylic pipes with a 5 cm diameter (D) are placed in the middle of the working section. The flow depth is kept in the range of 0.12-0.163 meters. The experimental duration for each experiment is set to 480 minutes as the scour depth generated after 300 minutes is deemed equilibrium scour depth in accordance with the previously published work (Mia and Nago 2003; Setia 2008; Yanmaz and Altinbilek 1991). For continuously monitoring the pattern of scour evolution around both the piers, a vernier point gauge of precision ± 0.1 mm is utilised. Vernier readings are recorded for 480 minutes in regular intervals, after every 30 minutes. After the completion of each experimental run, water from the flume section is drained out and scour depth around the twin piers is measured.

4.4.2 Results and Discussions

4.4.2.1 Temporal evolution of scour depth around two piers (side-by-side arrangement)

As stated earlier, experimental work is conducted for twin pier. **Fig. 4.30** depicts the scour hole pattern observed after water drainage from the flume section for all the pier positioning. For the $P_s = 1.5D$ one scour hole is formed around both the piers, and scoured sediment gets deposited in the middle of both the piers in the form of one tail scour. For $P_s = 2D$ a minor separation in the scour hole is observed, and only one tail scour deposition is noticed. For $P_s = 2.5D$, the formation of two separate scour holes started, but the tail scour one, and the outer circle is also one up to this pier spacing. At $P_s = 3D$ to $4.5D$, two separate scour holes are observed and scoured sediments get deposited in the middle of the two piers or along the centre line of flow. Up to $P_s = 4.5D$ strong vortices (Horseshoe and wake) are formed between the piers as a result sediment deposition mound is formed at the middle of the two piers. Whereas in the case of $P_s = 5D$ two separate holes are observed, but the deposition of sediment is observed at the rear of both the piers respectively, due to the weak interference force and separate vortices formation around both the piers.

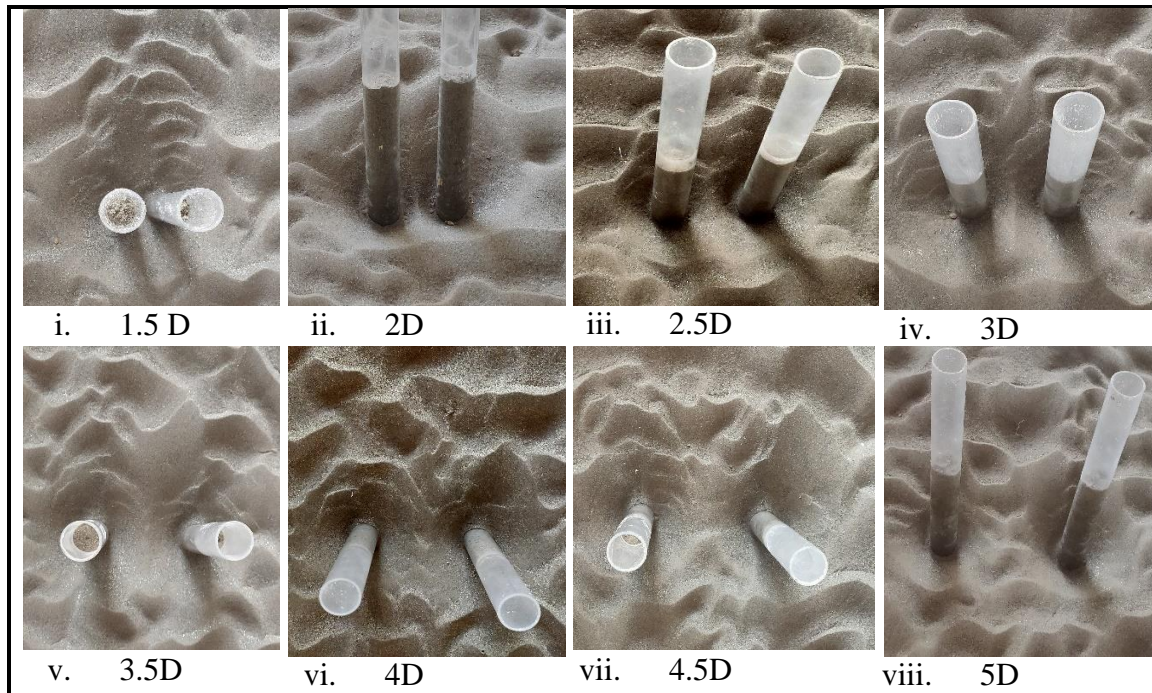
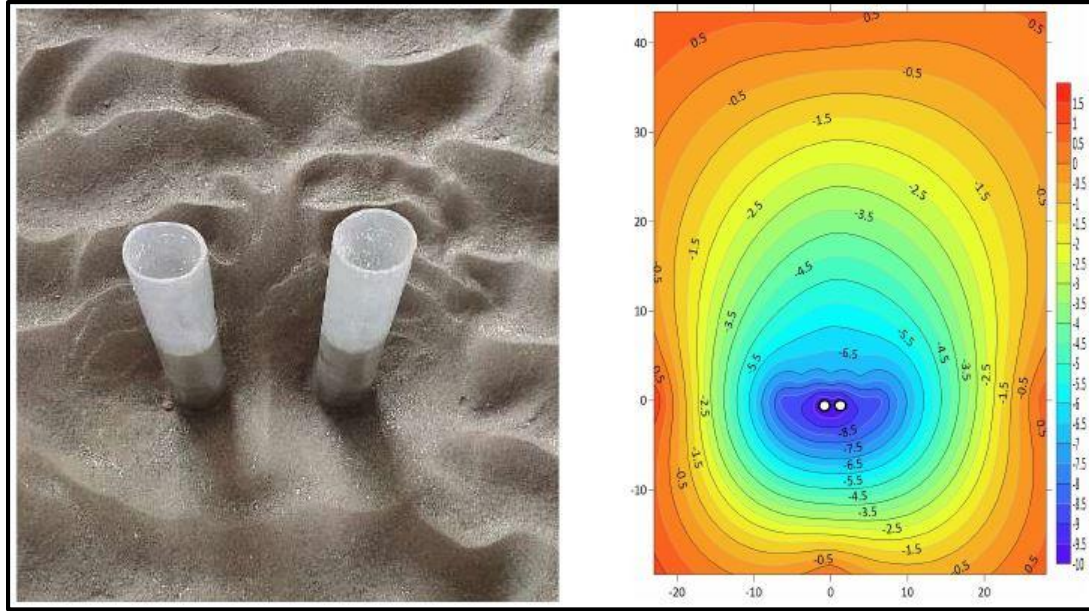


Fig. 4.30 Scour hole evolution after drainage of water for eight pier spacing arrangements



(a)

(b)

Fig. 4.31 Maximum scour depth in case of 2.5 D spacing (a) Experimental results (b) contour plot for maximum scour bed level in cm

MSD values for both the piers are normalized with the scour depth at the single pier, Y_{sul}/Y_u and Y_{sur}/Y_u . From the **Fig. 4.33**, it can be observed that the MSD increases with increase in the value of P_s/D and attains its peak value at $P_s/D = 2.5$, then it starts decreasing up to $P_s/D = 5$. The MSD is observed at the upstream end of the pier for $P_s/D = 2.5$ and $Q = 0.0537 \text{ m}^3/\text{sec}$. It is represented in the pictorial and contour form in **Fig. 4.31 a and b**, respectively. The analysis of the pier spacing effect is conducted on the basis of the scour hole developed after the lapse of 480 minutes. The scour holes formed around both piers merged, and the shape of the scour hole is identical to that of the single pier.

The scour holes formed around both piers merge in the $P_s/D = 1.5$ and 2 cases, and the shape of the scour hole is identical to that in the single-cylinder example. Even though the scour holes have merged in the $P_s/D = 2.5$ cases, there is some separation of the scour holes upstream of the cylinders. The scour depth between the two piers reduces as the distance between them expands because the jet-like flow, which drives flow acceleration and enhanced turbulence, is weakened. When the pier spacing P_s/D is more significant than 2.5, the local scour holes develop independently, resulting in isolated sedimentation mounds behind the individual piers. The pattern of the scour hole development for the 1.5

$\leq P_s / D \leq 2.5$ shows a highly complex behaviour due to the formation of large vortices between the piers. The scour depth results presented in this section are consistent with the results obtained by (Raudkivi 2020; Sumer et al. 2005).

Fig. 4.32 illustrates a bar plot for the equilibrium scour depth for the single pier for seven rate of flow. It can be observed that the rate of flow and scour depth have a linear relationship with each other, that is, as the rate of flow increases, the scour depth around the pier also increases. The increasing pattern of scour development is the same for all the seven flow conditions; however, MSD keeps on going deeper as the flow rate increases, as depicted in the plot.

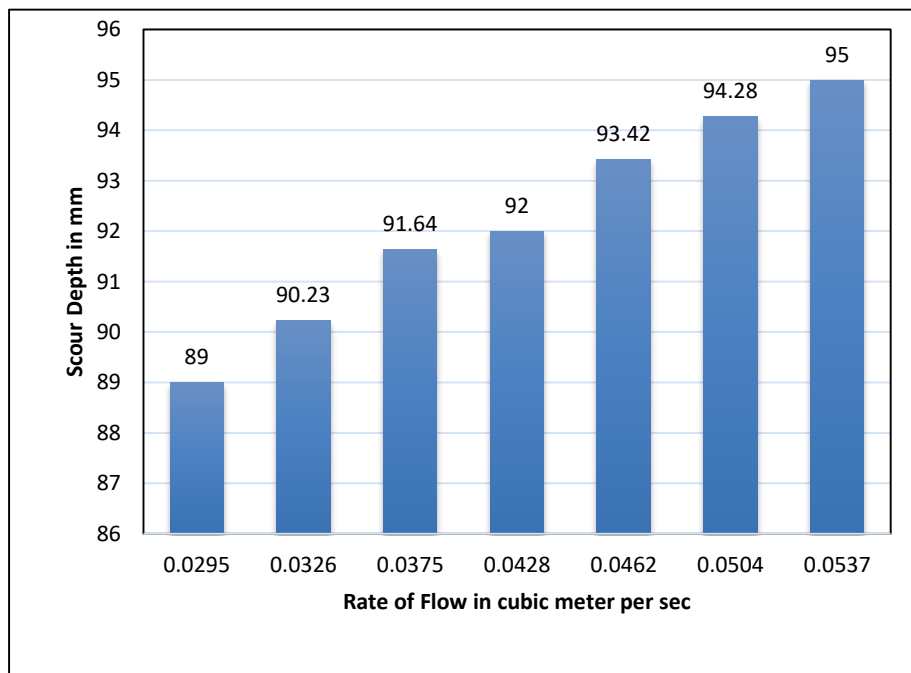


Fig. 4.32 Equilibrium scour depth for the seven-sets of rate of flow in m³/sec

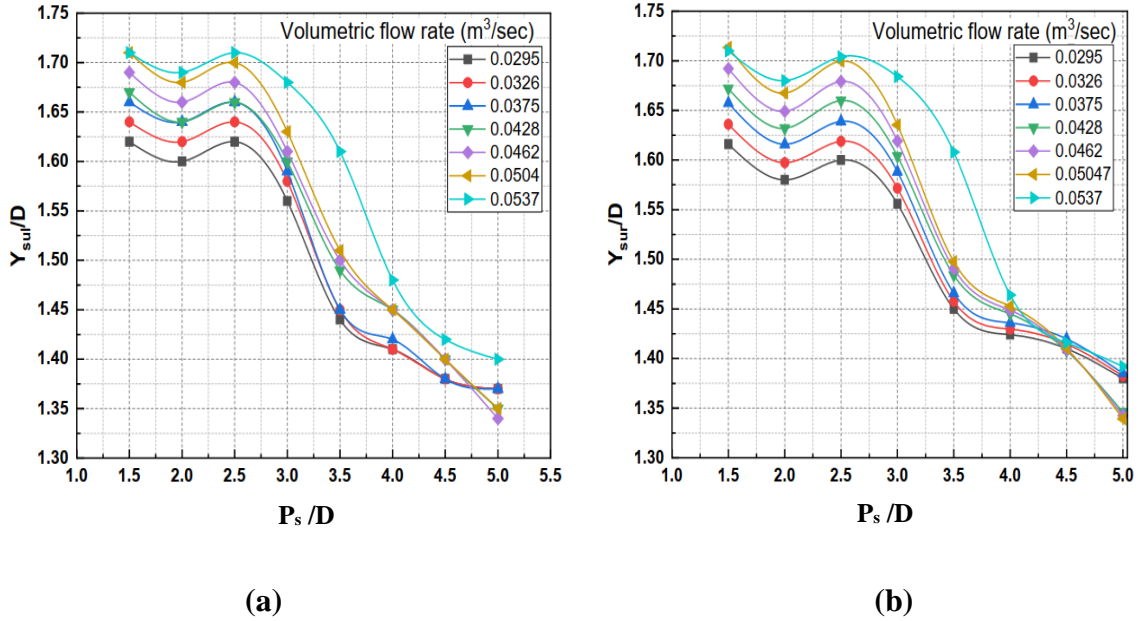


Fig. 4.33 Equilibrium scour depth for the seven-sets of rate of flow (m^3/sec) for (a) Left Pier, and (b) Right Pier.

Fig. 4.33 depicts the equilibrium scour depth variation with seven different rates of flow in m^3/sec . Scour trend for both the piers, the left pier and the right pier, is quite similar, as depicted in **Fig. 4.33 a and b**, respectively. For the pier spacing ranges from $1.5 \leq P_s/D \leq 2.5$, both the piers started behaving as a single body with a radius double in size; as a result the scour hole development is rather large in comparison with the single pier. For the pier spacing ranges from $2.5 < P_s/D < 4.5$, the scour hole evolution is partly divided into two parts, however, the influence of the presence of the two piers in the close proximity is still evident. For the pier spacing $P_s/D = 5$, both the piers start behaving like individual piers with the development of two separate scour holes, however, the development of scour is greater than the single pier. From the results of this experimental study, it can be concluded that the maximum scour depth is achieved when the pier is placed in a close vicinity as observed maximum scour depth in the case of P_s/D for $1.5D$ and $2.5D$ and the minimum scour depth is attained at the maximum spacing, that is $5D$, due to the individual behaviour of the piers.

4.4.2.2 Froude number effect

As per (Ettema et al. 1998) and (Ettema et al. 2006), the energy gradient for flow around piers might be characterized by the Froude number. The higher the Froude number, the

higher will be the scour depth. Ettema et al. (2006) developed the correction factor to account the Froude number effect in laboratory-based studies for testing scale. **Fig. 4.34 and Fig. 4.35** depicts the relationship between non-dimensional scour depth and Froude number. Effect of Froude number on the non-dimensional scour depth around both the piers (left and right) on upstream side has been depicted in **Fig. 4.34**. Both the piers behave identically, the non-dimensional scour depth has been varying non-linearly with the increase Froude number for various pier spacing. The seven Froude numbers are 0.20645 , 0.2019 , 0.21588 , 0.21644 , 0.22602 , 0.23294 , and 0.23724 . **Fig. 4.34** depicts the non-dimensional scour depth has been attained at the $F_r = 0.23294$ for the $P_s = 1.5D$ at the left pier and minimum has been attained at the $F_r = 0.22602$ for the $P_s = 5D$ at the left pier and right pier. Maximum value is attained for the $P_s = 1.5D$ and minimum values are attained for $P_s = 5D$ for all the Froude numbers at the nose of the pier because at small pier spacing pier are behaving like a one body with the large pier diameter.

The effect of Froude number on the non-dimensional scour depth around both the piers (left and right) on downstream side has been depicted in **Fig. 4.35**. The overall trend of the non-dimensional scour depth increases with the increase in the Froude number but it varies with the pier spacing. The maximum non-dimensional scour depth is attained at the $F_r = 0.23294$ for the $P_s = 2D$ at the both piers and minimum has been attained at the $F_r = 0.21588$ for the $P_s = 5D$ at the left pier and right pier. Maximum value is attained for the $P_s = 2D$ and minimum values are attained for $P_s = 5D$ for all the Froude numbers at the downstream side of the pier.

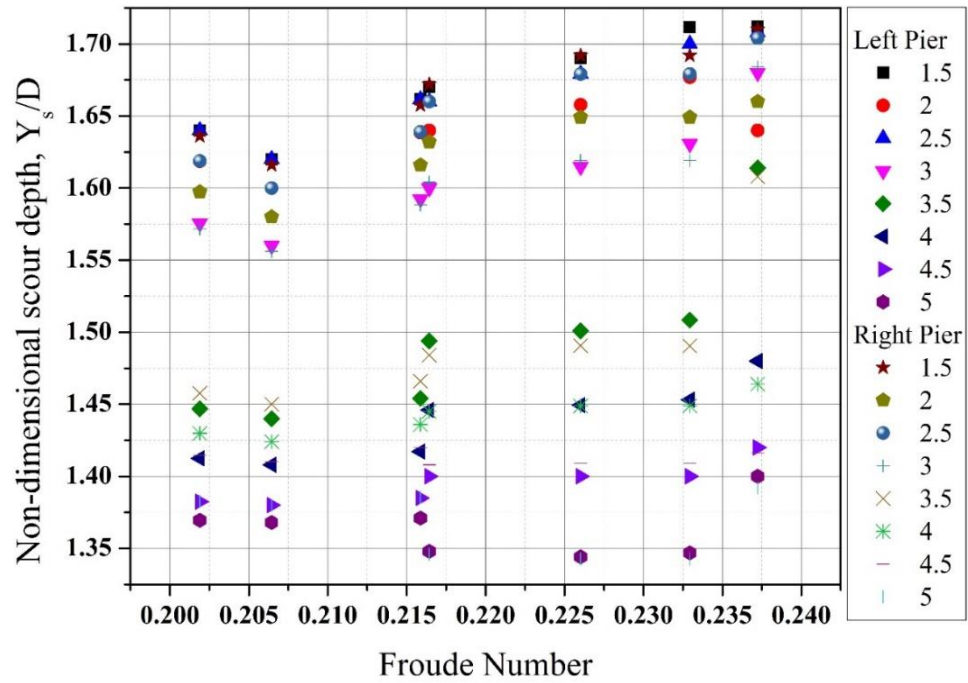


Fig. 4.34 Effect of the Froude number on scour depth upstream of the two piers in side-by-side arrangement

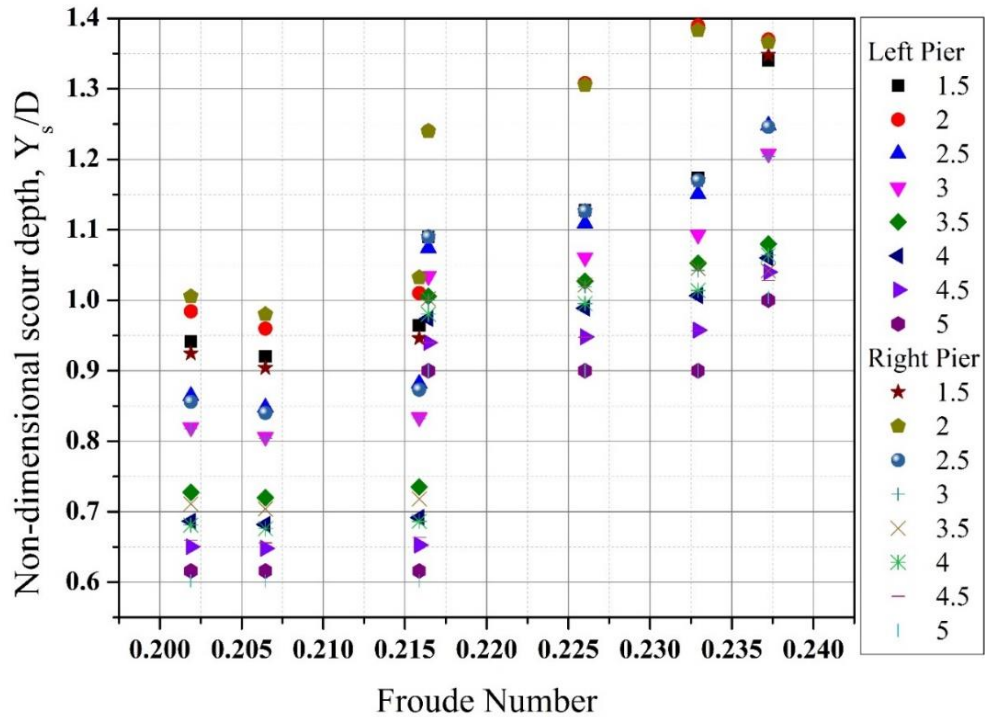


Fig. 4.35 Effect of the Froude number on scour depth downstream of the two piers in side-by-side arrangement

4.5 Two piers at an angle of 15° and 30° arrangement

4.5.1 Experimental Programme and flow characteristics

Details of the experimental setup and instruments used has been discussed in the **Chapter 3**. As discussed in previous chapter all the experiments have been carried out in a recirculating masonry flume, and experimental configuration for two piers at angle of 15° and 30° has been shown in **Fig. 4.36** and **Fig. 4.37**. Experimental programme has been conducted for uniform sediments under the five rate of flow conditions. Flow characteristics used during the experimental programme has been listed in **Table 4.5**. All the experiments have been carried out for eight centre-to-centre pier spacing (P_s) between the piers that are 1.5, 2, 2.5, 3, 3.5, 4, 4.5 and 5 times the diameter of the pier. Two piers of 5 cm diameter mounted with ultrasonic transducers has been utilized as pier model. The depth of flow has been kept in the range of 0.12-0.163 meters. The experimental duration for each experiment has been fixed to 480 minutes as discussed in the previous sections. The scour depth readings have been measured in regular intervals of 30 minutes. After the completion of each experimental run, water from the flume section has been drained out and scour depth around the twin piers has been measured.

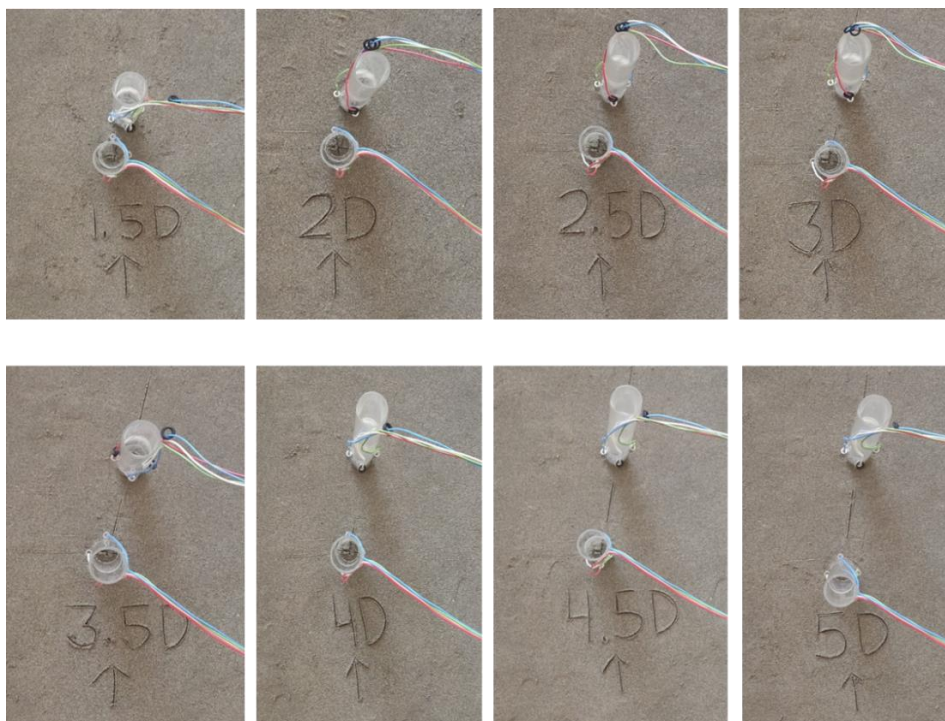


Fig. 4.36 Two piers aligned at 15° angle of attack to the direction of flow

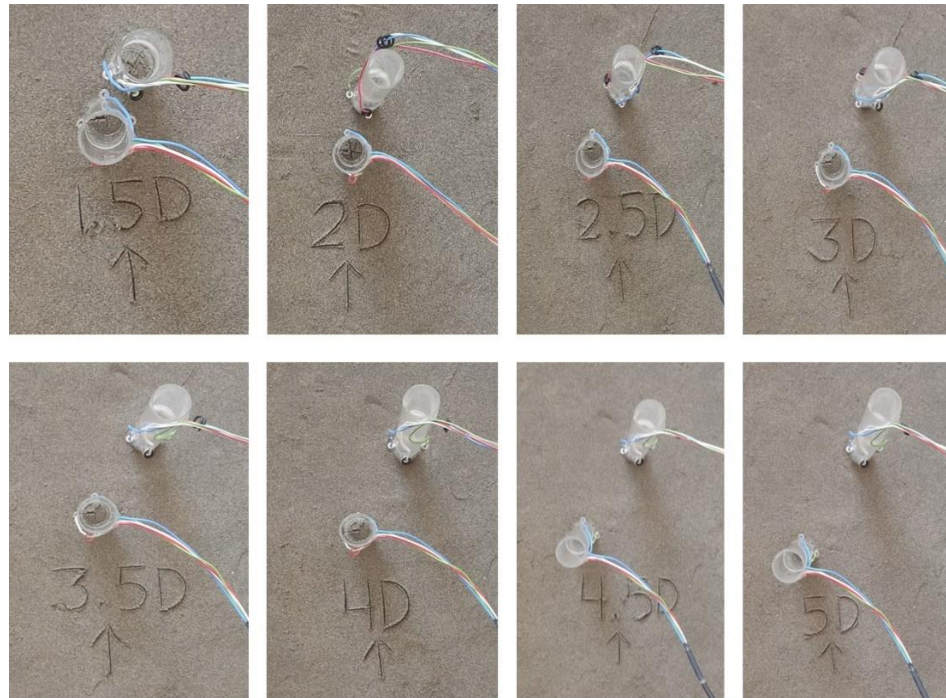


Fig. 4.37 Two piers aligned at 30° angle of attack to the direction of flow

Table 4.5 Flow characteristics for the two-pier aligned at an angle of 15 and 30 degree

Test classification	D (mm)	d_{50} (mm)	h (m)	V (m/sec)	Q (m ³ /sec)	F_r	V_c (m/sec)	V/V_c
A	50	1.75	0.120	0.224	0.0295	0.206	0.235	0.955
B	50	1.75	0.135	0.243	0.0361	0.211	0.239	0.974
C	50	1.75	0.149	0.262	0.0428	0.217	0.243	0.987
D	50	1.75	0.154	0.287	0.0486	0.233	0.244	0.996
E	50	1.75	0.163	0.300	0.0537	0.237	0.247	0.980

4.5.2 Results and Discussions

4.5.2.1 Temporal evolution of scour depth around two piers (angle arrangement)

When the attack angle is greater than zero, the maximum scour depth depends on the attack angle, pier diameter, and spacing. The maximum scour depth most likely occurs at the front pier. This is due to the strengthening of the horseshoe vortices when these vortices are superimposed with the wake vortices from the upstream pier. This superimposition increases as the sediment entrainment at the rear pier increases. And hence the maximum

scour depth around the front pier has been observed more than the rear pier. Maximum scour depth also varies with increasing the pier spacing. As the pier spacing increases, the interaction between two vortices is reduced as the wake vortices deviate away from the horseshoe vortices. And two separate scour holes have been observed around the front and rear pier. The maximum scour depth has been attained at an angle of 15° , and after that the scour depth starts reducing for 30° angle of attack. Temporal scour depth attained in both the cases of 15° and 30° has been presented in the **Fig. 4.38**. The scour depth at the front pier is higher than the scour depth at the rear pier for both angle of attack. However, the scour depth attained for the 30° angle of attack is comparatively less than the scour depth attained for the 15° angle of attack. As the angle of attack increases, the horseshoe vortices at the rear pier interact with the wake vortices from the upstream pier. However, as the attack angle increases to 30° , the maximum scour depth is reduced.

As shown in **Fig. 4.38 (a)**, the scour depth rate at the front pier is 0.0046 mm/sec in initial 60 minutes of experiment. In the next 300 minutes scour depth rate is 0.000105 mm/sec and in the last 120 minutes scour depth rate is 0.0008 mm/sec . Scour depth rate at the rear pier is 0.00417 mm/sec in initial 60 minutes of experiment. In the next 300 minutes scour depth rate is 0.00105 mm/sec and in the last 120 minutes scour depth rate is 0.00056 mm/sec . In the initial 60 minutes for both the piers scour depth increases at comparatively higher rate and in last 120 minutes the temporal scour depth curve is flattened. In **Fig. 4.38 (b)** temporal scour depth attained round the two piers for the 30° angle of attack has been presented. The scour depth around the piers for the 30° angle of attack is less for front and rear piers in comparison to the 15° angle. The scour depth rate at the front pier is 0.0046 mm/sec in initial 60 minutes of experiment, 0.00081 mm/sec in the next 300 minutes scour and in last 120 minutes the scour depth rate is 0.00138 mm/sec the rate of scour depth increases at the rear pier is a 0.0041 mm/sec in initial 60 minutes 0.00094 mm/sec in next 300 minutes and in the last 120 minutes scour depth rate is 0.00084 mm/sec .

For the temporal evolution, the maximum pier scour has been attained in case of 3D pier spacing at the front pier in both cases due to the presence of the interdependency of both the piers on each other. Both piers when placed in proximity at small angles, the effect of the flow field around the piers is increased. The flow field area transverse to the direction of flow, at the upstream of two piers positioned in the angled arrangement has been

increased, and consequently the scour depth has also been increased. As the pier spacing is increased the influence of the front pier on the rear pier has been reduced and consequently, a reduction in the scour depth has been recorded. The minimum scour depth has been attained in the case of 1.5D pier spacing at the upstream end of the rear pier.

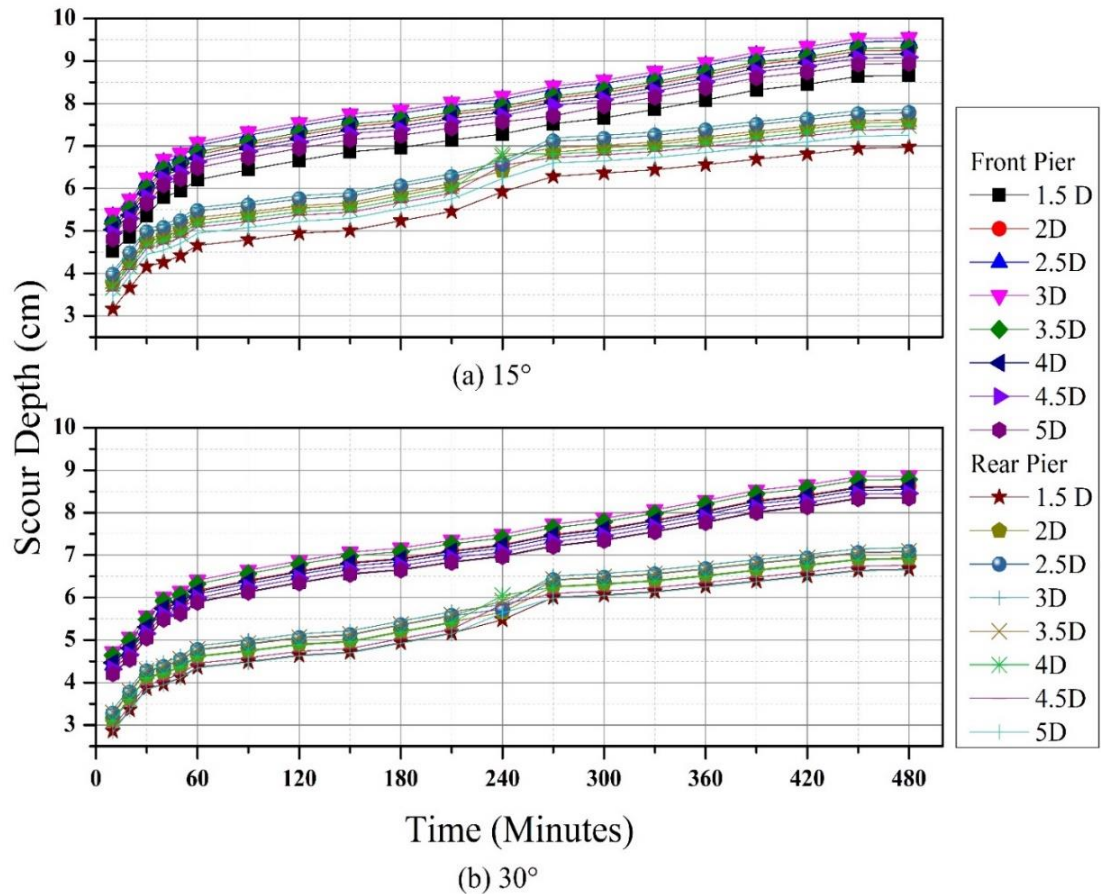


Fig. 4.38 Temporal Evolution of scour depth around two piers aligned at (a) 15° and (b) 30°

4.5.2.2 Effect of Pier Spacing on the Non-Dimensional Scour Depth

The effect of pier spacing plays an important role in the scour depth estimation process. The effect of pier spacing on the scour depth for both the angle (15° and 30°) arrangements has been presented in **Fig. 4.39 (a) and (b)**. The maximum scour depth observed for the 15° angle of attack is greater than the maximum scour depth observed for 30° angle of attack as shown in **Fig. 4.39**.

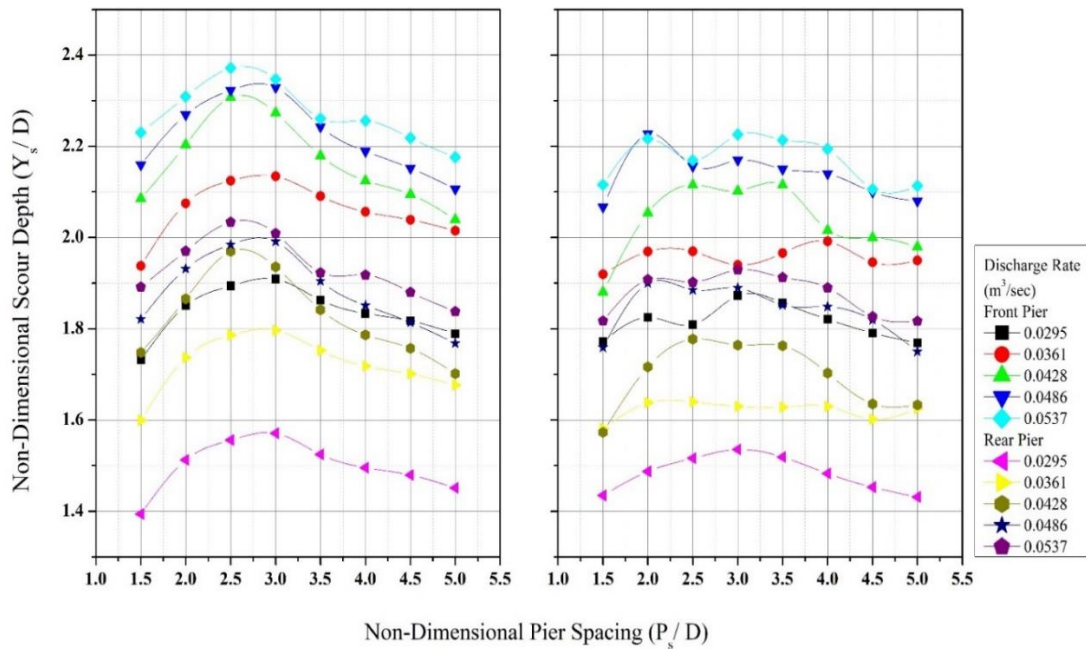


Fig. 4.39 Effect of angle of attack on the non-dimensional scour depth at two piers aligned at an angle of (a) 15° and (b) 30°

In both the cases the maximum scour depth has been observed for highest value of rate of flow $0.0537 \text{ m}^3/\text{sec}$. In case of 15° angle of attack the maximum scour, depth has been attained for the 2.5D pier spacing and minimum has been attained for the 5D pier spacing. Whereas for the 30° angle of attack maximum has been attained for the 2D pier spacing and minimum has been attained for the 5D pier spacing. The scour depth in both cases increases from 1D-2.5D, and afterwards scour depth starts reducing. Peak scour depth can be attained between 2D-3D, and minimum for the pier spacing $\geq 5D$. As the pier spacing increases from 1.5D-3D, the equivalent diameter of the pier for the 15° angle of attack has been increased, and then the maximum scour depth also increases. Maximum scour depth has been achieved at 2.5D pier spacing at 15° angle of attack on the upstream of the front pier, this is due to the presence of maximum drag force at the front pier. As per the (Sumer et al. 2005) the maximum scour depth is observed at the front pier at 2D-3D due to the increase in the horseshoe vortex formation. For small pier spacing the rear pier acts as a blockage in the flow direction and increases the size of the wake vortices and consequently the larger horseshoe vortices are formed on the front pier. The minimum scour depth has been achieved at 5D pier spacing on the rear pier for the $0.0295 \text{ m}^3/\text{sec}$ at 30° angle of attack.

4.6 Three piers in tandem arrangement

4.6.1 Experimental Programme and flow characteristics

Details of the experimental setup and instruments used has been discussed in the **Chapter 3**. As discussed in previous chapter all the experiments have been carried out in a recirculating masonry flume. Acrylic pipes of diameter, D , 50 mm, have been used as pier models, laid in the center of the working section at centre-to centre pier spacing, $P_s = 1, 2, 3, 4$ and 5 times the diameter of the pier. The arrangement of Pier models has been shown in **Fig. 4.40**. The whole experimental study has been conducted for three rates of flow (Q). Fifteen experiments have been performed using three piers in tandem arrangement. The experimental run has been conducted for 480 minutes. For precisely measuring the pattern of the scour evolutions, bed measurements have been recorded with the SeaTek ultrasonic ranging transducers. Transducers data has been recorded after every 10 minutes for the first 60 minutes, and after every 30 minutes for the next 420 minutes of the experimental duration. The water pump has been turned off at the completion of each experimental test, and water has been drained from the flume section. For final sand bed level measurements, a vernier-point gauge measurement with a precision of ± 0.1 mm has been utilized. The scour depth has been measured after 24 hours of water drainage using a vernier point gauge with ± 0.1 mm resolution, and an intense light was used to read the scour depth. The flow characteristics used during the experimental tests are tabulated below in **Table 4.6**:

Table 4.6 Flow characteristics for the three piers in the tandem and side by side arrangement

Set No.	d_{50} (mm)	Depth of flow, H (m)	V (m/sec)	Discharge, Q (m^3/sec)	Froude's Number, F_r	Reynolds' number, R_e	V_c (m/sec)	V/V_c
1	1.75	0.120	0.224	0.0295	0.206	30100	0.308	0.72
2	1.75	0.149	0.262	0.0428	0.217	43700	0.317	0.83
3	1.75	0.163	0.300	0.0537	0.237	54800	0.321	0.93

Where, D = pier diameter ; d_{50} = mean particle size; H = water depth above the sand bed; V = averaged velocity of approaching flow; Q = rate of flow; F_r = Froude number; V_c = critical velocity of the approaching flow; R_e = Reynold's number.



Fig. 4.40 Three piers positioned in the tandem arrangement

4.6.2 Results and discussion

4.6.2.1 Temporal evolution of scour depth around three piers in tandem arrangement

Temporal scour depth evolution around the three piers positioned in the tandem arrangement has been shown in **Fig. 4.41**, **Fig. 4.42** and **Fig. 4.43** for the three rate of flow conditions $0.0295 \text{ m}^3/\text{s}$, $0.0428 \text{ m}^3/\text{s}$ and $0.0537 \text{ m}^3/\text{s}$ respectively. The temporal scour depth for all the piers at the upstream side has been presented. For the rate of flow $0.0295 \text{ m}^3/\text{s}$ the scour depth at the front, mid and rear pier is presented in **Fig. 4.41**. The maximum scour depth has been obtained for the pier spacing $3D$ at the upstream of the front pier and minimum has been obtained for the pier spacing $5D$ at the rear pier. The scour depth at the rear pier has comparatively very less than the front pier. In the initial one hour of experiment, front and mid pier behave as one body and the scour depth observed is nearly same, whereas the rear pier has been behaving as a sheltered object and consequently the scour depth observed is comparatively very less. As the rate of flow increased the scour evolution pattern around the pier has also changed. As shown in the **Fig. 4.42** and **Fig. 4.43**, the scour depth evolution for the front and mid pier in the initial phase (60 minutes) for the rate of flow $0.0428 \text{ m}^3/\text{s}$ and $0.0537 \text{ m}^3/\text{s}$ is nearly same and rear pier is also participating in the same trend.

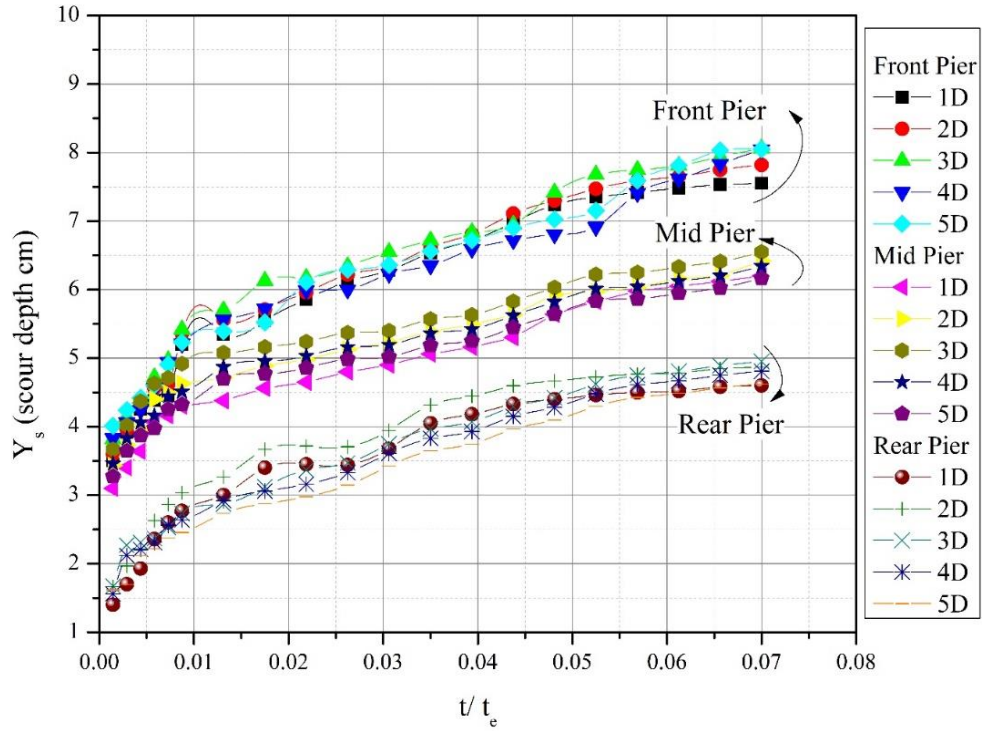


Fig. 4.41 Temporal evaluation of scour depth around three piers in the tandem arrangement at $0.0295 \text{ m}^3/\text{s}$ rate of flow

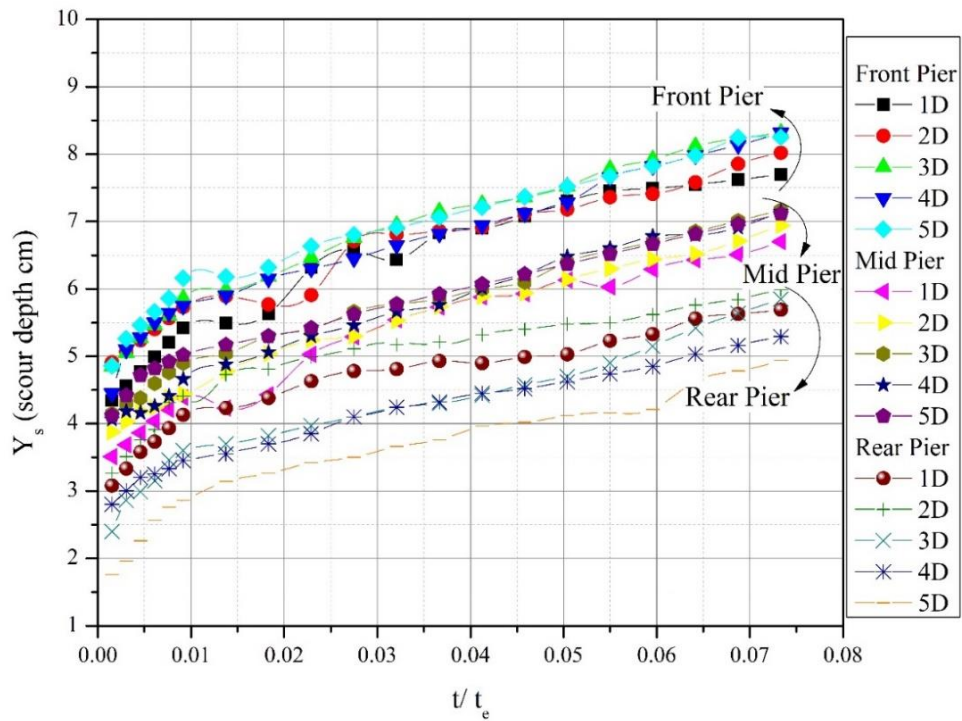


Fig. 4.42 Temporal evaluation of scour depth around three piers in the tandem arrangement at $0.0428 \text{ m}^3/\text{s}$ rate of flow

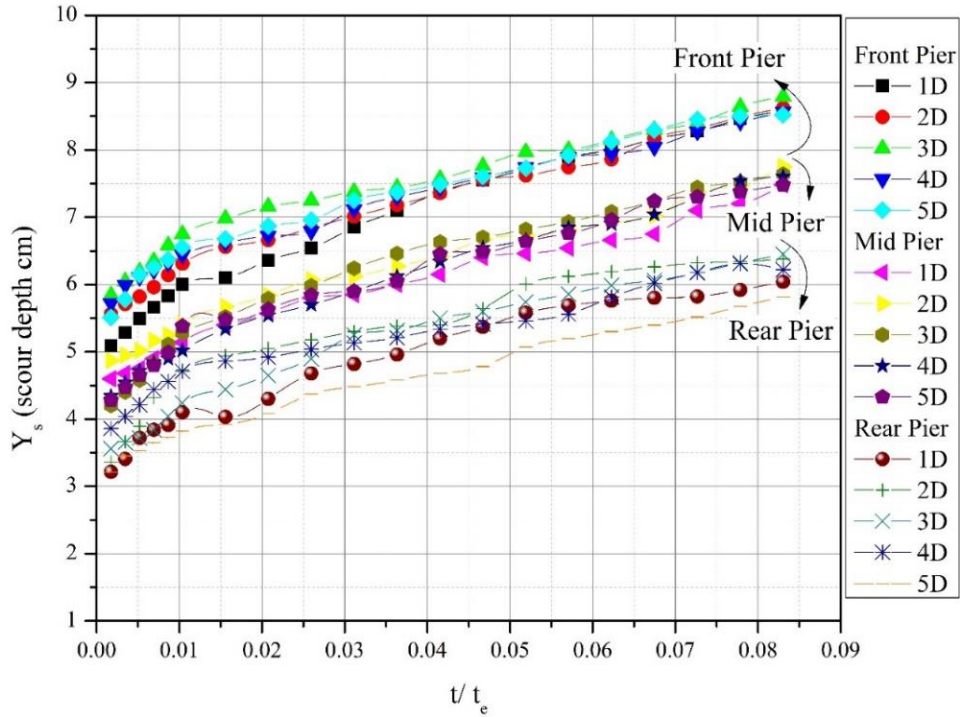


Fig. 4.43 Temporal evaluation of scour depth around three piers in the tandem arrangement at $0.0537 \text{ m}^3/\text{s}$ rate of flow

Results of the temporal study around three piers states that for the low rate of flow, all the three piers behave individually, and the scour depth observed is distinct for each pier. Whereas for the high rate of flow in the initial stage the scour depth around the piers may be nearly same but after the lapse of initial stage all piers behave individual, and the scour depth observed is also distinct. The difference between the scour depth observed for all the pier at the high rate of flow condition and low rate of flow condition is significant. As the rate of flow is increased the scour depth is also increased.

4.6.2.2 Effect of pier spacing on the three piers in tandem arrangement

As discussed, earlier scour phenomenon around the group of piers has been classified as global scour and local scour. The scour hole formed after the completion of the experimental duration for all the pier spacing has been presented in the **Fig. 4.44**. For the small pier spacing $1D$ and $2D$ both global and local scour holes are formed around the piers. For small pier spacing, three piers contact each other and the scour development pattern is similar to the single pier scour pattern but with the large pier diameter. The scour

depth at the upstream of the front pier increases for the pier spacing range 1D-3D and after that it starts decreasing up to 5D pier spacing.

For the pier spacing 1D, three small local scour holes have been formed around the pier and one big global scour hole around the three-pier group has been formed. Sediment has been deposited between the piers and on the downstream of the rear pier. Only one tail scour has formed, and its length has been reached up to 59 cm. Likewise 1D pier spacing, for 2D pier spacing also, three local scour holes and one global scour holes are formed around the piers. Dimensions of all the scour hole formed has been presented in **Fig. 4.44**. The scour hole formed in case of 2D pier spacing is bigger in size and the length of tail scour reaches up to 65.5 cm. For 3D pier spacing, three individual scour holes are formed around the three piers. Sediments gets deposited between the piers in the form of large mounds and on the downstream side of the rear pier. The tail scour depth reaches up to 65 cm in the straight direction behind the rear pier. For 4D pier spacing, piers started behaving partly independently, and three separate scour holes are formed around the piers.

A large amount of sediments has been deposited between the pier and the rest of the sediments gets deposited on the downstream side of the rear pier. The length of the tail scour depth has been observed as 36 cm, which is comparatively less than the 1D and 2D pier spacing. For 5D pier spacing only local scour has been observed, all the piers are behaving independently, and three separate scour holes are formed around individual pier. A part of the sediment transported from the upstream of the scour hole gets deposited behind the individual piers and the remaining part has been deposited on the downstream of the rear pier in the form of tail scour. The length of the tail scour depth observed in this case is 40 cm.

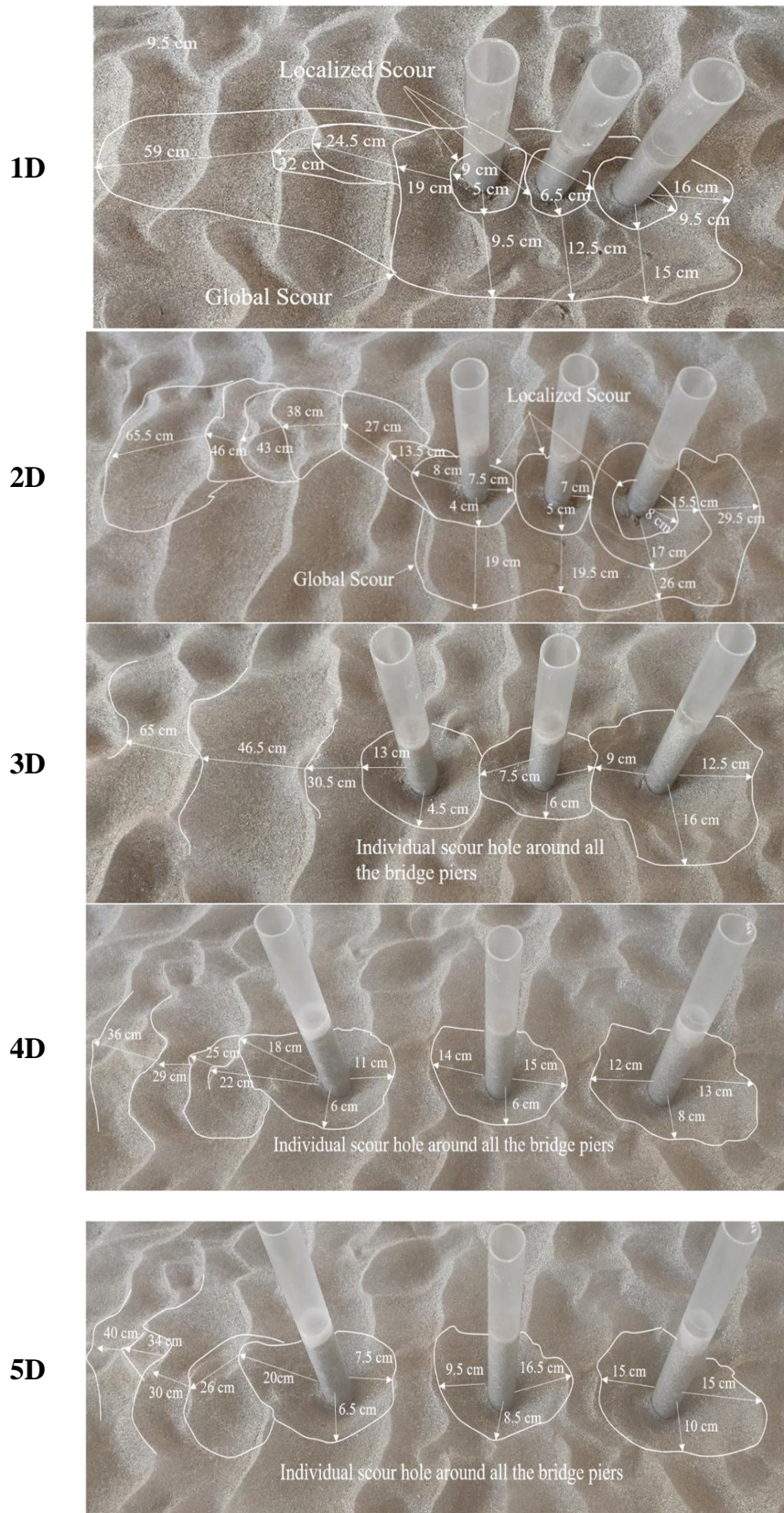


Fig. 4.44 Scour depth around the three piers in the tandem arrangement

As the pier spacing increases the scour depth around the three piers has increased. For the pier spacing range 1D-3D the piers have influence of each other, whereas for the pier spacing 4D-5D piers behave individually. The mutual interdependency of the piers is more prominent for the small pier spacing due to the interplay of the vortices between the pier spacing and at the toe of the front pier. Hence the pier spacing plays an important role in the understanding the scour depth pattern and this factor must be considered for the accurate estimation of the scour depth.

4.6.2.3 Froude number effect on the scour depth around three piers in tandem arrangement

Effect of the Froude number on the scour depth around the three piers at all the four observation points, upstream, right, left and downstream has been presented below in **Fig. 4.45, Fig. 4.46, Fig. 4.47 and Fig. 4.48**. In **Fig. 4.45**, variation of the non-dimensional scour depth (Y_s/D) around the three piers at the upstream side has been presented. As the Froude number increases the scour depth also increases, whereas with the increase in the pier spacing Y_s/D has been decreased. The maximum Y_s/D scour depth has been obtained at the front pier and minimum has been obtained at the rear pier. As the Froude number increases the difference between the scour depths observed at the front mid and rear pier has been reduced. Because, as the Froude number increases, velocity of flow also increases, due to this increase in the flow velocity the process of vortex formation around the piers has been accelerated. In this accelerated vortex formation, more sediment material has been taken away from the upstream sides of the pier and gets deposited on the downstream side of the rear pier. Particularly, in case of three piers more vortices are generated around the front pier, due to the increase in the attacking area of the flowing water.

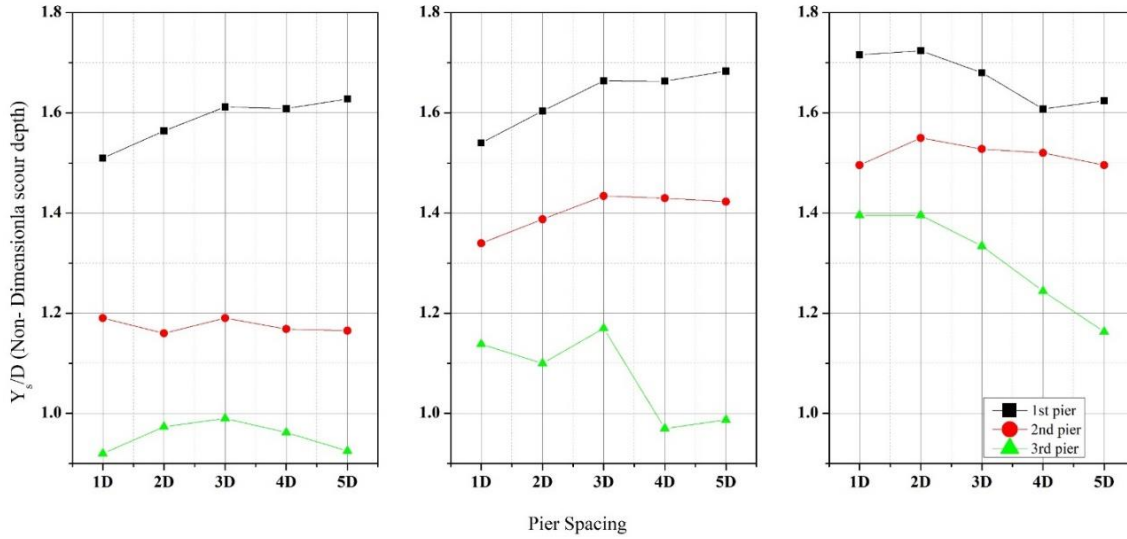


Fig. 4.45 Variation of non-dimensional scour depth with the pier spacing on the upstream side of the piers for the Froude number (a) 0.206, (b) 0.217 and (c) 0.237

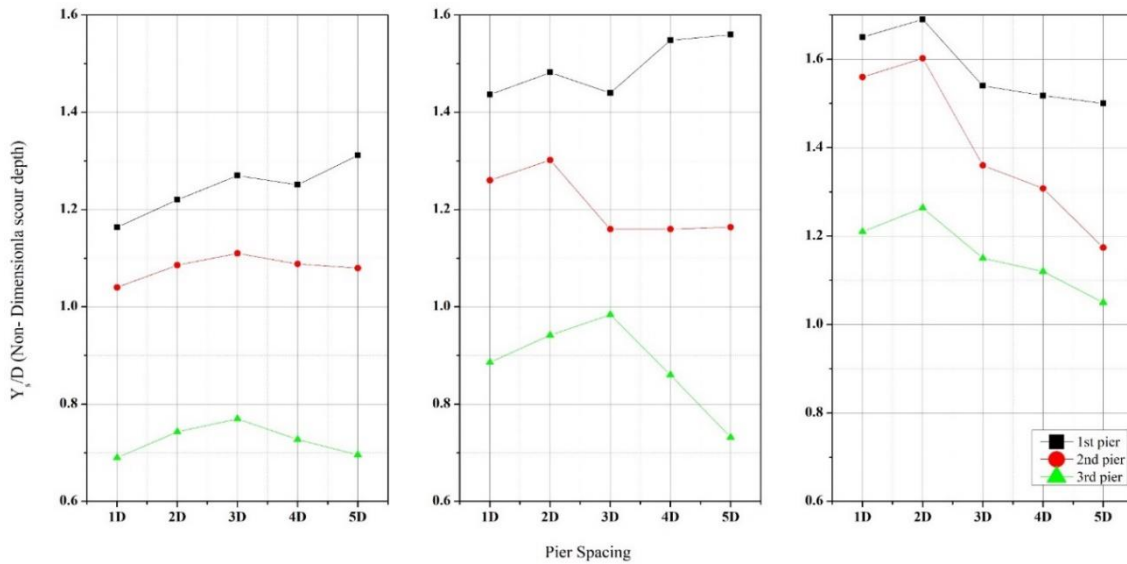


Fig. 4.46 Variation of non-dimensional scour depth with the pier spacing on the right side of the piers for the Froude number (a) 0.206, (b) 0.217 and (c) 0.237

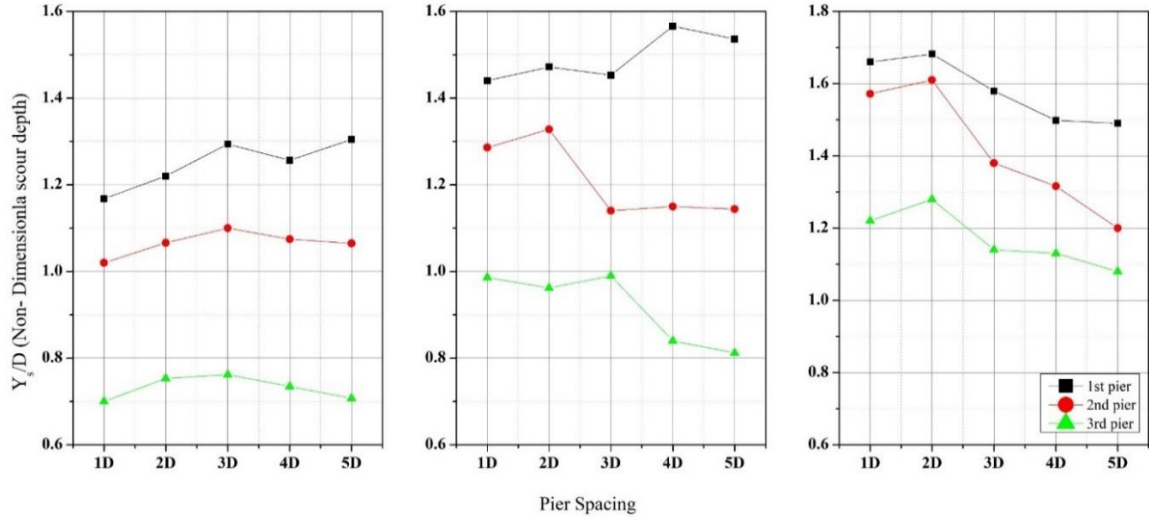


Fig. 4.47 Variation of non-dimensional scour depth with the pier spacing on the left side of the piers for the Froude number (a) 0.206, (b) 0.217 and (c) 0.237

In **Fig. 4.46** and **Fig. 4.47** the non-dimensional scour depth on the right and left side of the piers has been depicted. The trend of the scour depth on the left and right sides are quite similar. For the Froude number 0.206, and 0.217, the trend of scour depth starts changing from 3D pier spacing and for the Froude number 0.237 the trend changes from 2D pier spacing. Which means as the Froude number increases the trend of the scour depth changes for varying pier spacing. The scour depth at the rear pier decreases rapidly after 3D pier spacing for all the Froude number conditions.

Fig. 4.48 depicts the non-dimensional scour depth at the downstream side for all the piers. The downstream scour depth also increases with the increase in Froude number. The non-dimensional scour depth at the mid pier changes significantly with the increasing Froude number. For the 0.206 and 0.217 Froude number the scour depth at the mid and rear pier is approximately equal to each other. Due to the inflow and outflow of the sediment at the same time from the scour hole around the mid pier.

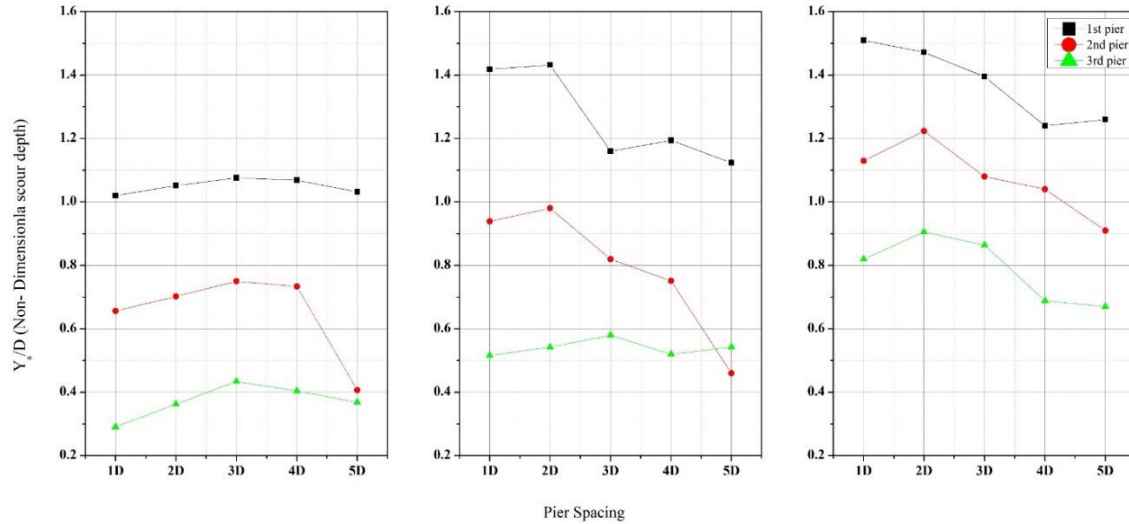


Fig. 4.48 Variation of non-dimensional scour depth with the pier spacing on the downstream side of the piers for the Froude number (a) 0.206, (b) 0.217 and (c) 0.237

4.7 Three piers in side by side arrangement

4.7.1 Experimental Programme and flow characteristics

Details of the experimental setup and instruments used has been discussed in the **Chapter 3**. As discussed in previous chapter all the experiments have been carried out in a recirculating masonry flume. Acrylic pipes of diameter, D , 50 mm, have been used as pier models, laid in the center of the working section at center-to-center pier spacing, $P_s = 1, 2, 3$, and 4 times the diameter of the pier. To avoid the channel wall effect in this section pier spacing has been restricted up to $4D$, details of the channel wall effect has been discussed in the **Chapter 3**. The arrangement of pier models has been shown in **Fig. 4.49**. The whole experimental study has been conducted for three rates of flow (Q). Twelve experiments have been performed using three piers in tandem arrangement. The experimental procedure and flow conditions are already explained in section **4.6.2**.



Fig. 4.49 Three piers in side by side arrangement

4.7.2 Results and discussion

4.7.2.1 Temporal evolution of scour depth around three piers in side-by-side arrangement

The temporal scour depth on the upstream side of the three piers in side-by-side arrangement has been shown in **Fig. 4.50**, **Fig. 4.51** and **Fig. 4.52** for the three rate of flow conditions respectively. As discussed in the section that scour depth increases with the increases in the pier spacing, same trend for the scour depth has also been observed in case of three piers in side-by-side arrangement. Hence the maximum scour depth has been observed in case of maximum pier spacing i.e. 4D and minimum has been observed for minimum pier spacing i.e. 1D. Three-piers in side-by-side arrangement behaves identical like two piers in side-by-side arrangement, the only difference is that the scour depth at the central pier is more in comparison with the two piers case and the scour hole developed in bigger in size. As the flow velocity increases scour depth also increases. As the time of experiment increases scour depth also increases, in the initial 60 minutes scour depth evolves rapidly. After 60 minutes to 300 minutes the rate of increase of scour depth has been reduced in comparison to the first 60 minutes. After lapse of 300 minutes the rate of scour process is relatively reduced and after 360 minutes rate of scour evolution becomes almost constant.

Maximum scour depth has been observed at the central pier, due to the interaction of the horseshoe and wake vortices at the nose of the central pier. At the central pier, horseshoe vortex, downward wave and flowing fluid attacks simultaneously at the toe of the pier, and erodes maximum sediment. Scour depth evolution pattern in side-by-side arrangement on

the upstream sides of the piers is completely different from tandem arrangement. As scour depth in tandem increases upto pier spacing 3D and then decreases upto 5D, whereas in case of side-by-side arrangement as the pier spacing increases scour depth also increases. Due to the experimental restrictions pier spacing upto 4D has only been considered.

The rate of scour evolution on the upstream side in side-by-side arrangement for the 1D pier spacing has been 0.00387 mm/sec , 0.00098 mm/sec and 0.00059 mm/sec for the initial 60 minutes, next 300 minutes and last 180 minutes respectively. For the 2D pier spacing rate of scour evolution has been observed as 0.00365 mm/sec , 0.00096 mm/sec and 0.00088 mm/sec for the initial 60 minutes, next 300 minutes and last 180 minutes respectively. For the 3D pier spacing 0.00395 mm/sec , 0.00096 mm/sec and 0.00089 mm/sec for the initial 60 minutes, next 300 minutes and last 180 minutes respectively. For 4D pier spacing 0.00383 mm/sec , 0.00096 mm/sec and 0.00096 mm/sec for the initial 60 minutes, next 300 minutes and last 180 minutes respectively. For the initial 60 minutes the rate of scour evolution remains almost constant for all the pier spacing, for the 300 minutes rate of scour evolution increases for the increasing pier spacing, whereas for the last 180 minutes this rate increases as the pier spacing increases.

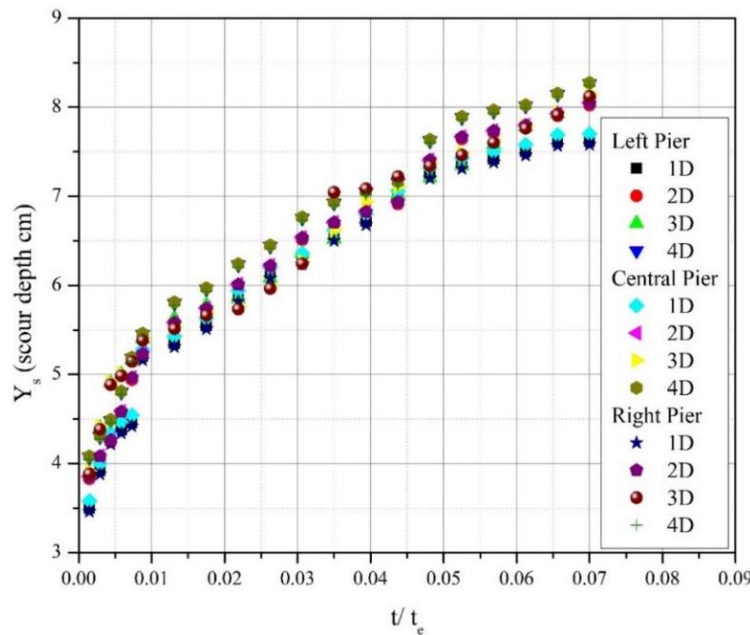


Fig. 4.50 Temporal evolution of scour depth on the upstream side of the side-by-side pier arrangement for $V= 0.224 \text{ m/sec}$

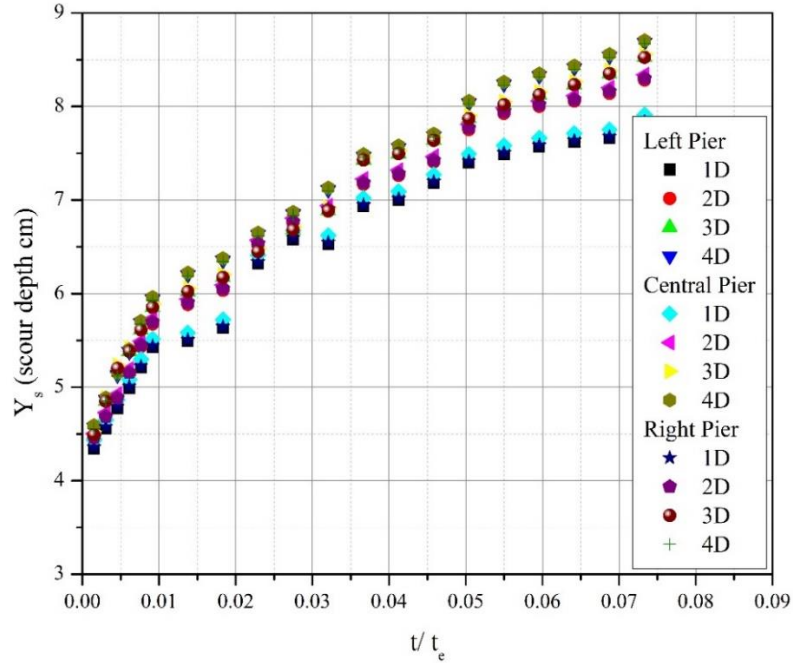


Fig. 4.51 Temporal evolution of scour depth on the upstream side of the side-by-side pier arrangement for $V= 0.262$ m/sec

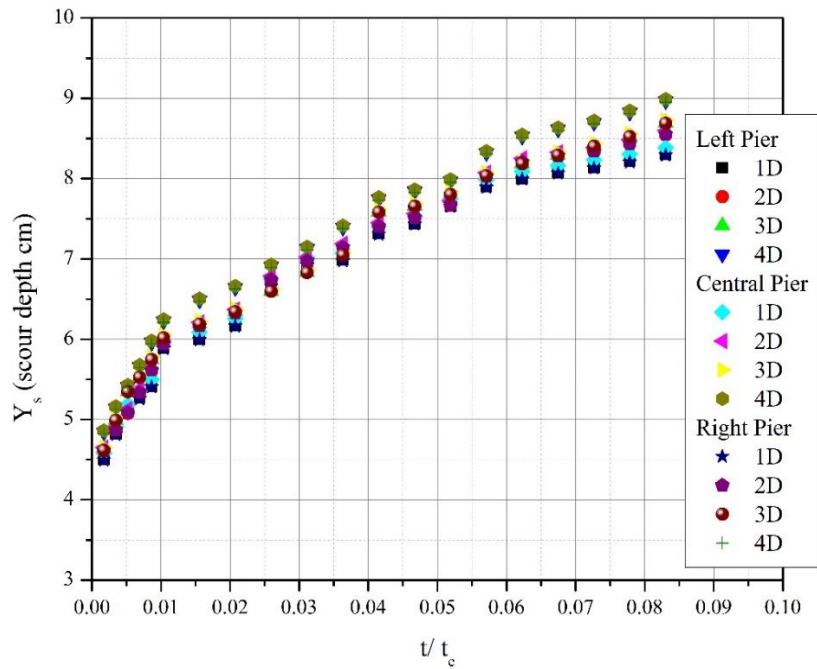


Fig. 4.52 Temporal evolution of scour depth on the upstream side of the side-by-side pier arrangement for $V= 0.3$ m/sec

The temporal evolution around the three piers in the side-by-side arrangement on the downstream side of the piers has been presented below in the **Fig. 4.53**, **Fig. 4.54** and **Fig.**

4.55 for the three rate of flow conditions respectively. Unlike the scour depth on the upstream side of the pier, scour depth at the downstream side of right, left and central piers is completely similar to each other for all the four pier spacing. Scour depth increases with the increase in the pier spacing. The scour evolution curve on the downstream side is more flat than the upstream curve. The rate of scour evolution on the downstream side is comparatively very less than the scour evolution rate on the upstream side. The rate of scour evolution on the downstream side of all the piers for four pier spacing remains almost similar as shown in the scour evolution curves below in the **Fig. 4.53, Fig. 4.54 and Fig. 4.55**.

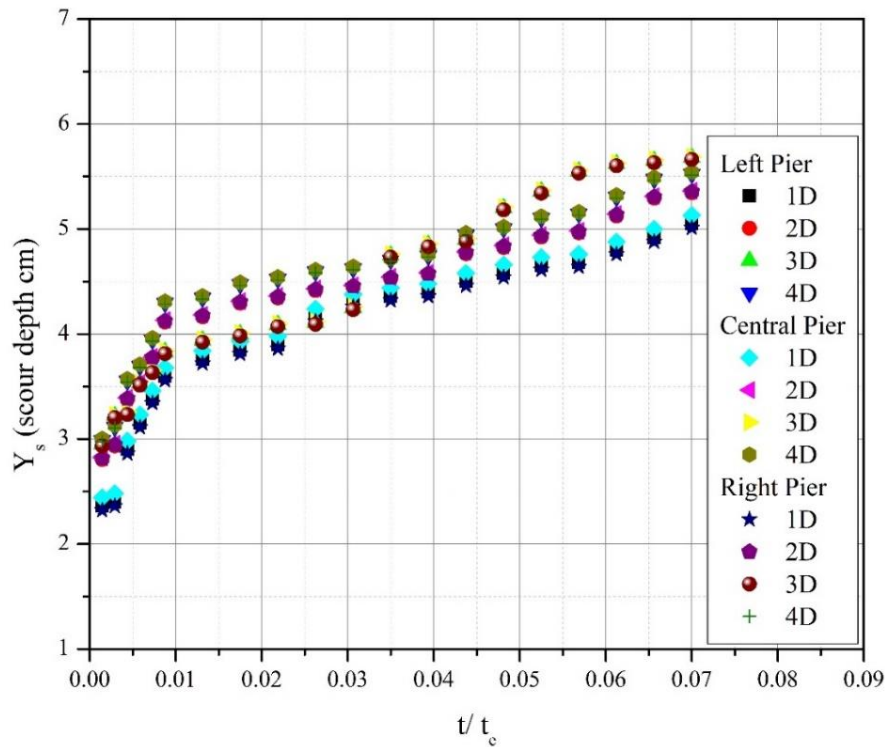


Fig. 4.53 Temporal evolution of scour depth on the downstream side of the side-by-side pier arrangement for $V= 0.224$ m/sec

The rate of scour evolution on the downstream side in side-by-side arrangement for the 1D pier spacing has been 0.00306 mm/sec, 0.00046 mm/sec and 0.00065 mm/sec for the initial 60 minutes, next 300 minutes and last 180 minutes respectively. For the 2D pier spacing rate of scour evolution has been observed as 0.00336 mm/sec, 0.00038 mm/sec and 0.00061 mm/sec for the initial 60 minutes, next 300 minutes and last 180 minutes respectively. For the 3D pier spacing 0.00269 mm/sec, 0.00053 mm/sec and 0.00070 mm/sec for the initial

60 minutes, next 300 minutes and last 180 minutes respectively. For 4D pier spacing 0.00336 mm/sec, 0.00040 mm/sec and 0.00059 mm/sec for the initial 60 minutes, next 300 minutes and last 180 minutes respectively.

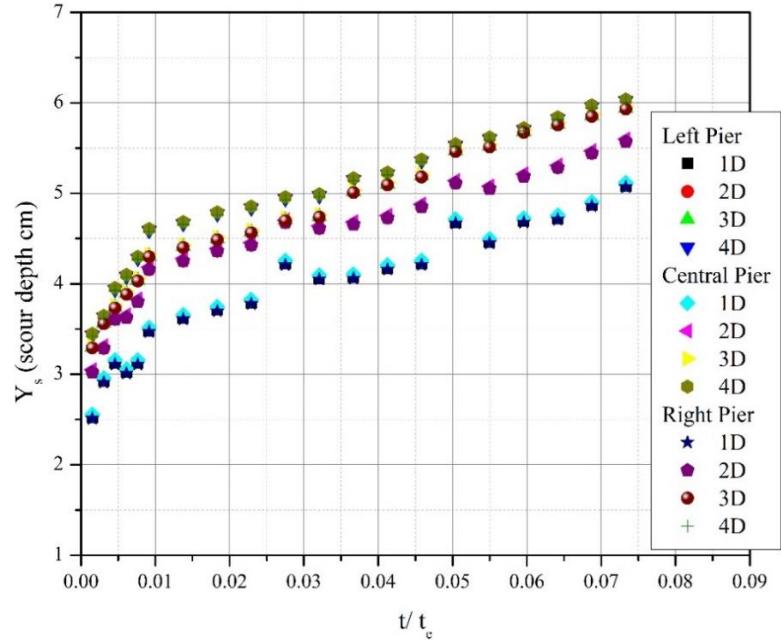


Fig. 4.54 Temporal evolution of scour depth on the downstream side of the side-by-side pier arrangement for $V=0.262$ m/sec

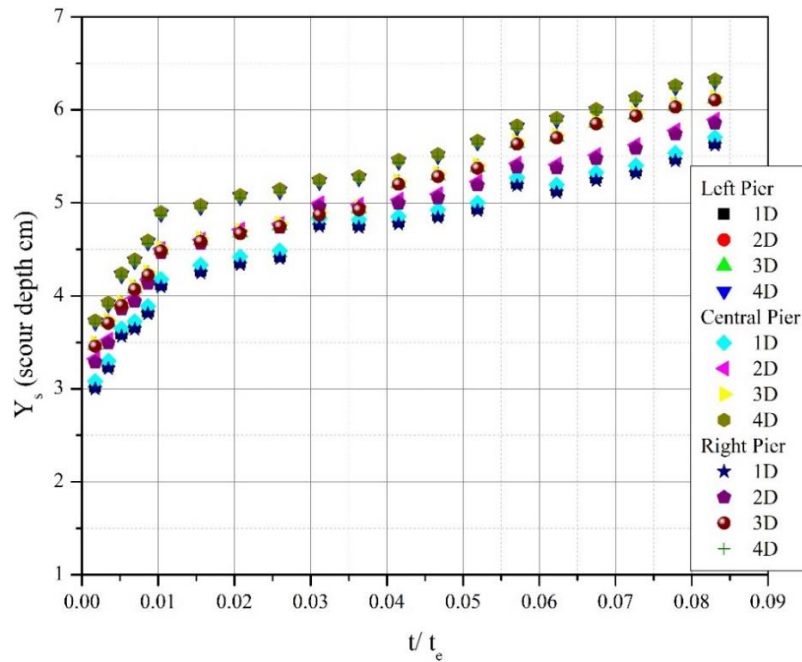


Fig. 4.55 Temporal evolution of scour depth on the downstream side of the side-by-side pier arrangement for $V=0.3$ m/sec

4.7.2.2 *Effect of pier spacing on the three piers in side-by-side arrangement*

To analyze the effect of pier spacing, scour hole pattern observed for all the four pier spacing has been presented in the **Fig. 4.56**. The scour depth around the piers has been categorized into two parts, global and local scour, details has been discussed earlier in section **4.3.3.1**. For 1D pier spacing local scour and global scour has been observed around the three piers, on the downstream side of piers three separate tail scour has been formed near the piers and ultimately merges into one tail scour. Sediment particles eroded from the upstream of the piers gets deposited on these tails scours. The maximum length of the tail scour for the 1D pier spacing has been observed as 48 cm. For the 2D pier spacing the scour hole observed on the upstream side of the left and right pier is of similar dimensions, whereas around the central pier more scour has been observed. For 2D pier spacing also both local and global scour has been observed and like in case of 1D pier spacing, in this case also three tails scours has been observed on the downstream side of the piers, and merges into one tail scour. The maximum range of the tail scour and sediment deposition goes upto 80 cm.

For 3D pier spacing only local scour around the piers has been observed. Three separate scour holes has been formed around the piers, scour holes formed are not interacting with each other. The scour hole on the upstream and downstream side of the piers is approximately similar. Three separate tail scours has been observed on the downstream side, which shows the complete independent behaviour of the bridge piers. The maximum range of the tail scour on the downstream side of the pier ranges upto 53 cm. Lastly, for the 4D pier spacing like in the case of 3D pier spacing, only local scour in the form of three separate scour holes has been observed. And on the downstream side of the piers three separate tail scours has been observed, which are ranging upto 52.5 cm. For 3D and 4D pier spacing piers are behaving completely independent, pier positioning has not influencing each other. The width of the scour hole observed in more for 3D and 4D than 1D and 2D due the increase in the attacking area and involvement of the vortices with each other.

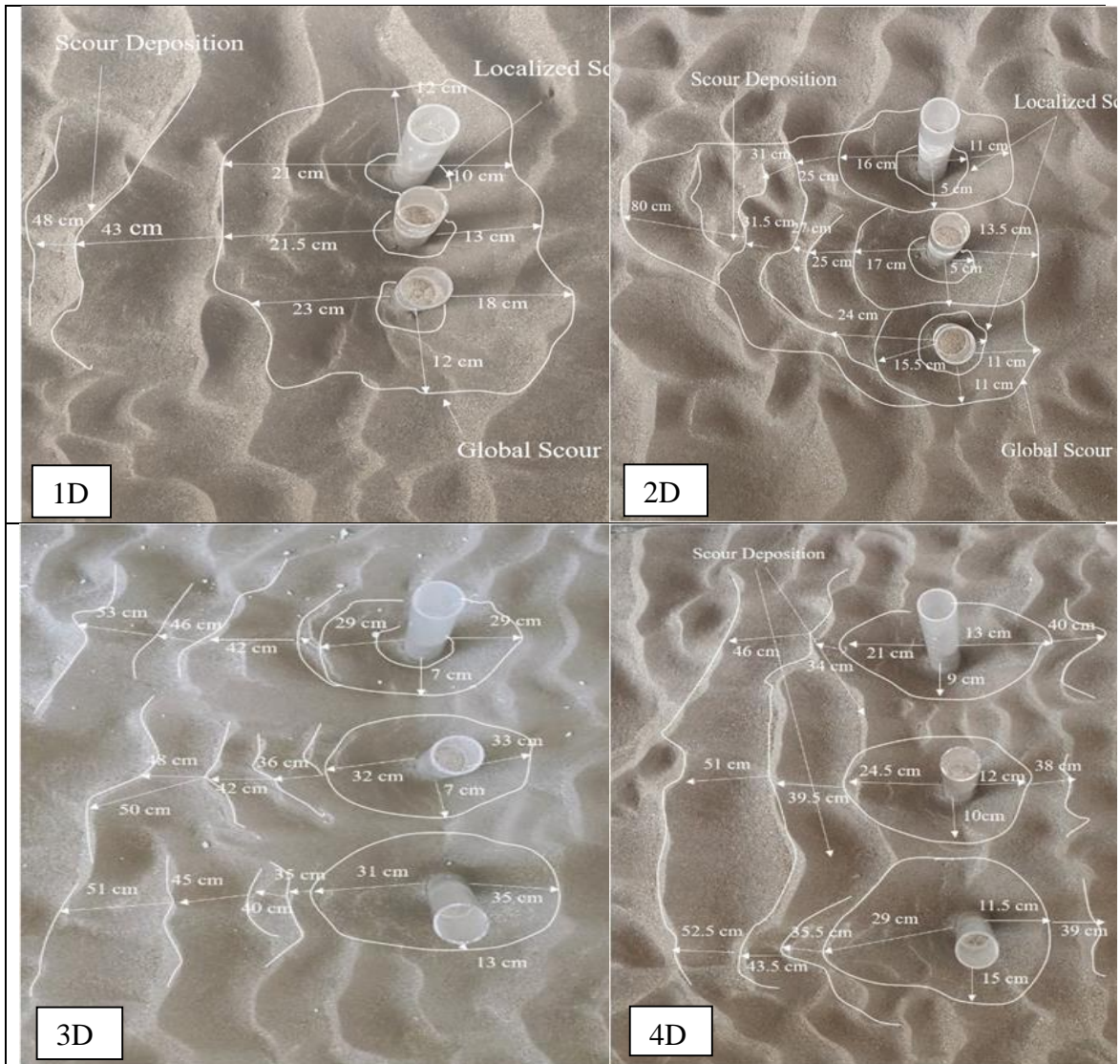


Fig. 4.56 Scour depth around the three piers in side-by-side arrangement

4.7.2.3 Froude number Effect on the Scour Depth

The effect of the Froude number on the scour depth on upstream side, right side, left side, and downward side has been shown in **Fig. 4.57** for the all four pier spacing. As discussed earlier in section 4.6.3.3, Scour depth increases with the increase in the Froude number, the trend has been shown below in **Fig. 4.57**. For the upstream side, **Fig. 4.57** (a) shows that the maximum scour depth has been attained at the central pier for all the pier spacing, and right and left piers have behaved almost identical. For the left and right side as shown in **Fig. 4.57** (b) and (c), pier have behaved identical for one pier spacing. And on

downstream side as shown in **Fig. 4.57** (d), maximum has been attained for the 4D pier spacing and minimum for 1D pier spacing.

Influence of Froude number on the scour depth for the two piers in side-by-side arrangement and three piers in side-by-side arrangement is similar. Hence it can be said that for the side-by-side arrangement pier scour behaves linearly with the Froude number and pier spacing.

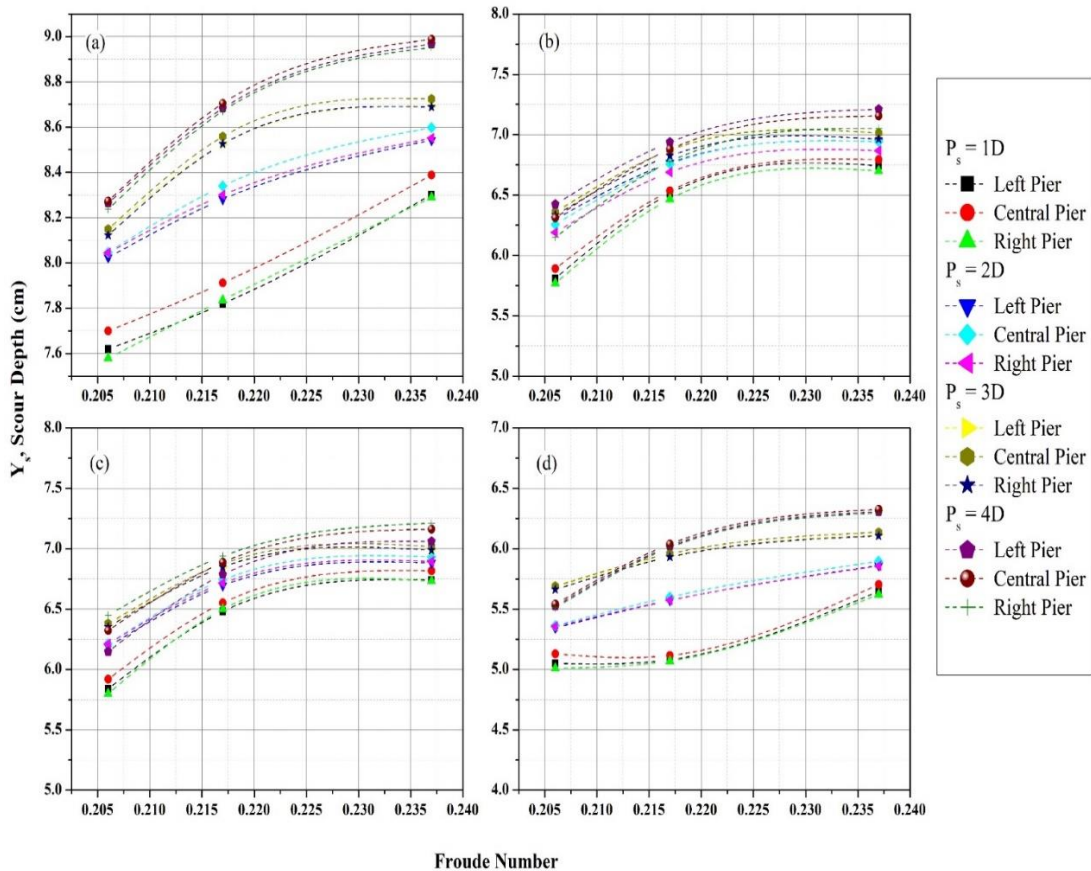


Fig. 4.57 Effect of Froude number on scour depth for side-by-side arrangement at (a) upstream side, (b) right side, (c) left side, and (d) downstream side

4.8 Three Piers in staggered arrangements

4.8.1 Experimental Programme and flow characteristics

Details of the experimental setup and instruments used has been discussed in the **Chapter 3**. As discussed in previous chapter all the experiments have been carried out in a

recirculating masonry flume. Acrylic pipes of diameter, D , 50 mm, have been used as pier models, laid in the center of the working section at center-to-center pier spacing, $P_s = 1.5, 2, 2.5, 3, 3.5, 4, 4.5$ and 5 times the diameter of the pier. As the flow-field is very complex in staggered arrangement so eight pier spacing has been considered. The arrangement of pier models has been shown in **Fig. 4.58**. The whole experimental study has been conducted for three rates of flow (Q). Twenty four experiments have been performed using three piers in staggered arrangement. The experimental procedure and flow conditions have been furnished in section 4.6.2.

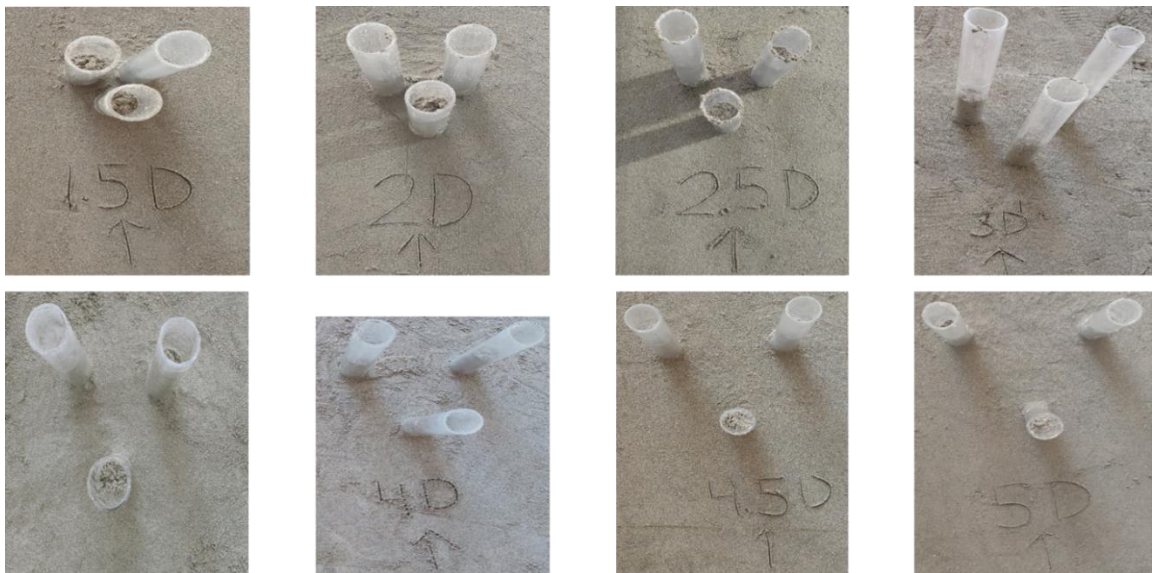


Fig. 4.58 Three piers in staggered arrangement

4.8.2 Results and discussion

4.8.2.1 Temporal evolution of scour depth around three piers in staggered arrangement

The temporal scour depth around the three piers in the staggered arrangement has been observed for all the three rate of flow conditions and results are presented in the **Fig. 4.59, Fig. 4.60 and Fig. 4.61**. Three piers placed in the staggered arrangement are named as, central pier (front pier), Right pier (downstream pier in the right side to the direction of flow), left pier (downstream pier in the left side to the direction of flow). The maximum scour depth has been observed at the central pier for the $P_s = 2.5-3D$ pier spacing for all the rate of flow conditions, and minimum scour depth at the central pier has been observed for the $P_s = 1.5D$. As downstream piers has similar behaviour for all the rate of flow, and

maximum scour erosion occurs at the node of the central pier. The horseshoe vortices generated from the upstream of the central pier gets merged with the wake vortices on the downstream piers and erodes the more sediment material from the pier vicinity. For the large pier spacing the scour depth at the downstream pier decreases due to the weakened wake vortices in the mid-section of the piers, this weak vortices flow acts on the downstream pier as approaching velocity.

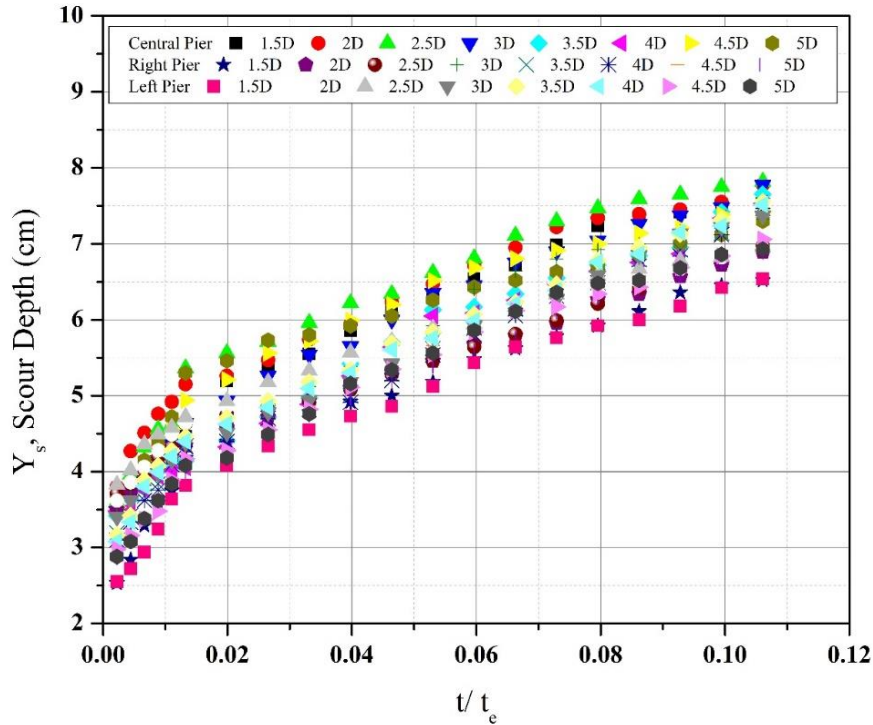


Fig. 4.59 Temporal scour depth around three piers aligned in staggered arrangement for $V=0.224$ m/sec

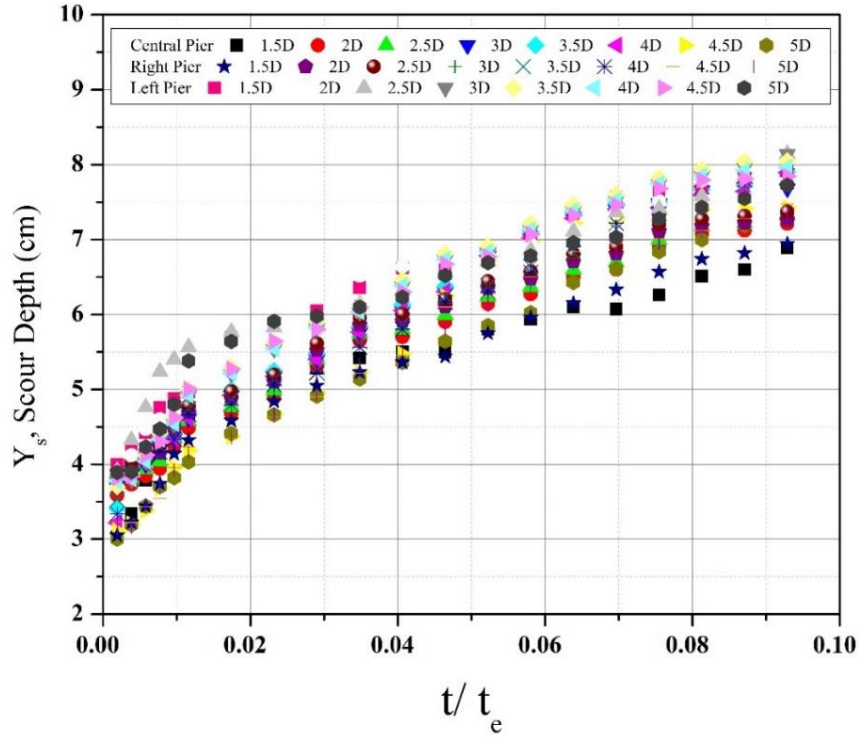


Fig. 4.60 Temporal scour depth around three piers aligned in staggered arrangement for $V= 0.262$ m/sec

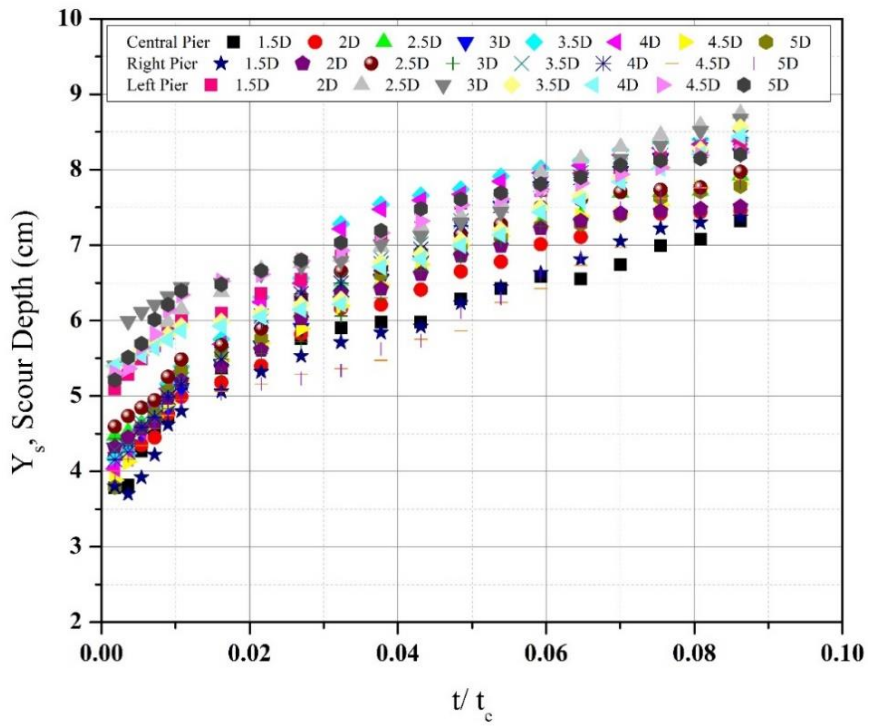
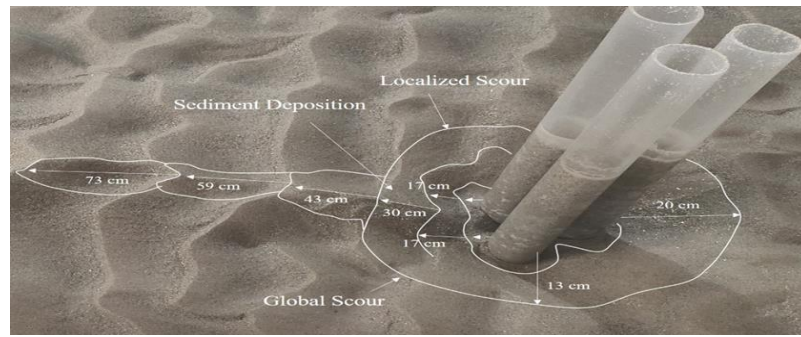


Fig. 4.61 Temporal scour depth around three piers aligned in staggered arrangement for $V= 0.30$ m/sec

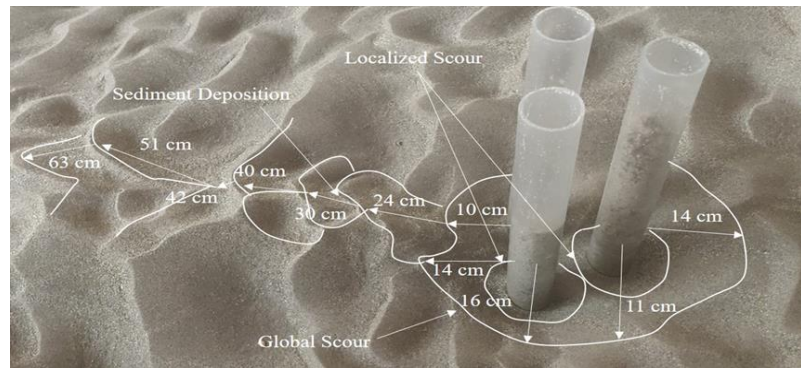
In **Fig. 4.59, Fig. 4.60 and Fig. 4.61**, shows that in the initial t/t_e range of 0.02 the scour evolution increases rapidly in the similar manner for the piers under same rate of flow conditions. For the next t/t_e range of $0.02-0.06$ the rate of scour evolution increases and for the t/t_e range of $0.06-0.085$ the rate becomes almost constant. So, it can be stated that the scour evolution increases with the increase in the time upto t/t_e range of 0.06 or upto 300 minutes of the initial experimental duration. After the 300 minutes the rate of scour evolution is reduced becomes almost constant. Hence, it can be concluded that for the staggered pier arrangement, after lapse of the 300 minutes the rate of scour evolution becomes constant so minimum duration should be kept 300 minutes.

Fig. 4.62 shows the pictures of the scour hole observed after the completion of the experiments for eight pier spacing. For the $1.5D$ pier spacing both local and global scour depth has been observed. For the close proximity of the piers three piers behaves as a single pier of larger diameter and scour hole observed is also in the form of single scour hole of bigger size. The scour on the upstream side of the pier is 20 cm. Scour hole developed is in the form of one local scour hole and one big scour hole. Sediment eroded from the upstream side has been deposited on the downstream side in the centre of two piers. Sediment has been deposited in the form of one tail scour and the length of this tail scour reaches upto 73 cm. Similar scour hole developments has been witnessed for the $2D$ and $2.5D$ pier spacing and tail scour depth approaches to 63 and 86 cm respectively. For the $3D$ pier spacing scour hole developed around the piers stars growing partially independently. And local scour holes are developed in the form of three separate scour holes, scour hole developed have merged into each other. Sediment has been deposited on the downstream side in the centre of two piers in the form of two separate tails which are ranging upto 71 cm. For $3.5D$ to $4.5D$ three separate scour holes have been observed, the boundaries of the scour holes are touching each other. The sediment has been deposited on the downstream side of the piers in the form of two scour tails ranging approximately 62 cm. For $5D$ pier spacing three completely separate scour holes has been observed, the scour deposition has been observed on the downstream side of both the piers, the length of tail scour for both the piers has been ranging upto 61 cm.

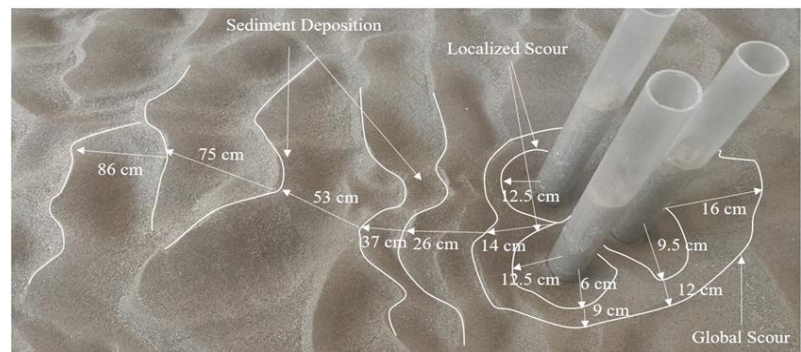
1.5D



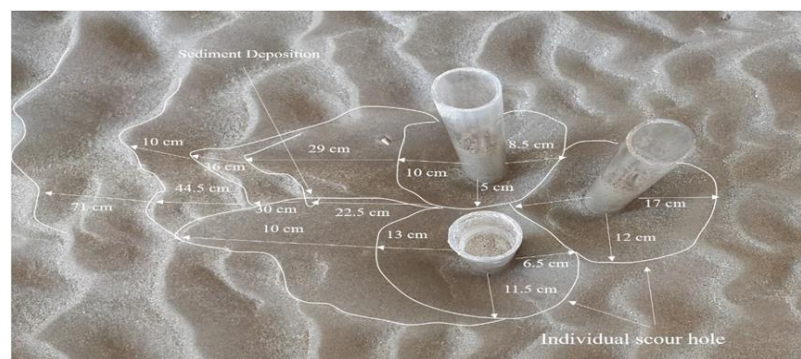
2D



2.5D



3D



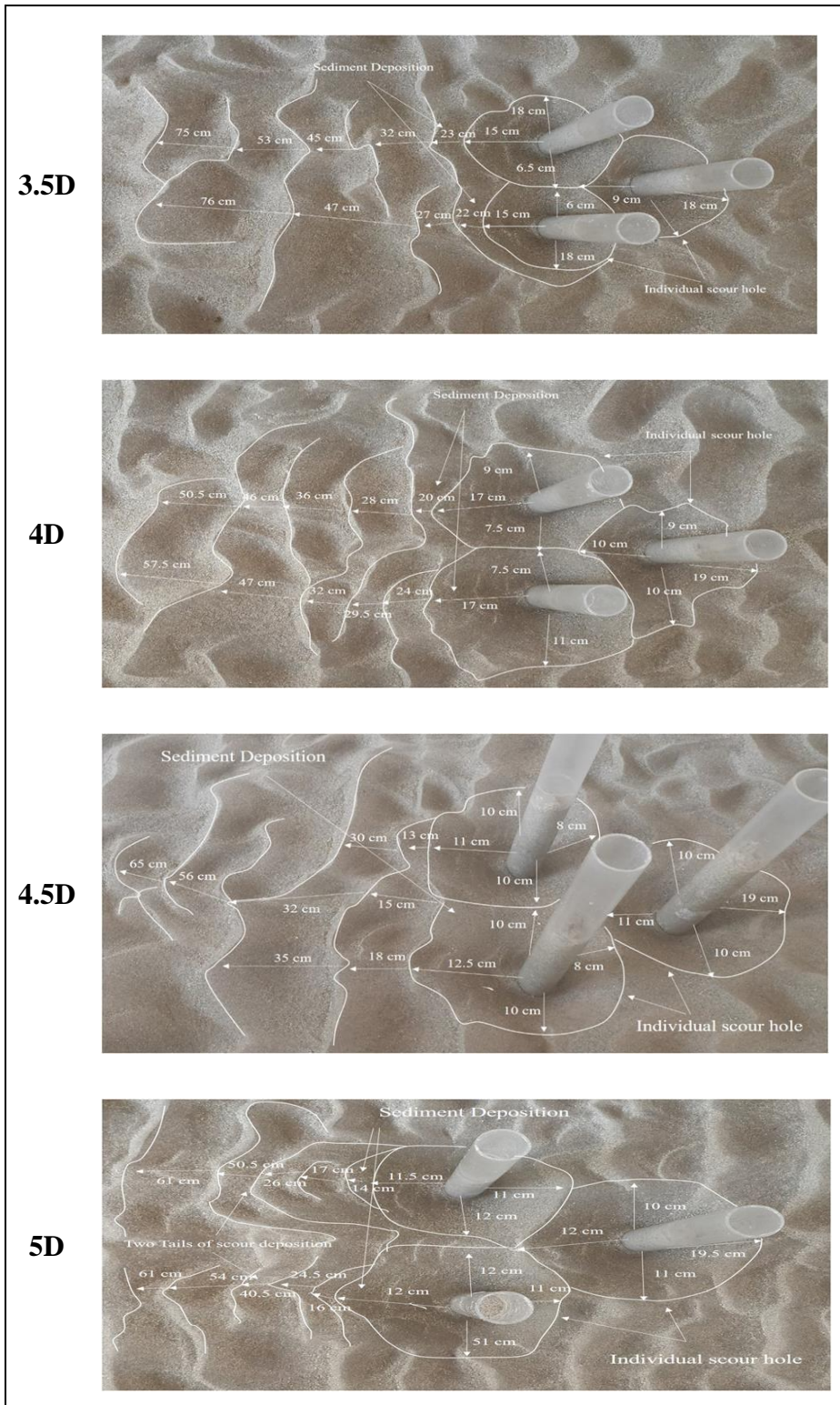


Fig. 4.62 scour depth around the three piers aligned in staggered positioning

4.9 Gene Expression Programming for tandem arrangement

4.9.1 GEP for scour depth prediction

Predictive approaches based on the artificial Intelligence such as Artificial Neural Networks (ANN) Adaptive Neuro-Fuzzy Inference Systems (ANFIS), Neuro-fuzzy Group Method of Data Handling (Neuro-fuzzy GMDH), Gene Expression Programming (GEP), Evolutionary Polynomial Regression (EPR), Model Tree (MT), and Multivariate Adaptive Regression Splines (MARS) have been studied by Azamathulla, 2012; Azamathulla et al., 2008; Azamathulla and Jarrett, 2013; Azmathullah et al., 2005; Najafzadeh, 2015; Najafzadeh and Azamathulla, 2015, to yield effective estimates of scour around hydraulic structures. Azmathullah et al. (2005) used ANN for the estimation of scour depth on the downstream of ski-jump bucket. Azamathulla et al. (2008) used neural networks to estimate the scour below spillways. Azamathulla (2012) has developed a predictive models for the abutment scour using GEP technique and concluded that the GEP models showed satisfactory estimations when compared to with the Artificial Neutral Network-Radial Basis Function (ANN- RBF) modulus. Whereas, Azamathulla and Jarrett (2013) assessed the potential of gene-expression programming (GEP) for estimating the Manning's n values. Najafzadeh, (2015) and Najafzadeh and Azamathulla, (2015) used Neuro-fuzzy GMDH systems to evaluate the scour depth around the piers. Additionally, Sharafati et al. (2020) utilized GMDH stochastic modelling technique to predict the local scour depth around the single pier in cohesive bed materials.

However, researchers have utilized GEP to model the scour prediction around the single pier. Najafzadeh et al. (2016) and Najafzadeh and Oliveto, (2021) developed nonlinear regression equations by utilizing four AI models including GEP, EPR, MT, and MARS to predict the equations for local scour depth around pile groups. Statistical assessment results obtained, shows that, the MARS approach provides more accurate prediction and equations obtained with GEP and MT models revealed convincing efficiency. Hassan and Jalal, (2021); Mohammed Saleh et al., (2019); Muzzammil et al., (2015) used GEP to formulate scour depth around single pier. Hassan et al. (2022) formulated expression for predicting the scour depth around the pile group by utilizing GEP, ANN Py-Torch. Whereas, (Devi and Kumar 2022b) used GEP to formulate the scour depth around two piers in the side by

side arrangement. Results of these studies shows that the GEP model indicated higher estimation accuracy compared to the established existing regression models.

By seeing the potential of the AI based methodologies for the prediction of the scour depth around the hydraulic structures and the only disadvantage of ANN that, it cannot provide a user friendly simplified equation that is practical for use by pavement engineering practitioners. This is one of the main reasons why ANN methods are considered “black boxes”. However, GEP methods provides equations that could be used to develop spreadsheets that are simple for use by practitioners. Through examination of literature, the approach using GEP for the estimation of scour depth for the tandem pier arrangements, has not been used. So, this problem is addressed in this section of dissertation for two piers positioned in the direction of the flow at the various pier spacing.

4.9.2 GEP Modelling

In the current study, the powerful software package GeneXpro Tools 5.0 has used to promote the development of GEP-based models for predicting the maximum scour depth that may occur at a bridge pier. Data sets from Keshavarzi et al., (2018); Liang et al., (2017); Malik and Setia, (2020, 2018) has been collected to develop the GEP model for predicting local scouring around a bridge pier. These data are then fed to the GEP in the form of a dependent variable (Y_s/d) and independent input variables (F_r , U/U_c , d/d_{50} , t/t_e , P_s/d), with the output variable Y_s/d then developed using the GEP.

The GEP randomly divided the data into validation and testing data (20%) and training data (80%), with the training data being used to build the GEP model. The GEP parameters and operations are then defined in 6 steps to stimulate the generation of the mathematical equation needed to predict local scouring around a bridge piers.

1. To begin with GEP modeling first step is generating an initial population. As suggested by (Ferreira 2001) any number of population can be utilized in the underlying populace but population of 30 to 100 offers optimal results.
2. After instating the population size, the fitness function is measured for measurement of fitness function for each individual chromosome by assessing RMSE.

3. After choosing the RMSE as fitness factor, the following stage is to select the function and terminals for each chromosomes. Functional series and terminals used in the present study are (+, -, *, /, *sqrt*) and (F_r , U/U_c , d/d_{50} , t/t_e , P_s/d).
4. Next advance is managing the architecture of the chromosomes by choosing the Gene numbers and length of head and tail for every gene.
5. The connecting function between the sub expression trees (sub-ETs) has been chosen in the following stage.
6. Following the preceding stage, genetic operators for chromosome design are chosen. These genetic operators include transposition (gene transposition, IS, and RIS), mutation (gene recombination, both one-point and two-point), inversion, and Dc-specific genetic operations and its rate.

After determining all genetic parameters, the model has been simulated for a number of generations in excess of 5,000,000. The values of all the parameters used in the present study are tabulated in **Table 4.7**. The description of the variables used in the proposed investigation to formulate GEP are presented in **Table 4.8**.

Table 4.7 Outline of the dimensional factors utilised in the formulation of the GEP

V	Variables Name	Range
V ₁	Diameter of pier (D)	5 cm
V ₂	Mean-Particle size of sediment used (d_{50})	1.75 mm
V ₃	Flume width	1.10 m
V ₄	Working section length	5 m
V ₅	Flow Depth (H)	0.12- 0.16 m
V ₆	Flow Velocity (U)	0.224-0.30 m/s
V ₇	Pier Spacing (P_s)	1.5D-5D
V ₈	Critical Velocity(U_c)	0.308-0.322 m/s
V ₉	Equilibrium time scour depth (t_e)	67-75 hours
V ₁₀	Experiment duration (t)	8 hours

The proposed scour depth (Y_s/d) equation is represented in the form of expression tree (ET) in **Fig. 4.63**. The ET's expression can be written in the simplified form as:

$$\frac{Y_s}{D} = \left\{ \frac{(d_2 \times d_1) + (C_9 + C_5)}{(C_6 - d_2) + d_4} \times (d_3 - \sqrt{C_1}) \right\} + \left\{ \frac{C_1}{\left[\frac{C_9/C_5}{d_3} + (C_1 + C_6) \right] + C_9} + d_1 \right\} + \left\{ \left[\frac{d_3}{\left(\frac{d_3}{d_4} + d_0 \right) \times C_0} + d_3 \right] \times C_3 \right\} \quad 54$$

By substituting the values of variables equation can be written as:

$$\frac{Y_s}{D} = \left\{ \frac{\left(\frac{P_s}{D} \times \frac{U}{U_c} \right) + (C_9 + C_5)}{\left(C_6 - \frac{P_s}{D} \right) + D/d_{50}} \times \left(\frac{t}{t_e} - \sqrt{C_1} \right) \right\} + \left\{ \frac{C_1}{\left[\frac{C_9/C_5}{t/t_e} + (C_1 + C_6) \right] + C_9} + \frac{U}{U_c} \right\} + \left\{ \left[\frac{t/t_e}{\left(\frac{t/t_e}{D/d_{50}} + F_r \right) \times C_0} + t/t_e \right] \times C_3 \right\} \quad 55$$

Further by substituting the values of the coefficients and simplifying the proposed equation can be written as:

$$\frac{Y_s}{D} = \left\{ \frac{\left(\frac{P_s}{D} \times \frac{U}{U_c} \right) - 14}{\left(\frac{D}{d_{50}} - \frac{P_s}{D} - 8.45 \right)} \times \left(\frac{t}{t_e} - 2.14 \right) \right\} + \left\{ \frac{7.48}{\left[\frac{0.242}{t/t_e} + 3.78 \right]} + \frac{U}{U_c} \right\} + \left\{ \left[\frac{t/t_e}{\left(\frac{t/t_e}{D/d_{50}} + F_r \right) \times (-8.70)} + t/t_e \right] \times 1.93 \right\} \quad 56$$

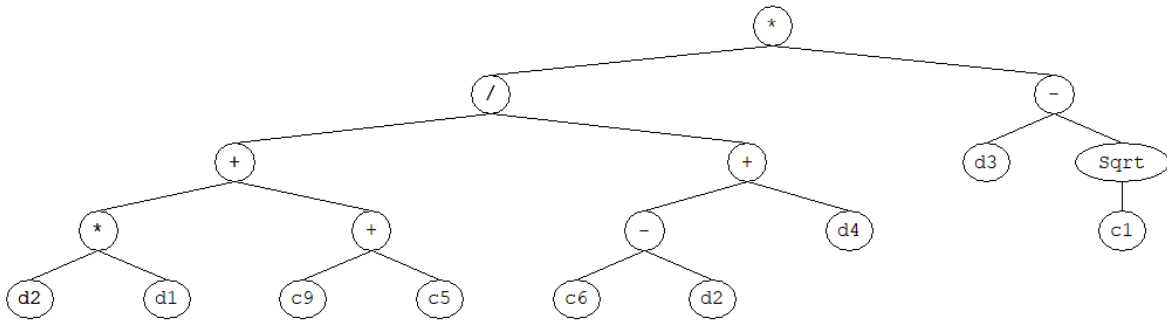
Table 4.8 Description of the variables used in the proposed investigation to formulate GEP

Variables	Description	Values
P ₁	Functional set	+, -, *, /
P ₂	Chromosomes Number	30
P ₃	Head Size	10
P ₄	Number of Genes	3
P ₅	Size of Gene	32
P ₆	Connecting Function	+
P ₇	Fitness Function	RMSE
P ₈	Inversion Rate	0.00546
P ₉	Mutation Rate	0.00138
P ₁₀	One-point recombination Rate	0.00277
P ₁₁	Two-point recombination Rate	0.00277
P ₁₂	Stumbling Mutation	0.00141
P ₁₃	Gene recombination Rate	0.00277
P ₁₄	Root insertion sequence transposition Rate	0.00546
P ₁₅	Gene Transportation Rate	0.00277
P ₁₆	Uniform Gene Recombination	0.00755

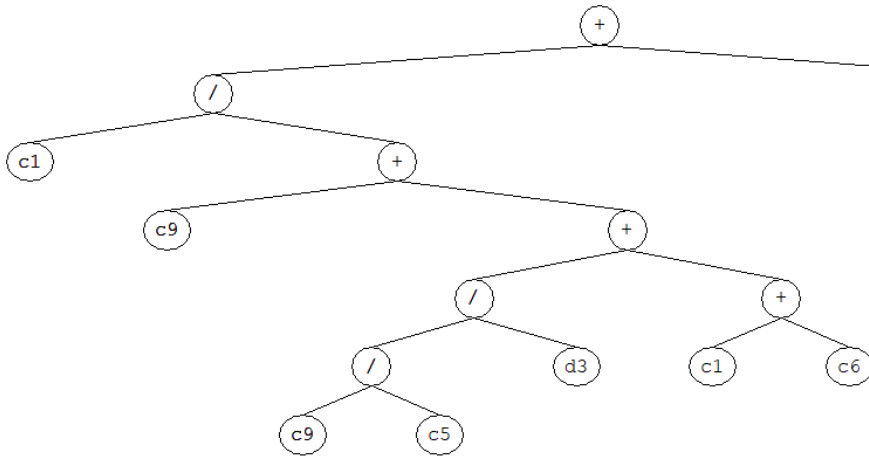
Table 4.9 Values of gene constants used in the proposed equation

Gene Number	Constant	Value
G1	C ₁	4.61
G1	C ₅	-6.17
G1	C ₆	-8.44
G1	C ₉	-7.83
G2	C ₁	-7.48
G2	C ₅	-8.14
G2	C ₆	1.73
G2	C ₉	1.97
G3	C ₀	-8.70
G3	C ₃	1.93

Sub-ET 1



Sub-ET 2



Sub-ET 3

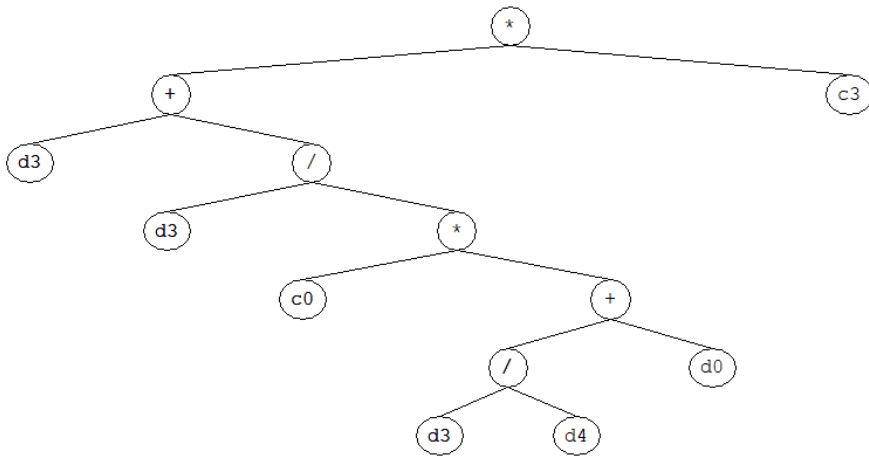


Fig. 4.63 Expression tree

4.9.3 GEP model performance analysis for equilibrium scour depth

A GEP formulation has proposed for the tandem arrangement has been written in **Eq. 56**. The performance analysis of the proposed equation has been carried out by comparing the GEP equation with the well-known existing equations, IRC equation (Congress 2016), Larsen and Toch equation (Laursen and Toch 1956), Melville and Coleman equation (Melville and Coleman 2000) and HEC-18 equation (Richardson and Davis 2001). The comparison of the proposed equation and already existing well-known equations has been illustrated in the **Fig. 4.64**. The proposed GEP equation is in good agreement with the present experimental results as the value of correlation coefficient (R^2) for training and testing has been observed 0.92 and 0.96 respectively.

As depicted in **Fig. 4.64**, the all the four equations over estimates the scour depth, whereas the proposed GEP equation is in a good agreement with the experimental results. In order to evaluate the prediction accuracy of all the five equations, statistical analysis of the predicted results have been carried out to measure the (Correlation Coefficient) R^2 , (Root Mean Square Error) RMSE, (Mean Absolute Error) MAE, (Mean Absolute Percentage Error) MAPE. Results of the statistical analysis are presented in **Table 4.10** and on the bases of these results five equations can be arranged in order of their prediction accuracy such as: proposed GEP equation, Melville and Coleman equation, IRC equation, HEC-18 equation and Larsen and Toch equation.

Table 4.10 Statistical analysis for the GEP and traditional regression based equations for the present experimental results

Performance Parameters	GEP	IRC Equation	Laursen and Toch Equation	Melville Equation	HEC-18 Equation
R^2	0.96	0.93	0.99	0.476	0.92
RMSE	3.77	35.14	32.99	15.02	35.92
MAE	2.83	31.06	32.87	13.57	32.41
MAPE	2.7	28.3	31.10	13.4	29.7

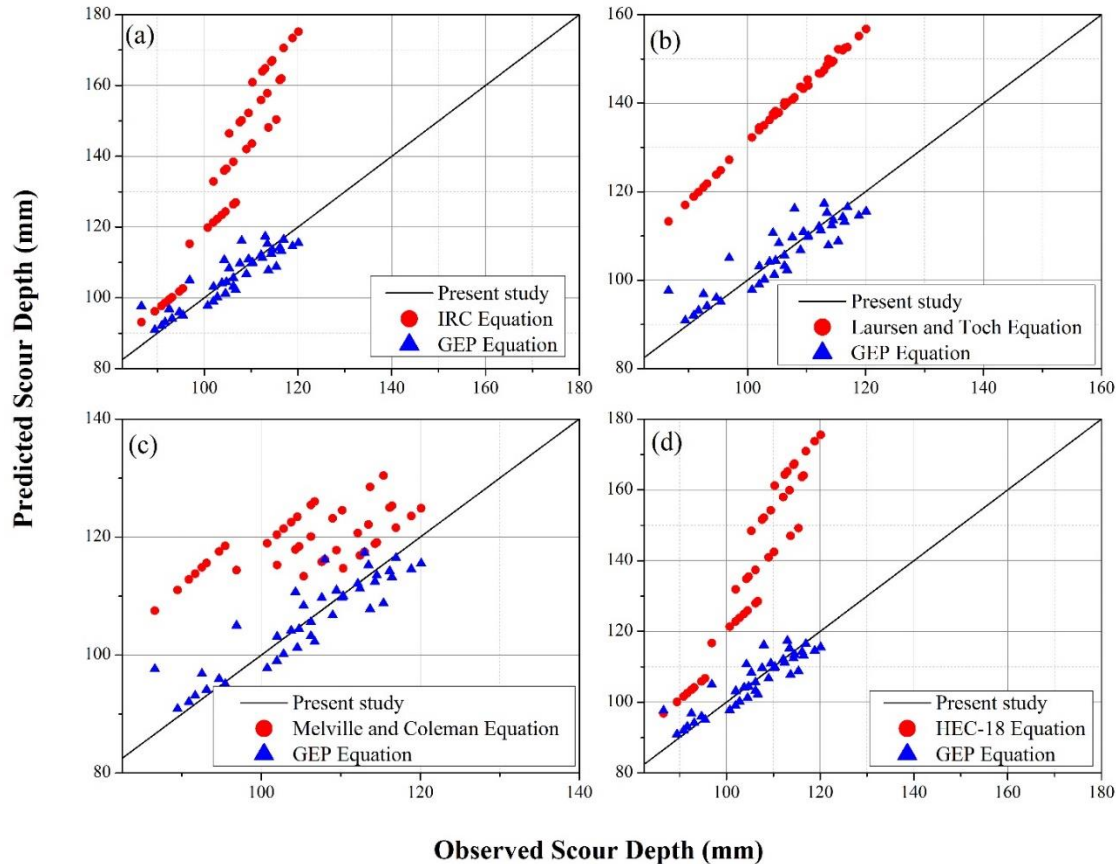


Fig. 4.64 Comparison of the GEP equation with the existing equations: (a) IRC equation; (b) Laursen and Toch equation; (c) Melville and Coleman equation; and (d) HEC-18 equation

4.10 Gene Expression Programming for side by side arrangement

4.10.1 Brief overview of Gene Expression Programming (GEP)

In a study (Ferreira 2006), Ferreira created Gene Expression Programming (GEP), which is an extension of genetic programming (GP). It combines the advantages of its forerunners: the genetic algorithm (GA) and genetic programming (GP). GEP is a proficient computing technique of genotype/phenotype system, with the separate functioning of genotype and phenotype, whereas these functions are mixed in GP (Ferreira 2006) and (Güven and Günel 2008). Seeing the potential of GEP in terms of simple modelling, easy coding, and faster computations, it has gained popularity over other tools. GEP develops computer programmes, which are subsequently encoded in linear chromosomes and generated or interpreted into expression trees (ETs). ET's are complex

computer programs that, in most cases, are created to address a specific problem and are chosen based on their functionality. As genetic operators act at the chromosomal level, an advantage of the GEP technique is that it simplifies the creation of genetic variation. Genetic operations including mutation, inversion, transposition, and recombination are used to reconfigure chromosomes containing one or more genes. After that, one of the fitness function equation available in the literature is used to evaluate the fitness of each chromosome in the original population. The second advantage of GEP is that it is mutagenic, allowing for the growth of more sophisticated applications. Seeing these benefits, GEP seems an excellent choice for a perfectly mathematical model the scour depth. For more insight on GEP, readers are encouraged to see (Ferreira 2006) and (Teodorescu and Sherwood 2008).

4.10.2 GEP Application: Formulation for Scour Depth

The equation for computing scours depth is formulated using GEP software (version 5.0), GeneXpro Tools 5.0. The experimental data set from this study is considered for the GEP formulation. For initiating the formulation, the whole data set is divided into two sets: the training set and the testing set. Further, the process of GEP formulation consists of five steps. The very first step is to choose the function of fitness for evaluating the fitness of chromosomes. For the present study, the Root Mean Square Error (RMSE) is chosen as a fitness function in accordance with the literature (Shiri et al. 2014). The second step is to choose the set of the terminal and set of functions for creating the chromosomes. For the present study, the terminal set, which consists of a set of an independent variables and a set of functions, is listed in

Table 4.12. For the precise prediction of the scour depth, ten-dimensional variables are listed in

Table 4.11. It is in accordance with the research work conducted by the author (Bateni et al. 2019), that the dimensional parameters give precise formulation than non-dimensional parameters. His investigation concludes that when dimensional data is used to train the GEP model, it provides better results than using non-dimensional data due to the enhanced flexibility in the fitting of variables. Therefore, based on the dimensional analysis, a set of

ten raw dimensional variables drawn from Eq. 57 to create the GEP modelling are written below:

$$Y_s = f(L, B, H, V, V_c, D_{50}, D, P_s, t, t_e) \quad 57$$

Where, L is the length of the flow section; B is the width of the flume section; H is the flow depth; V is the velocity of flow; V_c is the critical velocity; D_{50} is the mean-particle size; P_s is the centre-to-centre pier spacing between the piers; t is the time taken for the experiment; t_e is the time taken for achieving equilibrium scour depth.

The third step is to choose the architecture of the chromosomes, that is, head size and gene number. In the presented study, head size and gene number are chosen as ten and three, respectively. The fourth step is to select the connection function; in the presented study, a sign of addition is chosen. The last step is to choose the genetic operator and its rate. In the present study, a genetic operator such as mutation and inversion in combination are utilised with the rate of three types of a transportation insertion sequence, root insertion sequence transposition, and gene transpiration.

Table 4.11 List of the dimensional variables used for GEP formulation

Variables	Name	Range
V₁	Pier Diameter (D)	5 cm
V₂	Mean-Particle size(D ₅₀)	1.75 mm
V₃	Width of the flume section (B)	1.10 m
V₄	Length of the flow section (L)	5 m
V₅	Flow Depth (H)	0.12- 0.16 m
V₆	Velocity of flow (V)	0.224-0.30 m/s
V₇	Centre-to-Centre pier spacing between the Piers (P _s)	0.075-0.25 m
V₈	Critical Velocity(V _c)	0.308-0.322 m/s
V₉	Time taken for achieving equilibrium scour depth (t _e)	67-75 hours
V₁₀	Time taken for the experiment (t)	8 hours

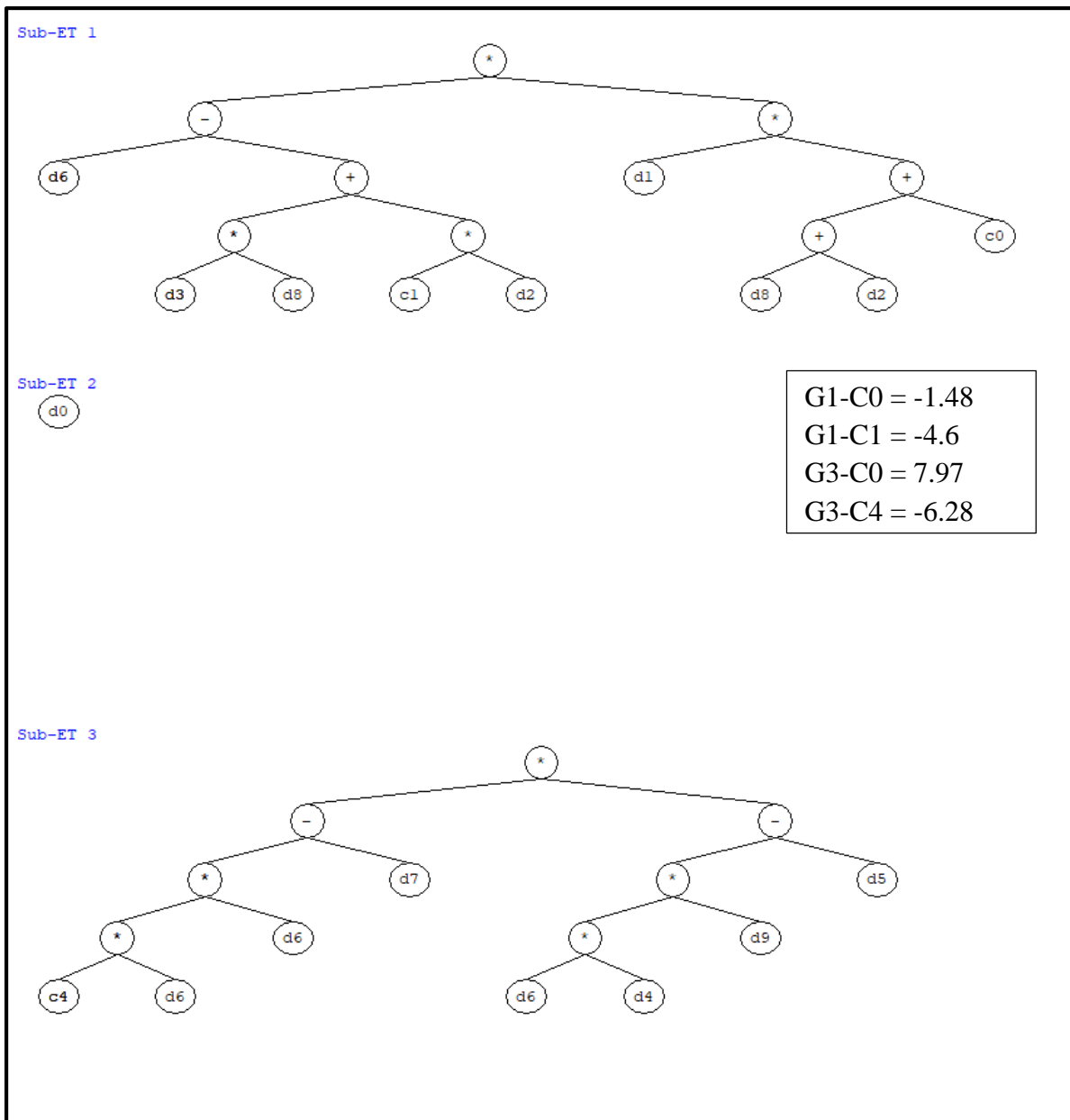


Fig. 4.65 Proposed GEP formulation in the form of expression tree's (ET's)

Here, GEP formulation for the reliable forecasting of scour depth is provided. The variables and parameters that are used for formulating non-linear equations are enumerated in **Table 4.11 and Table 4.12**, respectively. To formulate the GEP model, 60% of the total data set has been chosen randomly as training data sets, and the remaining 40% data set has been chosen as testing data sets. The results of the GEP modelling has been represented in **Fig. 4.65** in the form of ET's. **Fig. 4.65** consists of three expression trees which are linked with each other by the sign of addition. These gene pairs are a combination of constants whose values are also shown in the same **Fig. 4.65**.

Table 4.12 Definition of the parameters used in GEP formulation.

Parameters	Definition	Values
P ₁	Function set	+, -, x, /, Sqrt
P ₂	Chromosomes Number	30
P ₃	Head Size	10
P ₄	Genes Number	3
P ₅	Gene size	32
P ₆	Connecting Function	Addition
P ₇	Fitness Function	RMSE
P ₈	Rate of Inversion	0.00546
P ₉	Rate of Mutation	0.00138
P ₁₀	Rate of One-point recombination	0.00277
P ₁₁	Rate of Two-point recombination	0.00277
P ₁₂	Stumbling Mutation	0.00141
P ₁₃	Rate of Gene recombination	0.00277
P ₁₄	Rate of Root insertion sequence transposition	0.00546
P ₁₅	Rate of Gene Transportation	0.00277
P ₁₆	Uniform Gene Recombination	0.00755

A GEP-based explicit formulation for the maximum scour depth as a function of the dimensional parameters that have the largest effect on the scour process is written in **Eq. 58**.

$$Y_{su} = \{(d_6 - (d_3d_8 + C_1d_2)) \times (d_1 \times (d_8 + d_2 + C_0))\} + d_0 \quad 58$$

$$+ \{(C_4d_6^2 - d_7) \times ((d_6d_4 \times d_9) - d_5)\}$$

The values of actual parameters are: $d_0 = D$, $d_1 = D_{50}$, $d_2 = B$, $d_3 = L$, $d_4 = H$, $d_5 = V$, $d_6 = P_s$, $d_7 = V_c$, $d_8 = t_e$, $d_9 = t$. After substituting the corresponding values, the equation with the notation of the variables can be written as:

$$Y_{su} = \{(P_s - (Lt_e + C_1B)) \times (D_{50} \times (t_e + B + C_0))\} + D \quad 59$$

$$+ \{(C_4P_s^2 - V_c) \times ((P_sH \times t) - V)\}$$

It can be further simplified by substituting the values of the gene constants and can be written as in **Eq. 60**:

$$Y_{su} = \{(P_s - (Lt_e + 1.05B)) \times (D_{50} \times (t_e + B + 7.37))\} + D \quad 60$$

$$+ \{(1.05P_s^2 - V_c) \times ((P_sH \times t) - V)\}$$

Finally, the proposed equation using GEP Modelling for the evaluation of the scour depth in the simplified form is written in **Eq. 61**

$$Y_{su} = D + D_{50}t_e(P_s - Lt_e - LB - 7.37L - 1.05B) \quad 61$$

$$+ D_{50}B \left(P_s + \frac{7.37C_s}{B} - 1.05B - 1.05 - \frac{7.73}{d_{50}} \right) + 1.05P_s^3Ht - 1.05P_s^2V$$

$$- v_cP_sHt + VV_c$$

4.10.3 Performance analysis of the GEP model for equilibrium scour depth

Fig. 4.66 depicts a scatter-line plot of experimental observations versus GEP modeling predictions for relative scour depth for training and testing. It can be observed that the GEP results are the least dispersed from the experimental observations. The performance of the GEP modeling is analysed on the basis of a fitness function. The values of fitness function for training and testing is 0.00128 and 0.001424, respectively, while the correlation coefficient is 0.950 and 0.955, respectively. Consequently, GEP has proved its efficiency

in generalizing the proposed GEP formulation and has effectively captured the non-linear relationships between the parameters.

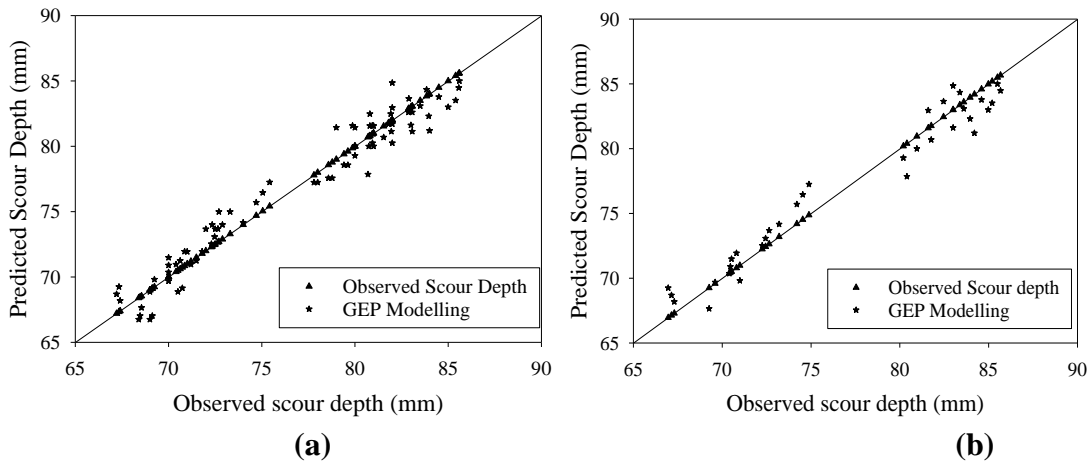


Fig. 4.66 GEP predicted equilibrium scour depth (Y_{su}) versus observations from the current Experimental Study (a) Training; and (b) Testing

The current study uses performance measures, R squared correlation (R^2), Root Mean Squared Error (RMSE) and Mean Absolute Error (MAE), to evaluate the performance of the various scour depth prediction equations. **Table 4.13** shows the efficacy of the proposed GEP based modelling in predicting the scour depth in comparison to previously reported results. It can be observed it provided lower values of R^2 , $RMSE$, and MAE . Overall, the findings of the presented study suggest that GEP based modelling is a potential alternative to existing equations, and it is reasonable to conclude that GEP based modelling has the best performance among all the mentioned scour prediction equations.

Table 4.13 Statistical error measures for the GEP and traditional regression based equations

Performance Parameters	GEP	Larsen and Toch Equation	Melville and Coleman Equation	HEC-18 Equation	Sheppard and Melville Equation
R^2	0.951	0.939	0.93	0.477	0.322
RMSE	0.00133	0.00161	0.0091	0.0216	0.0128
MAE	0.00113	0.00127	0.0089	0.0188	0.0104

Fig. 4.67 compares the GEP-based predicted equilibrium scour depth with four existing equations: (a) Laursen and Toch equation (Laursen and Toch 1956); (b) Melville and

Coleman equation (Melville et al.2000); (c) HEC-18 equation (Arneson et al. 2012); and (d) Sheppard/Melville equation (Sheppard et al. 2014). Larsen and Toch and Melville's equations provide satisfactory results, but HEC-18 and Sheppard's equations overestimated the equilibrium scour depth. The proposed GEP based modelling renders more accurate predictions of equilibrium scour depth. Its findings are mostly in the 1:1 range. This observation is perfectly depicted in the scatter plots.

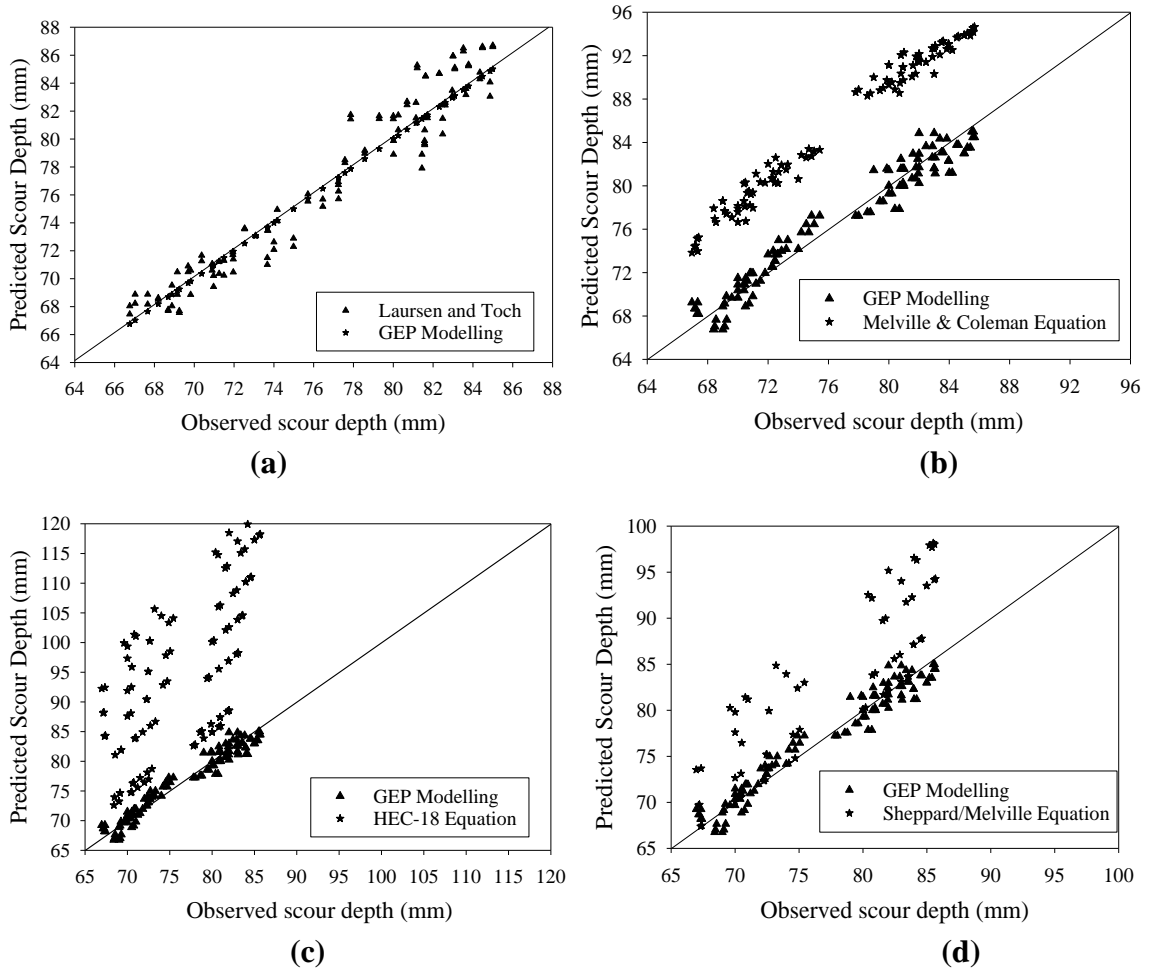


Fig. 4.67 Observed versus Predicted equilibrium scour depth using different equations: Present study (GEP) versus (a) Laursen and Toch; (b) Melville and Coleman; (c) HEC-18; (d) Sheppard/Melville

4.10.4 Sensitivity Analysis

Sensitivity analysis has been carried out to identify the impact of the various input variables on the scour depth prediction. This analysis facilitates the selection of the most sensitive variable for the accurate prediction of the scour depth. All the ten input variables used for

the GEP formulation are examined, and the results of the sensitivity analysis regarding the validation are illustrated in

Table 4.14. The sensitivity analysis is carried out by eliminating one input variable for each model. The main performance criteria of this process are the determination coefficient (R^2). The results presented in

Table 4.14 indicate that the pier spacing has the most significant influence in terms of scour depth prediction in comparison with the other input variables.

In very recent work, researchers utilised artificial intelligence-based approach to predict scour depth (Sharafati et al. 2020). Soft computing approaches have simplified this task and made it more acceptable and trustworthy than traditional ways of analysis (Muzzammil et al. 2015). Artificial Neural Networks (ANN), Genetic Programming (GP), Genetic Algorithms (GA), Group Method of Data Handling (GMDH), Gene Expression Programming (GEP), Adaptive Network-based Fuzzy Inference System (ANFIS), and Radial Basis Function (RBF) are among the Artificial Intelligence (AI) techniques now being used to solve various hydraulics engineering problems. Some of the studies, such as (Akib et al. 2014; Choi et al. 2017) utilised ANFIS model for solving different scour problems and (Pandey et al. 2020c; b) utilised GA approach for scour depth prediction. Furthermore, the work in (Najafzadeh et al. 2015; Najafzadeh and Azamathulla 2013) presented an application of GMDH to predict the scour depth around bridge pier. It utilised Levenberg–Marquardt (LM) method and compared their finding with ANFIS, RBF-NN, and certain empirical equations. It has been determined that the GMDH-LM offered more reliable predictions than the others. Even while ANN models outperform classic regression-based methods, they cannot give a direct relationship between scour depths and the variables that influence them, unlike GEP. In addition, the works in (Azamathulla 2012; Bateni et al. 2019; Guven and Gunal 2008; Muzzammil et al. 2015; Najafzadeh et al. 2016) have used GEP to evaluate scour depth and compared their findings with other regression-based equations, concluding that GEP is the most estimable modelling methodology for scour depth evaluation, among other tools.

Table 4.14 sensitivity analysis of the influencing parameters

Models	Variables	R²
Proposed GEP	$Y_s = f(D, D_{50}, B, L, H, V, P_s, V_c, t_e, t)$	0.933
Model 1	$Y_s = f(D_{50}, B, L, H, V, P_s, V_c, t_e, t)$	0.927
Model 2	$Y_s = f(D, B, L, H, V, P_s, V_c, t_e, t)$	0.933
Model 3	$Y_s = f(D, D_{50}, L, H, V, P_s, V_c, t_e, t)$	0.943
Model 4	$Y_s = f(D, D_{50}, B, H, V, P_s, V_c, t_e, t)$	0.930
Model 5	$Y_s = f(D, D_{50}, B, L, V, P_s, V_c, t_e, t)$	0.917
Model 6	$Y_s = f(D, D_{50}, B, L, H, P_s, V_c, t_e, t)$	0.891
Model 7	$Y_s = f(D, D_{50}, B, L, H, V, V_c, t_e, t)$	0.421
Model 8	$Y_s = f(D, D_{50}, B, L, H, V, P_s, t_e, t)$	0.930
Model 9	$Y_s = f(D, D_{50}, B, L, H, V, P_s, V_c, t)$	0.919
Model 10	$Y_s = f(D, D_{50}, B, L, H, V, P_s, V_c, t_e)$	0.926

In general, computational assessment of scour depth has been undertaken based on Artificial Intelligence methodologies and GEP in particular. This methodology is not frequently used, and there is an imperative need to carry out research in this area. Hence, the present study evaluates the capability of the GEP for predicting the scour depth around the twin piers configured side-by-side. In addition, to corroborate our proposed results, an experimental study is carried out which depicts the characteristics of flow around the piers and to train the proposed formulation. Finally, the precision ability of the proposed GEP formulation is compared with the experimental data as well as regression-based equations that are previously reported in the literature.

CHAPTER 5

SUMMARY AND CONCLUSIONS

5.1 Summary

5.1.1 Pier arrangements

In order to gain a better understanding of the scour phenomenon, it is important to consider various influencing parameters that affect scour depth. These parameters include pier spacing (P_s), flow depth (H), rate of flow (Q), Froude number (F_d), Reynolds number (R_e), angle of attack and relative velocity (R_v). Based on the temporal scour results discussed in this study, it is recommended to conduct the experimental study for a minimum duration of 450-500 minutes to effectively observe the scour depth around a single pier with uniform graded sediment. To achieve a state of real-time equilibrium, it is of utmost importance to maintain a controlled scour evolution rate around the pier. Specifically, this rate should be limited to no more than 3% of the pier diameter in last 24 hours of the experimental run. By adhering to this guideline, researchers can ensure accurate and reliable observations of the scour depth around the single pier for uniform graded sediment.

Through observations, it has been determined that the scour depth around the front pier in a tandem arrangement is 21.6% greater compared to a single pier, and 16% greater than the scour depth observed at the rear pier. When P_s/D ratio increases, the scour depth increases until reaching a P_s/D value of 3, at which point the piers behave as a single unit. However, for P_s/D values greater than 3, the scour depth starts to reduce, and both piers behave individually. Additionally, the maximum scour depth is observed at the highest F_d value ($F_{d84} = 1.83$), while the minimum scour depth is observed at the lowest F_d value ($F_{d84} = 1.37$). Similarly, the maximum and minimum scour depths are achieved at u/u_c ratios of 0.98 and 0.95, respectively.

In the experimental study, it was observed that the extent of scouring at the upstream and downstream sides of the left and right piers was approximately similar. The experimental results indicated that for pier spacing in the range of 1.5 times the pier diameter ($1.5D$) to 3 times the pier diameter ($3D$), a combined scour hole was formed for both piers, with

sediment deposition occurring in the form of a single tail scour deposition. For pier spacing in the range of $3.5D$ to $4.5D$, the piers behaved partially independently, resulting in two separate scour holes observed upstream of the piers, but with combined sediment deposition. When the pier spacing was equal to 5 times the pier diameter ($5D$), the piers behaved completely independently, leading to the observation of two separate scour holes, with sediment deposition observed at the rear of both piers (forming two tails of scour deposition). These findings highlight the importance of pier spacing in determining the behavior of scour and sediment deposition.

The maximum scour depth around bridge piers is affected by factors such as attack angle, pier spacing, and pier diameter. The highest scour depth is usually observed at the front pier due to the interplay between horseshoe and wake vortices. The maximum scour depth is typically seen at a pier spacing of 3 times the pier diameter at the front pier. However, the scour depth reduces as pier spacing increases due to reduced influence of the front pier on the rear pier. At a 15° angle of attack, the peak scour depth is observed between $2D$ and $3D$ pier spacing, while at a 30° angle of attack, the maximum scour depth occurs at a pier spacing of $2D$. The increase in scour depth for small pier spacing is due to larger equivalent diameter of the pier, increased drag force, and larger horseshoe vortices at the front pier.

In the staggered arrangement the maximum scour depth is observed at the central pier for pier spacing $P_s = 2.5-3D$. The minimum scour depth at the central pier is observed for a pier spacing, $P_s = 1.5D$. The downstream piers exhibit similar behavior across all rate of flow conditions, with maximum scour erosion occurring at the node of the central pier. This is due to the merging of horseshoe vortices generated upstream of the central pier with the wake vortices on the downstream piers, resulting in greater sediment erosion near the central pier. Larger pier spacing leads to a decrease in scour depth at the downstream piers due to weakened wake vortices in the mid-section of the piers. These weakened vortices act on the downstream pier as an approaching velocity, reducing scour depth.

Researchers can enhance their understanding of the scour phenomenon around piers by examining the various influencing parameters and their impact on scour depth. This comprehensive understanding enables engineers and researchers to make informed

decisions and incorporate necessary design considerations to effectively address scour-related issues in bridge and hydraulic structure design. By recognizing the relationships between these parameters, they can develop strategies to mitigate scour and ensure the structural integrity of these important infrastructure elements.

5.1.2 Traditional equation

The accuracy of predicting scour depth has been evaluated using five traditional equations. These equations were compared with the observed experimental results and their ability to forecast the ultimate asymptotic scour depth was assessed. Among the five equations, Larsen and Toch, Sheppard and Melville, HEC-18, and Melville equations demonstrated a mean absolute error percentage of less than 15% in predicting the scour depth. These equations provide reliable estimates for practical design purposes. However, it should be noted that the IRC recommended equation tended to overestimate the maximum scour depth. Despite this overestimation, the IRC equation may still be considered suitable for designs that require a high degree of conservatism or safety margin. The findings of this comparison study provide valuable insights into the performance of these traditional equations for predicting scour depth. Engineers and researchers can utilize these equations based on their specific design requirements and desired level of accuracy.

5.1.3 GEP

In addition to the comprehensive understanding of scour depth influencing factors, this study introduces a novel and efficient method for predicting local scour around bridge piers using the GEP modeling system. The proposed GEP formulations exhibit perfect agreement with experimental results and outperform traditional regression-based equations. These GEP equations are remarkably simple, allowing users unfamiliar with GEP to utilize them effectively. The promising findings of this study strongly advocate for the use of GEP in addressing complex water engineering problems. The prediction capability of the GEP formulation is compared to well-known traditional equations, demonstrating superior performance with statistical measures of R², MAE, and RMSE at 0.951, 0.00133, and 0.00113, respectively. Furthermore, sensitivity analysis reveals that pier spacing and rate of flow significantly influence scour depth estimation.

Overall, this study establishes the GEP modeling system as a valuable tool for accurate and efficient prediction of scour depth. Its simplicity and exceptional performance make it a promising approach for engineers and researchers in tackling scour-related challenges in bridge and hydraulic structure design.

5.2 Conclusion

In conclusion, the findings of this study shed light on the relationship between pier spacing and scour depths, providing valuable insights for engineers and researchers involved in bridge and hydraulic structure design.

1. To effectively observe scour depth around a single pier with uniform graded sediment, it is recommended to conduct experimental studies for a minimum duration of 450-500 minutes. Maintaining a controlled rate of scour evolution, limited to 3% of the pier diameter within last 24 hours of the experiment, is crucial for achieving real-time equilibrium.
2. The scour depth around bridge piers is influenced by various parameters, including pier spacing, flow depth, rate of flow, Froude number, Reynolds number, and relative velocity. Increasing pier spacing reduces interference and results in smaller scour depths, while smaller spacing leads to greater interference and increased scour depths. The behavior of the piers changes at different P_s/D ratios, with scour depth increasing until $P_s/D = 3$, and reducing thereafter.
3. The tandem arrangement of piers affects the distribution and magnitude of scour depth. In this arrangement scour depth around the front pier is greater than that of the rear pier. The interaction between vortices generated by adjacent piers in a tandem arrangement affects the scour depth. The presence of the front pier alter the flow patterns and scour depth around the rear pier. The spacing between the piers influence the development and intensity of horseshoe and wake vortices.
4. The side-by-side arrangement of piers significantly influences the scour depth. Closer spacing between piers increases mutual interference and the strength of horseshoe vortices, resulting in greater scour depths. The spacing between piers determines the level of mutual interference between the flow patterns generated by adjacent piers. Closer spacing leads to greater interference, resulting in increased

scour depths between the piers. The strength of horseshoe vortices are also affected by the side-by-side arrangement. Smaller spacing between piers results in larger and more pronounced horseshoe vortices, leading to greater scour depths. Smaller spacing tends to produce combined scour holes, whereas larger spacing allows for more independent scour holes with distinct sediment deposition patterns.

5. The angle of attack on a bridge pier has a direct impact on the scour depth. At a 15° angle of attack, the peak scour depth is observed between 2D and 3D pier spacing. This means that the scour depth is the highest within this range. On the other hand, at a 30° angle of attack, the maximum scour depth occurs at a pier spacing of 2D. The angle of attack affects the hydrodynamic forces acting on the pier. Higher angles of attack result in increased drag forces, which can enhance the scouring action and lead to greater scour depths.
6. The staggered arrangement of piers has a notable impact on scour depth. Maximum scour erosion occurs at the node of the central pier. This is due to the merging of horseshoe vortices generated upstream of the central pier with the wake vortices on the downstream piers, leading to intensified sediment erosion near the central pier. While the downstream piers are influenced by the merging of vortices, leading to increased erosion near the central pier. Pier spacing plays a crucial role, as smaller spacing increases scour depth at the central pier, while larger spacing reduces scour depth at the downstream piers. The downstream piers in the staggered arrangement exhibit consistent behavior across various flow conditions.
7. Traditional equations for predicting scour depth have been evaluated, with Larsen and Toch, Sheppard and Melville, HEC-18, and Melville equations demonstrating reliable estimates, having mean absolute error percentages of less than 15%. The IRC recommended equation tends to overestimate scour depth but may be suitable for conservative designs.
8. The introduction of the GEP modeling system provides a novel and efficient method for predicting local scour around bridge piers. The proposed GEP formulations show perfect agreement with experimental results and outperform traditional regression-based equations. The simplicity and user-friendliness of the GEP equations make them accessible to non-experts. The GEP-based predictions

exhibit high accuracy and reliability, as demonstrated by statistical measures such as R², MAE, and RMSE. Pier spacing and flow rate are identified as sensitive factors in scour depth estimation.

In conclusion, understanding the factors influencing scour depth, such as pier spacing, arrangement, angle of attack, and utilizing reliable prediction equations, is crucial for effective bridge and hydraulic structure design. By considering these findings, engineers can make informed decisions to mitigate scour-related issues, ensuring the stability and safety of piers in various arrangements.

5.3 Recommendation for further work

1. The possible extension of this study could be to application the numerical modelling on the group of piers.
2. Additional experimentation can be conducted by considering the angle of attack for the group of four and five piers.
3. Non-uniform sediment can be used to study the group effect.
4. More computational techniques can be used for the prediction of scour depth.

References

- Aguirre-Pe, J., Olivero, M. L., and Moncada, A. T. (2003). "Particle densimetric Froude number for estimating sediment transport." *Journal of Hydraulic Engineering*, 129(6), 428–437.
- Ahmed, F., and Rajaratnam, N. (1998). "Flow around bridge piers." *Journal of Hydraulic Engineering*, 124(3), 288–300.
- Akib, S., Mohammadhassani, M., and Jahangirzadeh, A. (2014). "Application of ANFIS and LR in prediction of scour depth in bridges." *Computers and Fluids*, Elsevier Ltd, 91, 77–86.
- Akilli, H., Akar, A., and Karakus, C. (2004). "Flow characteristics of circular cylinders arranged side-by-side in shallow water." *Flow Measurement and Instrumentation*, 15(4), 187–197.
- Albert Molinas. (2004). "Bridge scour in non uniform sediment mixtures and in cohesive materials : Synthesis report." *Federal Highway Administration Publication, FHWA-RD-03*(January).
- Alborzi, A., and Osouli, A. (2017). "Numerical simulation of pier scouring applying a Eulerian Multi-Phase model." *In Geotechnical Frontiers*, 426–436.
- Alemi, M., and Maia, R. (2018). "Numerical simulation of the flow and local scour process around single and complex bridge piers." *International Journal of Civil Engineering*, Springer International Publishing, 16(5), 475–487.
- Amini, A., Melville, B. W., and Ali, T. M. (2014). "Local scour at piled bridge piers including an examination of the superposition method." *Canadian Journal of Civil Engineering*, 41(5), 461–471.
- Amini, A., Melville, B. W., Ali, T. M., and Ghazali, A. H. (2012). "Clear-water local scour around pile groups in shallow-water flow." *Journal of Hydraulic Engineering*, 138(2), 177–185.

- Amini, A., and Mohammad, T. A. (2017). "Local scour prediction around piers with complex geometry." *Marine Georesources and Geotechnology*, 35(6), 857–864.
- Amini Baghbadorani, D., Ataie-Ashtiani, B., Beheshti, A., Hadjzaman, M., and Jamali, M. (2018). "Prediction of current-induced local scour around complex piers: Review, revisit, and integration." *Coastal Engineering*, 133, 43–58.
- Arneson, L. A., Zevenbergen, L. W., Lagasse, P. F., and Clopper, P. E. (2012). *Evaluating scour at bridges. National Highway Institute (US)*, (No. FHWA-HIF-12-003). National Highway Institute (US).
- Ataie-Ashtiani, B., and Aslani-Kordkandi, A. (2012). "Flow field around side-by-side piers with and without a scour hole." *European Journal of Mechanics, B/Fluids*, 36, 152–166.
- Ataie-Ashtiani, B., Baratian-Ghorghi, Z., and Beheshti, A. A. (2010). "Experimental investigation of clear-water local scour of compound piers." *Journal of Hydraulic Engineer*, 136(6), 343–351.
- Azamathulla, H. M. (2012). "Gene-expression programming to predict scour at a bridge abutment." *Journal of Hydroinformatics*, 14(2), 324–331.
- Azamathulla, H. M., Deo, M. C., and Deolalikar, P. B. (2008). "Alternative neural networks to estimate the scour below spillways." *Advances in Engineering Software*, 39(8), 689–698.
- Azamathulla, H. M., and Jarrett, R. D. (2013). "Use of gene-expression programming to estimate Manning's roughness coefficient for high gradient streams." *Water Resources Management*, 27(3), 715–729.
- Azmathullah, H. M., Deo, M. C., and Deolalikar, P. B. (2005). "Neural networks for estimation of scour downstream of a ski-jump bucket." *Journal of Hydraulic Engineering*, 131(10), 898–908.
- Baker, C. J. (1979). "Vortex flow around the bases of obstacles." University of Cambridge.

- Baker, R. E. (1986). "Local scour at bridge piers in non uniform sediment."
- Batani, S. M., Borghei, S. M., and Jeng, D. S. (2007). "Neural network and neuro-fuzzy assessments for scour depth around bridge piers." *Engineering Applications of Artificial Intelligence*, 20(3), 401–414.
- Batani, S. M., Vosoughifar, H. R., Truce, B., and Jeng, D. S. (2019). "Estimation of clear-water local scour at pile groups using genetic expression programming and multivariate adaptive regression splines." *Journal of Waterway, Port, Coastal and Ocean Engineering*, 145(1), 1–11.
- Beg, M. (n.d.). "Mutual interference of bridge piers on local scour." *Proceedings 2nd International Conference on Scour and Erosion (ICSE-2), 14-17, November 2004 singapore, 2004.*
- Beg, M., and Beg, S. (2015). "Scour hole characteristics of two unequal size bridge piers in tandem arrangement." *ISH Journal of Hydraulic Engineering*, 21(1), 85–96.
- Beheshti, A. A., and Ataie-Ashtiani, B. (2016). "Scour hole influence on turbulent flow field around complex bridge piers." *Flow, Turbulence and Combustion*, Springer, 97(2), 451–474.
- Behzad, A.-A., and Abolfazl, A.-K. (2013). "Flow field around single and tandem piers." *Flow Turbulence Combustion*, 90, 471–490.
- Behzad, A.-A., and Beheshti, A. A. (2006). "Experimental investigation of clear-water local scour at pile groups." *Journal of Hydraulic Engineering*, 132(10), 1100–1104.
- Bordbar, A., Sharifi, S., and Hemida, H. (2021). "Investigation of the flow behaviour and local scour around single square-shaped cylinders at different positions in live-bed." *Ocean Engineering*, 238, 109772.
- Bozkuş, Z., Özalp, M. C., and Dinçer, A. E. (2018). "Effect of pier inclination angle on local scour depth around bridge pier groups." *Arabian Journal for Science and Engineering*, 43(10), 5413–5421.

- Breusers, H. N. C., Nicollet, G., and Shen, H. W. (1977). "Local scour around cylindrical piers." *Journal of Hydraulic Research*, 15(3), 211–252.
- Breusers, H. N. C., and Raudkivi, A. J. (1991). *Scouring*. Balkema Rotterdam.
- Cardoso, A. H., and Bettess, R. (1999). "Effects of time and channel geometry on scour at bridge abutments." *Journal of Hydraulic Engineering*, 125(4), 388–399.
- Chabert, J., and Engeldinger, P. (1956). "Study of scour around bridge piers." *Rep. Prepared for the Laboratoire National d'Hydraulique*.
- Chang, K., and Constantinescu, G. (2015). "Numerical investigation of flow and turbulence structure through and around a circular array of rigid cylinders." *Journal of Fluid Mechanics*, Cambridge University Press, 776, 161–199.
- Chang, W.-Y., Constantinescu, G., Miyawaki, S., Tsai, W. F., and Lien, H.-C. (2010). "The flow and turbulence structure at a rectangular bridge pier with a low angle of attack." *River Flow 2010*, Karlsruhe, 681–690.
- Chee, R. K. W. (1982). "Live-bed scour at bridge piers." *Publication of: Auckland University, New Zealand*, (290).
- Cheng, N.-S., Wei, M., Lu, Y., and Chiew, Y.-M. (2020a). "Evaluation of sediment gradation effects on clear-water pier scour with densimetric Froude number." *Journal of Engineering Mechanics*, 146(12), 04020133.
- Cheng, N.-S., Wei, M., Lu, Y., and Chiew, Y.-M. (2020b). "Evaluation of Sediment Gradation Effects on Clear-Water Pier Scour with Densimetric Froude Number." *Journal of Engineering Mechanics*, 146(12), 04020133.
- Cheng, Z., Koken, M., and Constantinescu, G. (2018). "Approximate methodology to account for effects of coherent structures on sediment entrainment in RANS simulations with a movable bed and applications to pier scour." *Advances in Water Resources*, 120, 65–82.
- Chiew, Y.-M. (1995). "Mechanics of riprap failure at bridge piers." *Journal of Hydraulic*

Engineering, 121(9), 635–643.

- Chiew, Y. M. (1984). “Local scour at bridge piers.” ResearchSpace@ Auckland.
- Choi, S., and Cheong, S. (2006). “Prediction of local scour around bridge piers using artificial neural networks 1.” *JAWRA Journal of the American Water Resources Association*, Wiley Online Library, 42(2), 487–494.
- Choi, S. U., Choi, B., and Lee, S. (2017). “Prediction of local scour around bridge piers using the ANFIS method.” *Neural Computing and Applications*, Springer London, 28, 335–344.
- Coleman, B. S. E., and Melville, B. W. (2001). “Case study: New Zealand bridge scour experiences.” *Journal of Hydraulic Engineering*, 127(7), 535–546.
- Coleman, S. E. (2005). “Clearwater local scour at complex piers.” *Journal of Hydraulic Engineer*, 131(4), 330–334.
- Coleman, S. E., Lauchlan, C. S., Melville, B. W., and Giri, S. (2005). “Clear-water scour development at bridge abutments.” *Journal of Hydraulic Research*, 43(4), 445–448.
- Congress, I. R. (2016). “Standard specifications and code of practice for road bridges.” Indian Road Congress (IRC).
- Dargahi, B. (1989). “The turbulent flow field around a circular cylinder.” *Experiments in fluids*, Springer, 8(1), 1–12.
- Das, R., Khwairakpam, P., Das, S., and Mazumdar, A. (2014). “Clear Water Local Scour Around Eccentric Multiple Piers to Shift the Line of Sediment Deposition.” *Asian Journal of Water, Environment and Pollution*, 11(3), 47–54.
- Das, S., Das, R., and Mazumdar, A. (2015). “Comparison of local scour characteristics around two eccentric piers of different shapes.” *Arabian Journal for Science and Engineering*, 41(4), 1199–1213.
- Debnath, K., and Chaudhuri, S. (2010). “Bridge pier scour in clay-sand mixed sediments at near-threshold velocity for sand.” *Journal of Hydraulic Engineering*, 136(9), 597–

609.

- Deng, L., and Cai, C. S. (2010). “Bridge Scour: Prediction, Modeling, Monitoring, and Countermeasures—Review.” *Practice Periodical on Structural Design and Construction*, 15(2), 125–134.
- Devi, G., and Kumar, M. (2022a). “Countermeasures against local scouring at circular bridge piers using collar and combination of slot and collar.” *River Hydraulics: Hydraulics, Water Resources and Coastal Engineering Vol. 2*, R. Jha, V. P. Singh, V. Singh, L. B. Roy, and R. Thendiyath, eds., Springer International Publishing, Cham, 289–296.
- Devi, G., and Kumar, M. (2022b). “Estimation of local scour depth around twin piers using gene expression programming (local scour around twin piers).” *Water Supply*, 22(6), 5915–5932.
- Dey, S., Bose, S. K., and Sastry, G. L. N. (1995). “Clear water scour at circular piers: A model.” *Journal of Hydraulic Engineering*, 121(12), 869–876.
- Dey, S., and Raikar, R. V. (2007). “Characteristics of horseshoe vortex in developing scour holes at piers.” *Journal of Hydraulic Engineering*, 133(4), 399–413.
- Diab, R., Link, O., and Zanke, U. (2009). “Experimental investigation of 3D flow field around square pier.” *33rd IAHR Congress: Water Engineering for a Sustainable Environment*.
- Ebtehaj, I., Bonakdari, H., Moradi, F., Gharabaghi, B., and Khozani, Z. S. (2018). “An integrated framework of extreme learning machines for predicting scour at pile groups in clear water condition.” *Coastal Engineering*, 135, 1–15.
- Elliott, K. R., and Baker, C. J. (1985). “Effect of pier spacing on scour around bridge piers.” *Journal of Hydraulic Engineering*, 111(7), 1105–1109.
- Escauriaza, C., and Sotiropoulos, F. (2011). “Initial stages of erosion and bed form development in a turbulent flow around a cylindrical pier.” *Journal of Geophysical Research: Earth Surface*, 116(3), 1–24.

- Ettema, R. (1976). *Influence of bed material gradation on local scour*. University of Auckland.
- Ettema, R. (1980). "Scour at bridge piers."
- Ettema, R., Constantinescu, G., and Melville, B. W. (2017). "Flow-field complexity and design estimation of pier-scour depth: Sixty years since Laursen and Toch." *Journal of Hydraulic Engineering*, 143(9), 1–14.
- Ettema, R., Kirkil, G., and Muste, M. (2006). "Similitude of large-scale turbulence in experiments on local scour at cylinders." *Journal of Hydraulic Engineering*, 132(1), 33–40.
- Ettema, R., Melville, B. W., and Barkdoll, B. (1998). "Scale effect in pier-scour experiments." *Journal of Hydraulic Engineering*, 124(6), 639–642.
- Ettema, R., Melville, B. W., and Constantinescu, G. (2011). *Evaluation of bridge scour research: Pier scour processes and predictions*. Washington, DC, USA: Transportation Research Board of the National Academies.
- Ferreira, C. (2001). "Gene expression programming: a new adaptive algorithm for solving problems." *arXiv preprint cs/0102027*.
- Ferreira, C. (2006). *Gene expression programming: mathematical modeling by an artificial intelligence*. Springer.
- Garde, R. J., and Raju, K. G. R. (2000). *Mechanics of sediment transportation and alluvial stream problems*. Taylor & Francis.
- Garg, V., Setia, B., Singh, V., and Kumar, A. (2021). "Scour protection around bridge pier and two-piers-in-tandem arrangement." *ISH Journal of Hydraulic Engineering*, Taylor & Francis, 28(3), 1–13.
- Gaudio, R., Tafarojnoruz, A., and De Bartolo, S. (2013). "Sensitivity analysis of bridge pier scour depth predictive formulae." *Journal of Hydroinformatics*, 15(3), 939–951.
- Gazi, A. H., and Afzal, M. S. (2020). "A new mathematical model to calculate the

- equilibrium scour depth around a pier.” *Acta Geophysica*, Springer International Publishing, 68(1), 181–187.
- Ghaemi, N., Etemad-Shahidi, A., and Ataie-Ashtiani, B. (2013). “Estimation of current-induced pile groups scour using a rule-based method.” *Journal of Hydroinformatics*, 15(2), 516–528.
- Goel, A., and Pal, M. (2009). “Application of support vector machines in scour prediction on grade-control structures.” *Engineering Applications of Artificial Intelligence*, 22(2), 216–223.
- Grimaldi, C. (2005). “Non-conventional countermeasures against local scouring at bridge piers.” *D. Università 'della Calabria, Cosenza, Italy*.
- Guan, D., Chiew, Y. M., Wei, M., and Hsieh, S. C. (2019). “Characterization of horseshoe vortex in a developing scour hole at a cylindrical bridge pier.” *International Journal of Sediment Research*, 34(2), 118–124.
- Güven, A., and Günel, M. (2008). “Genetic programming approach for prediction of local scour downstream of hydraulic structures.” *Journal of Irrigation and Drainage Engineering*, 134(2), 241–249.
- Hancu, S. (1971). “Computation of local scour in the vicinity of bridge piers.” *Proc., 14th Int. Association of Hydraulic Research (IAHR) Congress*, 299–305.
- Hannah, C. R. (1978). *Scour at pile groups*. Dept. of Civil Engineering, University of Canterbury, Christchurch, N.Z.
- Hassan, W. H., Hussein, H. H., Alshammari, M. H., Jalal, H. K., and Rasheed, S. E. (2022). “Evaluation of gene expression programming and artificial neural networks in PyTorch for the prediction of local scour depth around a bridge pier.” *Results in Engineering*.
- Hassan, W. H., and Jalal, H. K. (2021). “Prediction of the depth of local scouring at a bridge pier using a gene expression programming method.” *SN Applied Sciences*, Springer International Publishing, 3(2), 1–9.

- Heidarpour, M., Afzalimehr, H., and Izadinia, E. (2010). "Reduction of local scour around bridge pier groups using collars." *International Journal of Sediment Research*, International Research and Training Centre on Erosion and Sedimentation and the World Association for Sedimentation and Erosion Research, 25(4), 411–422.
- Hong, Y., Ph, D., Kan, Y., Ph, D., Zeng, J., Lin, H., and Ph, D. (2018). "Multiphysics coupling model for computing pier scour upon simulation and experiment." *Journal of Computing in Civil Engineering*, 32(1), 1–15.
- Hosseini, R., and Amini, A. (2015). "Scour depth estimation methods around pile groups." *KSCE Journal of Civil Engineering*, 19(7), 2144–2156.
- Huang, W., Yang, Q., and Xiao, H. (2009). "CFD modeling of scale effects on turbulence flow and scour around bridge piers." *Computers and Fluids*, Elsevier Ltd, 38, 1050–1058.
- Jahangirzadeh, A., Shamshirband, S., and Aghabozorgi, S. (2014a). "Neurocomputing A cooperative expert based support vector regression (Co-ESVR) system to determine collar dimensions around bridge pier." *Neurocomputing*, 140, 172–184.
- Jahangirzadeh, A., Shamshirband, S., Petković, D., Basser, H., Sedaghat, A., Akib, S., and Karami, H. (2014b). "Adaptive neuro-fuzzy estimation of the influence of slot on local scour at bridge pier groups." *Journal of Coastal Conservation*.
- Jain, R., Lodhi, A. S., Oliveto, G., and Pandey, M. (2021). "Influence of cohesion on scour at piers founded in clay–sand–gravel mixtures." *Journal of Irrigation and Drainage Engineering*, 147(10), 04021046.
- Jaman, H., Das, S., Kuila, A., and Mazumdar, A. (2017). "Hydrodynamic flow patterns around three inline eccentrically arranged circular piers." *Arabian Journal for Science and Engineering*, 42(9), 3973–3990.
- Jiang, W., and Lin, C. (2021). "Scour effects on vertical effective stresses and lateral responses of pile groups in sands." *Ocean Engineering*, 229, 109017.

- Jiang, W., and Lin, C. (2022). "Scour effects on lateral responses of pile groups in clays." *Computers and Geotechnics*, 149, 104851.
- Jiao, H., and Wu, G. X. (2018). "Analysis of fluctuating force acting on two cylinders in different arrangements through Lattice Boltzmann Method." *Journal of Fluids and Structures*, 82, 101–120.
- Johnson, P. A., Clopper, P. E., Zevenbergen, L. W., and Lagasse, P. F. (2015). "Quantifying uncertainty and reliability in bridge scour estimations." *Journal of Hydraulic Engineering*, 141(7), 4015013.
- Johnson, P. A., and Torrico, E. F. (1994). "Scour around wide piers in shallow water." *Transportation Research Record*, US National Research Council, (1471), 66–70.
- Jones, J. S., and Sheppard, D. M. (2004). "Local scour at complex pier geometries." *Joint Conference on Water Resource Engineering and Water Resources Planning and Management 2000: Building Partnerships*, 104(1), 1–9.
- Keshavarzi, A., Sarmadian, F., Shiri, J., Iqbal, M., Tirado-Corbalá, R., and Omran, E.-S. E. (2017). "Application of ANFIS-based subtractive clustering algorithm in soil cation exchange capacity estimation using soil and remotely sensed data." *Measurement*, 95, 173–180.
- Keshavarzi, A., Shrestha, C. K., Melville, B., Khabbaz, H., Ranjbar-Zahedani, M., and Ball, J. (2018). "Estimation of maximum scour depths at upstream of front and rear piers for two in-line circular columns." *Environmental Fluid Mechanics*, 18(2), 537–550.
- Khan, M., Tufail, M., Azmathullah, H. M., Aslam, M. S., and Khan, F. A. (2017). "Experimental analysis of bridge pier scour pattern." *Journal of Engineering and Applied Sciences (JEAS)*, 36(1).
- Khaple, S., Reddy, P., and Roberto, H. (2017). "Interference of an upstream pier on local scour at downstream piers." *Acta Geophysica*, Springer International Publishing.
- Khassaf, S. I., and Shakir, S. S. (2013). "Evaluation of The Local Scour Around Group

- Piers (Babil Bridge as Case Study).” *International Journal of Innovative Research in Science, Engineering and Technology*, 2(12), 7409–7420.
- Kim, H. S., Roh, M., and Nabi, M. (2017). “Computational modeling of flow and scour around two cylinders in staggered array.” *Water (Switzerland)*, 9(9), 1–19.
- Kirkil, G., Constantinescu, G., and Ettema, R. (2009). “Detached eddy simulation investigation of turbulence at a circular pier with scour hole.” *Journal of Hydraulic Engineering*, 135(11), 888–901.
- Kirkil, G., Constantinescu, S. G., and Ettema, R. (2008). “Coherent structures in the flow field around a circular cylinder with scour hole.” *Journal of Hydraulic Engineering*, 134(5), 572–587.
- Klinga, J. V, and Alipour, A. (2015). “Assessment of structural integrity of bridges under extreme scour conditions.” *Engineering Structures*, 82, 55–71.
- Kothyari, U. C. (1989). “Scour around bridge piers.” University of Roorkee.
- Kothyari, U. C. (2007). “Indian practice on estimation of scour around bridge piers - A comment.” *Sadhana - Academy Proceedings in Engineering Sciences*, 32(3), 187–197.
- Kothyari, U. C., Garde, R. C. J., and Ranga Raju, K. G. (1992a). “Temporal variation of scour around circular bridge piers.” *Journal of Hydraulic Engineering*, 118(8), 1091–1106.
- Kothyari, U. C., Garde, R. C. J., and Ranga Raju, K. G. (1992b). “Temporal variation of scour around circular bridge piers.” *Journal of Hydraulic Engineering*, 118(8), 1091–1106.
- Kothyari, U. C., Hager, W. H., and Oliveto, G. (2007). “Generalized Approach for Clear-Water Scour at Bridge Foundation Elements.” *Journal of Hydraulic Engineering*, 133(11), 1229–1240.
- Kothyari, U. C., and Kumar, A. (2012). “Temporal variation of scour around circular

- compound piers.” *Journal of Hydraulic Engineering*, 138(11), 945–957.
- Kumar, A., and Kothiyari, U. C. (2012). “Three-Dimensional flow characteristics within the scour hole around circular uniform and compound piers.” *Journal of Hydraulic Engineering*, 138(5), 420–429.
- Lança, R., Fael, C., and Cardoso, A. (2011). “Effect of relative sediment size on clear-water equilibrium scour depth at single cylindrical piers.” *Proceedings of the 34th World Congress of the International Association for Hydro-Environment Research and Engineering: 33rd Hydrology and Water Resources Symposium and 10th Conference on Hydraulics in Water Engineering, Brisbane, QLD, Australia*.
- Lança, R., Fael, C., Maia, R., Pêgo, J. P., and Cardoso, A. H. (2013). “Clear-Water Scour at Pile Groups.” *Journal of Hydraulic Engineering*, 139(10), 1089–1098.
- Laursen, M. E., and Toch, A. (1956). *Scour around bridge piers and abutments (1956)*. Iowa Institute of Hydraulic Research.
- Lauth, T. J., and Papanicolaou, A. N. (2008). “Experimental/feasibility study of radio frequency tracers for monitoring sediment transport and scour around bridges.” *World Environmental and Water Resources Congress: Ahupua’a*, 1–10.
- Lee, S. O., and Sturm, T. W. (2009). “Effect of sediment size scaling on physical modeling of bridge pier scour.” *Journal of hydraulic engineering*, 135(10), 793–802.
- Liang, F., Wang, C., Huang, M., and Wang, Y. (2017). “Experimental observations and evaluations of formulae for local scour at pile groups in steady currents.” *Marine Georesources and Geotechnology*, 35(2), 245–255.
- Liang, F., Wang, C., and Yu, X. (2019). “Performance of existing methods for estimation and mitigation of local scour around bridges : Case studies.” *Journal of Performance of Constructed Facilities*, 33(6)(04019060), 1–15.
- M. Lança, R. M., Simarro, G., S. Fael, C. M., and Cardoso, A. H. (2016). “Effect of viscosity on the equilibrium scour depth at single cylindrical piers.” *Journal of Hydraulic Engineering*, 142(3), 6015022.

- Ma, L., Wang, L., Guo, Z., Jiang, H., and Gao, Y. (2018). "Time development of scour around pile groups in tidal currents." *Ocean Engineering*, 163, 400–418.
- Majedi-Asl, M., Daneshfaraz, R., Abraham, J., and Valizadeh, S. (2021). "Effects of hydraulic characteristics, sedimentary parameters, and mining of bed material on scour depth of bridge pier groups." *Journal of Performance of Constructed Facilities*, 35(2), 04020148.
- Malik, A., Singh, S. K., and Kumar, M. (2021). "Experimental analysis of scour under circular pier." *Water Science and Technology: Water Supply*, 21(1), 422–430.
- Malik, R., and Setia, B. (2018). "Local scour around closely placed bridge piers." *ISH Journal of Hydraulic Engineering*, Taylor & Francis, 27(4), 1–8.
- Malik, R., and Setia, B. (2020a). "Prediction of scour depth in a group of piers in staggered arrangement using experimental and regression models." *Journal of The Institution of Engineers (India): Series A*, 101(1), 141–152.
- Malik, R., and Setia, B. (2020b). "Interference between pier models and its effects on scour depth." *SN Applied Sciences*, 2(1), 1–12.
- Melville, B. W. (1975). "Local scour at bridge sites." (Doctoral dissertation researchspace@ auckland).
- Melville, B. W. (1984). "Live-bed scour at bridge piers." *Journal of Hydraulic Engineering*, 110(9), 1234–1247.
- Melville, B. W. (1992). "Discussion of 'Study of Time-Dependent Local Scour Around Bridge Piers' by A. Melih Yanmaz and H. Dog˘ an Altmbilek (October, 1991, Vol. 117, No. 10)." *Journal of Hydraulic Engineering*, 117(10), 1593–1595.
- Melville, B. W. (1997). "Pier and abutment scour: Integrated approach." *Journal of Hydraulic Engineering*, 123(2), 125–136.
- Melville, B. W., and Chiew, Y. (1999). "Time scale for local scour at bridge piers." *Journal of Hydraulic Engineering*, 125(1), 59–65.

- Melville, B. W., and Coleman, S. E. (2000). *Bridge scour*. Water Resources Publication.
- Melville, B. W., and Raudkivi, A. J. (1977). “Flow characteristics in local scour at bridge piers.” *Journal of Hydraulic Research*, 15(4), 373–380.
- Melville, B. W., and Sutherland, A. J. (1988). “Design method for local scour at bridge piers.” *Journal of Hydraulic Engineer*, 114(10), 1210–1226.
- Memar, S., Zounemat-Kermani, M., Beheshti, A., Rahimpour, M., De Cesare, G., and Schleiss, A. J. (2020). “Influence of collars on reduction in scour depth at two piers in a tandem configuration.” *Acta Geophysica*, 68(1), 229–242.
- Meneghini, J. R., Saltara, F., Siqueira, C. de L. R., and Ferrari Jr, J. A. (2001). “Numerical simulation of flow interference between two circular cylinders in tandem and side-by-side arrangements.” *Journal of fluids and structures*, 15(2), 327–350.
- Mia, M. F., and Nago, H. (2003). “Design method of Time-Dependent local scour at circular bridge pier.” *Journal of Hydraulic Engineering*, 129(6), 420–427.
- Mohammed Saleh, L. A., Majeed, S. A. A. din, and Alnasrawi, F. A. el kadhium M. (2019). “Numerical study of the bridge pier scour using gene expression programming.” *Journal of Applied Water Engineering and Research*, 7(4), 287–294.
- Moreno, M. (2016). “Experimental study of local scour around complex bridge piers.” 268.
- Muzzammil, M., Alama, J., and Danish, M. (2015). “Scour prediction at bridge piers in cohesive bed using Gene Expression Programming.” *International conference on water resources, coastal and ocean engineering: Aquatic Procedia*, 789–796.
- Muzzammil, M., and Gangadhariah, T. (2010). “The mean characteristics of horseshoe vortex at a cylindrical pier.” *Journal of Hydraulic Research*, 41(3), 285–297.
- Nagel, T., Chauchat, J., Bonamy, C., Liu, X., Cheng, Z., and Hsu, T. J. (2020). “Three-dimensional scour simulations with a two-phase flow model.” *Advances in Water*

Resources, 138, 1–76.

Najafzadeh, M. (2015). “Neuro-fuzzy GMDH systems based evolutionary algorithms to predict scour pile groups in clear water conditions.” *Ocean Engineering*, 99, 85–94.

Najafzadeh, M., and Azamathulla, H. M. (2013). “Group method of data handling to predict scour depth around bridge piers.” *Neural Computing and Applications*, 23, 2107–2112.

Najafzadeh, M., and Azamathulla, H. M. (2015). “Neuro-Fuzzy GMDH to Predict the Scour Pile Groups due to Waves.” *Journal of Computing in Civil Engineering*, 29(5).

Najafzadeh, M., Balf, M. R., and Rashedi, E. (2016). “Prediction of maximum scour depth around piers with debris accumulation using EPR, MT, and GEP models.” *Journal of Hydroinformatics*, 18(5), 867–884.

Najafzadeh, M., Barani, G. A., and Azamathulla, H. M. (2013). “GMDH to predict scour depth around a pier in cohesive soils.” *Applied Ocean Research*, 40, 35–41.

Najafzadeh, M., Barani, G. A., and Hessami-Kermani, M. R. (2015). “Evaluation of GMDH networks for prediction of local scour depth at bridge abutments in coarse sediments with thinly armored beds.” *Ocean Engineering*, Elsevier, 104, 387–396.

Najafzadeh, M., and Oliveto, G. (2021). “More reliable predictions of clear-water scour depth at pile groups by robust artificial intelligence techniques while preserving physical consistency.” *Soft Computing*, Springer Berlin Heidelberg, 25(7), 5723–5746.

Nazariha, M. (1996). *Design relationships for maximum local scour depth for bridge pier groups*. University of Ottawa (Canada).

Okhravi, S., Gohari, S., Alemi, M., and Maia, R. (2022). “Effects of bed-material gradation on clear water scour at single and group of piles.” *Journal of Hydrology and Hydromechanics*, 70(1), 114–127.

- Oliveto, G., and Hager, W. H. (2002). “Temporal evolution of clear-water pier and abutment scour.” *Journal of Hydraulic Engineer*, 128(9), 811–820.
- Oliveto, G., Hager, W. H., and Asce, F. (2005). “Further results to time-dependent local scour at bridge elements.” *Journal of Hydraulic Engineering*, 131(2), 97–106.
- Oliveto, G., Unger, J., and Hager, W. H. (2003). “Discussion of ‘Design method of time-dependent local scour at circular bridge pier’ by Md. Faruque Mia and Hiroshi Nago.” *Journal of Hydraulic Engineer*, 129(6), 1211–1215.
- ÖZALP, M. C. (2013). *Experimental investigation of local scour around bridge pier groups. Thesis.*
- Pandey, M., Oliveto, G., Pu, J. H., Sharma, P. K., and Ojha, C. S. P. (2020a). “Pier scour prediction in non-uniform gravel beds.” *Water (Switzerland)*, 12(6), 13–17.
- Pandey, M., Zakwan, M., Khan, M. A., and Bhave, S. (2020b). “Development of scour around a circular pier and its modelling using genetic algorithm.” *Water Science and Technology: Water Supply*, 20(8), 3358–3367.
- Pandey, M., Zakwan, M., Sharma, P. K., and Ahmad, Z. (2020c). “Multiple linear regression and genetic algorithm approaches to predict temporal scour depth near circular pier in non-cohesive sediment.” *ISH Journal of Hydraulic Engineering, Taylor & Francis*, 26(1), 96–103.
- Parola, A. C., Hagerty, D. J., Mueller, D. S., Melville, B. W., Parker, G., and Usher, J. S. (1997). “The need for research on scour at bridge crossings.” *Stream Stability and Scour at Highway Bridges: Compendium of Stream Stability and Scour Papers Presented at Conferences Sponsored by the Water Resources Engineering (Hydraulics) Division of the American Society of Civil Engineers, ASCE*, 1020.
- Pasupuleti, L. N., Timbadiya, P. V., and Patel, P. L. (2022). “Flow fields around tandem and staggered piers on a mobile bed.” *International Journal of Sediment Research*, 37(6), 737–753.
- Pu, J. H., Wallwork, J. T., Khan, M. A., Pandey, M., Pourshahbaz, H., Satyanaga, A.,

- Hanmaiahgari, P. R., and Gough, T. (2021). “Flood suspended sediment transport: Combined modelling from dilute to hyper-concentrated flow.” *Water (Switzerland)*, 13(3), 1–24.
- Qadar, A. (1981). “The vortex scour mechanism at bridge piers.” *Proceedings of the Institution of Civil Engineers*, Thomas Telford-ICE Virtual Library, 71(3), 739–757.
- Qi, M., Chiew, Y.-M., and Hong, J.-H. (2013). “Suction effects on bridge pier scour under clear-water conditions.” *Journal of Hydraulic Engineering*, 139(6), 621–629.
- Qi, W. G., Li, Y. X., Xu, K., and Gao, F. P. (2019). “Physical modelling of local scour at twin piles under combined waves and current.” *Coastal Engineering*, 143, 63–75.
- Raikar, R. V, and Dey, S. (2008). “Kinematics of horseshoe vortex development in an evolving scour hole at a square cylinder.” *Journal of hydraulic research*, Taylor & Francis, 46(2), 247–264.
- Raudkivi, A. J. (2020). *Loose boundary hydraulics*. CRC Press.
- Raudkivi, A. J., and Ettema, R. (1983). “Clear-Water scour at cylindrical piers.” *Journal of Hydraulic Engineering*, 109(3), 338–350.
- Richardson, E. V., and Davis, S. R. (2001). *Evaluating scour at bridges*. National Highway Institute (US).
- Richardson, E. V, and Davis, S. R. (1995). “Evaluating scour at bridges, Report No. FHWA-IP-90-017, Hydraulic Engineering Circular No. 18 (HEC-18).” Office of Technology Applications, HTA-22, Federal Highway Administration
- Richardson, E. V, Lagasse, P. F., Schall, J. D., Ruff, J. F., Brisbane, T. E., and Frick, D. M. (1987). “Hydraulics, erosion and channel stability analysis of the schoharie creek bridge failure, New York.” *Resource Consultants, Inc.*
- Richardson, J. E., and Panchang, V. G. (1998). “Three-dimensional simulation of scour-inducing flow at bridge piers.” *Journal of Hydraulic Engineering*, 124(5), 530–540.
- Roulund, A., Sumer, B. M., Fredsoe, J., and Michelsen, J. (2002). “3-D numerical

- modeling of flow and scour around a pile.” *First International Conference on Scour of Foundations*. November 17-20, 2002, College Station, USA, 795–809.
- Roulund, A., Sumer, B. M., Fredsøe, J., and Michelsen, J. (2005). “Numerical and experimental investigation of flow and scour around a circular pile.” *Journal of Fluid Mechanics*, 534, 351–401.
- Salim, M., and Jones, J. S. (1996). “Scour around exposed pile foundations.” *North American water and environment congress & destructive water*, 2202–2211.
- Sarker, A. (1998). “Flow measurement around scoured bridge piers using Acoustic-Doppler Velocimeter (ADV).” *Flow Measurement and Instrumentation*, 9, 217–227.
- Şarlak, N., and Tiğrek, Ş. (2011). “Analysis of experimental data sets for local scour depth around bridge abutments using artificial neural networks.” *Water Sa*, 37(4), 595–602.
- Setia, B. (2008). “Equilibrium scour depth time.” *3rd IASME / WSEAS Int. Conf. on Water Resources, Hydraulics & Hydrology (WHH '08)*, University of Cambridge, UK, 114–117.
- Sharafati, A., Tafarjnoruz, A., and Yaseen, Z. M. (2020). “New stochastic modeling strategy on the prediction enhancement of pier scour depth in cohesive bed materials.” *Journal of Hydroinformatics*, 22(3), 457–472.
- Shen, H. W., Schneider, V. R., and Karaki, S. (1969). “Local scour around bridge piers.” *Journal of the Hydraulics Division*, 95(6), 1919–1940.
- Shen, H. W., Schneider, V. R., and Karaki, S. S. (1966). “Mechanics of local scour.”
- Sheppard, D. M., Melville, B., and Demir, H. (2014). “Evaluation of existing equations for local scour at bridge piers.” *Journal of Hydraulic Engineer*, 140(1), 14–23.
- Sheppard, D. M., and Miller, J. W. (2006). “Live-Bed local pier scour experiments.” *Journal of Hydraulic Engineering*, 132(7), 635–642.

- Sheppard, D. M., Odeh, M., and Glasser, T. (2004). "Large scale clear-water local pier scour experiments." *Journal of Hydraulic Engineering*, 130(10), 957–963.
- Sheppard, D. M., and Renna, R. (2010). "Bridge scour manual. 605 Suwannee Street." *Tallahassee, FL*, 30450–32399.
- Shiri, J., Marti, P., and Singh, V. P. (2014). "Evaluation of gene expression programming approaches for estimating daily evaporation through spatial and temporal data scanning." *Hydrological Processes*, 28(3), 1215–1225.
- Simarro, G., Fael, C. M. S., and Cardoso, A. H. (2011). "Estimating Equilibrium Scour Depth at Cylindrical Piers in Experimental Studies." *JOURNAL OF HYDRAULIC ENGINEERING*, 137(9), 1089–1093.
- Smith, D. W. (1976). "Bridge failures." *Proceedings of the institution of civil engineers*, Thomas Telford-ICE Virtual Library, 60(3), 367–382.
- Sreedhara, B. M., Rao, M., and Mandal, S. (2019). "Application of an evolutionary technique (PSO–SVM) and ANFIS in clear-water scour depth prediction around bridge piers." *Neural Computing and Applications*, 31(11), 7335–7349.
- Sumer, B. M., Fredsøe, J., and Bundgaard, K. (2005). "Global and local scour at pile groups." *The Fifteenth International Offshore and Polar Engineering Conference*, OnePetro.
- Sumner, D., Wong, S. S. T., Price, S. J., and Païdoussis, M. P. (1999). "Fluid behaviour of side-by-side circular cylinders in steady Cross-Flow." *Journal of Fluids and Structures*, 13(3), 309–338.
- Tafarojnoruz, A., Gaudio, R., and Calomino, F. (2012). "Bridge pier scour mitigation under steady and unsteady flow conditions." *Acta Geophysica*, 60(4), 1076–1097.
- Tang, H. W., Wang, H., Liang, D. F., Lv, S. Q., and Yan, L. (2013). "Incipient motion of sediment in the presence of emergent rigid vegetation." *Journal of Hydro-Environment Research*, 7(3), 202–208.

- Teodorescu, L., and Sherwood, D. (2008). "High energy physics event selection with Gene Expression Programming." *Computer Physics Communications*, 178(6), 409–419.
- Tipireddy, R. T. R., Barkdoll, B. D., and Asce, F. (2019). "Scour reduction by air injection at a cylindrical bridge pier : Experimental determination of optimal configuration." *Journal of Hydraulic Engineering*, 145(1), 1–4.
- Török, G. T., Baranya, S., and Rütther, N. (2017). "3D CFD modeling of local scouring, bed armoring and sediment deposition." *Water (Switzerland)*, 9(1).
- Umeda, S., Yamazaki, T., and Yuhi, M. (2010). "An experimental study of scour process and sediment transport around a bridge pier with foundation." *Proceedings 5th International Conference on Scour and Erosion (ICSE-5)*, ASCE, San Francisco, USA, 66–75.
- Vijayasree, B. A., and Eldho, T. I. (2021). "A modification to the Indian practice of scour depth prediction around bridge piers." *Current Science*, 120(12), 1875–1881.
- Wang, C., Yu, X., and Liang, F. (2017a). "Comparison and estimation of the local scour depth around pile groups and wide piers." *Geotechnical Special Publication*, (GSP 279), 11–21.
- Wang, C., Yu, X., and Liang, F. (2017b). "A review of bridge scour: mechanism, estimation, monitoring and countermeasures." *Natural Hazards*, 87(3), 1881–1906.
- Wang, H., Tang, H., Liu, Q., and Wang, Y. (2016a). "Local scouring around twin bridge piers in open-channel flows." *Journal of Hydraulic Engineering*, 142(9), 06016008.
- Wang, H., Tang, H. W., Xiao, J. F., Wang, Y., and Jiang, S. (2016b). "Clear-water local scouring around three piers in a tandem arrangement." *Science China Technological Sciences*, 59(6), 888–896.
- Wardhana, K., and Hadipriono, F. C. (2003). "Study of recent building failures in the United States." *Journal of performance of constructed facilities*, 17(3), 151–158.

- Xiong, W., Tang, P., Kong, B., and Cai, C. S. (2016). “Reliable bridge scour simulation using Eulerian two-phase flow theory.” *Journal of Computing in Civil Engineering*, 30(5), 4016009.
- Xiong, W., Tang, P., Kong, B., and Cai, C. S. (2017). “Computational simulation of Live-Bed bridge scour considering suspended sediment loads.” *Journal of Computing in Civil Engineering*, 31(5), 04017040.
- Yang, F., Liu, X., Cao, S., and Huang, E. (2010). “Bed load transport rates during scouring and armoring processes.” *Journal of Mountain Science*, 7(3), 215–225.
- Yang, Y., Melville, B. W., Sheppard, D. M., and Shamseldin, A. Y. (2018). “Clear-Water local scour at skewed complex bridge piers.” *Journal of Hydraulic Engineering*, 144(6), 4018019.
- Yang, Y., Melville, B. W., Sheppard, D. M., and Shamseldin, A. Y. (2019). “Live-bed scour at wide and long-skewed bridge piers in comparatively shallow water.” *Journal of Hydraulic Engineering*, 145(2017), 6019005.
- Yang, Y. S., Melville, B. W., Macky, G. H., and Shamseldin, A. Y. (2020). “Temporal evolution of clear-water local scour at aligned and skewed complex bridge piers.” *Journal of Hydraulic Engineering*, 146(2016), 04020026.
- Yanmaz, A. M., and Altinbilek, H. D. g ~ an. (1991). “Study of time-depenbent local scour around bridge piers.” *Journal of Hydraulic Engineering*, 117(10), 1247–1268.
- Yanmaz, A. M., and Kose, O. (2007). “Time-wise variation of scouring at bridge abutments.” *Sadhana - Academy Proceedings in Engineering Sciences*, 32(3), 199–213.
- Zaid, M., Yazdanfar, Z., Chowdhury, H., and Alam, F. (2019). “Numerical modeling of flow around a pier mounted in a flat and fixed bed.” *Energy Procedia*, 160(2018), 51–59.
- Zhao, W., and Huhe, A. (2006). “Large-eddy simulation of three-dimensional turbulent flow around a circular pier.” *Journal of Hydrodynamics*, 18(6), 765–772.

Zhou, K., Duan, J. G., and Bombardelli, F. A. (2020). “Experimental and theoretical study of local scour around three-pier group.” *Journal of Hydraulic Engineering*, 146(10), 04020069.